

**DEVELOPMENT OF ABS COMPOSITE MATRIX BASED 3D
PRINTED PROTOTYPES FROM INDUSTRIAL WASTE FOR
NON-STRUCTURAL APPLICATIONS**

Thesis Submitted For the Award of the Degree of

DOCTOR OF PHILOSOPHY

In

(Mechanical Engineering)

By

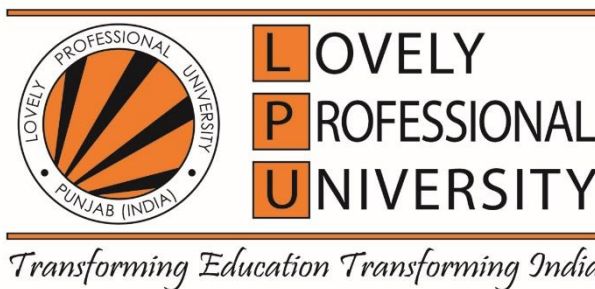
**Kapil Chawla
(41800161)**

Supervised By

Dr. Jaspreet Singh

Co-Supervised by

Prof. Rupinder Singh

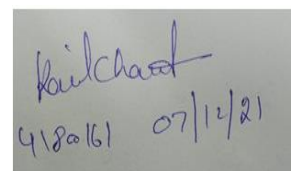


**LOVELY PROFESSIONAL UNIVERSITY
PUNJAB
2022**

CANDIDATE'S DECLARATION

I hereby certify that the work which is being presented in the thesis, entitled “Development of ABS Composite Matrix Based 3D Printed Prototypes from Industrial Waste for Non-Structural Applications”. in fulfilment of the requirements for the award of the degree of Doctor of Philosophy in Lovely Faculty of Technology and Science submitted in Lovely Professional University, Jalandhar is an authentic record of my own work carried out during a period from August, 2018 to April, 2021 under the supervision of Dr. Jaspreet Singh and Prof. Rupinder Singh.

The matter embodied in this thesis has not been submitted by me for the award of any other degree of this or any other University/Institute.



(Kapil Chawla)

This is to certify that the above statement made by the candidate is correct to the best of my knowledge.

(Dr. Jaspreet Singh)

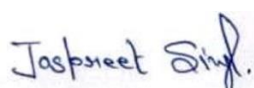
(Supervisor)

Department of Mechanical Engineering
Lovely Professional University, Phagwara-144411, Punjab (India)

(Prof. Rupinder Singh)

(Co- Supervisor)

Department of Mechanical Engineering
National Institute of Technical Teacher Training and Research, Chandigarh- 160019, Punjab (India)



Signature of Supervisor

Signature of Co-Supervisor

ABSTRACT

The present research work primarily focuses on printing of non-structural component by utilizing various industrial wastes to address the global issue of recyclability. In this work, the researchers utilized secondary recycled acrylonitrile butadiene styrene (ABS) as base material and bakelite powder (BP), wood dust (WD) and Fe powder as reinforcements. The particular reinforcements were selected to prepare composite filaments to induce some specific properties in the smart tiles that can be employed in low-temperature regions.

The entire research was divided into three phases. In the first phase, recycled ABS based composite filaments reinforced with industrial wastes such as WD, BP, and Fe powder respectively were fabricated through three different blending routes (mechanical, mechanical-hybrid and chemical assisted mechanical) by altering the selected parameters of Twin Screw Extruder (load, temperature and speed) using L9 Orthogonal array. The results highlighted that melt flow rate (MFR) being a rheological property increases with the addition of any of the reinforcements up to a certain critical level irrespective of the type of blending. The chemical assisted blending of BP, WD and Fe as reinforcement in ABS matrix yields improved mechanical properties as compared to mechanical blending. However, thermal properties in terms of heat-carrying capacity achieved through chemical blending were degraded may be due to the presence of a higher porosity percentage. The composite filaments fabricated through mechanical-hybrid blending possess relatively poor mechanical properties due to the brittle nature of the fabricated filaments. Finally, optimization was performed to investigate the optimum parametric settings for preparation of composite filaments with regard to all the three blending routes. The filaments fabricated at optimum settings were utilized in second phase for printing.

In second phase, mechanically and chemically assisted composite filaments were used to print multilayer tensile and flexural specimen through FDM whereas single filament based tensile and flexural specimens were printed from composite filament prepared by mechanical-hybrid assisted blending by varying the printing parameters such as raster angle, infill pattern and infill speed. Infill density and infill speed during printing come out as the most influential parameter that affects the properties of all prepared specimens. The tensile and flexural specimens printed from mechanical-hybrid blended composite filaments exhibit minimum

strength and elongation among all the printed specimens. The SEM characterization indicated that higher density and lower raster angle results in uniform deposition of layers that leads to lesser void formation and consequently good bonding between the adjacent layers. Finally, multi-objective optimization was performed to investigate the optimum printing settings and the rectangular strips were printed on the obtained optimized settings.

The third phase involves the post processing of printed strips to improve their surface quality and shore hardness. The post processing was performed through two separate techniques (chemical vapour smoothing (CVS) and heat treatment) to analyse and compare their impact on surface properties. Both the CVS and heat treatment processes improve the surface finish of ABS based rectangular printed specimen significantly. Improvement in surface finish of more than 90% and 80% was achieved through CVS and heat treatment process respectively. An improvement in shore hardness of 12% was observed after CVS and heat treatment process. In last, the work summarizes the successful utilization of secondary recycled ABS reinforced with BP, WD and Fe powder respectively (to achieve desired properties) in the form of composite filament for 3D printing applications.

ACKNOWLEDGEMENT

First and foremost, I am thankful to the Almighty God for planning everything for my life and choosing me to perform this research work. Whenever things got tough while performing this work, my firm belief in Him strengthened me to accept these challenges with smile and bestow courage to work hard for solving these difficulties.

I would like to express my sincere thanks to Associate Professor (Dr.) Jaspreet Singh and Professor Rupinder Singh for being my research supervisors and for giving me an opportunity to do research in the area of fused deposition modelling assisted investment casting. Their valuable guidance, positive thoughts, encouragement, understanding and kindness proved the existence of GOD in him as a teacher. I really feel fortunate to have a chance to perform this research under their guidance

I am also highly thankful to Dr. Vijay Kumar (Associate Dean, Lovely Professional University), and my wife Mrs. Himani Mehta for encouraging me during my research work. I am greatly indebted to technical staff of GNDEC, Ludhiana and Central Instrumentation Facility Laboratory in Lovely Professional University for providing the technical support during the course of experimental work.

My special thanks to Mr. Puran Singh (Manufacturing Research Lab, GNDEC, Ludhiana) and Mrs. Anita (CIF Lab, LPU) for his help in performing the experimental work.

Finally, I want to thank all my family members, friends and colleagues. I could not have reached today's point without their help and best wishes.

LIST OF ABBREVIATIONS AND SYMBOLS USED

ABS	Acrylonitrile butadiene styrene
AM	Additive manufacturing
Al ₂ O ₃	Aluminum oxide
ANOVA	Analysis of Variance
Adj. SS	Adjusted Sum of Square
Adj. MS	Adjusted Mean Square
BS	Break Strength
BL	Break Load
%BE	Percentage Break Elongation
BP	Bakelite powder
CAD	Computer aided design
CB	Carbon black
CF	Carbon fibre
CNT	Carbon nanotube
CVS	Chemical Vapor Smoothing
DOF	Degree of Freedom
DOE	Degree of Experiments
E	Modulus of Elasticity
Fe	Iron Powder
FDM	Fused deposition modeling
F- value	Fisher's value
GF	Glass fibre
HT	Heat Treatment
HDPE	High density polyethylene
LDM	Liquid deposition modeling
LDPE	Low density polyethylene
MFR	Melt flow rate
OA	Orthogonal array
PS	Peak strength

PL	Peak Load
%PE	Percentage Peak Elongation
PA6	Polyamide
PBT	Polybutylene terephthalate
PC	Polycarbonate
PCL	Polycaprolactone
PET	Polyethylene terephthalate
PEEK	Polyether ether ketone
PEI	Polyetherimide
PLA	Polylactic acid
PP	Polypropylene
PVC	Polyvinyl chloride
PVDF	Polyvinylidene difluoride
p- value	Probability Value
Ra	Surface roughness
S/N	Signal to Noise
SLA	Stereolithography
.STL	Standard triangulation language
TiO ₂	Titanium dioxide
TSE	Twin screw extruder
T	Toughness
WD	Wood Dust
μ	Mean
α	Significance level
°	Degree

TABLE OF CONTENT

	Page No.
Candidate's Declaration	i
Abstract	ii-iii
Acknowledgement	iv
List of Abbreviations and symbols used	v-vi
Table of Content	vii-viii
List of Figures	ix-xiii
List of Tables	xiv-xvi
List of publications	xvii
Chapter 1: Introduction	1-13
1.1 Introduction	1-5
1.2 Recycling Techniques	5-7
1.3 Recycled polymer with reinforced materials	8-12
1.4 Organization of thesis	12-13
Chapter 2: Literature Review	14-41
2.1 Review of Fused Filament Preparation	14-22
2.2 Review of Fused deposition modelling review	23-35
2.3 Review of Post Processing review	35-38
2.4 Bibliographic Analysis	38-41
Chapter 3: Problem formulation and objective	42-44
3.1 Need of research	42
3.2 Findings from literature survey	42-43
3.3 Objectives	43-44
Chapter 4: Methodology and Experimentation	45-68
4.1 Selection of base material and reinforcement material	47
4.2 Melt Flow Rate	47-50
4.3 Twin screw extruder	50-51
4.4 Tensile Testing	51

4.5 Flexural Testing	52
4.6 Mechanical and thermal testing	52-55
4.7 Fused Deposition Modeling setup	55-57
4.8 Chemical vapor smoothing (CVS)	58-59
4.9 Shore Hardness Tester	59
4.10 Heat Treatment	59-60
4.11 Surface roughness measurement	60-61
4.12 Pilot experimentation	61-64
4.13 Design of experiment	64-65
4.14 Orthogonal array selection	65-66
4.15 Signal to Noise- ratio	66-67
4.16 Analysis of variance (ANOVA)	67-68
Chapter 5: Result and Discussion	69-154
5.1 Phase1- (Fused Filament preparation)	69-118
5.2 Phase 2- (3D printing)	119-143
5.3 Phase 3- (Pre and Post Processing)	144-154
Chapter 6: Conclusions	155-157
Limitations and Scope of Future Research Work	158
References	159-179

LIST OF FIGURES

Figure No.	Title	Page No.
1.1	Polymer structure	1
1.2	Production and consumption of polymer waste in tonnes	3
1.3	Different recycling techniques used in recycling polymer waste	7
1.4	Schematic diagram of FDM	10
2.1	Bibliographic Analysis	40
2.2	Research Gap analysis based upon Figure 3.1	41
4.1	Steps involved in present study	46
4.2	MFR Tester setup	48
4.3	Flakes prepared by reinforcement of a) WD and b) BP c) Fe in ABS through chemical blending	49
4.4	ABS after hybrid blending	49
4.5	Schematic diagram of Single Screw Extruder	50
4.6	Schematic diagram of Tensile Testing	51
4.7	Schematic diagram of Flexural Testing	52
4.8	Schematic diagram of Differential Scanning Calorimeter	53
4.9	Scanning Electron Microscopic setup	53
4.10	Fourier Transform Infrared Spectroscopy setup	55
4.11	Fused Deposition Modelling setup	55
4.12	Repetier- Host software working	56
4.13	CAD model of tensile specimen	57
4.14	Chemical Vapor Smoothing station setup	58
4.15	a) Feedstock filament prepared by reinforcing WD in ABS b) Feedstock filament prepared by reinforcing Fe in ABS c) Feedstock filament prepared by reinforcing BP in ABS	62
5.1	SEM image of BP reinforced filament at X 2000	72
5.2	SEM image of WD reinforced filament X 2000	72
5.3	SEM image of Fe reinforced filament X 3000	73
5.4	EDS analysis of filament possessing maximum PS fabricated by	73

	reinforcing BP	
5.5	EDS analysis of filament possessing maximum PS fabricated by reinforcing WD	74
5.6	EDS analysis of filament possessing maximum PS fabricated by reinforcing Fe	74
5.7	Stress versus strain curve of ABS reinforced with BP	75
5.8	Stress versus strain curve of ABS reinforced with WD	75
5.9	Stress versus strain curve of ABS reinforced with Fe	76
5.10	FTIR of composite filaments having maximum PS (a) mechanically blended ABS+BP, (b) mechanically blended ABS+WD, (c) mechanically blended ABS+Fe	77
5.11	Photomicrographs at cross-section for BP reinforced filament having maximum and minimum peak strength	77
5.12	Photomicrographs at cross-section for WD reinforced filament having maximum and minimum peak strength	78
5.13	Photomicrographs at cross-section for Fe reinforced filament having maximum and minimum peak strength	78
5.14	Mean S/N ratio plots for PS and % BE of ABS reinforced with BP	80
5.15	Mean S/N ratio plots for PS and % BE of ABS reinforced with WD	80
5.16	Mean S/N ratio plots for PS and % BE of ABS reinforced with Fe	81
5.17	Porosity analysis of BP reinforced composite filaments having (a) minimum and (b) maximum porosity percentage	84
5.18	Porosity analysis of WD reinforced composite filaments having (a) minimum and (b) maximum porosity percentage	84
5.19	Porosity analysis of Fe reinforced composite filaments having (a) minimum and (b) maximum porosity percentage	85
5.20	3D rendered images of filaments having minimum and maximum porosity	85-87
5.21	Thermal analysis of BP and WD reinforced filaments containing minimum and maximum porosity	88
5.22	Thermal analysis of Fe reinforced filaments containing minimum and maximum porosity	88
5.23	Stress versus strain curve of BP reinforced ABS filaments	92

5.24	Stress versus strain curve of WD reinforced ABS filaments	93
5.25	Stress versus strain curve of Fe reinforced ABS filaments	93
5.26	FTIR of composite filaments having maximum PS (a) chemically blended ABS+BP, (b) chemically blended ABS+Fe, and (c) chemically blended ABS+WD	95
5.27	S/N analysis for peak strength and %BE of BP reinforced filaments	96
5.28	S/N analysis for percentage Peak strength and %BE of WD reinforced filaments	97
5.29	S/N analysis for percentage Peak strength and %BE of Fe reinforced filaments	97
5.30	(a) Minimum and (b) Maximum porosity at break cross-section of filaments reinforced with BP	100
5.31	Minimum and (b) Maximum porosity at break cross-section of filaments reinforced with WD	100
5.32	Minimum and (b) Maximum porosity at break cross-section of filaments reinforced with Fe	101
5.33	Photomicrograph analysis at the cross-section of samples reinforced with BP	102
5.34	Photomicrograph analysis at the cross-section of samples reinforced with WD	102
5.35	Photomicrograph analysis at a cross-section of samples reinforced with Fe	103
5.36	Surface morphology of BP (a, b), WD (c, d) and Fe (e,f) reinforced filaments possessing lowest and highest porosity respectively	103-105
5.37	SEM analysis of filament at $\times 5000$ (BP reinforced)	105
5.38	SEM analysis of filament at $\times 5000$ (WD reinforced)	106
5.39	SEM analysis of filament at $\times 10,000$ (Fe reinforced)	106
5.40	EDS analysis of filament possessing maximum PS fabricated by reinforcing BP	107
5.41	EDS analysis of filament possessing maximum PS fabricated by reinforcing WD	107
5.42	EDS analysis of filament possessing maximum PS fabricated by reinforcing Fe	107

5.43	Thermal analysis of BP and WD composite filaments	108
5.44	Thermal analysis of Fe composite filaments	109
5.45	Stress-strain curve for prepared filaments	111
5.46	Optical Photomicrograph of filaments having least and highest voids	112
5.47	FTIR of composite filaments having maximum PS prepared by mechanical-hybrid blended	112
5.48	Surface topology of filaments having a) minimum and b) maximum voids	113
5.49	Porosity presence along with percentage in composite filaments	114
5.50	SEM analysis of filament prepared by hybrid blending	114
5.51	EDS analysis of filament prepared by hybrid blending	115
5.52	Mean S/N ratio for a) PS b) %BE of composite filaments	116
5.53	Thermal analysis of filaments having maximum and least porosity	117
5.54	Stress-Strain curve of 3D printed specimens after tensile testing	120
5.55	Stress-Strain curve of 3D printed specimens after flexural testing	120
5.56	SEM analysis of 3D printed tensile specimen	121
5.57	SEM analysis of 3D printed Flexural specimen	122
5.58	EDS analysis of 3D printed tensile specimen a) shows wt.% of carbon particles b) shows wt.% of iron particles	122
5.59	EDS analysis of 3D printed flexural specimen a) shows wt.% of carbon particles b) shows wt.% of iron particles	123
5.60	Mean S/N ratio plots for PS of tensile and flexural specimen	124
5.61	Mean S/N ratio plots for %BE of tensile and flexural specimen	125
5.62	Stress-Strain curve of 3D printed specimens after tensile testing	129
5.63	Stress-Strain curve of 3D printed specimens after flexural testing	129
5.64	SEM analysis of 3D printed tensile specimen	130
5.65	SEM analysis of 3D printed flexural specimen	130
5.66	EDS analysis of 3D printed tensile specimen a) shows wt.% of carbon b) shows wt.% of iron particles	131
5.67	EDS analysis of 3D printed flexural specimen a) shows wt.% of carbon b) shows wt.% of iron particles	131
5.68	S/N ratio peak strength of the tensile and flexural specimen	132

5.69	S/N ratio %BE of tensile and flexural specimen	133
5.70	Stress- Strain curve of 3D printed specimens after tensile testing	136
5.71	Stress-Strain curve of 3D printed specimens after Flexural testing	137
5.72	SEM analysis of tensile specimen	138
5.73	SEM analysis of flexural specimen	138
5.74	EDS analysis of hybrid specimen a) shows wt.% of carbon b) shows wt.% of iron particles	139
5.75	Mean effect plot for PS of 3D printed flexural and tensile specimen	140
5.76	Mean effect plot for %BE of 3D printed flexural and tensile specimen	140
5.77	Different pre-processing parameters of FDM	146
5.78	2D drawing and 3D CAD model of a rectangular specimen	146
5.79	SEM image before and after CVS	149
5.80	Mean SN ratio plot of percentage change in a) surface roughness and b) shore Hardness after CVS	150
5.81	Mean SN ratio plot of percentage change in a) surface roughness and b) shore Hardness after CVS	151
5.82	Surface roughness profile shows improvement in a) surface roughness and b) shore hardness after CVs treatment	153
5.83	Surface roughness profile shows improvement in a) surface roughness and b) shore hardness after heat treatment	153

LIST OF TABLES

Table No.	Title	Page No.
1.1	Different plastic polymers with their applications	4-5
1.2	Different AM techniques along with advantages and disadvantages	9
2.1	Fabricated composite filaments with properties for 3D printing applications	21-22
2.2	Relevance score for selected terms (as per Scopus data base)	38-40
4.1	Control Log of experimentation	51
4.2	Specification of FTIR setup	54
4.3	Fixed parameters of FDM	56
4.4	Control log of experimentation applied on FDM	57
4.5	Control log of experimentation applied on smoothing station	59
4.6	Control log of experimentation applied on hot air oven	60
4.7	Specifications of the surface roughness tester	61
4.8	Final Parameters for Experimentations	64
4.9	ANOVA Table	68
5.1	MFR of 2° recycled ABS with and without reinforcements	69
5.2	Responses for 2°recycled ABS filament reinforced with BP (90:10)	70
5.3	Responses for 2°recycled ABS filament reinforced with WD (90:10)	71
5.4	Responses for 2°recycled ABS filament reinforced with Fe (90:10)	71
5.5	S/N ratios for PS and %BE	79
5.6	Results of ANOVA for PS of BP reinforced filament	81
5.7	Results of ANOVA for %BE of BP reinforced filament	82
5.8	Results of ANOVA for PS of WD reinforced filament	82
5.9	Results of ANOVA for %BE of WD reinforced filament	82
5.10	Results of ANOVA for PS of Fe reinforced filament	83
5.11	Results of ANOVA for %BE of Fe reinforced filament	83
5.12	Suggested parametric levels	89
5.13	MFR of 2° recycled ABS with and without reinforcements	90
5.14	Responses for 2°recycled ABS reinforced with 10% BP	91

5.15	Responses for 2 ⁰ recycled ABS reinforced with 10% WD	91
5.16	Responses for 2 ⁰ recycled ABS reinforced with 10% Fe	92
5.17	S/N ratios for peak strength and percentage break elongation	95
5.18	ANOVA analysis for PS of BP reinforced filament	98
5.19	ANOVA analysis for %BE of BP reinforced filament	98
5.20	ANOVA analysis for PS of WD reinforced filament	99
5.21	ANOVA analysis for %BE of WD reinforced filament	99
5.22	ANOVA analysis for PS of Fe reinforced filament	99
5.23	ANOVA analysis for %BE of Fe reinforced filament	99
5.24	Optimized levels for different responses	110
5.25	Different Mechanical properties obtained aster tensile testing	111
5.26	Calculated S/N values for PS	115
5.27	ANOVA analysis for PS of composite filaments	116
5.28	ANOVA analysis for %BE of composite filaments	116
5.29	Comparison of properties for composite filaments	118
5.30	Different observations obtained during tensile testing	119
5.31	Different observations obtained during flexural testing	119
5.32	S-N ratio analysis of peak strength and % break elongation for both tensile and flexural specimen	124
5.33	ANOVA analysis for PS of 3D printed Tensile specimen	125
5.34	ANOVA analysis for %BE of 3D printed Tensile specimen	126
5.35	ANOVA analysis for PS of 3D printed Flexural specimen	126
5.36	ANOVA analysis for %BE of 3D printed Tensile specimen	126
5.37	Multi response of 3D printed specimens	127
5.38	Obtained mechanical properties of 3D Printed tensile specimens	128
5.39	Obtained mechanical properties of 3D Printed flexural specimens	128
5.40	S-N ratio analysis of peak strength and % break elongation for both tensile and flexural specimen	132
5.41	ANOVA analysis of PS for the tensile specimen	133
5.42	ANOVA analysis of %BE for tensile specimen	134
5.43	ANOVA analysis of PS for Flexural specimen	134
5.44	ANOVA analysis of %BE for flexural specimen	134
5.45	Multi response analysis of 3D printed specimens	135

5.46	Obtained mechanical properties of 3D Printed tensile specimens	136
5.47	Obtained mechanical properties of 3D Printed flexural specimens	137
5.48	S-N ratio analysis of peak strength and % break elongation for both tensile and flexural specimen	139
5.49	ANOVA analysis for PS of tensile specimen	141
5.50	ANOVA analysis for %BE of tensile specimen	141
5.51	ANOVA analysis for PS of flexural specimen	141
5.52	ANOVA analysis for %BE of flexural specimen	142
5.53	Multi response analysis of 3D printed specimens	142
5.54	Comparison of properties for composite filaments	143
5.55	Percentage change in Shore Hardness and Surface Roughness after CVS	148
5.56	Percentage change in Shore Hardness and Surface Roughness after Heat treatment	148
5.57	S/N ratio after CVS and Heat treatment	150
5.58	ANOVA analysis of percentage change in Shore Hardness after CVS	151
5.59	ANOVA analysis of percentage change in surface roughness after CVS	152
5.60	ANOVA analysis of percentage change in shore Hardness after heat Treatment	152
5.61	ANOVA analysis of percentage change in Surface roughness after heat Treatment	152

LIST OF PUBLICATIONS FROM THE THESIS

Research Publications in International Journals

S.No	Title	Journal	Impact Factor/ SJR	Status
1	On recyclability of thermosetting polymer and wood dust as reinforcement in secondary recycled ABS for non-structural application	Journal of Thermoplastic Composite Materials (SCIE)	3.33	Published
2	On recyclability of thermoplastic ABS polymer as fused filament for FDM technique of additive manufacturing	World Journal of Engineering (Scopus)	0.2 (SJR)	Published
3	Investigation on flexural strength of multi- material ABS based composite specimen fabricated through FDM technique	Material Today: Proceedings (Scopus)	0.34 (SJR)	Published
4	On Comparative analysis of recycled ABS composite filaments prepared by different blending routes for 3D printing of smart tiles	Material Letters (SCIE)	3.423	Under Review
5	On Chemical assisted blending of secondary Recycled ABS with bakelite and wood dust: mechanical, rheological, morphological and thermal investigations	Advances in Material Processing and Technology (Scopus)	0.27	Under Review
6	Investigation on mechanical properties of secondary recycled ABS reinforced with Fe powder for 3D printing applications	Material Today: Proceedings (Scopus)	0.34	Published
7	Fused Deposition Modeling as Secondary recycling process for preparation of sustainable structures	Tayor and Francis (Scopus)	-	Published
8	Applications of thermoplastic polymer in 3D printing	Encyclopedia of Materials: Plastics and Polymers (Scopus)	-	Published
9	Chemical based blending of reinforced in ABS for 3D printing applications	Encyclopedia of Materials: Plastics and Polymers (Scopus)	-	Published
10	Mechanical and rheological investigation of bakelite reinforced ABS	Encyclopedia of Materials: Plastics and Polymers (Scopus)	-	Published

CHAPTER-1

INTRODUCTION

1.1 INTRODUCTION

Polymers have become an important part of our daily life after World War II as they are polymeric in nature therefore they offer properties the same as rubbers. They also have properties of elongation, good strength, shock resistance, resilience, etc same as metals and other materials. Polymers are generally composed of several molecules known as macromolecules [1]. The word polymer is a Greek word that comprises two words first is “poly” means ‘many’ and the second is “mer” which means “parts”. Polymer has two categories the first category of polymers is Natural Polymers also known as biopolymers such as wool, rubber, starch, silk etc. second category is Synthetic Polymer. Synthetic polymers are those which prepared by chemical reactions in labs or we can say which are prepared artificially. Examples of Synthetic polymers are PVC, ABS, Polystyrene, nylon, polyethylene, bakelite etc. [2]. Polymer generally comprises of long chain of Carbon and Hydrogen atoms as shown below in Figure 1.1.

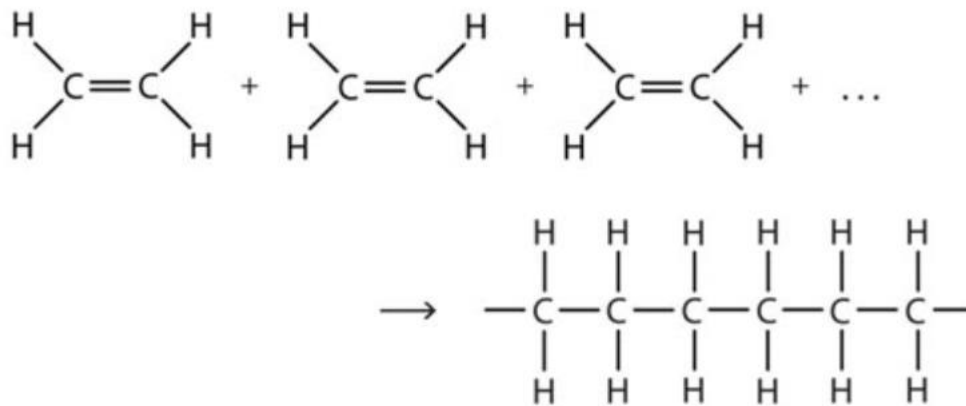


Figure 1.1 Polymer structure [3]

Polymers are growing faster as compared to engineering metals, materials, wood almost in every part of life due to their easy processability. Polymers can also be classified as elastic rubbery, opaque, strong, stiff etc. depending upon their applications [4-5]. Polymers have high degree of crystallinity known as crystalline polymers. The enormous applications of plastics in daily life make them an essential part of human life. Their unique features such as low density, low weight, high strength, low cost and easy processing make them

indispensable materials [6]. Due to these unique properties and features, polymers have numerous applications in the field of construction, transportation, industries, etc. But their repeated, long-chain and stable polymeric structure does not allow them to degrade easily in natural conditions and they remain in the same form for hundreds of years. Landfilling is commonly employed for polymeric waste (PW) in many countries. Decomposing polymer waster via landfill generates harmful gases which affect human health and leads to global warming [7]. The rapid increase of PW induces several critical socio-environmental complications such as reduction in geographic space due to landfills, terrestrial and marine pollution, adverse effect on biological life and freshwater resources, etc. [8-12]. These problems mainly arise due to low cost and unmatched applications of polymeric materials, especially in the packaging industry where they are generally used once or for a short service span. To generate virgin plastics, 4% of the world's oil production is consumed each year [13]. It has been reported that 10% of the PW comes from municipal waste which ultimately increases the demand for open space for landfilling [14]. In 2018, plastic production reached the value of 359 million tons globally increased approximately 20 times in the last 50 years [15]. The variation in consumption and production of plastic products which in turn depends upon demand and supply also influences the generation of PW. The analysis performed by Tata Strategic indicated a huge variation in consumption and production of plastic products in India as shown in Figure 1.2. The rapidly increasing plastic solid waste (PSW) becomes a serious issue throughout the world. In most countries, landfilling is commonly employed to handle the PSW. In 2018, plastic production reached the value of 359 million Tons globally increased approximately 20 times in the last 50 years and is expected to reach 1600 million tons by 2050 [16]. The Central Pollution Control Board (India) highlighted the plastic waste generation of 26,000 Tons per day (based on the 2019-2020 report) out of which 60% is recycled and the remaining 40% either polluting the groundwater resources or streams or landfilled. For managing the PSW, conserving the available resources, and protecting the environment, plastic recycling becomes the leading issue worldwide as approximately 3.8 barrels of crude oil were conserved by recycling one Ton of PSW ([www. sciencing.com](http://www.sciencing.com), accessed 08-11-2021).

The worldwide existing polymers are broadly classified into three categories: elastomers, thermoplastics (materials that can be recycled up to a certain extent), and thermosetting (that cannot be recycled) [17].

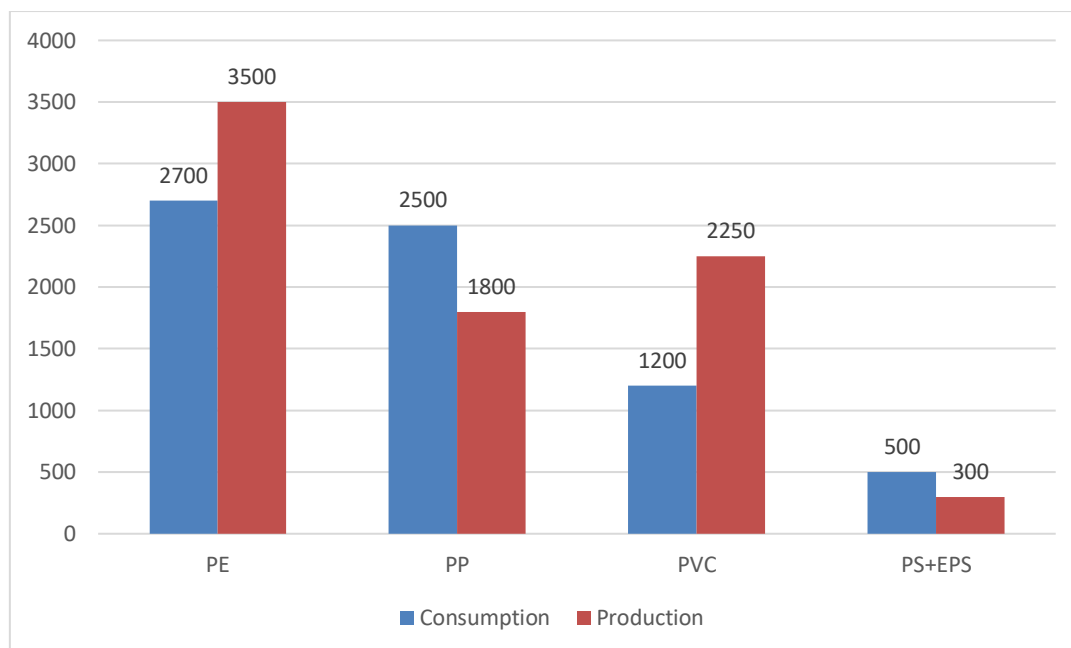


Figure 1.2 Production and consumption of polymer waste in tonnes [7]

Among all these materials, thermoplastics address the significant gathering and replacing a large portion of the materials in different applications ranging from packaging, automotive, medicine, construction, agriculture as well as in electronic industry [14]. Thermosetting are monomers used to fabricate polymeric frameworks with a high thickness of cross-connecting synthetic bonds by a restoring cycle. Among thermosetting and thermoplastic polymers nowadays thermoplastic polymers are widely used and they occupied 80% share of the market volume. The main reason behind accommodating 80% market share is their fabrication and processing techniques. The most commercially utilized thermoplastics and thermosetting along with their certain applications were represented in Table 1.1. Polyolefins being one of the elastomers are highly popular due to their low density, cheap production and relatively low cost for multiple applications [17]. Irrespective of a large number of available polymers, the PW found on earth mainly consists of five thermoplastics namely polystyrene, low and high-density polyethylene (available in packaging material form), polypropylene, polyethylene terephthalate [18]. The demand for new material with required properties by blending thermoplastic polymers with other materials and elastomers leads to the development of new polymer material. Thus, it leads to the development of PW therefore for managing the PW and protecting the environment, plastic recycling becomes the leading issue worldwide.

Table 1.1 Different plastic polymers with their applications [19-20]

Thermosetting	Applications
Polyurethane (PU)	Medical devices, footwear, automobile components, Freezers and refrigerators, bedding, and furniture
Bakelite	The insulating material in various equipment and household utensils, electrical systems
Epoxy	Adhesive and coating substance, potting
Polyester	Staple fiber, bottles of beer and juices, adhesives
Vinyl ester	Laminating process, vessels, and tanks, marine industry
Phenol formaldehyde	Adhesive and coating substance, fiberglass cloths, circuit boards, billiard balls
Silicon	Electrical and thermal insulations, adhesive, kitchen and medical utensils
Melamine	Kitchen utensils, dinnerware, laminating flooring
Thermoplastics	Applications
Poly Carbonate (PC)	Electronic and Telecommunications appliances
Polypropylene (PP)	Clear bags, food packaging, mats, and carpet
Polyamides (PA)	Toothbrushes, textile industry, cams, gears, ropes
Polyethylene terephthalate (PET)	Wires, beverage bottles, food packaging, staple fiber
High-density polyethylene (HDPE)	Automotive parts, tubes, buckets, cable and wire insulations, pipes
Low-density polyethylene (LDPE)	Screen cards, plastic bags, food containers, trays, general packaging films
Polystyrene (PS)	Thermal insulations, food packaging, toys, electronic appliances, dinnerware, CD cases
Polyvinyl chloride (PVC)	Serum and blood bags in the medical field, automobile parts, fittings and tubes, medicine and food packaging
Polylactic acid (PLA)	Disposable garments, hygiene products, bags, cups,

	medical implants
Acrylonitrile butadiene styrene (ABS)	Automotive components, electronic components, musical instruments, drain pipes

1.2 RECYCLING TECHNIQUES

With an aim to reduce the generation of PW and its harmful impact on the socio-environment, a strategy based on 3R (reduce, reuse and recycle) has been adopted by the developed and various developing countries. As per the 3R approach for PW management, any product irrespective of its materials should follow these guidelines during the entire life cycle: (i) non-generation of waste, (ii) reduction of waste, (iii) re-use, (iv) recycling, (v) landfilling (treated as last option). Recycling involves a process in which waste material is re-utilized for fabricating any product or can be re-used in any useful application by enhancing or transforming its properties and other characteristics. As per the literature survey, polymer recycling is broadly classified into the following four categories [21-24].

1.2.1 Primary (1^o) recycling: This type of recycling involves sorting plastic waste from high purity or semi-clean PW. It is generally preferred by industries to reduce their own PW by separating the easily identifiable clean scrap from the contaminated parts. Sometimes, the clean scrap is added into collected waste to improve their properties as well as performance. More often the PW collected from household applications is treated by 1^o recycling. This type of recycling is particularly helpful in reducing the emission of toxic gases such as sulphur dioxide, nitrogen oxides and carbon dioxide [25]. Since municipal solid waste contains highly contaminated PW, so it restricts the applicability of this particular recycling technique in such applications.

1.2.2 Secondary (2^o) recycling: This type of recycling is particularly accomplished by mechanical means and hence it is also called mechanical recycling. It is the widely accepted technique for recycling of large-scale PW in the world due to following reasons [26]:

- lower infrastructure cost for sorting and treating the PW as compared to other recycling techniques.
- low operational cost due to already established and existing standards along with equipment for processing the PW.

The presence of multiple polymers along with impurities in the PW hampers their re-usability and thus, sorting and separation steps become essential before their processing [25]. The existence of different polymers in the PW causes phase partition and results in the development of compatibility issues, thus adversely affecting the mechanical performance of the newly fabricated component. Moreover, it offers significant challenges during the processing of PW. Impurities (like inks and particulates) limit the creation of superior grade and homogeneous final recyclates [27-28]. So, it becomes necessary to develop highly advanced techniques to separate the postconsumer polymers from different existed materials as far as possible. Apart from this, the thermomechanical degradation that occurred during the processing of PW imparts major challenges. The recycling of PW is restricted by the frequency of cycles that the material can withstand without affecting its performance/properties beyond a specified level [29].

2° recycling involves the following steps during the processing of PW:

- Separation of PW: The first step involves sorting and separating different materials from the collected PW. Different polymers are segregated based on their chemical composition, color, density or any other specific property.
- Form transformation: The next step after separation is to transform the collected PW in the form of small flakes, powder or granules through rotary mills.
- Wash: Chemical washing needs to be performed for removing glue, organic and inorganic compounds from the polymer. Mostly, caustic soda and surfactants are commonly used for cleaning and washing purpose.
- Drying: It is an important step for reducing the degradation of polymer during mechanical recycling. For example, polymers (polyesters or polyamides) are susceptible to hydrolysis as they are obtained by polycondensation.
- Agglutination: Next step is to reduce the volume of the binder to ensure its homogenization after washing and drying. This encourages the last cycle that is completed in an extruder.
- Reprocessing: The last step is the transformation of polymer in the form of polymer grains. After this, the grains are packed and send to industries for manufacturing of new parts.

1.2.3 Tertiary (3°) recycling: In this type of recycling, monomers of different polymeric materials are recovered from the PW through the depolymerization process [13]. In other

words, through this recycling, the basic raw materials required to form various plastics are generated and hence it contributes largely towards energy sustainability as polymers are petroleum-based products [30-31]. This type of recycling is also called chemical recycling. Depolymerization of PW can be performed either chemically (solvolysis) or through thermal (thermolysis) means. Further, the process can be executed in the absence of air (pyrolysis) or under controlled conditions (gasification).

1.2.4 Quaternary (4^o) recycling: This type of recycling is particularly performed on the PW that cannot be recycled such as waste generated from medical applications and packing of hazardous products and is mostly suitable for thermosetting polymers [32]. After over and over reusing, polymer begins to lose its properties and ultimately leads to landfilling that contaminates the earth's surface as well as generates toxic gases. With the advancements of new incinerators, numerous analysts proposed that by incineration (burning) energy can be recuperated from PW which leads to a reduction in waste; thus, 4^o recycling is also called energy recovery technique. Thermal and electrical energy is generated from the energy (chemical) present in the bonds of the long-chain structure of PW. During incineration, plastics generally produce gases like CO₂, SO_x, NO_x as they are derived from crude oils [33-34]. Certain techniques can be used to control the harmful pollutant particles like (i) filtration, (ii) addition of ammonia in the combustion chamber, (iii) flue gas cooling, (iv) acid neutralization, (v) flue gas cooling [29,35]. The above-discussed recycling techniques are summarized in Figure 1.3.

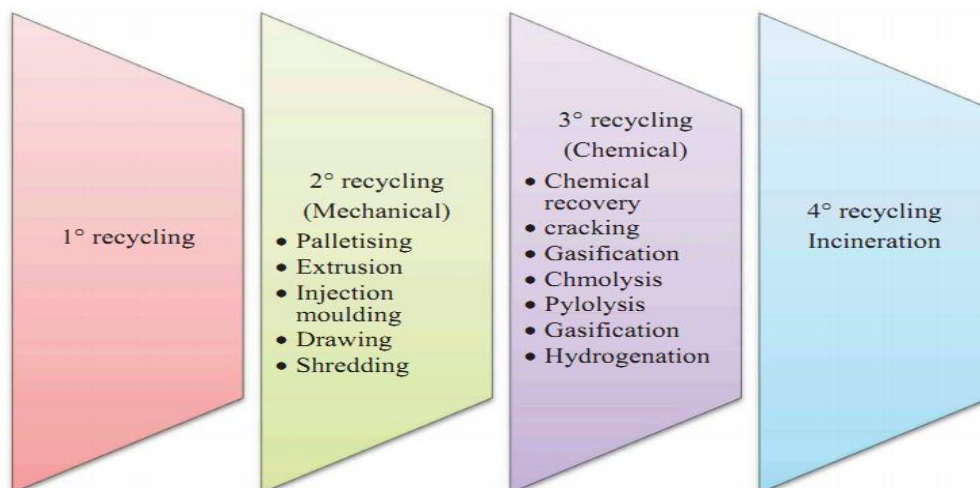


Figure 1.3 Different recycling techniques used in recycling polymer waste

1.3 RECYCLED POLYMERS WITH REINFORCED MATERIALS

Competition among the manufacturing industries forces them to reduce the cost of their products. The usage of recycled material is quite helpful in achieving this goal and at the same time, it reduces industrial and municipal waste also. Chemical recycling (pyrolysis) of PW results in various environmental hazards and landfilling generates green-house effect gases. So, mechanical/2^o recycling comes out as the only solution to manage/reduce the continuously increasing PW. The new advanced technologies to process the PW with cost-effective solutions need to be developed urgently. Additive manufacturing (AM) has the potential to meet the rapid demand of customized products in which parts are fabricated by depositing a layer on a layer under control path without any need of expensive tools, also initial cost in operating AM is very less as compared to conventional machining process [36-37]. In AM, computer-aided design is developed and converted into STL files to create three-dimensional (3D) desired shaped parts with the help of AM equipment. There are different AM techniques categorized based on different raw materials used to make 3D components are illustrated below. Selective Laser Sintering (SLS) utilizes powder bed fusion technology, it starts with the melting of powder below its melting temperature. The polymer material in the form of powder has been sintered with the help of a CO₂ laser beam and solidifies to form the desired shape. This technique is suitable only for small production parts as it requires advanced material handling techniques therefore lead time is more. A second technique is Stereolithography (SLA) which cured the polymer resin with the help of a laser beam. But it only uses brittle polymers instead of ductile polymers, also materials prepared by this technique have poor impact strength, poor mechanical property, and low service life. Because of poor mechanical properties they generally get degraded in the presence of sunlight therefore they are suitable for functional applications. A third technique is Fused deposition modeling (FDM) as shown in Figure 1.4, which utilizes thermoplastic and thermosetting polymers in the form of fused filament for making parts [38]. Different AM techniques are illustrated below as shown in Table 1.2.

Table 1.2 Different AM techniques along with advantages and disadvantages

Technique	Polymer material	Starting material	Principle	Advantage and Disadvantage	References
SLA	Photocurable resin (epoxy or acrylate-based resin)	Liquid photopolymer	Laser scanning and UV-induced curing	High printing resolution, Material limitation, cytotoxicity, and high cost	[39]
SLS	PCL and polyamide powder	Powder	Laser scanning and heat-induced sintering	Good strength, easy removal of support powder, High cost and powdery surface	[40]
3DP	Any materials can be supplied as powder and binder needed	Powder	Drop-on-demand binder printing	Easy removal of support powder Clogging of binder jet and binder contamination	[41]
FDM	Thermoplastics, such as PC, ABS, PLA and nylon	Filament	Extrusion and deposition	Good strength and multi-material capability Anisotropy and nozzle clogging	[42]

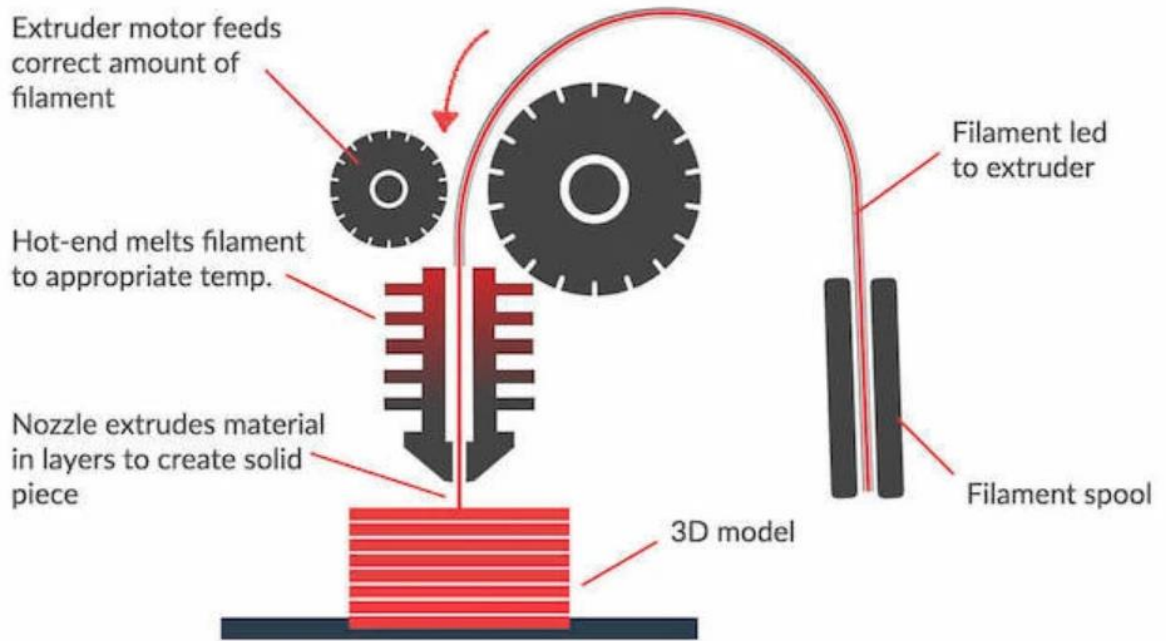


Figure 1.4 Schematic diagram of FDM [45]

Additive manufacturing (AM) being one of the relatively new technology, becomes quite popular in a very short time due to its capability to fabricate complex features and it is expected to rise with 23% market growth by 2021 compared to 2016 [43]. AM techniques such as fused deposition modeling (FDM) and 3D printing have the capability to utilize filament prepared from waste materials and thus offer a potential solution to reduce the PW generated from different applications [44]. Researchers proposed to utilize recycled thermoplastics in an open-source 3D printer/FDM set up by preparing the filament through plastic extruders [45]. FDM process is being given continuous attention to utilize recycled plastic materials with the use of proper reinforcements for cement-based building materials [46-48].

The most commonly employed thermoplastic filaments in FDM/3D printing are PLA, PC, ABS, LDPE, HDPE, PET, PS, polyetheretherketone (PEEK) and these filaments are generally prepared from polymer powder or granules through an extrusion process. Currently, ABS, LDPE, HDPE, PP, PET, PS and PC are being recycled globally for the fabrication of 3D printing filaments. But these recycled polymers cannot be utilized directly due to their poor mechanical and physicochemical properties [49]. These properties have a critical impact on the quality of the printed product. Also, multiple recycling of polymers causes degradation in properties (such as break strength, viscosity, molecular weight, etc) due to high

temperature and shear stresses that occurred during the extrusion process and ultimately affect the quality of the extruded products.

Most of the commercially available 3D printers utilize ABS and PLA as filament. Although ABS is toxic it exhibits enormous applications (particularly in the electronic and automobile industry) due to its high corrosion resistance and impacts strength. On the other hand, PLA is a bio-compatible and biodegradable polymer but highly sensitive to elevated temperature [50]. Researchers reported 30% and 60% degradation in PLA after recycling 3 and 7 times respectively [51]. Some of the researchers studied the effect of multiple recycling of PLA polymer and reported that the polymer chain length reduces as the injection cycles increases which ultimately increases the melt flow rate (rheological property) and decreases the various mechanical properties (break tensile strength and break tensile strain) [24]. It is well-established fact that multiple recycling of PLA has an adverse effect on mechanical properties and viscosity of polymer which prohibits its further utilization for 3D printing applications [52]. As the mechanical strength of PLA reduces significantly with the recycling cycles, it was proposed to apply polydopamine (PDA) coating on the recycled polymer filaments [53]. Some researchers suggested adding virgin PLA to the shredded and recycled PLA filament to improve the thermal and mechanical properties along with the viscosity of the blend [54].

A lot of researchers reinforced materials like carbon nanotubes, nano-particles, metallic powders, fibers (glass, jute, sisal, coconut, carbon), wood, bamboo, etc in mechanically recycled (1^o and 2^o) thermoplastics and thermosetting with an aim to enhance certain properties [55-61] reported that the addition of nano metallic powders (Fe-Si-Al or Fe-Si-Cr) in recycled HDPE and PP filaments improves Young's modulus and yield strength significantly. Further, the authors identified that the probability of cracks formation in the base matrix reduces with the introduction of metallic powders. In another study, the introduction of SiC/Al₂O₃ in recycled HDPE with paraffin wax as a binder dramatically increases the mechanical strength of filaments [36]. Some authors reported improved dimensional stability and mechanical properties when wood fibers were reinforced in plastics [55,62]. The bonding between the base matrix and the reinforced material plays an important role to achieve the desired properties. To improve the bonding between the base matrix and the reinforced material, certain bonding agents such as silanes, organo-titanes, maleated polypropylene, etc were employed by different researchers [63].

Taking into account the importance and recent advances in the field of recycling, countless surveys have just examined the problem and solution of polymer waste. But very less work has been done on 2^o recycled thermoplastic polymers for preparations of sustainable structures [21, 26, 63-67]. Also, the mechanical behavior of 3D printed structures with multiple materials (multi-layer printing) has not been extensively explored. Also, very little work has been done on the implementation of post-processing techniques for the improvement of surface roughness and shore hardness on multi-layered 3D printed specimens. So, in this research work, an effort has been performed to print multi-layered specimens fabricated through 2^o recycled ABS thermoplastic with the reinforcement of BP, Fe and WD. The particular reinforced materials were selected keeping in mind that BP powder can improve thermal properties (heat carrying capacity) of ABS, WD can impart insulating properties whereas Fe powder for magnetic properties. The structure/tiles printed by these multi-layered composite filaments can be utilized in cold regions for keeping the heat inside the confined space.

1.4 ORGANIZATION OF THE THESIS

Present research work is divided into the following six-chapter:

Chapter 1 highlights the brief discussion on the applications, limitations of the Fused Deposition Modeling (FDM). It also highlights the different types of polymers along with their applications, various work done by the researchers in the field of Additive manufacturing. The aim of the present research work and a brief introduction of the thesis has been explained.

Chapter 2 includes the work done by various researchers in the field of FDM. The complete literature survey has been divided into three parts first part reviewed the work done by the various researchers related to the Feedstock filament preparation, in the second part literature review was done related to various parameters applied to the FDM for printing tensile and flexural specimens. In the third part, various techniques were used by the researchers for improving surface finish and shore hardness.

Chapter 3 depicts the problem formulation, need of the research based on a literature survey. This chapter deals with various objectives used in the present work.

Chapter 4 summarizes the detailed methodology used in doing the experiments for the present study. Different techniques, testing methods and equipment used in the present study have been discussed.

Chapter 5 summarize the result and discussion based on the experiments. This chapter also highlights the significant factors responsible for the good properties based on Taguchi experimentation and ANOVA analysis. This chapter also highlights the different post-processing techniques used for the improvement of surface finish and shore hardness.

Chapter 6 highlights the conclusions drawn from the research work and scope for the future research work. In last references has been shown.

CHAPTER-2

LITERATURE REVIEW

A detailed literature review has been done and presented in the chapter which would help in finding out research objectives. The literature review includes literature related to the FDM process, the role of FDM in printing tensile and flexural specimens, it also includes various post-processing techniques applied on FDM printed specimens for improving their surface properties.

2.1 LITERATURE RELATED TO FUSED FILAMENT PREPARATION

Fabrication of Fused filament is one of the primary steps in 3D printing which includes various parameters such as type of the polymer, reinforcement type and other parameters used while making filament with the help of a Twin Screw Extruder. Various researchers have done work in the field of fabricating Fused Filament with the help of TSE [68-69].

Ryder et al. developed a new methodology to prepare feedstock filament by the chemical blending of ABS with Stainless steel (SS420) by varying weight proportion of SS420 with 10, 15 and 23% wt. for investigating different mechanical properties (Tensile, thermal behavior and SEM) of prepared composite. The author found that filaments prepared at 15% wt. SS420 and ABS have superior mechanical properties as compared to filaments prepared without reinforcement. On further increase in wt.% of SS 420 in the base material, there was a drastic reduction in mechanical properties has been found [70].

Sezer et al. compared mechanical and electrical properties of multi-wall carbon nanotubes (MWCNT) reinforced with ABS matrix composite by varying 0-10%. The authors reported that with 7% addition of MWCNT by weight in ABS, the tensile strength of the 3D printed part increased by 288% as well as Melt flow Rate (MFR) was improved compared to ABS without reinforcement. When ABS was reinforced with 10%wt. MWCNT a drastic reduction in MFR was observed it could be due to nozzle clogging, at the same time the improved tensile strength was also observed [71].

Mojarrad et al. studied the rheological properties of ABS and PA6 blended with nanoclay and reported that with the addition of nanoclay in the base matrix, there was a

significant improvement in storage modulus. Also, the rheological and morphological analysis showed good bonding between reinforced and base material [72].

Billah et al. prepared different filaments by reinforcing ABS with 20%wt. glass fiber and short glass carbon fiber for studying mechanical stiffness and thermal behavior with the help of Differential scanning calorimetry. They have prepared different filaments at constant barrel temperature (200°C) and extrusion speed (50rpm) and the found that mechanical stiffness of ABS reinforced with short carbon fiber was improved by 272% where was for ABS reinforced with Glass fiber was improved by 84% as compared ABS filament without any reinforcement. Also, there was a significant improvement in the thermal stiffness of the ABS reinforced with short carbon fiber as compared to ABS reinforced with Glass fiber and neat ABS [73].

Leon et al. prepared novel material for enhancing adhesive properties of additive manufacturing by blending thermoplastic polymer ABS with another thermoplastic polymer polyurethane (TPU). Initially, they prepared filament with the help of a single screw extruder at a screw speed of 60rpm, extruder temperature 230°C by varying weight proportion of TPU from 10-30%wt. in ABS. They prepared different filaments for studying different mechanical properties of a printed tensile specimen. From FTIR analysis it has been found that with an increase in wt.% of TPU in ABS there was good adhesion have been seen between the layers along with this an improved yield strength was found at 30wt.% TPU [74].

Kumar et al. studied the rheological, morphological and thermal properties of secondary recycled ABS. They prepared different ABS filaments with the help of TSE (Twin Screw extruder) at different parameters such as load (10kg, 11.5kg,13kg), temperature (190°C, 200°C, 210°C) and torque (0.3, 0.4,0.5Nm). They found that better mechanical and thermal properties were observed at 210°C, 13kg load and 0.3Nm. Modulus of toughness was improved up to 3.216Mpa. from 0.191 MPa (for non-TSE processed) and 0.081 for virgin ABS [75].

Kumar et al. studied the 4D capabilities of 3D printed chemically assisted ABS-Gr composite. They prepared ABS-Gr composite by varying weight proportion of Gr (10%, 15% and 20%) in ABS for preparing feedstock filament with the help of a Twin Screw Extruder. For verifying the 4D capabilities of ABS-Gr composite they have evaluated magnetic properties with the help of a vibration scanning magnetometry (VSM) test. With the help of Fourier transform infrared spectroscopy (FTIR) they found that at 20% wt. the proportion of

Gr in ABS there was good bonding between the adjacent layers and also they shows maximum magnetization, therefore, it can be used for self-assembly applications [76].

Tambrallimathy et al. investigated the properties of two different polymers through the addition of filler materials to achieve different mechanical properties. Poly Carbonate and ABS were blended with the addition of Graphene (Gr) as filler material in a ratio of (0.2-0.8%) by weight to prepare feedstock filament for FDM. The researchers have observed that with the addition of graphene, there was a significant improvement in young's modulus, thermal behavior, and glass transition temperature because of good dispersion and interfacial bonding between composite. They also observed that the addition of Gr 0.8% by wt. glass transition temperature was increased by 7.6% and thermal degradation by 3.8% [77].

Weng et al. studied the thermal and mechanical properties of fused filament prepared by reinforcing Acrylonitrile butadiene styrene (ABS) nanocomposites with organic modified montmorillonite (OMMT). They prepared fused filament with the help of a Single Screw Extruder and further processed it on the 3D printer for printing 3D samples to determine tensile, flexural and thermal properties. They found that with the addition of 5wt%. OMMT the tensile strength of the 3D printed sample was improved by 43% and also there was significant improvement seen in the flexural modulus [78].

Torrado et al. studied the impact of 5% by weight of strontium titanate (SrTiO_3) as fired fillers on ABS polymer. The blending of SrTiO_3 and ABS was executed with the help of TSE. Tensile strength of ABS and ABS/ SrTiO_3 were obtained as 33.96 and 1.74 MPa and 21.60 and 0.63 MPa respectively. Poor mechanical properties of ABS/ SrTiO_3 composite were due to the presence of small voids and their brittle nature. Besides SrTiO_3 , the authors also used Al_2O_3 as reinforced material in the ABS matrix. Similar to the results of ABS/ SrTiO_3 composite, the tensile strength of ABS/ Al_2O_3 composite (28.8 MPa) was lesser than virgin ABS (33.96 MPa) [79].

Schmitz et al. studied the effect of material composition along with the electrical conductivity effect on prepared composite. They prepared three compositions for filaments in the following proportion ABS with 5 wt% of CB, ABS with 5 wt% of CNT, and a hybrid composite with 5 wt% total of additive but a (75:25) fraction of CNT: CB. They also prepared specimens in three directions horizontal at $\pm 45^\circ$ raster angle, horizontal concentric, perpendicular concentric for evaluating the effect of reinforcement percentage on electrical

conductivity. It was observed that the electrical conductivity of the printed samples was highly influenced by the CNT presence in the composition, and increased with its incorporation. The electrical conductivity values for ABS with 5 wt% of CB were in the range of 10^{-12} S. cm^{-1} , while for hybrid composite and ABS with 5 wt% of CNT values between 10^{-8} and 10^{-5} S. cm^{-1} were observed [80].

Kariz et al. studied the effect of wood content in PLA used for 3D printing. The author prepared six filaments by varying the loading level of wood from 0 to 50% by weight and observed that the density of 3D filament decreases with an increase in wood content. Also, the tensile strength of 57 MPa was observed for filament with 10% wood addition but it decreases up to 30 MPa with 50% wood content. Further, with an increase in wood percentage, the surface becomes rough due to more void formation [81].

Kumar et al. studied the mechanical properties of four different filaments, namely PLA with WD, PLA with polyvinyl chloride, PLA with Fe_3O_4 , and virgin PLA, for multi-material 3D printing. The authors observed significant improvement in mechanical properties with the addition of Fe_3O_4 as compared with other reinforcements. Also, with the reinforcement of polyvinyl chloride, peak elongation, and break elongation (BE) decrease. Further, with the addition of reinforcements, the melt flow rate (MFR) of composite increases except in the case of WD due to clogging of the nozzle [82].

Yang et al. studied the effect of Carbon Nanotube (CNT) content on the melt flow rate (MFR), mechanical properties of PLA/CNT composite. CNT reinforcement was varied between 0 to 8% by weight in PLA and it has been observed that CNT percentage of 6% showed improved tensile strength by 64.12%. But there was a significant reduction in the MFR value of PLA/CNT blend as MFR of virgin PLA was 29.38g/10min, but MFR with 8% of CNT was 6.91g/10min. It was primarily due to the nucleation effect between PLA and CNT, which enhances the intermolecular forces and results in decreasing the MFR [83].

Singh et al. prepared feedstock with the help of biodegradable food waster i.e almond skin powder reinforced with polylactic acid for biomedical implants having good mechanical performance. They prepared feedstock filament with the help of a Twin Screw Extruder by reinforcing almond skin powder varies from 0-5wt.% in PLA, from melt flow index analysis it was observed that maximum melt flow rate was observed at 2.5wt.% reinforcement as

compared to 5wt.% reinforcement. Similar behavior was observed while analyzing the thermal behavior and mechanical properties of the feedstock filament [84].

Stoof et al. performed the experimentation for analyzing the mechanical properties of reinforced hemp and harakeke in 0 to 30% by weight in PLA. The feedstock filament of 3mm diameter was prepared to utilize for 3D printing. It has been observed that the highest value of tensile strength (38MPa) was found in the composite of PLA + hemp (10% by weight) and the second-highest tensile strength (37MPa) was found in the composite of PLA + harakeke (20% by weight). And the maximum value of Young's modulus i.e. more than 4GPa was found only in the case of harakeke reinforced composite 20,30% by weight in PLA [85].

Montava et al. examined the effect of linseed oil (LO) for enhancing the adhesion between the PCL and walnut shell flour (WSF) reinforcement with PLA. They found that without reinforcement of linseed oil in PLA matrix there was a significant reduction in mechanical strength and thermal stability. It has been noted that 48wt.% PLA+ 12wt.% PCL+ 40wt.% WSF+ LO has maximum tensile strength i.e 10.4 MPa and tensile modulus is 714 MPa whereas impact strength is 9.4MPa as compared to 48wt.% PLA+ 12wt.% PCL + 40 wt.% WSF. Also with morphological analysis, it has been found that there was a significant improvement in mechanical properties with the use of linseed oil for reinforcements [86].

Singh et al. Singh et al. have developed feedstock filaments for industrial application with reinforcement of Fe powder at different wt.% (i.e. 6% and 10%by weight) in HDPE and LDPE. They have found that HDPE reinforced with 10%wt. of Fe shows maximum peak strength compared to LDPE filaments [87].

Kumar et al. have reported an improvement in mechanical properties of recycled HDPE and LDPE with reinforcement of Fe powder from 0 to 25% by weight used for FDM filament. The authors investigated that Fe powder reinforcement increases the maximum HDPE hardness by 36.66% whereas LDPE hardness improved by 64%. Despite this, with the addition of Fe powder MFR of LDPE and HDPE increased as Fe has good heat-retaining capacity due to which polymer viscosity gets reduced. They also revealed from SEM images that the surface roughness of HDPE is less as compared to LDPE, so it gives better results in terms of mechanical properties [88].

Liu et al. investigated the mechanical, thermal, water absorption and morphological properties of HDPE and Nylon6 reinforced with banana jute fiber and reported that thermal

properties and water absorption capacity of the Nylon6 composite were far better as compared to HDPE composite due to fractionated crystallization structure [89].

Masood et al. developed a new composite material by mixing Fe powder with P301 polyamide (Nylon) to make feedstock filament for FDM. The authors used two different particle sizes (coarse and fine) of Fe and reported that with an increase of filler material, the thermal conductivity of material composite increases along with MFR, Fe is a good heat retainer and they have found that thermal conductivity directly depends upon particle size therefore fine particle size shows more thermal conductivity as compared to coarse particle [90].

Singh et al. prepared PA6-TiO₂ (70%–30%by weight) composite filament for obtaining optimum working condition of twin-screw extruder (TSE) by varying three parameters namely extrusion load (10 kg, 15 kg, 20 kg), speed (50, 60, 70 rpm) and temperature (240°C, 250°C, 260°C). Better mechanical properties were observed at 250°C, 50 rpm, and 10 kg load [91].

Mergen et al. prepared a composite of polymethyl methacrylate reinforced with multi-walled carbon nanotube (MWCNT) for studying the effect of percentage variation of reinforcement (MWCNT) on electrical and mechanical properties. It has been highlighted that the addition of 10% by weight of MWCNT improves the electrical conductivity and tensile strength without any significant improvement in toughness [92].

Chen et al. studied the effect of organoclay on the electrical conductivity of the PC/PVDF/CNT blend. The authors varied organoclay from 0.05% to 0.25% by weight and CNT from 0.1% to 0.5% in PC/PVDF composite. From scanning electron microscopy, it has been observed that organoclay and CNT morphology in the PC/PVDF blend has been changed from a typical sea-island structure to a quasi-continuous structure. Also, with the addition of organoclay improved electrical resistivity has been observed [93].

Novais et al. used Glass fiber waste (GFW) generated from wind turbine blades as a reinforcement agent in geopolymer to determine the effect of fiber length and fiber content percentage on compressive and tensile strength of geopolymer. The authors selected two parameters first glass fiber content (0-2%) by weight and second is fiber length (6 mm, 20 mm) to determine the effect of reinforcement percentage on prepared composite strength. They found that with the addition of GFW in base material both compressive and tensile

strength has been increased by 162% and 77%. They also reported that glass fiber content plays important role in improving different mechanical properties such as peak strength, break strength as compared to fiber length [94].

Sodefian et al. investigated different mechanical, rheological and morphological properties of polypropylene (PP)/glass fiber (GF) composite containing maleic anhydride polyolefin (POE-g- MA) at three different weight percentages (10,20,30 wt%). They also compared the properties of composites prepared by FDM and compression modeling (CM). They found that with the addition of GF the modulus and strength of the composite was increased but flexibility was decreased. Whereas the addition of POE-g-MA composite showed the opposite characteristic. While comparing the composite prepared by both methods it was observed that the CM method have better results as compared to the composite prepared by FDM [95].

Colorado et al. prepared two composite materials by mixing wollastonite powder and phosphoric acid with reinforcement of glass and carbon fibers respectively for studying the creep behavior and revealed that composite reinforced with carbon fibers shows better results as compared to glass fibers which could be due to a reduction in creep effect with the addition of carbon fibers [96].

Sharma et al. investigated 4D printing applications of polyvinylidene fluoride (PVDF) reinforced with Barium Titanate (BaTiO_3) and Graphene (Gr) with the help of D33 meter for investigating 4D properties. They also prepared different feedstock filaments with the help of a Twin Screw Extruder (TSE) for studying mechanical and rheological properties of prepared feedstock filament by varying different weight proportions of Graphene, BaTiO_3 . They found that the best mechanical and rheological properties were obtained for composition PVDF (78% wt.) + Gr (2 wt.) + BaTiO_3 (20% wt.) as compared with reinforcement of BaTiO_3 (0-25% wt) and for Gr (0-5% wt) [97].

The work performed by the various researchers for composite filament fabrication along with obtained mechanical properties has been summarized in Table 2.1.

Table 2.1 Fabricated composite filaments with properties for 3D printing applications

Base Matrix	Reinforced material with %	Tensile Modulus (GPa)	Tensile Strength (MPa)	Flexural Modulus (GPa)	Flexural Strength (MPa)	Reference
ABS	CF (10%)	1.67	32.78	-	-	[98]
ABS	CF (12%)	2.72	31.70	-	43.80	[99]
ABS	CF (7.5%)	2.5	41.5	-	-	[100]
	CF (15%)	2.25	35	-	-	
ABS	CF (10%)	7.7	52	-	-	[101]
	GF (18%)	-	58.6	-	-	
ABS	CF (20%)	8.4	66.8	-	-	[102]
ABS	CF (13%)	8.15	53	-	-	[103]
ABS	C (1.6%)	-	43	-	-	[104]
ABS	Fe (10%)	0.96	43.4	-	-	[105]
	Fe (40%)	0.95	36.2	-	-	
	Cu (30%)	0.91	26.5	-	-	
ABS	GF (20%)	5.7	54.3	-	-	[106]
	GF (40%)	10.8	51.2	-	-	
ABS	Jute fiber (5%)	1.54	25.9	-	-	[107]
PLA	Talc (2%)	1.47	57.9	-	-	[108]
	CF (5%)	1.10	31.7	-	-	
PLA	CF (15%)	7.54	53.4	-	-	[109]
PLA	CF (20%)	4.54	29.96	-	-	[110]
PET-G	CF (20%)	4.26	32.79	-	-	

PLA	CF	0.74	41.3	2.93	75.6	[111]
	Al	0.83	51.1	3.27	97.8	
	Ceramic	1.05	46.5	4.62	100.1	
PLA	Cu (10%)	0.93	42	-	-	[112]
	CF (27%)	-	-	30	355	
Nylon	C (6.6%)	19.5	185.2	-	-	[113]
	C (6.9%)	14	140	-	-	
	C (20.7%)	35.7	464.4	-	-	
Nylon	Aramid (2%)	-	51.45	-	98.16	[114]
Nylon	Kevlar (4.04%)	1.77	31	-	-	[115]
	Kevlar (8.08%)	6.92	60	-	-	
	Kevlar (10.1%)	9	84	-	-	
Nylon	AF (8%)	4.23	110	-	-	[116]
	AF (10%)	4.76	161	-	-	
	GF (8%)	3.29	156	-	-	
	GF (10%)	4.91	212	-	-	
PEI	CNT (4.7%)	3	125.3	-	-	[117]
PE	Cu (25%)	0.7	17.12	-	-	[118]
	Cu (50%)	0.79	18.25	-	-	
	Cu (75%)	1.2	19.41	-	-	
	Cardboard (50%)	0.12	2.05	-	-	

2.2 STUDIES ON FUSED DEPOSITION MODELING PROCESS

Fabrication of parts via FDM is one of the most important steps in any printing process. Preparation parts via conventional machining and Investment casting process is a very time consuming and costly process. The use of AM allows manufacturers to fabricate parts with minimum cost and least lead time [119]. Work done by various researchers in the field of FDM is summarized as below.

Azadi et al. studied the effect of print direction on the print quality of 3D printed parts and their mechanical properties. They prepared 3D printed specimens of ABS and PLA with an infill percentage of 50% of thickness layer 0.15mm. They printed fatigue specimens in both horizontal and vertical directions and found that PLA specimens printed in the horizontal direction have better fatigue strength than specimens prepared in the vertical direction [120].

Singh et al. prepared a pen drive case with the help of ABS thermoplastic polymer for industrial applications as per DIN 16901 standard and ISO standard UNI EN 20286-I standard with the help of an FDM machine for the dimensional and economic point of view. The prepared specimen at three different orientations between 0-90° with a layer thickness of 0.254mm in the x-y-z direction. Further, they calculated dimensional accuracy and shore Hardness of all 9 prepared specimens. It has been found that specimens prepared at 0° inclination in the horizontal direction have maximum shore hardness and better morphology as compared to other samples prepared at different orientations [121].

Liu et al. studied tensile and flexural properties of FDM printed PLA composites reinforced with different additives like WD, ceramics, copper, aluminum and carbon fiber at raster angle of 0°/90° and +45°/-45°. The authors have found that reinforcement of copper, aluminum and ceramics results in improved mechanical properties whereas poor mechanical properties were obtained when it was reinforced with WD and carbon fiber due to poor adhesion between filaments as compared to virgin PLA. They also observed that PLA composite samples fabricated at an orientation of +45°/-45° raster angles have the highest mechanical strength [122].

Maurya et al. highlighted the effect of selected FDM parameters (infill density, build orientation, layer thickness and infill pattern) on cylindricity, flatness and dimensional accuracy of three-dimensional printed connecting rod of PLA polymer. They have revealed

that optimum parameters for all the responses were different. Further, the researchers investigated the properties of RGD840 material by varying the selected process parameters of the polyjet process and concluded that glossy surface, flat orientation and 90° raster angle provide optimum results about the modulus of elasticity, true stress and tensile strength [123].

Anderson et al. compared the mechanical properties of virgin and recycled PLA under similar conditions. The authors prepared dumbbell-shaped specimens with the help of a 3D printer to determine different mechanical properties like tensile strength, shear, modulus of elasticity and hardness. They investigated that with the addition of almond skin powder by 2.5wt% in PLA matrix mechanical properties of filament have been improved by 40% [52].

Kumar et al. prepared 3D printed tensile specimens as per ASTM D 638 standards. They used three polymers one was ABS, the second was HIPS and the third was PLA for studying thermal, mechanical properties of multilayer 3D printed tensile specimens. They varied two printing parameters one was infill density i.e 50%, 60%, 100% and the second was printing speed i.e. 50, 60 and 70mm/sec. They have found that multilayer printed specimens gave maximum tensile and flexural strength as compared to specimens printed separately [124].

Schirmeister et al. studied different properties (young modulus, tensile strength) of 3D printed HDPE thermoplastic by fused deposition modeling by varying different parameters like diameter and temperature of nozzle, build plate temperature, extrusion rate. It has been found that the mechanical properties do not depend upon printing speed and nozzle diameter but surface quality depends upon nozzle diameter and printing speed. They have compared all these properties of HDPE thermoplastic prepared by injection molding and found that it exhibits similar properties but break elongation of a specimen prepared by 3D printing was more as compared to specimen prepared by injection molding [125].

Lohar et al. prepared a nanocomposite polymer for studying the mechanical properties of polypropylene and ABS reinforced with Carbon Black (CB) in different weight proportions for high load-bearing capacity. They varied proportion of CB from 0-10%wt. in the proportion of ABS/PP (80/20) and it has been found that impact strength and tensile strength of specimens have 2.5%wt. CB was more superior as compared to specimens prepared at different compositions [126].

Mu et al. prepared tensile specimens of ABS with the help of 3D printing by varying three orientations i.e. horizontal, vertical and perpendicular for studying the effect of vapor smoothing on the tensile specimen of all three orientations. For studying the effect of vapor smoothing they took two vapor smoothing chemicals acetone and ethyl acetate, they have taken 200ml of each and exposure time 10, 30 and 50sec. They have found that with an increase in exposure time tensile strength of specimens treated with acetone showed good results as compared to tensile specimens treated with ethyl acetate. While studying the effect of build orientation on surface roughness and tensile strength it was found that specimens prepared in the vertical direction have the least tensile strength as compared to specimens prepared in a perpendicular direction [127].

Singh et al. prepared a bio-compatible implant (hip joint) prepared with stainless steel 316L because of its superior mechanical properties and easy manufacturing ability. They have prepared a bio-compatible hip joint with the help of FDM at the different orientations of 0° and 90° and further post-treatment was done with the help of CVS to reduce the surface irregularities. They found that a better surface finish was observed at 90° build orientation with solid part density at three cycles [128].

Bharath et al. explored the effect of layer thickness, build direction, air gap, and build temperature and printing direction surface finish of the specimen manufactured by FDM 1650 using L18 orthogonal array and found that both layer thickness and part direction have a significant effect on the surface roughness. They found that 0.007 Layer thickness and 70° build orientation give superior results in terms of surface roughness. It was also highlighted that by using an optimum setting of FDM surface roughness of printed parts can be improved up to 60% [129].

Chakraborty et al. developed a new technique of depositing layer known as curved layer fused deposition modeling (CLFDM), in this technique layers are deposited along the curved path instead of the horizontal path. They have concluded that parts printed with this technique have more tensile strength, were also helpful in reducing staircase effect and also help in reducing build time and the number of layers [130].

Lay et al. compared physical and mechanical properties of ABS, nylon6 and PLA filaments prepared by FDM with physical and mechanical properties of filaments prepared in investment casting. For analyzing tensile properties of 3D printed tensile specimens it has been found that nylon 6 has the lowest young modulus as compared to ABS and PLA printed

tensile specimens. Also, it has been found that the crystallinity of FDM printed PLA and nylon 6 was more as compared to injection molding. It was also found that the water absorption capacity of FDP printed PLA, ABS and nylon specimens were 133%, 102% and 89% respectively as compared to samples prepared with injection casting [131].

Roy et al. studied the tribological behavior of 3D printed specimens of ABS and PLA thermoplastic polymer by varying different printing parameters such as infill density, layer thickness and orientation. For printing parts, they have varied two levels of infill density one is 45% and second is 80%, infill angle 45° and 90° after printing both PLA and ABS specimens tribological test was performed with the help of tribological tester TR-25, they have found that specimens printed in vertical orientation has more wear as compared to other specimens and also the wear of PLA was more as compared to ABS specimens [132].

Yap et al. investigated the effect of raster angle (0° and 90°) and orientation on the elastic properties of 3D printed PC-ABS polymers. The effects of raster angle and orientations on the elastic properties of the 3D-printed PC-ABS material were investigated with both mechanical testing (four-point bending test and impact test) and numerical finite element simulation. They found that raster and orientations have a significant influence on the mechanical properties of the FDM printed PC-ABS. Specimen printed in the X-orientation and 0° raster, gave a better modulus of elasticity and yield strength as compared to specimens printed at another raster angle and configuration [133].

Rashid et al. Studied the effect of chemical, physical and mechanical properties of nanocomposite prepared by reinforcing ABS with TiO₂ in different weight proportions 1%, 5% and 10% by wt. for printing specimens. They have used acetone for the chemical mixing of base material with reinforced material. They prepared specimens of tensile and flexural with the help of a 3D printer. When the mechanical properties of all prepared composites were measured. It has been found that specimens prepared with the addition of 5% and 10% give maximum breaking point as compared to the non-reinforced polymer. Also, it has been revealed that the effective size of TiO₂ plays important role in evaluating tensile and flexural strength as more is the particle size less will be the bonding between the base material and reinforced material and this directly result in decreasing strength of the composite [134].

Petroni et al. developed a new highly sensitive electrical conductive thermoplastic composite prepared by depositing graphite layer on ABS. They have prepared samples by reinforcing 45% by wt. of Graphene in ABS, also, they have prepared samples of PLA/CB

composite for printing highly conductive electrical sensors. They found that 3D printed electrodes using G/ABS have high peak current also they have good stability in terms of (relative standard deviations (RSDs) reproducibility as compared to PLA/CB [135].

Kaur et al. studied the effect of raster angle, infill density, air gap and raster angle on tribological behavior of 3D printed ABS specimens. They revealed that process parameters are the most significant factor responsible for influencing the tribological behavior of the specimen as compared to other factors such as working temperature, working conditions. With the addition of graphite, PTFE, Zirconia, CaCO₃, carbon fiber, etc. wear resistance can be improved up to 30% [136].

Boparai et al. studied the effect of thermal properties of 3D printed parts using Bakelite and ceramic reinforced acrylonitrile butadiene styrene (ABS). They compared thermal analysis of virgin ABS with reinforced ABS and found that the composites prepared with higher loading of reinforced particles showed maximum storage modulus and were also suitable as FDM feedstock filament. The reinforcement of filler materials in the ABS matrix has also resulted in enhanced viscoelastic properties as compared with virgin ABS material. [137].

Jayanth et al. have studied the conductive nature of the sensor prepared by reinforcing ABS with carbon Black for void measurement. They prepared ABS-CB filament for printing sheets of length 94mm with a layer thickness of 0.2mm with the help of a 3D printer with nozzle temperature of 230°C and bed temperature of 80°C. It was observed that there was a constant effect of layer thickness on the conductivity of the sensor [138].

Dul et al. prepared nano-composite for FDM filament by using ABS as base material with reinforcement of (2%,4%,8%) of graphene by weight. They used these prepared filaments for printing specimens with the help of FDM at various build orientations (horizontal, vertical and perpendicular). They have observed that with the addition of graphene in ABS matrix, elastic modulus and thermal stability of 3D printed parts increases along all the three build orientations [139].

Sahay et al. studied the effect of SiC on mechanical properties of 3D printed ABS composite. They varied the percentage of SiC between 0 and 4%wt in steps of 2%wt. The twin-screw extrusion technique was employed to develop ABS + SiC filament suitable for the FDM printing process. 3D printed pure ABS and ABS + SiC composites were subjected to a

tensile test as per ASTM standards. Results showed the SiC filled ABS composite provides a remarkable improvement in ultimate tensile strength as compared to pure ABS. Further, Ultimate tensile strength increases with an increase in SiC content. With SEM analysis they found that pure ABS shows microscopic ductile fracture whereas SiC-ABS reinforced filament has brittle fracture due to the presence of SiC particles in the composite [140].

Abdullah et al. studied the effect of raster angle and layer thickness on tensile and flexural specimen fabricated by ABS and PLA thermoplastic polymer. They prepared tensile and flexural specimens as per ASTM D638 standard and D790 standard, to determine the effect of raster angle and layer thickness on tensile and flexural property they used ANOVA analysis. They varied layer thickness in three intervals 0.2mm, 0.3mm and 0.4mm and raster angle 0°- 90° at an interval of 30° by using a rectilinear type infill pattern. It was observed that both variables affect flexural strength more as compared to tensile strength, also specimen printed with PLA has more strength as compared to ABS printed specimen [141].

Singh et al. prepared tensile, flexural and compressive components with the help of a 3D printer by reinforcing ABS with 10%wt. copper. They prepared feedstock filament with the help of a twin-screw extruder by keeping screw speed constant 85rpm, nozzle temperature 230°C For printing 3D specimen they varied three parameters of 3D printer one is printing temperature (i.e 230°, 240°, 250°), layer thickness (0.1mm, 0.15mm, 0.20mm) and pattern (i.e ZigZag, line or triangular), they found that specimen printed at 230°C, zig-zag pattern and 0.1mm layer thickness has maximum strength compared to other printing parameters [142].

Kumar et al. prepared two circular specimens of PA6 and ABS matrix with Fe powder reinforcement of (0-40%) by weight for structural applications (joining of sheets, pipeline assembly). These circular filaments were used on friction welding setup under best conditions of feed, rpm, etc. The authors investigated that with the addition of Fe powder, it was possible to join two dissimilar materials at a particular 40% of Fe reinforcement in the ABS and PA6 matrix. Better mechanical and metallurgical properties were obtained at high rpm and low feed rate [143].

Rodríguez et al. evaluated the fatigue behavior of PLA polymer reinforced with wood. They compared the mechanical properties of non-reinforced PLA polymer with PLA polymer reinforced with wood. They evaluated the effect of layer thickness, infill percentage and nozzle diameter on the printed specimen and found that fatigue property directly depends

upon these properties. It has been observed that the maximum stress found was 17.9Mpa in specimens reinforced with wood [144].

Yubo et al. determined the effect of different printing parameters like layer height (0.1 mm, 0.2 mm, 0.3mm), raster angle (0°, 45°, 90°), printer speed(20mm/sec, 30mm/sec, 40mm/sec) on the different mechanical properties (like elastic modulus, tensile strength, and elongation at break) of poly-lactic acid (PLA) based 3D printed dumbbell specimen as per ASTM D638 standards. They observed that enhanced tensile property was observed at layer thickness (0.3mm) and lowest printing speed (20mm/sec) at 45° raster angle poor strength was observed [145].

Kumar et al. investigated both flexural and pullout strength of the PLA hybrid composite (PLA: 50wt.%, PVC: 25wt.%, WD: 5 wt.% and magnetite (Fe₃O₄): 20 wt.%). In their study, they varied three input parameters i.e infill speed, infill density and raster angle for the 3D printing of specimens. They found that optimized parameters for getting maximum strength are infill density: 100%, infill angle of 45°, and infill speed of 90mm/s Maximum flexural strength and pullout strength observed in the experimentation were 14.14 MPa and 45.74MPa respectively [146].

Gavali et al. revealed that raster angle is an important parameter in 3D printing of carbon fiber reinforced in thermoplastics (such as PLA, ABS, polyethylene, nylon) as it affects the mechanical properties of the specimen. It has been found that specimen printed at 0° and 90° raster angle shows superior tensile and young modulus as compared to specimen printed at 45° raster angle. They found that with the reinforcement of carbon fiber up to 15% by weight, the brittleness of thermoplastic composites increases but the toughness of thermoplastic composites decreases [147].

Kwok et al. explored the possibility of utilizing conductive thermoplastic composites in FDM printing. An electrically conductive filament was fabricated through the mixing of PP, homo polypropylene, and carbon black (CB) in a single screw extruder. Results demonstrated that with a 30% weight percentage of CB, the electrical resistivity of 10–2 ohms was accomplished, making it reasonable for printing 2D or 3D printed circuits and sensors. The potential application of the electrically conductive thermoplastic composites is for electromagnetic shielding, sensors, 2D and 3D circuit printing [148].

Torrado et al. have prepared two polymer blends of ABS/styrene ethylene butadiene styrene (SEBS) in the ratio of 95:5% and 80:20% by weight reinforced with ultra-high molecular weight polyethylene (UHMWPE) with the help of a single screw extruder. With the increase in the percentage of UHMWPE, no significant improvement in ultimate tensile strength has been observed due to the occurrence of higher plastic deformation. The blends show spheroids and fibrils at the fractured region which indicates improper mixing of UHMWPE in the ABS/SEBS matrix. Also, the ultimate tensile strength of the hybrid blend was less as compared to virgin ABS [149].

Angelopoulos et al. investigated the effect of expanded perlite as filler for the preparation of ABS composite filament through an extrusion process and printed composite filament was further used for printing tensile samples with the help of 3d printer. They prepared different composite filaments by varying filaments size from 90 μ m to 355 μ m in a different weight proportion of 10, 20, and 40% by volume. From morphological and tensile testing of prepared tensile specimens, it has been found that perlite having fine particle size has superior printing properties, and also filaments having reinforced content more than 20% by volume has poor properties and as compared to specimens having lesser filler percentage [150].

Jiang et al. prepared fused filament with the help of biodegradable polymer PLA reinforced with stainless steel 316L varies from 5% vol. to 15% vol. using fused filament fabrication technique. They studied the effect of reinforcement percentage on thermal, mechanical, and vitro properties, and from the morphological analysis, it was observed that there was a significant improvement in surface roughness with the addition of 316L powder. While analyzing linear and thermal expansion and glass transition temperature it was found that both were not affected by the reinforcement of steel powder whereas compressive and elastic modulus were improved with reinforcement at 10 vol.% and 15vol% [151].

Sang et al. developed a thermoplastic composite filament with the help of polylactic acid (PLA), Polycaprolactone (PCL) and Basal (KBL) to determine mechanical & thermal properties of 3D honeycomb and circular structures. They prepared different honeycomb structures by varying PCL from (0-40%) by weight and observed that the honeycomb structure of PLA-PCL30/KBL filament shows better energy absorption capacity as compared to the other two honeycomb structures [152].

Leist et al. studied the 4D printing behavior of PLA combined with nylon fabrics for creating smart textiles. The authors printed PLA onto nylon to form 4D printing smart textile and concluded that smart textile can be made into custom shapes when heat treated and return to their original shape when heated above glass transition temperature [153].

Bilkar et al. investigated the effect on mechanical properties of carbon nanofiller reinforced with ABS composite prepared with FDM for studying tensile, dimensional and surface properties of 3D printed tensile specimens. They have used a twin-screw extruder for preparing filament with the addition of nanocarbon filler in ABS by varying percentages from 0-2%wt. With an increase in wt% of nanocarbon filler, there was a reduction in tensile strength of 3D printed specimen as compared to tensile specimen prepared with 1%wt. carbon fiber [154].

Peng et al. studied the effect of different processing parameters on tensile specimens prepared with carbon fiber reinforced with polyamide (PA6) with a 6.8 volume fraction. For examining the effect of different printing properties they prepared feedstock filament as per the above conditions with the help of co-rotating twin-screw extruder, along with build plate temperature they varied raster angle in three proportions 0°, 45°, 90°. While analyzing their mechanical properties it was found that with an increase in build plate temperature there was a significant reduction in voids which ultimately helps in increasing the mechanical properties of a 3D printed tensile specimen [155].

Ramesh et al. prepared both tensile and flexural specimens as per ASTM standards for improving different mechanical properties such as ultimate tensile strength, flexural strength, shore Hardness and impact strength. For optimizing the different properties they used Nylon polymer and they varied different printing parameters such as infill density, layer thickness and printing speed. While analyzing with the help of ANOVA analysis it has been found that maximum tensile and flexural strength was obtained with an increase in layer thickness and infill density [156].

Yao et al. studied the tensile strength of 3D printed polymer at different raster angles as per ISO (527-2-2012). They have prepared 7 different tensile specimens by varying raster angle from 0°- 90° at an interval of 15° and layer thickness (0.1 mm, 0.2 mm, 0.3 mm). From experiment analysis, they found that tensile failure strength increases with the increase of the printing angle or the decrease of the layer thickness [157].

Singh et al. prepared a tensile specimen of ABS polymer with the help of FDM as per ASTM standards by varying infill density i.e. 20, 60 and 100% and they performed heat treatment on the printed specimen at three different temperatures (105°C,115°C, 125°C) and time duration of 20,25 and 30min for investigating the effect of these input parameters on surface roughness, tensile strength, flexural strength, dimensional accuracy and hardness. From annealing treatment, it was found that better mechanical property was obtained at 100% infill density, 125°C annealing temperature and 30min, heating time because with an increase in heating temperature and time heat flow between the adjacent layers and helps in filling the air gap between the layers and ultimately it gives better mechanical property as compared to other parameters [158].

Wittbrodt et al. found that with the addition of barium titanate into acrylonitrile butadiene styrene, the polymeric matrix dielectric constant has been improved up to 40%. They found that peak load and mechanical properties of 3D printed specimens were dependent upon the crystallinity of the composite as it was one of the important factors, which has an important role in the mechanical behavior of 3D printed specimens [159].

Tao et al. examined the effect of wood powder reinforcement percentage in the PLA matrix and observed that more % of wood makes polymer matrix less tensile and reduces the tensile strength of the component and also reduced mechanical properties of the prepared filament. They also observed that high wood content in base matrix leads to poor printing i.e nozzle clogging of 3D printers which directly print specimens having poor surface finish and this has been proved by thermal analysis. Wood percentage poor is more thermal analysis will be poor because the reinforcement level affects the thermal stability of filament [160].

Wu et al. examined the effect of raster angle and layer thickness on mechanical properties of the 3D printed specimen. They prepared different samples of PEEK and ABS polymer for testing their compressive, tensile and bending strength. From analysis, they have found that the peak strength of PEEK parts was 114% more than samples prepared with ABS, when they compared the compressive and bending strength of prepared specimen it was found that maximum is of PPEK polymer as compared to ABS polymer. The test samples fabricated at a raster angle of 0°/90° had more mechanical strength as compared to ABS parts [161].

Shenavar et al. evaluated that with reinforcement of graphene into ABS matrix both modulus of elasticity and toughness of the specimen has been increased by 120%. Further, the addition of CB in ABS helps in increasing thermal stability but there was a decrease in the strength with the addition of graphene and carbon black in the ABS matrix [162].

Roberson et al. reported that mechanical properties of parts prepared with FDM depend upon infill density, infill pattern, raster angle, print speed. It was observed that tensile strength and elongation were maximum when tensile strength was applied along the print direction instead of the perpendicular direction [163].

Gkartzou et al. reported that the addition of lignin biopolymer reduces Young's modulus and tensile strength of PLA specimen by 6% and 18% respectively whereas melting properties improve as compared to pure PLA samples [164].

Idrees et al. highlighted that higher thermal resistance along with improved tensile strength (32%) and modulus of elasticity (60%) of PET material was obtained when biocarbon (< 100 μm) was added into it [165].

Singh et al. prepared composite filament by reinforcing zirconium oxide in recycled HDPE and investigated that the coefficient of friction of composite filaments was 40% lower than those of unreinforced filaments. The authors proposed the composite material to be used for low-temperature bearing applications [166].

Alexander et al. studied the effect of raster angle on accuracy and cost of parts fabricated via FDM and stereolithography process. They improved the surface finish by reducing the cusp height. Further, they have suggested different build orientations to reduce fabrication cost [167].

Tong et al. suggested that the dimensional accuracy of the printed parts can be improved by using the compensation method to minimize dimensional errors in both STL file formats and .STL. They found that after applying the compensation method on STL file volumetric error and dimension error were reduced by 30% [168].

Noriega et al. developed a methodology for improving the dimensional accuracy of parts printed through FDM by using an artificial neural network (ANN) in combination with an optimization algorithm. Firstly a part was fabricated with FDM with any application of

algorithm and ANN, secondly, the same parts were fabricated with FDM with the application of ANN and algorithm. It has been found that external and internal dimensions were improved by 50% and 30% respectively by employing this methodology [169].

Hur et al. developed a new algorithm to determine the optimum orientation and layer thickness required during printing of the part. They developed this model for the stereolithography process and one of the major advantages of developing this technique was that it helps in calculating the staircase [170].

Zhang et al. compared the pattern resolution of scaffold structure using PLA printed via FDM and the same scaffold were prepared by combining FDM with electrohydrodynamic (EHD). While preparing the scaffold they varied different parameters such as printing speed, flow rate and found that pattern resolution was improved by 10 μ m as compared to the pattern prepared by the FDM process [171].

Ramos et al. developed a new methodology for making biomedical implants in small quantities for performing vitro and vivo analysis. They have used SolidWorks software for making CAD models and Room Temperature Vulcanizing (RTV) rubber mould was used for making wax patterns. Different surface roughness characteristics of fabricated implants have been measured because of the addition of different metal alloys and the final geometry of the implant was decided based on various parameters [172].

Peres et al. used the FDM process for making patterns and core box for the valve body and found that the FDM process saves 73% manufacturing time as compared to conventional methods. They also compared the results of parts fabricated via FDM and additive manufacturing techniques and found that FDM is superior in terms of time-saving and printing time [173].

Chua et al. highlighted that tooling cost, lead time of conventional machining process was more for small quantity production as compared to additive manufacturing techniques. Further, additive manufacturing can be used to create a pattern for Investment casting for reducing manufacturing costs up to 87.5% as compared to conventional machining methods [174].

Kumar et al. investigated the effect of different parameters on the hardness of the hip joint fabricated by IC and found that mold thickness of the casting plays an important role

while calculating the thickness. They have also optimized the dimensional accuracy of the hip joint fabricated with the help of FDM assisted with IC process and found that dimensions were in the acceptable range as per international standards i.e UNI EN 20286-I (1995) [175].

2.3 WORK PERFORMED TO IMPROVE SURFACE QUALITY OF FDM PARTS

In this context surface roughness and shore Hardness were considered as the important surface properties of FDM parts. They play an important role in FDM printing and are required to be improved [176]. In the FDM air gap, bed temperature, extrusion temperature plays an important role in affecting the surface properties of the parts [177-178]. Therefore work done by some researchers to improve surface properties are illustrated below.

Grenda et al. revealed that layer thickness and nozzle diameter were one of the major limitations in getting précised model with the help of FDM. Layer-by-layer material deposition gives an error concerning the amount of material shown by the computer-aided design model. It influences the dimensional accuracy as well as the surface roughness for various part build directions [179].

Bakar et al. found that parts having an orientation in the horizontal direction has a superior surface finish as compared to parts having orientation vertical and circulation. It could be due to the reason that the parts printed in circular shape have elliptical curves which result in poor bonding between the adjacent layer and ultimately reduce the part strength [180].

Percoco et al. evaluated the effect of surface roughness and compressive strength of FDM printed part treated chemically with a solution of 90% dimethyl ketone and 10% water. They observed that after chemically treating for 300s with acetone solution the surface roughness of the printed part has been reduced up to 90%. Along with this the chemical treatment also helps in improving the compressive strength of the chemically treated part as compared to non-treated parts [181].

Boschetto et al. have stated that many models are available in the market to evaluate surface roughness of printed FDM parts but these models are unable to measure and predict roughness in the range of 0–30° and 150–180° with respect to deposition angle is a superior way. Therefore they developed a new model with the help of neural networks which could apply to an entire printed surface. After being examined by ANN architectures and they verified the results obtained from the new model for calculating surface roughness were

verified by ANOVA and they revealed that this designed model is suitable for calculating surface roughness [182].

Ayrilmis et al. studied the effect of layer thickness on surface roughness and wettability on the 3D printed samples were prepared from PLA/wood flour (70%+30%) by weight. The authors prepared the specimen by varying the layer thickness (i.e. 0.05mm, 0.1mm, 0.2mm and 0.3mm) and concluded that surface roughness as well as wettability increases with an increase in layer thickness [183].

Chouhan et al. studied the effect of using acetone as a smoothing agent on ABS-prepared replicas. In this study, they found that with an increase in exposure time with acetone vapors better surface finish was found but on further increasing the exposure time there was an adverse effect on the surface finish of the prepared replica. With an increase in exposure time there a change in dimension and surface property of replica has been found [184].

Garg et al. examined the dimensional accuracy and improvement in the surface finish of FDM fabricated parts when treated with dimethyl ketone. They have concluded that after vapor treatment the surface finish of the components was improved dramatically with minimum change in part dimensions [185].

Boschetto et al. prepared a new geometrical model to predict the surface roughness of parts fabricated by barrel finishing (BF) and by FDM. The model predicts the roughness of the parts prepared by the FDM process by varying parameters i.e raster angle and layer thickness and the material removed by the BF operation. The experiment showed that BF operation is affected mainly by the morphology of the profile which depends upon the FDM process parameters. The comparison between experimental data and theoretical model shows a significant reliability of the theoretical conclusions [186].

Turner et al. have stated some tests for evaluating both surface roughness and dimensional accuracy. They studied the effect of different design variables on surface roughness for determining surface roughness. It was found that process optimization is a must and it also helps in minimizing the surface roughness of 3D printed parts during printing, which directly helps in reducing time and cost utilized during post-processing [187].

Jin et al. determine the effect of different process variables on the surface finish of the parts fabricated with the help of FDM. They have considered two types of the model first model was preprocessed parameters and the second model was printing variables for determining the change in surface profile of surfaces top as well as a side surface. The values obtained from these models were compared with the values obtained from the experiments to check whether is there any reliability or validity of the proposed model or not. It was found that the surface roughness of the top surface was mainly affected due to variation between the ratio of flow are and feed rate of the nozzle. While evaluating the surface roughness of the side surface it was found that it was maximum because the side surface was mostly affected by the staircase effect [188].

Rattanawong et al. designed a part orientation system for RP by considering the volumetric error (VE) developed during the process. The designed approach showed the VE at different orientations and suggested the optimized orientation for less VE. They also revealed based on results that in the case of the cylinder and cube 0° and 90° build orientations are suitable for reducing VE [189].

Pennington et al. found that the dimensional accuracy of ABS parts fabricated via FDM process was mainly affected by the build temperature, part size and layer thickness [190]. **Gregorian et al.** found that 1.007 was shrinkage compensation factor (SCF) for FDM to improve the dimensional accuracy and surface finish of the fabricated parts [191].

Idris et al. fabricated hollow and solid H-shaped ABS patterns with the help of an FDM machine to determine the size distortion, surface finish and dimensional accuracy. They have revealed that dimensional accuracy of the hollow pattern was more accurate as compared to the solid pattern, but surface roughness of both patterns was the same, whereas the size distortion of the hollow pattern was more as compared to the solid pattern was more i.e around 33% [192].

Volpato et al. revealed that the dimensional accuracy and dimensional errors of parts fabricated by FDM in Z-direction can be enhanced by improving the quality of the support base and it has been found that by using improved quality of the support base dimensional error has been improved by 50% [193].

Nunez et al. examined the effect of layer thickness and part density on surface roughness and dimensional accuracy of the ABS parts prepared by FDM. They have found

that the least dimensional deviation was achieved with solid part density having a layer thickness of 0.254mm. They also found that part density was one of the major process parameters that affect dimensional accuracy [194].

Thrimurthulu et al. developed a new model for improving surface finish and for reducing the build time with the help of an adaptive slicing technique for the FDM. They found that surface finish and build time both are opposite to each other [195].

Mahapatra et al. studied the effect of build parameters on the surface finish of FDM parts using Artificial Neural Network and Lavenberg- Marquardt algorithm for optimizing surface finish of the bottom, top and side surface of the printed part. The advanced algorithm technique showed that raster angle was more significant for the top surface while layer thickness was significant for the bottom and side surface [196].

2.4 Bibliographic Analysis

For bibliographic analysis Scopus data base for past 20 Years has been explored with keyword ‘multi material 3D printing’ and 2329 results were obtained. The top 2000 results were processed with VOS viewer open-source software. Further by selecting minimum occurrence of terms as 5, out of 5073 terms, 148 meet the threshold. For each of 148 terms, a relevance score was calculated. Based on this score, the most relevant terms were selected. For analysis 60% most relevant terms (89) were selected (Table 2.2).

Table 2.2: Relevance score for selected terms (as per Scopus data base)

Id	Term	Occurrences	Relevance score
1	3d bioprinting	19	0.5425
2	3d printer	22	1.0741
3	4d printing	30	0.5684
4	Accuracy	13	0.5603
5	Additively	5	0.7905
6	Advance	9	0.6831
7	Architecture	16	0.889
8	Art	5	0.8302
9	Bioink	14	0.6062
10	Biomaterial	10	0.7775
11	Biomedical application	7	0.9147
12	Bioprinting	19	1.0301
13	Bone tissue engineering	5	0.9749
14	Carbon	5	0.917

15	Carbon nanotube	14	0.6499
16	Challenge	20	0.8112
17	Color	7	1.1697
18	Construction	13	0.7503
19	Current status	6	0.9908
20	Deposition modeling	9	0.4896
21	Dimensional printing	27	0.9768
22	Direct ink writing	10	1.6203
23	Effect	43	0.5022
24	Electric field	6	1.4929
25	Electronic	12	2.4546
26	Experiment	8	1.6091
27	Experimental investigation	9	0.7144
28	Fdm	13	0.4667
29	Feasibility study	5	1.2108
30	High performance	5	2.7841
31	High resolution	5	1.5382
32	Hydrogel	37	0.7134
33	Influence	18	0.5165
34	Interface	14	1.1228
35	Investigation	23	0.729
36	Laser powder bed fusion	5	0.6741
37	Layer	16	1.1199
38	Mechanical	6	1.0033
39	Mechanical behavior	8	0.8768
40	Mechanical characterization	8	1.2924
41	Microstructure	13	0.8423
42	Multi jet fusion	6	1.0033
43	Multi material 3d printer	6	2.8013
44	Multi objective optimization	6	0.78
45	Multi scale	6	1.1148
46	Multifunctional material	9	1.1901
47	Multimaterial 3d printing	12	1.03
48	New method	5	1.0333
49	Novel	5	1.9161
50	Object	23	0.6538
51	Opportunity	6	0.9354
52	Overview	7	1.3616
53	Parameter	12	0.575
54	Performance	25	0.6837
55	Perspective	10	0.546
56	Pla	8	0.6488
57	Poly	11	0.6709
58	Polyjet	6	0.8267
59	Polylactic acid	10	0.6532
60	Polymer composite	13	0.6539

61	Prediction	6	1.8101
62	Printability	6	0.8736
63	Printer	19	0.55
64	Proceeding	8	0
65	Process parameter	10	0.6393
66	Production	15	0.2789
67	Progress	9	0.8381
68	Rapid prototyping	7	2.3116
69	Recent advance	10	0.9079
70	Recent development	6	0.9064
71	Recent progress	6	1.1462
72	Research progress	6	1.315
73	Selection	10	0.8625
74	Selective laser	8	1.169
75	Self	8	1.5632
76	Shape memory polymer	9	1.0671
77	Smart material	9	0.8516
78	Soft robotic	9	1.813
79	State	7	0.7959
80	Stem cell	7	0.5076
81	Step	8	1.028
82	Stereolithography	12	0.6453
83	Stiffness	16	1.1856
84	T3dp	6	1.3327
85	Testing	13	1.2142
86	Tissue	20	0.8257
87	Tissue engineering	21	0.6952
88	Tissue engineering application	7	1.425
89	Voxel	9	1.0832

Based upon Table 2.2, bibliographic analysis is shown in Figure 2.1. Further based upon Figure 2.1, the research gap is highlighted in Figure 2.2.

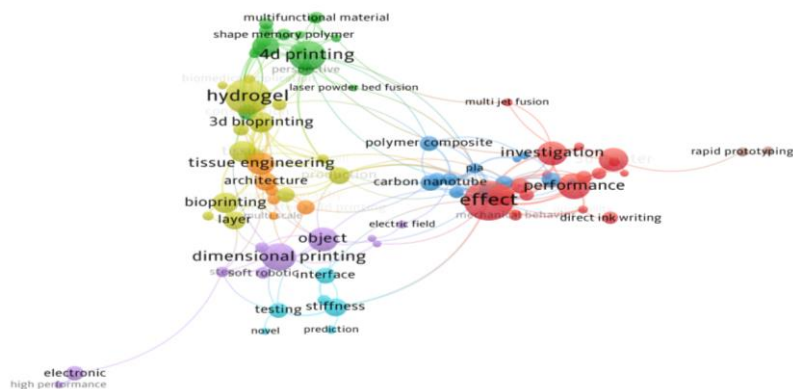


Figure 2.1: Bibliographic analysis

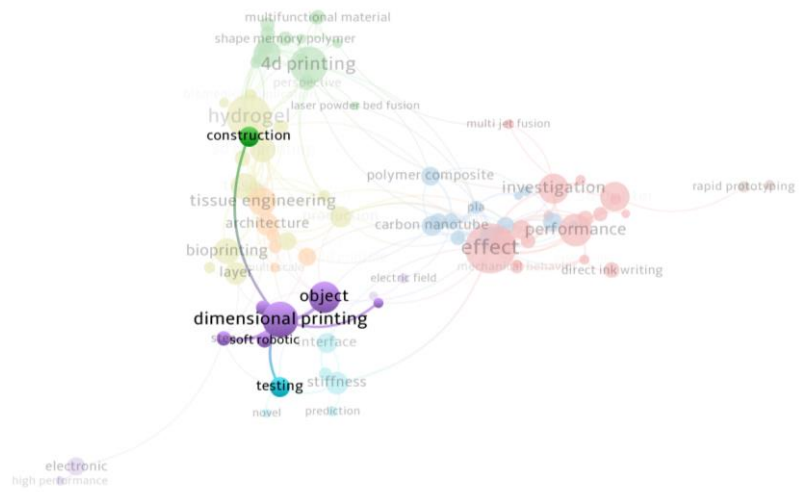


Figure 2.2: Research gap based upon Figure 2.1

CHAPTER- 3

PROBLEM FORMULATION AND OBJECTIVE

3.1 NEED FOR RESEARCH

In developing and underdeveloped countries human beings use either land filling or incineration for polymer waste management. But both these techniques produced harmful gases like methane which directly contributes to global warming. So, recycling is a better way of managing plastic waste. Recycling of waste polymer includes various steps such as segregation, washing, drying, extruding and granule forming. But recycled polymers start losing their mechanical properties after the certain number of cycles. So, one of the solutions could be the reinforcement of different materials into polymer waste to enhance its properties.

Researchers nowadays use reinforced materials such as graphene, carbon nanotubes (CNT), Aluminum oxide (Al_2O_3) and some other external particles to enhance the properties of polymer wastes. Some researchers reported that reinforcement of metal powder results in an improvement in mechanical properties as well as the composite formed becomes conducting in nature [197-198]. Also, such composites may be traced easily with different testing techniques like ultrasonic testing, eddy current and magnetic particle inspection testing. From last few decades, extruded filament wire made from plastic waste has been successfully utilized in FDM, being one of the most economical AM techniques for various applications such as construction, tissue engineering, electronic, dentistry for dentures fabrication etc [199]. FDM requires filament wire especially of polymeric material extruded either by single screw or twin-screw extruder. FDM allows high degree of freedom to the operator to fabricate the desired specimen. This design flexibility may help in improving the mechanical as well as morphological properties of the material.

3.2 FINDINGS FROM LITERATURE SURVEY

The literature review reveals that FDM has the capability to prepare complex shaped components, surgical equipment's, electronic sensors, outlet ducts, truck fanders, turbine blades, biomedical implants etc. with additional features such as reliability, low tooling cost, less lead time as compared to conventional machining process. FDM is one of the techniques having the potential to meet the rapid demand of the product in the shortest possible time but parts fabricated by FDM have poor surface quality due to various reasons and therefore, it resists the FDM application in the field of structural applications. Therefore, to improve the

properties as well as applications of FDM in structural applications, the mechanical and surface properties of FDM printed parts should be improved.

Various researchers utilized different techniques to improve surface characteristics and mechanical properties of FDM printed parts with reinforcement of suitable materials in thermoplastic polymer but hitherto very less has been explored on printing of recycled thermoplastic composite matrix with reinforcement of waste thermosetting, WD and Fe particles for multi/hybrid blend without any alteration in FDM software/hardware. The use of multi and hybrid blend in 3D printed prototypes is expected to enhance the mechanical, rheological, surface and morphological properties. The BP is one of the thermosetting polymers extensively used in metallurgical labs for specimen mounting and thus generating a large quantity of PSW [200]. BP consists of 3D cross-linked structure having high hardness, chemical resistance and strength, hence can be used as reinforcement for enhancing the properties of the base matrix. Further, the utilization of WD and Fe as reinforcement has been little explored in 3D printed functional prototypes for non-structural applications.

So, in the proposed research work, primary recycled ABS (collected from local industry) will be used as a base matrix with BP (thermosetting waste collected from labs), WD (waste collected from saw mill) and Fe metal powder (waste collected from machining industry) as reinforcement. The composite filaments would be fabricated through three different blending routes (mechanical, chemical assisted mechanical and mechanical-hybrid). The prepared composite filaments would be employed to print multi and hybrid blended smart tiles that can be used in low-temperature regions for nonstructural applications. The particular reinforcements were selected to induce some specific properties in the FDM printed smart tiles (BP can increase the heat-carrying capacity, WD can induce insulating properties to retain the heat inside the cabin and Fe powder to impart magnetic properties for self-assembly features).

3.3 OBJECTIVES

The main objectives of the proposed research work are:

1. To prepare ABS composite matrix by mechanical and chemical blending based upon rheological, morphological and surface properties.
2. To prepare feed stock filament for FDM setup by using twin screw extrusion (for mechanical and chemical blended composite matrix) and its process parametric optimization.

3. To print the prototype (for tensile and flexural properties) on FDM by using a multi/hybrid blend and its process parametric optimization.
4. To study the effect of pre and post processing on the surface and mechanical properties of 3D printed functional prototypes.

CHAPTER-4

METHODOLOGY AND EXPERIMENTATION

STEPS INVOLVE IN PRESENT RESEARCH

The present research has divided into three steps:

- 1) **First phase (filament preparation):** After the selection of suitable weight percentage of reinforcements (based on MFR results) in the ABS base matrix, the composite filaments were fabricated with the help of TSE by varying different input variables (load, speed, and temperature) using L₉ orthogonal array. The levels of chosen parameters were decided by performing pilot experiments. The universal testing machine (UTM) was then employed to measure various characteristics of the composite filaments like peak load, PS, peak elongation, breaking load, break strength, break elongation, modulus of elasticity, and modulus of toughness. To examine the mechanical behavior of composite filaments in terms of PS, the porosity analysis was also performed as per ASTM B276 standard. Finally, FTIR (Make: PerkinElmer Spectrum IR Version 10.6.1) was performed to determine the presence and nature of bonds formed between the base and reinforced material that might affect the mechanical strength of the composite.
- 2) **Second Phase (3D printing):** In this phase tensile and flexural specimen were printed on FDM from the fabricated composite having maximum peak strength. The mechanical and chemical-assisted blending-based composite filaments were utilized to print multi-layer (layer of different composite material) tensile and flexural specimens whereas single-layered tensile and flexural specimens were printed from composite filament based on mechanical-hybrid blending. The outer three layers on both sides of the multi-layered specimen were printed with filament reinforced with BP and Fe powder whereas the inner layers were composed of WD reinforced filaments. Further different mechanical properties have been measured for the optimization of multi-material 3D printing of specimens.
- 3) **Third Phase (post Processing):** A post-processing technique has been applied on rectangular specimens for determining the effect of chemical vapor smoothing and heat treatment techniques on surface roughness and shore hardness. Vapor smoothing was done with the help of a smoothing apparatus using acetone as a smoothing solution by varying different parameters such as smoothing time, soaking time, and

number of cycles. The steps involved in the present research work have been illustrated in Figure 4.1.

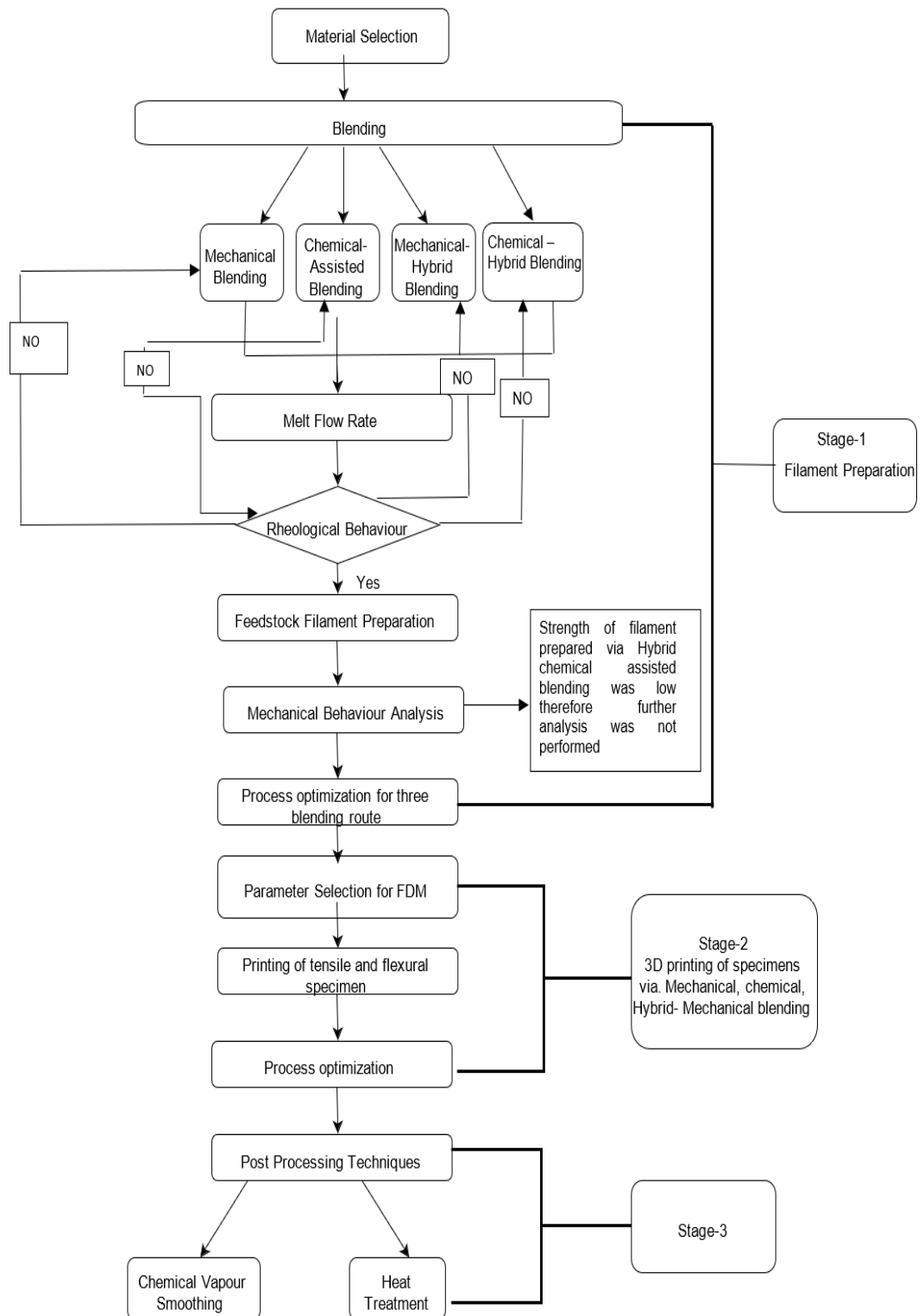


Figure 4.1 Steps involved in the present study

This section of the report explains the detailed methodology, materials, techniques, equipment, and testing techniques used in the present research.

4.1 SELECTION OF BASE MATERIAL AND REINFORCEMENT MATERIAL

The polymer used in the present work was secondary recycled Acrylonitrile Butadiene Styrene (ABS). It has a carbon chain co-polymer belonging to a styrene-terpolymer chemical family. Which contains monomers of acrylonitrile, butadiene, and styrene i.e 15%–35% acrylonitrile, 5%–30%butadiene, and 40%–60% styrene with three structural units having good mechanical and thermal properties. After the selection of base material, the next steps were the selection of reinforcement material and its percentage. Waste WD was procured from a local sawmill and Fe was collected from the machine shop of the institute both were segregated by sieve shaker and a particle size of 50 μm was selected for the research work. Similarly, waste BP was collected from the metallurgical lab, crushed in a cryogenic environment (-196°C), and particle size similar to WD reinforcement was selected for the composite filament.

4.2 MELT FLOW RATE

Initially, the procured 2° recycled ABS was kept in a vacuum oven at 50°C (temperature lower than the glass transition temperature) for 4 h to ensure the removal of moisture present in the granules. Before preparing feedstock filament for FDM, the Melt Flow Rate (MFR) of the 2° recycled ABS was calculated. Figure 4.2 shows the setup of MFR tester. MFR is an analytical technique used for determining the flow ability of the polymer under different conditions such as temperature and nozzle diameter as per American society for testing materials D1238 standards [201]. MFR was represented in g/10 min, which indicates the amount of polymer flows through a nozzle in 10 min [202]. After doing five repeated trails for 2° recycled ABS, MFR comes out as 16.2 g/10 min as per ASMTM D1238 standard (230°C and 3.8 kg load). The three-dimensional printers (Stratasys) using virgin ABSplus P430 thermoplastic usually have an MFR of 2.415 g/10 min. This huge difference in the MFR may be attributed to the variable percentage of monomers (15%–35% acrylonitrile, 5%–30%butadiene, and 40%–60% styrene) in the recycled ABS. Figure 4.2 shows the setup of the MFR tester.

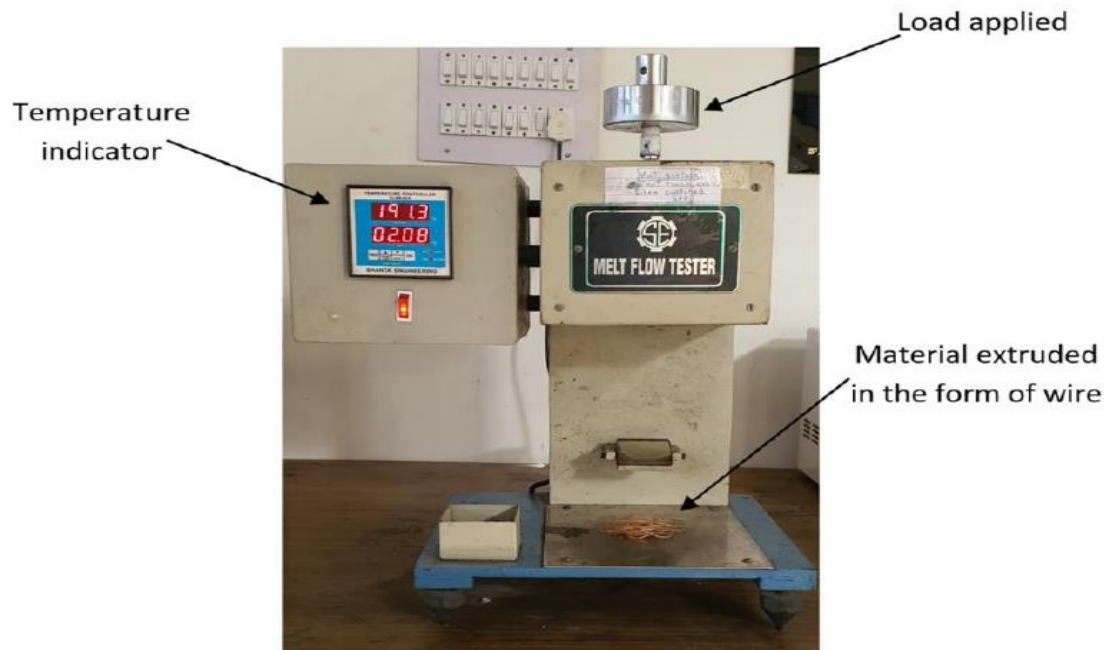


Figure 4.2 MFR Tester setup

4.2.1 Mechanical Assisted Blending

Before preparing fused filament first step was the preparation of composite with the addition of different reinforcements (BP, Fe, and WD) by varying their proportion of 2.5–10% by weight separately to the base matrix by mechanical blending their MFR has been investigated under ASTM D1238 standards. The MFR indicates the flow rate of thermoplastic polymer per unit time (g/10 min). It also ensures the ability to print thermoplastic for 3D printing applications. From MFR analysis it has been observed that on increase in the proportion of reinforcement beyond 10% by weight there was a sudden reduction in MFR and resulting in clogging the nozzle. Also the MFR in (ABS + BP, ABS + Fe, and ABS + WD) with reinforcement of 10% by weight results in MFR near to recycled ABS, therefore 10% reinforcement in ABS matrix has been selected for the fabrication of fused filaments by TSE.

4.2.2 Chemical Assisted Blending

First of all acetone $[(CH_3)_2CO]$ has been procured from the local market (Shiva Chemical, Ludhiana) as ABS can dissolve with acetone. For chemical assisted blending, 100 ml of acetone was blended with 50 gm of ABS with the help of a stirrer and kept it 2-3 hours for proper mixing at room temperature. After that reinforced materials (BP, Fe, and WD)

were added separately at different weight proportions of 2.5%, 5%, 7%, and 10% respectively. Then the composite was stirred for 30 min so that both base and reinforced materials mixed properly. In the next step, a glass sheet was taken and the composite was poured over it and placed in an oven at 100°C for 4 hours so that traces of acetone vaporized completely. Once composite was dried, small flakes were produced (Figure 4.3) and then utilized for preparing composite filaments. Further MFR of prepared composite has been calculated as per ASTM D1238 standards. From MFR results it has been found that reinforcement of 10% by weight results into MFR near to recycled ABS, therefore 10% reinforcement in ABS matrix has been selected for the fabrication of fused filaments by TSE.



Figure 4.3 Flakes prepared by reinforcement of a) WD and b) BP c) Fe in ABS through chemical blending

4.2.3 Mechanical- Hybrid assisted blending

The secondary recycled ABS was reinforced with WD taken from the sawmill, Fe powder from the milling shop, and BP from the metallurgical lab of particle size 50 μ m by taking 90% ABS and 10% reinforcements.



Figure 4.4 ABS after hybrid blending

Then the MFR of the prepared composite was determined as per ASTM D1238 standards and after doing five repeated trials for the prepared composite, MFR comes out as 18.35g/10min. On further increase in reinforcement proportion, MFR decreases drastically.

4.3 TWIN SCREW EXTRUDER

The reinforcement percentage was selected after calculating the MFR next step is a fabrication of feedstock filament with the help of a Twin Screw Extruder (TSE). The twin-screw extruder consists of a number of parts such as die, heater, hopper, twin screw. The material in the form of granules was fed into the extruder with the help of a hopper. The heater present in the barrel melts the material and the screw forces the material in a forward direction towards the die. Some parameters that affect the wire formation are: the first factor is speed, which is one of the most important parameters that affect the strength of filament wire. At maximum speed obtained filament would be of poor strength as compared to filament prepared at a lower speed. The second parameter is pressure, high pressure sometimes in creating back pressure which means material starts coming out from the backside instead from the forward direction. Therefore, pressure should be up to 500psi so that material should come out from the die in the form of semi-molten Figure 4.5 shows a schematic diagram of a single screw extruder is shown below:

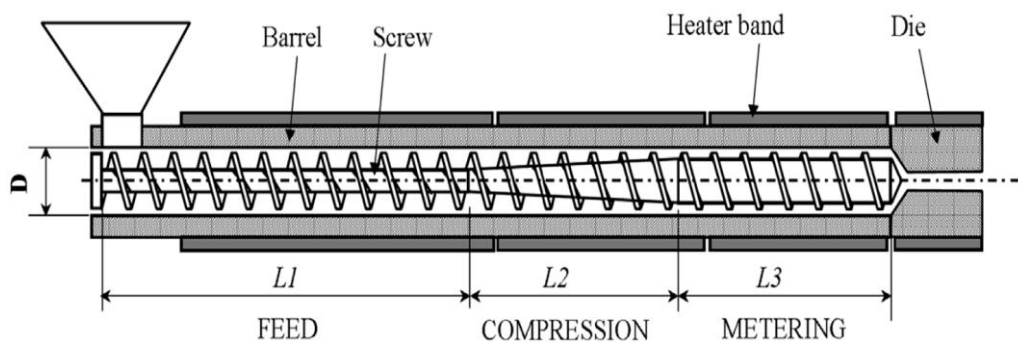


Figure 4.5 Schematic diagram of Single Screw Extruder [203]

While preparing feedstock filament with the help of TSE number of parameters can be varied such as externally applied load, screw speed, extruder temperature. In the present study for preparing feedstock filament design of experiment (DOE) employing Taguchi's L9 orthogonal array (OA) has been applied to avoid experimentation error. Pilot experiments were performed for the selection of different parameters and their levels. Table 4.1 shows the control log of experimentation for the preparation of feedstock filament with TSE.

Table 4.1 Control Log of experimentation

S. No	Load (kg)	Temperature (°C)	Speed (rpm)
1	10	225	70
2	10	235	80
3	10	245	90
4	12.5	225	80
5	12.5	235	90
6	12.5	245	70
7	15	225	90
8	15	235	70
9	15	245	80

4. 4 TENSILE TESTING

After preparing fused filaments on the basis of control log of experimentation as mentioned in Table they further processed on a Universal Testing Machine (UTM, Shanta Engineering Works, India) having a load-carrying capacity of 5000N for determining different mechanical properties like peak strength, break strength, modulus of toughness, break elongation with a separation distance of 60mm between the jaws as shown in the Figure 4.6

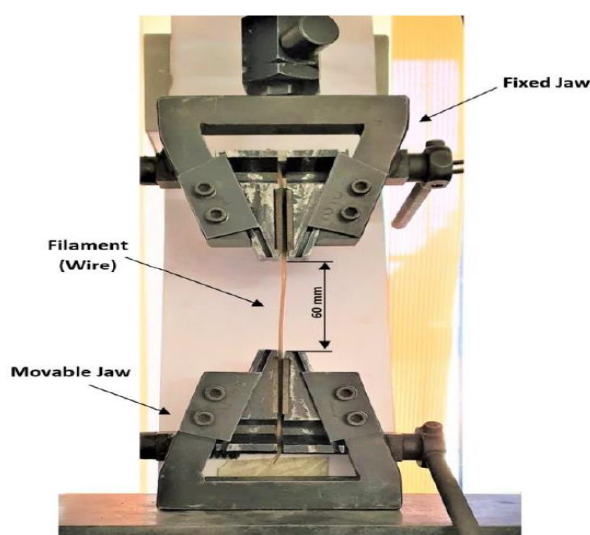


Figure 4.6 Schematic diagram of Tensile Testing

4.5 FLEXURAL TESTING

3D printed flexural specimens were further processed for determining their mechanical properties such as Peak Load, Break Load, Peak strength, Break Strength with the help of UTM having load capacity of 5KN. The schematic diagram of flexural testing via UTM is shown in the Figure below 4.7.



Figure 4.7 Schematic diagram of Flexural Testing

4.6 MECHANICAL AND THERMAL TESTING

After tensile testing of feedstock filament, the next step is the determination of mechanical and thermal behavior of the prepared feedstock filament. Few mechanical and thermal techniques that have been employed in the present study for studying their behavior are illustrated below.

4.6.1 Differential Scanning Calorimeter (DSC)

Differential scanning calorimeter (DSC) is an analytical technique used for determining glass transition temperature (T_g), heat-carrying capacity (j/g), solidification temperature, etc. The process consists of repeated heating and cooling of the composite sample by flowing air (50 ml/min) at $-10^\circ\text{C}/\text{min}$ for endothermic reaction and $10^\circ\text{C}/\text{min}$ for an exothermic reaction. The amount of heat absorbed and released during the particular reaction gives the estimation of the heat-carrying capacity of the samples. These properties

are defined under the controlled continuous heating (endothermic reaction) and controlled continuous cooling (exothermic reaction). DSC setup analyzed the thermal behavior of applied samples by taking references from the standard sample and it uses two separate crucibles for cooling and heating as shown in Figure 4.8.

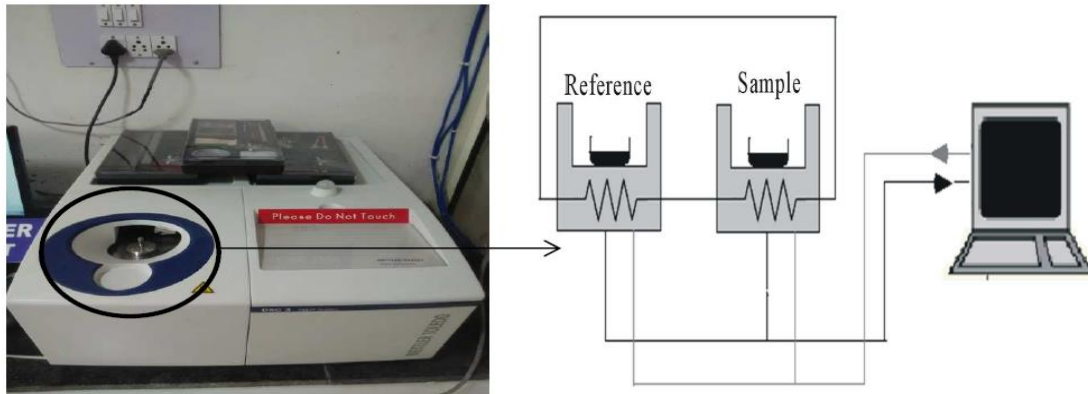


Figure 4.8 Schematic diagram of Differential Scanning Calorimeter

4.6.2 Scanning Electron Microscopic (SEM)

SEM is a surface imaging technique used to observe the change in morphology of a specimen after different processes. However, changes in surface topology, particle distribution, cracks, peaks, and valleys are not visible via naked eyes but with the help of SEM micrographs at different resolutions it is possible.



Figure 4.9 Scanning Electron Microscopic setup

Micrographs obtained from SEM helps in providing exact information for change in surface topology which would help in better understanding the phenomena responsible for showing different behaviors. In the present study JEOL, JSM 7610F plus SEM machine has been used with a resolution of 1.0nm and magnification up to 1000KX as shown in Figure 4.9. A sample size of 5X5X4mm has been used in the SEM machine and the polymer specimen was coated with gold before viewing micrographs of the sample.

4.6.3 Electron Dispersive Spectroscopy (EDS)

EDS is a surface analytical technique used to determine the compositional proportion of various materials in the composite filaments and is also used for elemental analysis in coexistence with Scanning Electron Microscopy. EDS systems generally used X-ray detectors and software to analyze and collect energy spectra. One of the biggest advantage of EDS is it helps in collecting the electron component of the material from different spots and creating all elements in the form of an element composition grid.

4.6.4 Fourier Transform Infrared Spectroscopy (FTIR)

FTIR was used to determine the nature and type of bond with the help of infrared spectroscopy by applying Fourier transform. FTIR analysis can be done on samples either in solid or liquid form no further preparation is required. FTIR apparatus used in the present study has the following specifications.

Table 4.2 Specification of FTIR setup

Make	Perkin Elmer
Optics	KBr
Sensitivity	32,000:1 peak to peak for 1 minute scan
Resolution	0.5cm ⁻¹
Scan range	8300-350cm ⁻¹
ATR accessory	Diamond
Software	Spectrum 10 software



Figure 4.10 Fourier Transform Infrared Spectroscopy setup

4.7 FUSED DEPOSITION MODELING SETUP

The filaments prepared with the help of TSE were further processed on the FDM model: Accuraft 250D for the printing of Tensile specimen (as per ASTM D 638 type IV) and flexural specimen (as per ASTM D 790 standards) as shown in Figure 4.11. Significance of flexural testing is to determine both flexural modulus and flexural strength. It is used to determine the maximum tensile and compressive stresses that the specimen can bear. Moreover, more flexural strength gives good restoration ability of the specimen.

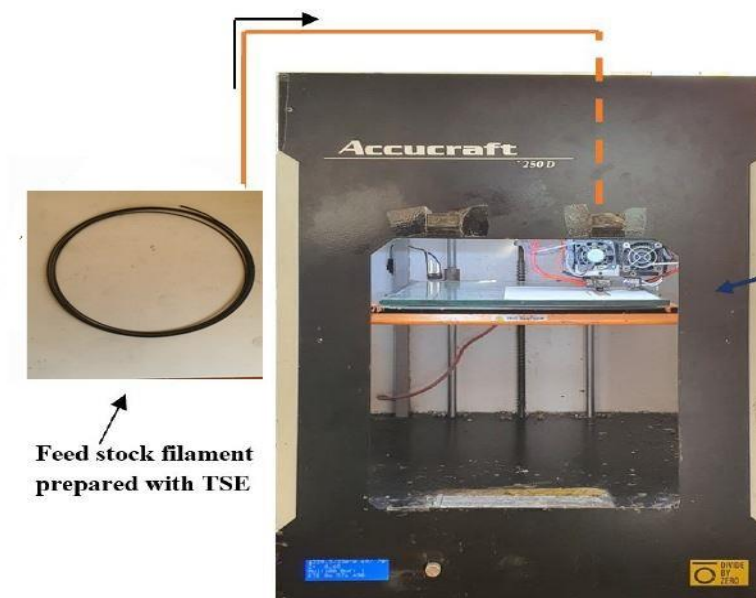


Figure 4.11 Fused Deposition Modelling setup

. Initially, the three-dimensional CAD file of a tensile and flexural specimen is generated with the help of “Solidworks 2014” software. Further prepared CAD file is

processed in Slice3r to converted into STL format and then G- codes were generated. Once the G-Code is generated, Repetier-Host V2.1.6 software utilizes to execute the printing as demonstrated in Figure 4.12. This Repetier-Host instruct the 3D printer to execute printing operation by reading G-codes. Then the printer prints these cross-sections by depositing a layer on layer through extrusion.

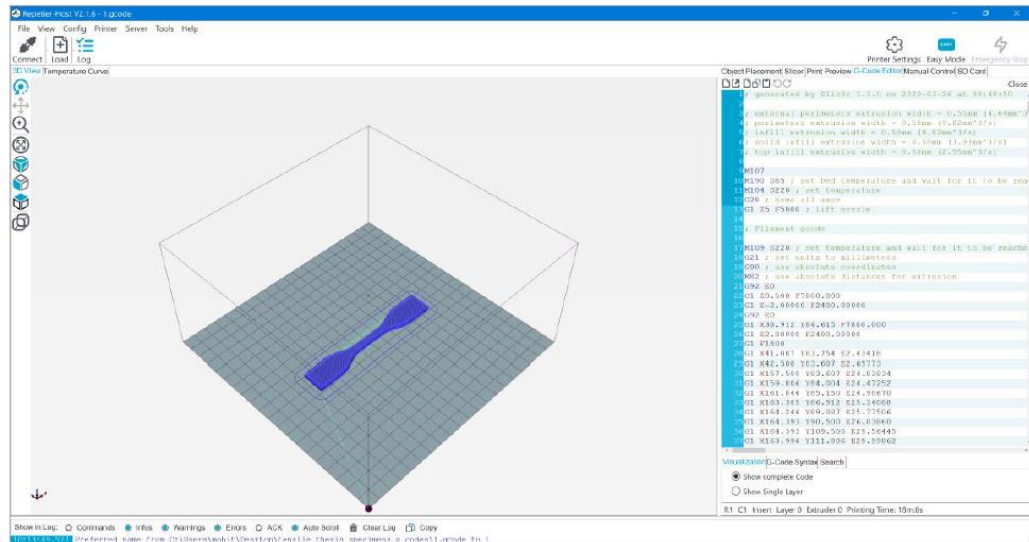


Figure 4.12 Repetier- Host software working

FDM used in the present work can go up to maximum nozzle temperature 270⁰C and bed temperature 80⁰C. FDM was used in the current study having features of replacing fused filament manually at the desired time. It has two nozzles namely; the model material nozzle and support material nozzle from where the respective material is extruded. In FDM few parameters have been fixed they are listed in Table 4.3.

Table 4.3 Fixed parameters of FDM

Fixed parameters of 3D printing	
Raster width (mm)	0.254
Air Gap (mm)	0
Layer thickness(mm)	0.4070
Nozzle Temperature	270 ⁰ C
Bed Temperature	80 ⁰ C
Infill pattern	Rectilinear

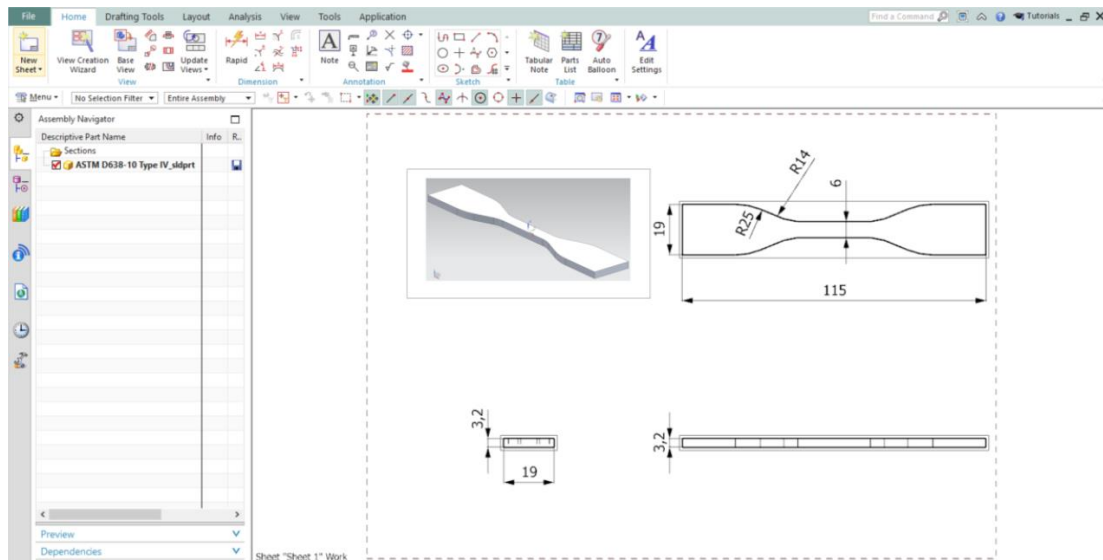


Figure 4.13 CAD model of tensile specimen

Before printing parts on FDM three input parameters (Infill density, Raster angle, and Infill speed) have been selected along with layer combination. Therefore, three combinations of layers i.e 2° ABS- BP, 2° ABS- WD, and 2° ABS-Fe have been used for the preparation of the multi- layer 3D printed prototype. The material selection was done based on the MFR, tensile and thermal properties of the fused filament. While preparing 3D specimens first 3 layers of 2° ABS-Fe next three layers of 2° ABS- WD and the last three layers of 2° ABS- BP were printed at a uniform height to prepare a multi-layer specimen for non-structural applications. To avoid receptions an L9 orthogonal array has been applied on the FDM printer as per Table 4.4.

Table 4.4 Control log of experimentation applied on FDM

S. No	Units	1	2	3	4	5	6	7	8	9
Raster angle	Degree	0	0	0	30	30	30	60	60	60
Infill density	%	80	90	100	80	90	100	80	90	100
Infill speed	mm/sec	20	30	40	30	40	20	40	30	20

After fabrication of tensile and flexural specimens, parts are further processed on UTM for calculating their mechanical properties and further parts can be further processed for the improvement of surface finish.

4.8 CHEMICAL VAPOR SMOOTHING APPARATUS (CVS)

CVS apparatus used in the present study as shown in Figure 4.14 consist of two chambers one is cooling and the other is a smoothing chamber. The cooling chamber is equipped with cooling coils maintained at 0°C, whereas the smoothing chamber consists of a heater installed at the bottom maintained at 65°C where the smoothing fluid is heated.



Figure 4.14 Chemical Vapor Smoothing station Setup

The process starts when the smoothing fluid flows the tank into the smoothing chamber from the reservoir. When the fluid reaches up to heating temperature, the fumes rise in the chamber and get deposited on the surface of the specimen. The gathered liquid is reused once more into a smoothing chamber through the smoothing reservoir. The pneumatically powered lid is used for closing and opening of smoothing chamber which gets compressed air from the reciprocating compressor. The parts are needed to be cooled for a few moments prior for better outcomes. At first, 20 litres of smoothing liquid were filled in a vapor smoothing device. The smoothing fluid utilized in this work was acetone because of its high diffusion and low toxicity. The acetone is exceptionally unpredictable which dissipates even at room temperature. An exhaust fan has been given at the lower part of the cooling chamber to extricate the leftover fumes from part surfaces and push them out into the open air. Vapor smoothing was done on prepared rectangular specimens by varying different

parameters like cycle time (seconds), soaking time (minutes), and No of cycles. To avoid repetitions L9 orthogonal array has been applied on the vapor smoothing working station as shown in Table 4.5.

Table 4.5 Control log of experimentation applied on smoothing station

Cycle Time (Sec.)	Soaking Time (Min.)	No. of cycles
15	15	2
15	20	3
15	25	4
20	15	3
20	20	4
20	25	2
25	15	4
25	20	2
25	25	3

4.9 SHORE HARDNESS TESTER

The Digital Durometer was used for measuring shore D hardness (Hd) of 3D printed specimens. as shown in Figure 4.17. The hardness of prepared specimens has been measured as per the ASTM D2240 standard. The hardness tester has a measuring range from 0 to 100 Hd with the least count of 0.5Hd. The hand pressure foot is used to apply on the surface with a uniform force of 5 kg for 6 seconds during each measurement. The indentation hardness is inversely proportional to the penetration and the indenter is directly connected with the spring with gives deflection to spring. The force given by the spring to indenter has been calibrated with Durometer units as $1 \text{ Hd} = 0.4445 \text{ N}$ Thus, the output in form of durometer units can be suitably converted as a force on spring upon requirement. The three readings are measured for each specimen before tensile testing.

4.10 HEAT TREATMENT

Heat treatment of 3D printed specimens was done above the glass transition temperature of the polymer with the help of a hot air oven. In a hot air oven, both heating time and heating temperature can change with the help of a control panel available in the front of the hot air oven. It has one steel plate for placing the specimen in the oven, once the

specimen is placed in the oven, close the door and then set temperature and time. Before opening the door make ensure heating time has been completed and take out the hot steel plate with gloves. While doing heat treatment on prepared specimens two variables have been taken one was heating time and the second was heating temperature. To avoid experimentation repetitions L9 orthogonal array was applied as shown in Table 4.6 below.

Table 4.6 Control log of experimentation applied on hot air oven

Heating Temp. (°C)	Heating Time (Min.)
100	10
110	15
120	20
100	15
110	20
120	10
100	20
110	10
120	15

4.11 SURFACE ROUGHNESS MEASUREMENT

The surface roughness (R_a) of the 3D printed specimen was measured with the help of Mitutoyo Surftest SJ-210. The device can measure more than thirty types of roughness parameters as per international standards. It displays output on a 2.4-inch liquid crystal display (LCD) screen and data can be stored on the desktop through synchronization. While measuring surface roughness, the sensor is placed on the surface whose roughness is to be measured as the sensor has the property of sliding along the surface to collect information regarding surface roughness with the help of an inbuilt diamond probe. The surface roughness given by the tester is in the form of an analog signal which is in proportion to the surface roughness at the output end of the phase-sensitive rectifier and surface roughness profiles are directly plotted on the desktop. The surface roughness of prepared specimens is measured before and after vapor smoothing for getting a valuable comparison between surface roughness. Specification of surface roughness tester is mentioned in Table 4.7 below.

Table 4.7 Specifications of the surface roughness tester

Parameter	Specification
Mass	190gm
Stylus	Diamond cone
Measuring speed	0.25mm/s and 0.5mm/s
Returning speed	0.8mm/s
Measurement Range	12.5mm along x-axis
Measurement force	0.75mN
Tip radius	2 μ m
Roughness standards	ISO, JIS, ANSI, DIN

4.12 PILOT EXPERIMENTATION

Initially, a pilot experiment was conducted to determine the rheological behavior of thermoplastic polymer as per ASTM D1238 standards by varying weight proportion of reinforcement. ABS was reinforced separately with Fe (collected from machine shop), WD (collected from Local SAW Mill), and BP (collected from the metallurgical lab) in different weight proportions i.e 2.5% wt., 5% wt., 7.5% wt., 10% wt. and 12.5% wt. It has been found that at 12.5% wt. nozzle clogging took place and there was a drastic decrease in MFR of prepared composite beyond reinforcement 10% wt. From MFR results, it has been concluded that at 10% wt. of reinforcements, the MFR of all composites was near to MFR of 2^o recycled ABS. Also, this wt.% of reinforcement gives maximum utilization of waste material.

After the selection of the maximum weight proportion of reinforcement, the next step was the preparation of feedstock filament with the help of TSE. From literature review it was found that mechanical properties of feedstock filament depends upon speed, load, and temperature, instead of environmental conditions. Therefore, three parameters have been selected (speed, temperature and load) while preparing feedstock filament. On increasing extruder speed beyond 100rpm, it has been found that the wire obtained from the extruder was very thin and it was not of uniform dia. throughout. Also, on speed 100rpm the wire obtained has not made proper bonding with the base matrix and gives more brittle wire. On selection of speed less than 70rpm, it was difficult to get filament from the nozzle.

Because this lower extruder speed was not sufficient to melt and force the material from the nozzle. The second parameter was load on increasing load beyond 15kg, the flow of

wire from the nozzle was high, and obtained filament obtained was hollow from inside. The third parameter was extruder temperature, the maximum temperature selected was 245°C because it was near to melting temperature of ABS. Therefore, the suitable parameters selected for preparing feedstock filament were speed (70rpm,80rpm, and 90rpm), load (10kg, 12.5kg, and 15kg.), and temperature (225°C, 235°C, and 245°C) were selected for preparation of feedstock filament. 27 filaments of 2⁰ABS reinforced separately with Fe, BP, and WD via mechanical blending have been prepared similarly 27 filaments of 2° ABS reinforced separately with Fe, BP, and WD via chemical assisted blending as shown in Figure 4.15 below and 9 filaments via. Mechanical- hybrid assisted blending has been prepared. Further, all prepared feedstock filaments were processed on UTM for optimizing filament fabrication conditions at a constant load of 5KN for determining the mechanical properties. All prepared filaments were undergoing three cycles of tensile testing, in the last, the average of all mechanical properties was measured to avoid an error.

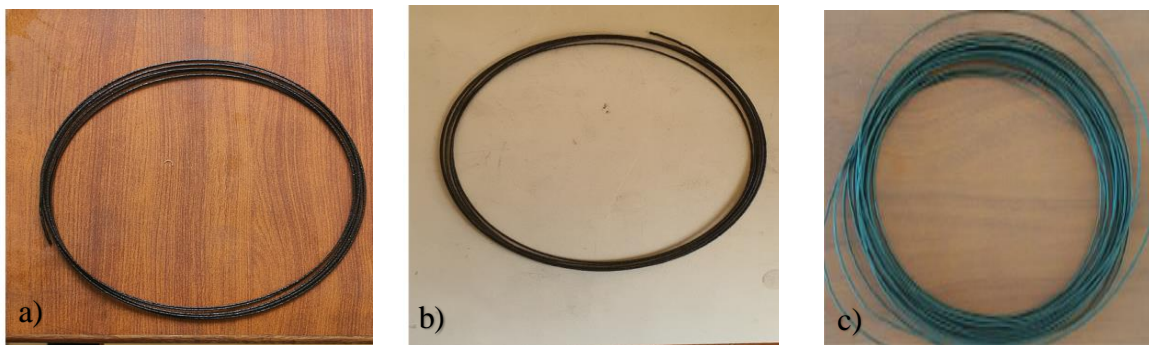


Figure 4.15 a) Feedstock filament prepared by reinforcing WD in ABS b) Feedstock filament prepared by reinforcing Fe in ABS c) Feedstock filament prepared by reinforcing BP in ABS

To examine the printability of recycled ABS-based filaments, tensile and flexural specimens were printed on FDM from the fabricated composite filaments having maximum PS. The mechanical and chemical assisted blending-based composite filaments were utilized to print multi-layered (layers of different composite material) tensile specimens whereas single-layered tensile specimen was printed from composite filament based on mechanical-hybrid blending. The outer three layers on both sides of the multi-layered tensile specimen were printed with filament reinforced with BP and Fe powder whereas the inner layers were composed of WD reinforced filaments. During this trial printing process, it has been found that nozzle temperature should be equal to and more than the melting temperature of base material because by keeping extruder temperature lower than 245°C the material coming from the nozzle was not in molten form therefore it was kept constant 270°C. A second fixed

parameter was the infill pattern while doing pilot experimentation it has been found that specimens prepared at multi-layer printing having honeycomb infill pattern show very little peak strength, therefore, the rectilinear pattern has been selected in the present study. While doing multi-layer printing layer combination was done on the thermal analysis as mentioned above. The first three layers of ABS+ BP next three layers of ABS+WD and the last three layers of ABS+ Fe were done. While selecting different variables such as infill density, raster angle, and infill speed from the literature it has been found that at low raster angle strength will be maximum and raster angle should vary in the interval of 45 therefore pilot experiment was done at 0° and 90° raster angle and it was found that maximum strength was obtained at 0° and minimum at 90°. Similarly, in the case of infill density and speed. Therefore, parameter selected in present study are raster angle (0°, 60° and 90°), infill speed (20mm/sec, 30mm/sec, 40mm/sec) and infill density (80%,90% and 100%). After studying the different mechanical properties of all prepared specimens next step is post-processing. For post-processing two techniques have been used one is chemical vapor smoothing (CVs) and the second technique is heat treatment. While using the CVs technique three parameters have been selected one is smoothing time, second is soaking time and third is the number of cycles. Initially while doing CVs for 10s it was found that small vapors get deposited with an increase in smoothing time by 20 sec it was found that more vapors get deposited on the surface. Similarly, with an increase in the number of cycles more surface get smoothed by depositing acetone. On further increase in the number of cycles beyond 4, it was found that change in surface roughness becomes constant. Therefore, the first parameter used in CVs is the number of cycles (2,3,4) second parameter is smoothing time (15sec, 20sec, and 25sec) and the third parameter is soaking time (15min, 20min, and 25min.) for evaluating the change in surface roughness and shore Hardness.

The second post-processing technique was heat treatment, from the literature it was found that on heating 3D printed specimen around its glass transition temperature the gap between the adjacent layer gets filled, and also surface roughness also gets improved due to reflow of the ABS between the adjacent layers. While using this post-processing technique three parameters have been selected first in heating temperature and second in heating time. Initially, the heating temperature taken was 90°C and the heating time was 10 min and it was found that there was no improvement in the surface roughness of the specimen. On further increase in heating temperature, i.e 100°C and heating time 20min there was an improvement in surface roughness was found. Therefore, parameters selected for heat treatment were

heating time (15min, 20min, and 30min) and heating temperature (100°C, 110°C, and 120°C). So, in the present study, different parameters have been selected based on pilot experimentation as shown in Table 4.8 below.

Table 4.8 Final Parameters for Experimentation

Stages	Process	Parameters	Level
Stage 1	Fused Filament	Load (kg)	10,12.5,15
		Extruder Temperature (°C)	225,235,245
		Screw speed (rpm)	70,80,90
Stage 2	FDM	Infill density (%)	80,90,100
		Infill speed (mm/s)	20,30,40
		Raster angle (degree)	0°,30°,60°
Stage 3	CVS	Cycle Time (sec)	15,20,25
		Soaking Time (min)	15,20,25
		Number of cycles	2,3,4
	Heat Treatment	Heating temperature (°C)	100,110,120
		Heating time (min.)	10,15,20

4.13 DESIGN OF EXPERIMENT

The Design of Experiment (DOE) is a scientific approach used to investigate several factors at a time to get generalized conclusions. DOE is a general approach to improve product quality with limited use of resources. The DOE strategy empowers users to assess the individual effect of every parameter along with the interactions because of different parameters. The full factorial plan is another DOE device that takes all potential combinations to examine the impact of every interaction and parameter on response. The design can adequately contemplate two, three, or four parameters however as the number of parameters increases, the number of experiments will also increase which would require more time and cost. Taguchi DOE approach has been applied for optimizing the process parameters. The Taguchi techniques were created by a Japanese analyst G. Taguchi who backs limiting the deviation from target esteem which gives a strong design for controlling uncontrollable noise factors.

The Taguchi method divides all the problems into two classes one is static and another is dynamic. The static issues don't have signal variables and the enhancement is accomplished with three kinds of SN ratio one is larger the best, smaller the best, and nominal the best. Taguchi has proposed three phases in process development [204] through tolerance design, system, and parameter design. In the last few decades, many manufactures and researchers have used Taguchi's DOEs technique in process optimization and product design. As already mentioned, the goal of this strategy is to design the experiment with the parameters which give ideal outcomes. The Taguchi DOE technique has been used by many researchers for optimizing various input parameters and found that it is a suitable tool for optimizing the cost of Additive manufacturing [205-206]. The Taguchi procedure is a methodology for product optimization strategy and recommends eight stages of preparation, leading and assessing results of the examination runs to decide the best parametric condition. The essential objective is to keep the fluctuation very low made a robust design against all variations.

4.14 ORTHOGONAL ARRAY SELECTION

To solve complex systems special orthogonal array (O.A) is used in which entire process parameters can be studied with a small number of experiments. The utilization of the term OA with Taguchi's strategy permits the impacts of a few parameters to be determined efficiently and is a significant method in robust design [207]. When the controllable parameters influencing have been identified, the levels at which these parameters affect the process to be identified and should be varied. Deciding on levels of a variable to test requires a top to bottom comprehension of the interaction, including the maximum, minimum, and current value of the parameter. For the choice of a proper OA, the accompanying technique should be utilized [208]:

- Define the number of factors and their levels
- Determine Degree of freedom (DOF)
- Selection of orthogonal array
- Consider any interaction

The degree of freedom is defined as the minimum number of treatment conditions. According to Taguchi's technique, the DOF of selected OA should be more or equivalent to the DOF desired as per the experiment. In this investigation, there are three variables

with three levels each. DOF of each level is given by (n-1), where 'n' is the number of levels of the factor. In this way, all the factors have 2 DOF, in this way, the most reasonable symmetrical cluster of three-level components was described as L9 with 8 degrees of freedom. This OA comprises 3 columns allocating factors and 9 rows for assigning the test conditions. Section 1 can oblige factors with two levels, though any remaining segments can oblige factors with three levels. The table shows the assigned factors and their levels to three columns of L9 OA. Raster angle is assigned to row 1, infill density and infill speed are assigned to row2 and 3. The table shows the assigned factors and their levels to four columns of L9 OA. The response parameters selected in the present study were peak strength, % Break elongation, and shore hardness of specimen prepared with the help of a 3D printer.

4.15 SIGNAL-TO-NOISE RATIO (S/N)

Taguchi helps in defining the deviation between the experimental value and the target value [208]. This deviation is then transformed into a signal-to-noise ratio, which is a statistical tool for measuring performance. S/N ratio determines the inverse of the coefficient of variation, i.e. it determines the ratio μ/σ , where μ defines the process means (signal) and σ (noise) the process standard deviation [210]. In the Taguchi method, a larger value of the S/N ratio is desirable because a larger S/N ratio will result in a smaller product variance around the target value. So, the level with maximum S/N ratio is considered as the optimal level of the control factor. The S/N ratios can be classified into three categories [208]:

Larger the better;

$$\frac{S}{N} = -10 \times \log_{10} \left\{ \frac{1}{n} \sum_{i=1}^n \frac{1}{Y_i^2} \right\} \quad (1)$$

Smaller the better;

$$\frac{S}{N} = -10 \times \log_{10} \left\{ \frac{1}{n} \sum_{i=1}^n Y_i^2 \right\} \quad (2)$$

Where 'n' is the number of measurements and 'Yi' is the observed characteristic value

Nominal the best;

$$\frac{S}{N} = 10 \times \log_{10} \left(\frac{\mu^2}{\sigma^2} \right) \quad (3)$$

Where μ is mean and calculated with the help of the below relation

$$\frac{1}{n} \sum_{i=1}^n Y_i^2 \quad (4)$$

Similarly, variance is calculated with the help of the following relation.

$$\sigma^2 = \frac{\sum_{i=1}^n (Y_i - \sigma)^2}{(n-1)} \quad (5)$$

Where 'n' represents the number of observations, Y is the observed data and S/N is the signal-noise ratio.

4.16 ANALYSIS OF VARIANCE (ANOVA)

ANOVA is one of the most powerful tools used for analyzing the data. ANOVA is utilized to determine the impact of the control factors on the experimental outcomes. It helps in anticipating the meaning of each input variable and the percentage contribution of each variable to the required output. More percentage contribution shows more effect of input variable on output. By controlling the variables having maximum contribution, the output can be improved by reducing the variations that help in improving the process performance. The following steps are used in ANOVA for analyzing the experiment.

- (i) Calculate the total number of readings of individual repetitions:

$$= \sum Y_{ij} \quad (6)$$

Where i represents number of repetitions and j is number of runs.

- (ii) Determine the Correction Factor:

$$CF = \frac{T^2}{n} \quad (7)$$

Where n represents number of runs

(iii) Calculate Sum of the squares (SS_T) for all readings.

$$SS_T = \sum_{j=1}^R Y_{ij}^2 - CF \quad (8)$$

Where R is the repetitions

(iv) Calculate Sum of Square between the repetitions (SS_{between})

$$SS_{\text{between}} = \sum T_j^2 / n - CF \quad (9)$$

(v) Find out sum of square with in the repetition (SS_{within}).

$$\sum_{j=1}^R Y_{ij}^2 - CF - \sum T_j^2 / n - CF \quad (10)$$

(vi) Find out Degree of Freedom (DOF)

$$\text{Total DOF } (f_T) = (\text{total number of trials} - 1) = (R \times n - 1)$$

$$\text{DOF between the samples} = (\text{number of repetitions} - 1) = (i - 1)$$

$$\text{DOF within the samples} = (\text{number of runs} - 1) = (j - 1)$$

(vii) F- ratio is refined as the ratio of variance of each factor to the error variance.

In last represent all above calculated values in ANOVA Table 4.9

Source of Variation	Sum of Squares (SS)	Degree of Freedom (DOF)	Mean of square (MS)	F- ratio
Between the repetitions	SS_{between}	$i - 1$	$\frac{SS_{\text{between}}}{i - 1}$	$\frac{MS_{\text{between}}}{MS_{\text{within}}}$
With in the repetition	SS_{within}	$j - 1$	$\frac{SS_{\text{within}}}{i - 1}$	
Total	SS_T	$RXn - 1$	$\frac{SS_T}{RXn - 1}$	

The value of the calculated F-ratio for a factor is then compared with the critical value of F which is tabulated at a chosen level of significance α (95% confidence level). When the calculated F-ratio value for a factor is greater than the tabulated value of F-ratio, then the factor is a significant factor. If the calculated value of the F-ratio is less than the tabulated F-ratio, then that factor is considered to be an insignificant factor.

CHAPTER-5

RESULT AND DISCUSSION

5.1 PHASE 1- (FUSED FILAMENT PREPARATION)

5.1.1 Mechanical Assisted Blending

MFR: In the present work, 2° recycled ABS purchased from the local market (Batra Polymers, Ludhiana) has been selected as a base material for the fabrication of FDM fused filament. The results of MFR performed as per ASTM D 1238 standard (230°C, 3.8 kg load) with a different weight percentage of reinforced materials have been presented in Table 5.1. Initially, the MFR of recycled ABS without any reinforcement was investigated (average of 5 repetitions) and found to be 16.32 g/10min. In the next step, different reinforcements (BP, WD and Fe) in the proportion of 2.5 % to 10 % by weight have been added separately to the ABS matrix and their MFR has been investigated.

Table 5.1 MFR of 2° recycled ABS with and without reinforcements

S. No.	Sample	MFR (g/10 min)					Average MFR (g/10 min)	Standard Deviation
1	2°recycled ABS	17.0	16.2	16.5	15.9	16.0	16.32	0.44
2	2°recycled ABS +2.5% BP	20.5	21.7	21.8	20.8	21.5	21.26	0.57
3	2°recycled ABS +5% BP	18.0	17.2	18.7	18.4	19.1	18.28	0.72
4	2°recycled ABS +7.5% BP	16.1	16.1	16.2	16.3	16.5	16.24	0.16
5	2°recycled ABS +10% BP	14.4	15.1	14.3	14.8	15.2	14.76	0.40
6	2°recycled ABS +2.5% WD	20.8	21.8	22.2	21.2	21.5	21.50	0.53
7	2°recycled ABS +5% WD	26.7	28.5	27.5	27.3	28.4	27.68	0.76
8	2°recycled ABS +7.5% WD	17.7	18.4	18.8	17.8	18.5	18.24	0.47
9	2°recycled ABS +10% WD	14.1	13.8	14.8	13.6	14.2	14.10	0.45
10	2°recycled ABS + 2.5% Fe powder	20.5	18.9	21	19.9	21.3	20.32	0.95
11	2°recycled ABS +5% Fe powder	21.3	22.7	24.8	23.2	22.9	22.98	1.25
12	2°recycled ABS + 7.5% Fe powder	20.3	19.4	20.2	19.8	20.1	19.96	0.36
13	2°recycled ABS + 10.0% Fe powder	20.2	19	16.8	18.4	17.5	18.38	1.31

From Table 5.1, it has been observed that the addition of any reinforcements (BP/WD/Fe) initially increases the MFR of composite filament as compared to 2° recycled ABS

filament. However, with an increase of reinforcement level from 5%-10% in ABS, the MFR of all three composite filaments starts decreasing. It may be due to improper mixing of reinforced particles in the ABS matrix which resists the flow of heat. An increase in reinforcement percentage (of BP/WD/Fe) beyond 10% leads to nozzle clogging in the case of WD whereas highly brittle wire was formed in the case of both BP and Fe. Since, the MFR in all three cases (ABS+BP, ABS+WD and ABS +Fe) at reinforcement of 10% by weight is near to the MFR of recycled ABS, therefore 10% reinforcement in ABS matrix has been selected for the fabrication of fused filaments by TSE. Also, this level of reinforcements results in better utilization of waste material in the present case.

Tensile Testing: The fused filaments were prepared by taking 90% 2° recycled ABS and 10% reinforcement (BP, WD and Fe) respectively using TSE as per the conditions mentioned in Table 1.1. For analyzing various mechanical properties like peak strength, break strength, peak elongation, break elongation, modulus of toughness and modulus of elasticity of the fabricated filaments, a tensile test has been performed on UTM on load rate of 25mm/min. The results obtained for filament reinforced with BP, WD and Fe have been shown in Table 5.2, 5.3 and 5.4 respectively.

Table 5.2 Responses for 2° recycled ABS filament reinforced with BP (90:10)

S.No	PS (MPa)	BS (MPa)	% PE	% BE	E (GPa)	T (MPa)
1	30.82±1.7	27.74±1.6	4.4±0.6	5.3±0.7	0.695±0.15	0.835±0.3
2	28.36±1.5	26.42±1.4	3.5±0.4	4.2±0.5	0.746±0.25	0.544±0.2
3	23.85±0.9	21.47±0.8	3.8±0.5	3.8±0.4	0.636±0.2	0.408±0.15
4	29.10±1.4	26.82±1.3	3.1±0.3	3.7±0.4	0.919±0.35	0.467±0.2
5	26.33±1.2	26.19±1.2	2.8±0.2	3.1±0.3	0.924±0.4	0.539±0.25
6	29.80±1.4	23.69±1.1	3.1±0.2	4.9±0.6	0.917±0.3	0.525±0.2
7	27.20±1.3	27.74±1.4	2.2±0.3	2.7±0.3	0.781±0.3	0.615±0.25
8	30.82±1.6	24.48±1.5	4.3±0.4	5.0±0.5	0.573±0.2	0.736±0.35
9	28.23±1.3	22.71±1.2	3.4±0.3	4.4±0.4	1.323±0.4	0.252±0.15

Based on Table 5.2, Table 5.3 and 5.4, it has been observed that with the increase in speed, the PS and %BE of all the filaments start decreasing. This may be due to the improper bonding between matrix material and reinforcement at high speed that resulted in poor mechanical properties.

Table 5.3 Responses for 2° recycled ABS filament reinforced with WD (90:10)

S.No	PS (MPa)	BS (MPa)	% PE	% BE	E (GPa)	T (MPa)
1	25.66±1.4	22.01±1.5	5.3±0.6	6.0±0.7	0.477±0.1	0.697±0.2
2	24.46±1.5	23.10±1.4	3.1±0.3	4.1±0.4	0.772±0.25	0.475±0.15
3	21.60±1.1	19.44±1.2	2.8±0.3	3.8±0.5	0.758±0.2	0.369±0.15
4	23.84±1.3	21.45±1.4	2.8±0.4	3.7±0.6	0.396±0.1	0.679±0.25
5	20.15±1.0	16.11±1.2	2.8±0.3	3.1±0.3	0.711±0.2	0.255±0.1
6	24.13±1.2	21.72±1.1	4.8±0.5	5.7±0.5	0.862±0.25	0.378±0.2
7	18.84±0.8	20.39±1.1	2.8±0.3	3.4±0.4	0.632±0.15	0.372±0.15
8	22.66±1.3	16.96±1.2	4.5±0.4	5.4±0.6	0.894±0.2	0.232±0.1
9	20.21±1.2	18.19±1.2	2.5±0.2	3.3±0.4	0.836±0.25	0.230±0.15

Table 5.4 Responses for 2° recycled ABS filament reinforced with Fe (90:10)

S.No	PS (MPa)	BS (MPa)	% PE	% BE	E (GPa)	T (MPa)
1	32.82±1.1	28.98±1.3	2.85±1.2	3.17±1.5	0.942±1.1	0.46±1.0
2	30.36±1.3	26.43±1.0	3.48±1.3	3.85±1.1	0.504±1.0	0.50±0.9
3	28.99±1.5	23.09±0.8	3.48±1.5	3.98±1.2	0.907±0.8	0.45±1.2
4	30.77±1.3	29.88±1.4	2.85±1.1	4.32±1.5	0.892±1.5	1.10±1.3
5	28.51±0.8	27.69±1.1	3.48±0.8	8.25±1.0	0.813±1.1	1.57±1.0
6	35.43±1.4	25.65±1.5	7.28±1.2	3.18±1.1	1.115±1.5	0.61±1.1
7	26.46±1.0	26.70±1.5	2.85±1.3	6.97±1.2	0.542±1.2	0.541.0
8	31.43±1.5	23.82±1.3	5.38±0.4	3.82±1.3	0.450±1.0	0.83±1.1
9	29.67±1.2	28.12±1.2	2.85±0.2	3.87±1.4	0.537±1.5	0.42±1.0

At low speed, composite gets sufficient time and uniform blending of reinforcement into ABS matrix takes place which helps in exhibiting ductile behavior. Also, the PS of filaments reinforced with Fe was quite higher as compared to filament reinforced with WD and BP at the same parametric settings. It was mainly because of the high specific heat capacity of reinforced Fe in the ABS matrix. Due to its high specific heat capacity, the composite can retain a high amount of heat (energy) which in turn ensures smooth flow of material and thus exhibit better mechanical properties. Further, the spherical structural shape of BP in the ABS matrix can also be responsible for superior mechanical properties as compared to WD particles having a 2-D structure. As the spherical shaped BP and Fe particles occupied more volume in the ABS matrix as compared to 2-D structured WD

particles, the porosity of the Fe reinforced composite filament decreases which ultimately results in high PS.

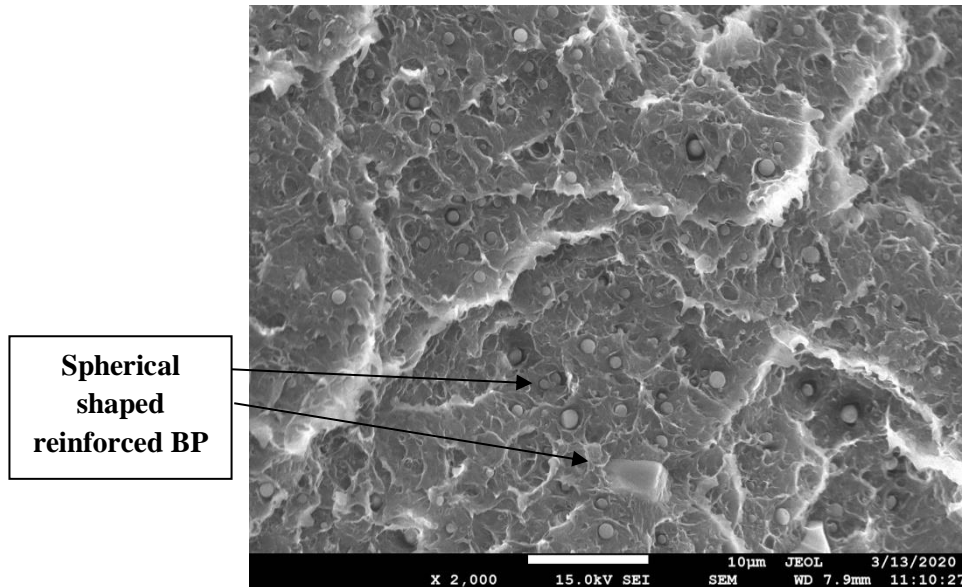


Figure 5.1 SEM image of BP reinforced filament at X 2000

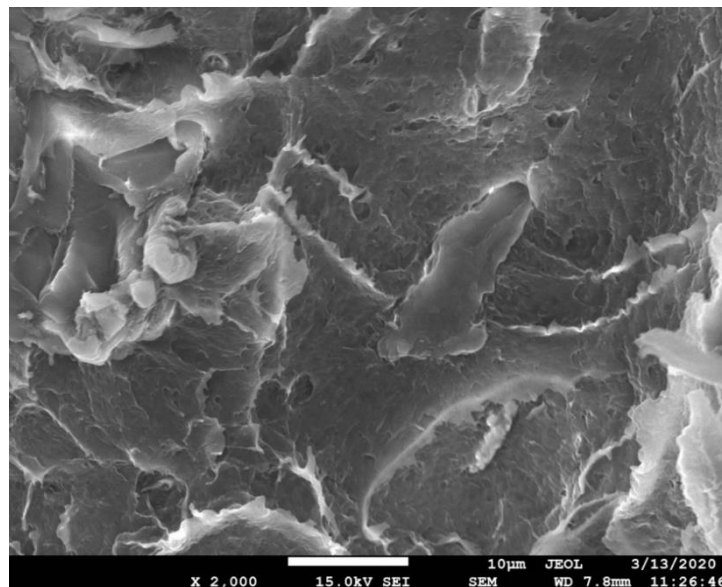


Figure 5.2 SEM image of WD reinforced filament X 2000

The scanning electron microscopic (SEM) images at the break cross-section of all three filaments (having maximum PS) reinforced with Fe, BP and WD have been shown in Figures 5.1-5.3 respectively which indicates the presence of spherical shaped reinforced BP

and Fe in the ABS matrix. However, the WD particles were not visible in the SEM image due to their highly non-conductive nature.

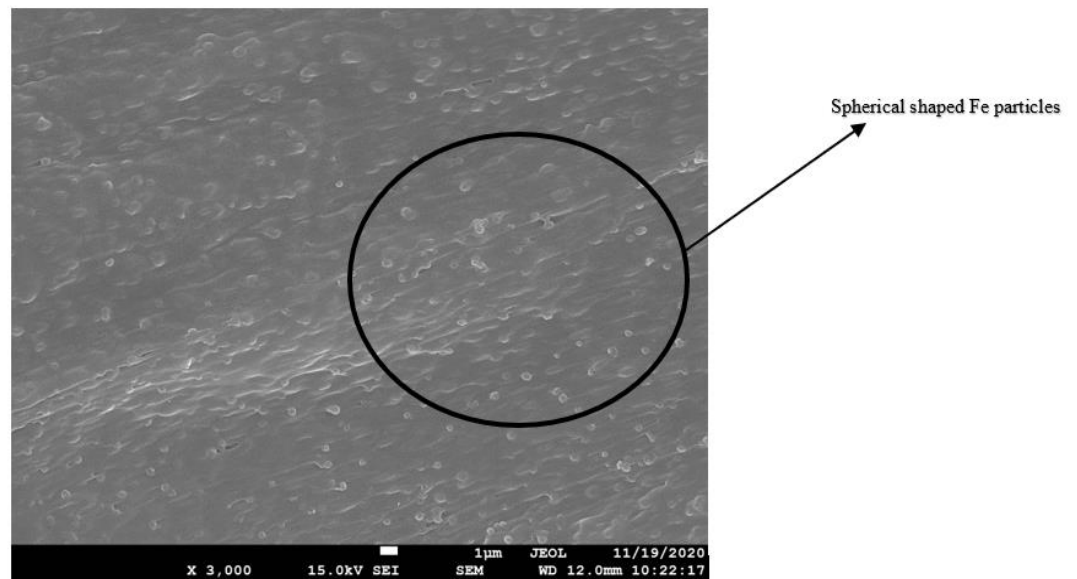


Figure 5.3 SEM image of Fe reinforced filament X 3000

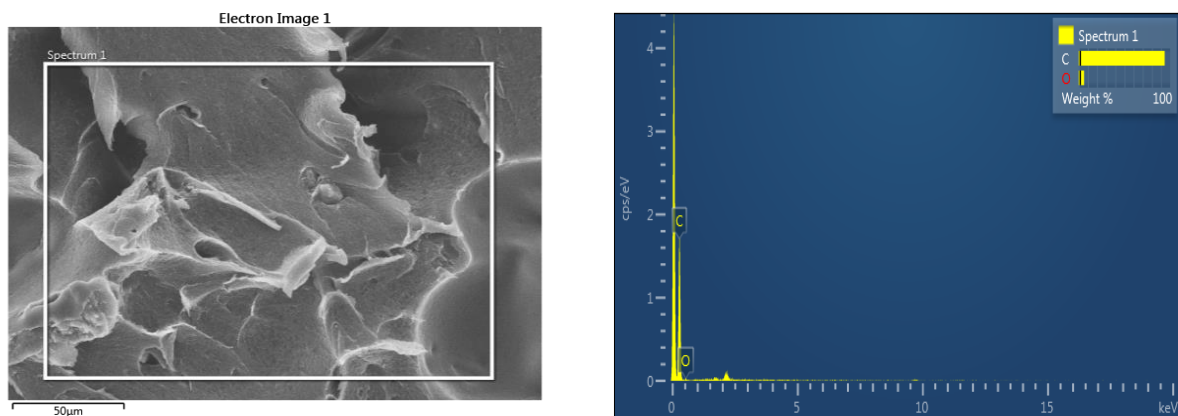


Figure 5.4 EDS analysis of filament possessing maximum PS fabricated by reinforcing BP

Further EDS analysis (point mapping) has been done for determining the composition percentage of elements present in filaments as shown in Figure 5.4-5.6. From EDS analysis it has been found that element composition in BP fused filament was 95.43% atomic weight % of C, 4.57% atomic weight % of O, whereas element composition of WD reinforced filament was 95.47% atomic weight %, 4.53% atomic weight % of O, similarly for Fe reinforced filament element composition was 99.87% atomic weight% was C and 0.13% atomic weight % was Fe.

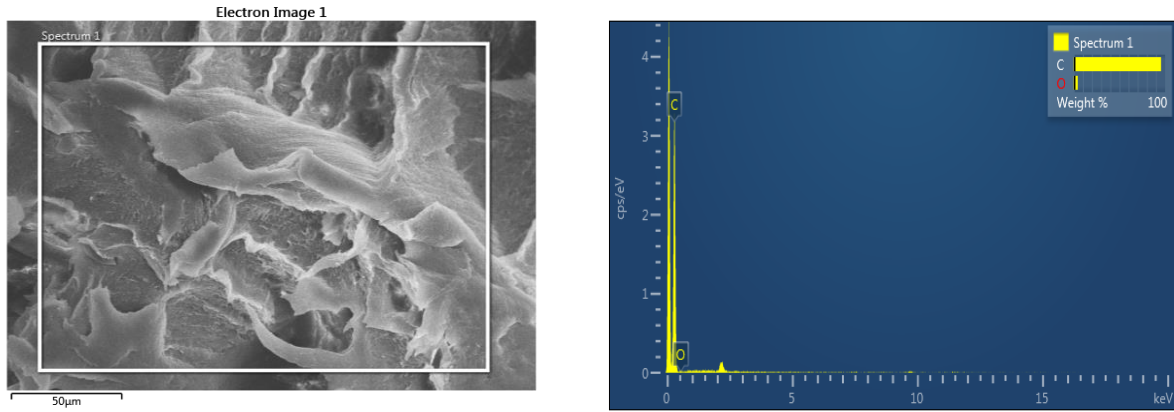


Figure 5.5 EDS analysis of filament possessing maximum PS fabricated by reinforcing WD

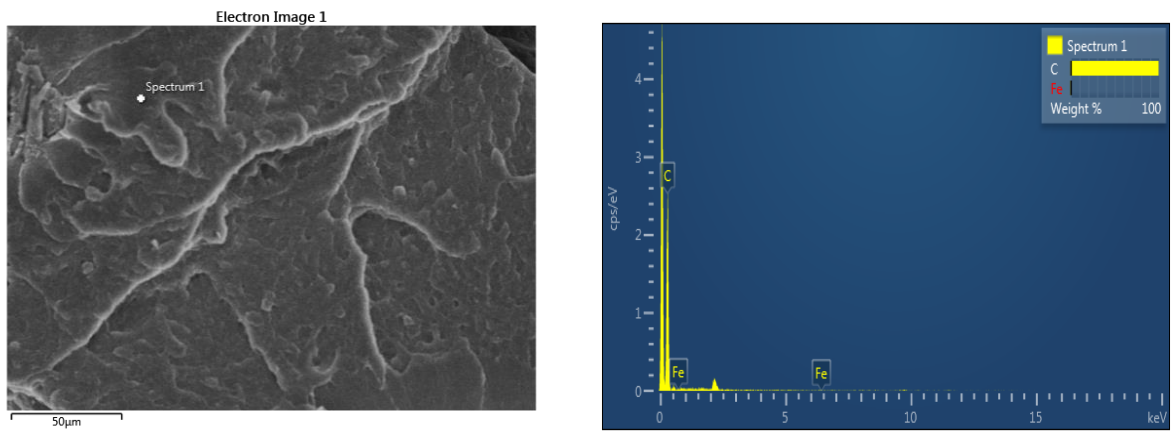


Figure 5.6 EDS analysis of filament possessing maximum PS fabricated by reinforcing Fe

The Stress-Strain curve of ABS reinforced with BP, WD and Fe has been shown in Figures 5.7, 5.8 and 5.9 respectively. While doing tensile testing, it has been observed that strain was in the direction of load and no negative strain was investigated. Modulus of elasticity (E) and modulus of toughness (T) for the fabricated filaments were calculated based on the data collected (Table 5.2, 5.3 and 5.4) as follows:

$$\text{Modulus of Elasticity (GPa)} = \frac{\text{Peak Strength}}{\text{Peak Elongation}} \times \text{Original length} \quad (11)$$

$$\text{Modulus of Toughness (MPa)} = \frac{1}{2} \times \text{Break Strength} \times \frac{\text{Break Elongation}}{\text{Original length}} \quad (12)$$

Modulus of Toughness (T) indicates the amount of energy absorbed by the filament per unit volume before fracture. It also represents the area under the stress-strain curve. From Table 5.2, the highest value of T (0.835 MPa) was observed for Sample 1 while a low value of T was observed for Sample 9 (0.252 MPa) when ABS was reinforced with BP.

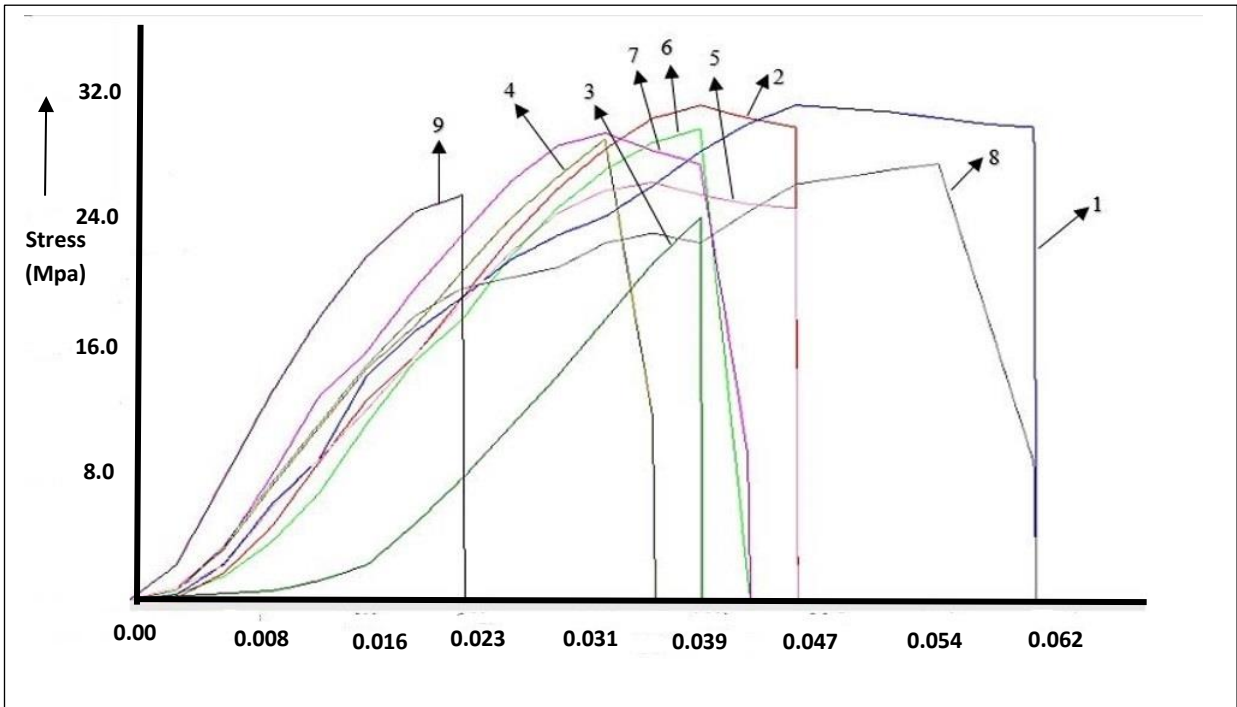


Figure 5.7 Stress versus strain curve of ABS reinforced with BP

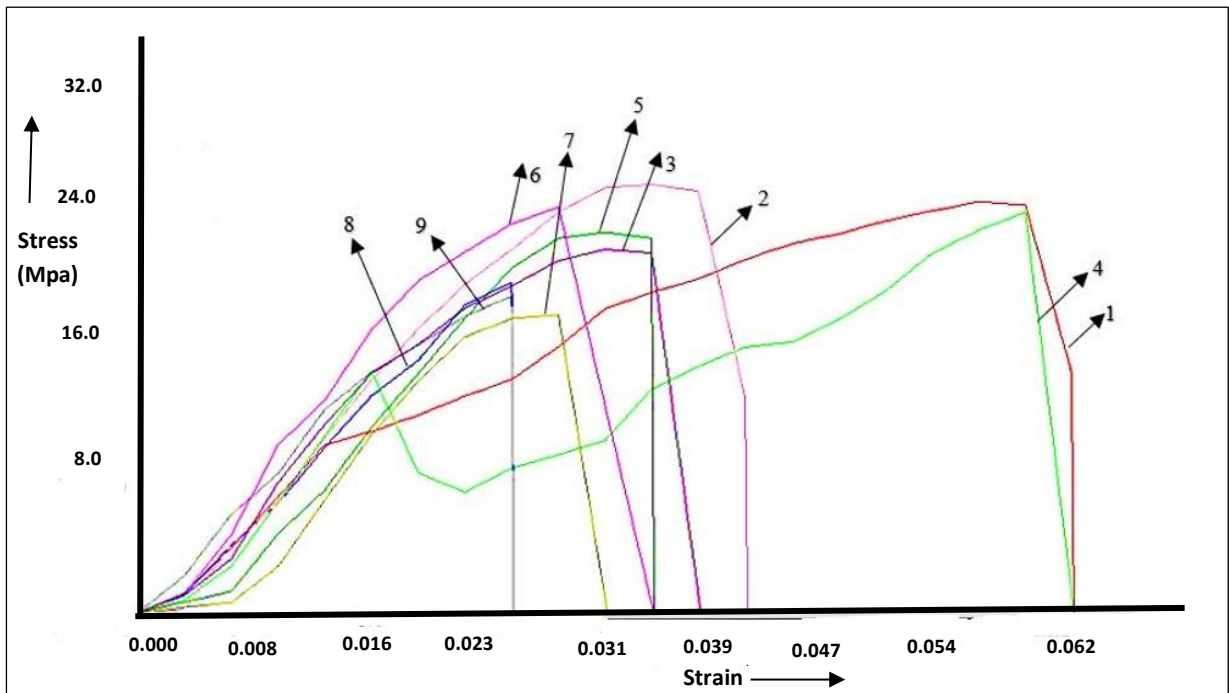


Figure 5.8 Stress versus strain curve of ABS reinforced with WD

Similarly (Refer Table 5.3), when ABS is reinforced with WD, Sample 1 (0.697 MPa) yields the highest value of T and a lesser value of T was observed for Sample 9 (0.230 MPa). From Table 5.4 when ABS reinforced with Fe Sample No. 5 has maximum toughness i.e 1.57 MPa

were as sample 9 has minimum toughness i.e 0.42 MPa. Also, filament fabricated by reinforcing Fe possesses higher T (more energy absorbing capacity) as compared to filament reinforced with WD (Refer Table 5.2-5.4).

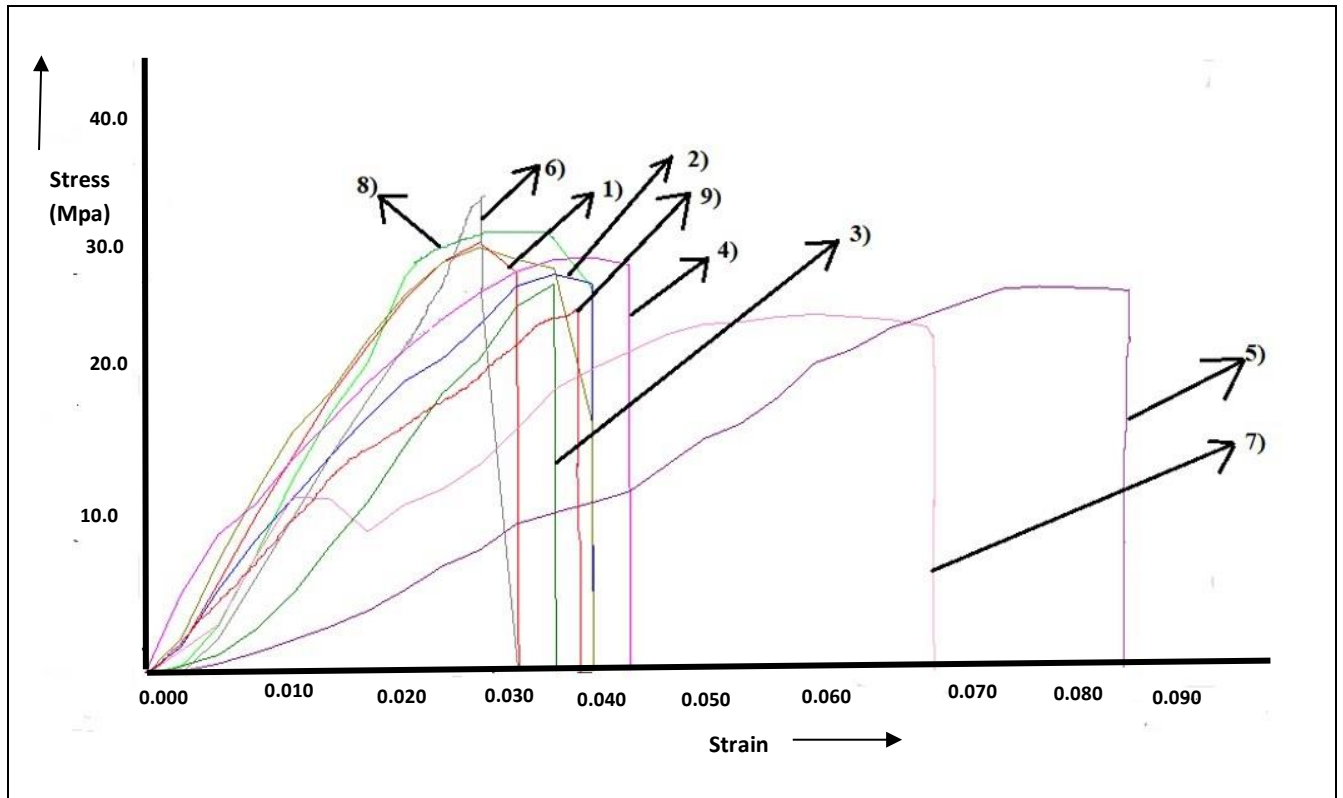


Figure 5.9 Stress versus strain curve of ABS reinforced with Fe

To determine the presence and nature of bonds formed between the base and reinforced materials that ultimately effects the PS of the composite filament, FTIR analysis was performed. The FTIR analysis of filaments having maximum PS fabricated by different blending techniques is shown in Figure 5.10. During FTIR analysis of BP, WD and Fe reinforced composite filament ((a-c)), the formation of a first medium peak at wave number in the range of 3725 cm^{-1} to 3750 cm^{-1} represents O-H bond stretching confirming the presence of bakelite in the prepared composite. The second sharp peak at wavenumber close to 2925 cm^{-1} indicates C-H bond stretching of ABS thermoplastic (alkane). Both the O-H and C-H bonds require significantly higher bond dissociation energy that ultimately corresponds to better strength of the BP reinforced composite filaments. the third medium peak at a wavenumber of 1480 cm^{-1} represents C-H bond bending and C-C bond stretching due to aromatic rings present in ABS thermoplastic

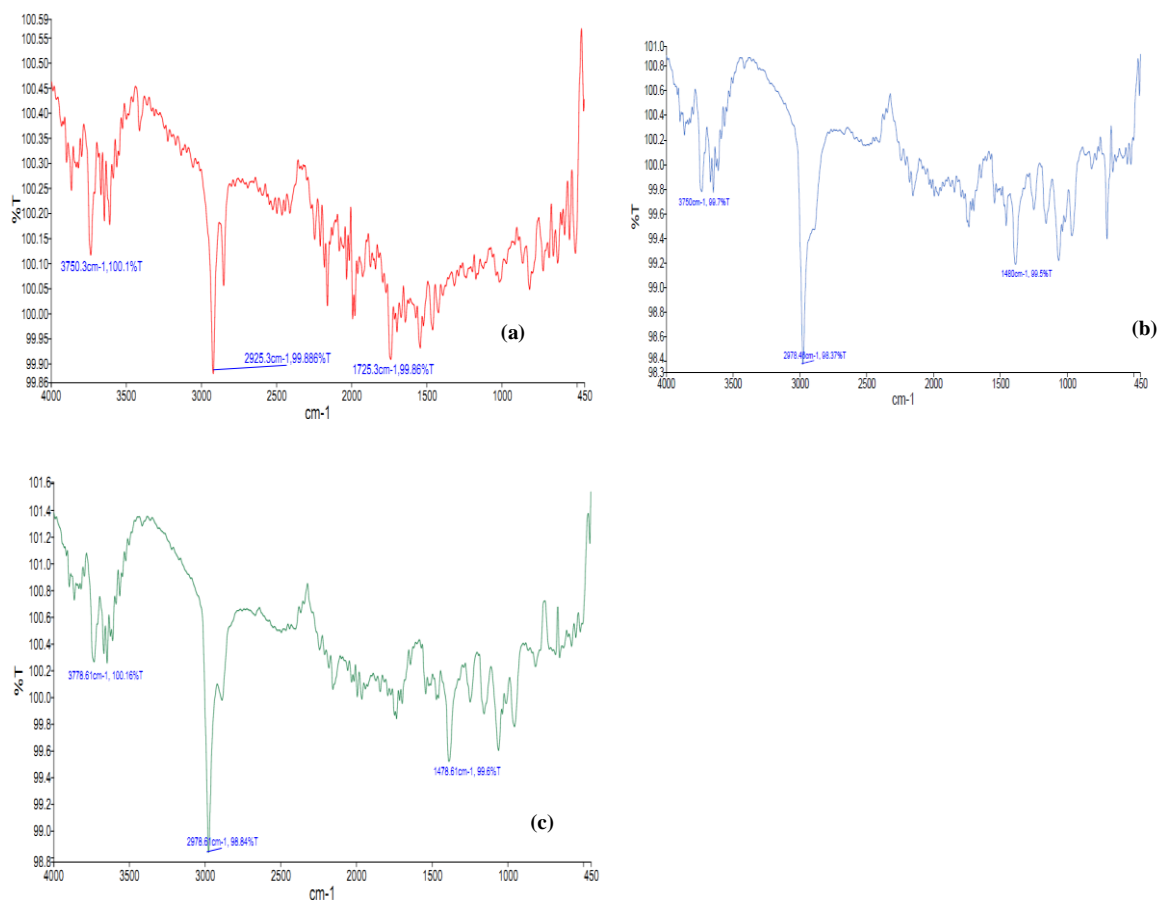


Figure 5.10 FTIR of composite filaments having maximum PS (a) mechanically blended ABS+BP, (b) mechanically blended ABS+WD, (c) mechanically blended ABS+Fe.

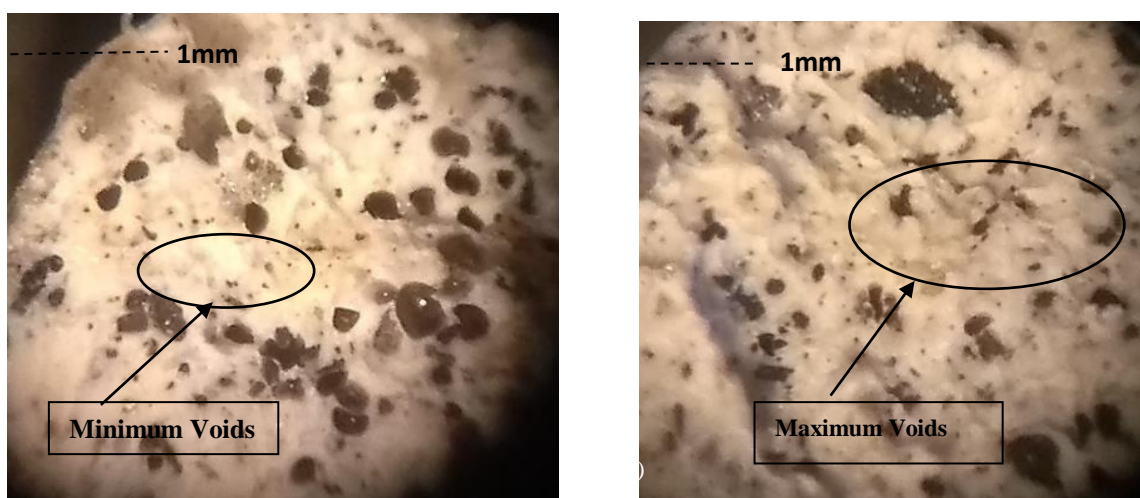


Figure 5.11 Photomicrographs at cross-section for BP reinforced filament having maximum and minimum peak strength

Further, photomicrographs at the break cross-section for the filaments having maximum and minimum peak strength were taken at X 30 (Figure 5.11-5.13). From the photomicrographs, it has been ascertained that more asperities at the cross-section were responsible for poor mechanical properties.

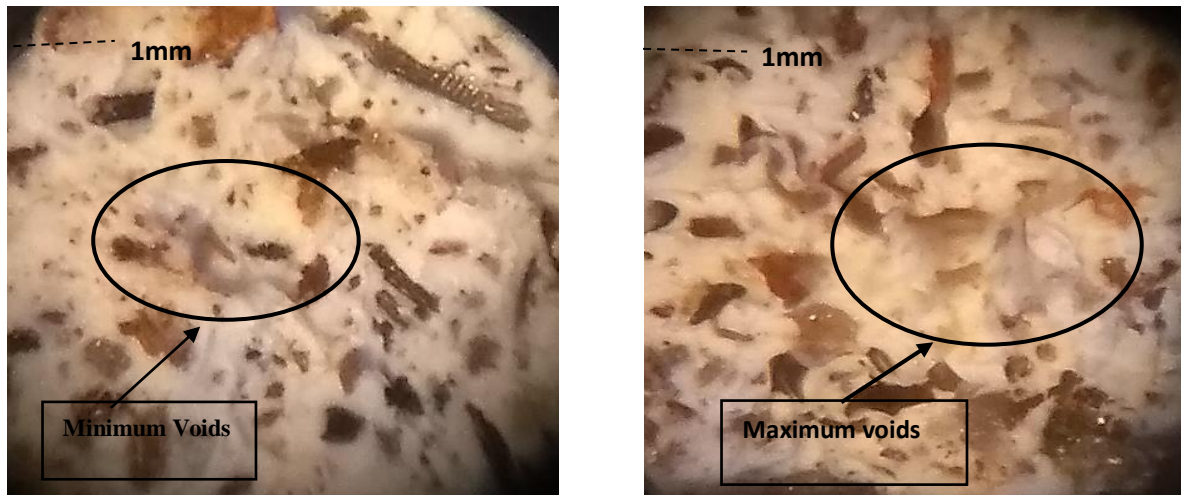


Figure 5.12 Photomicrographs of cross- section for WD reinforced filaments having maximum and minimum peak strength

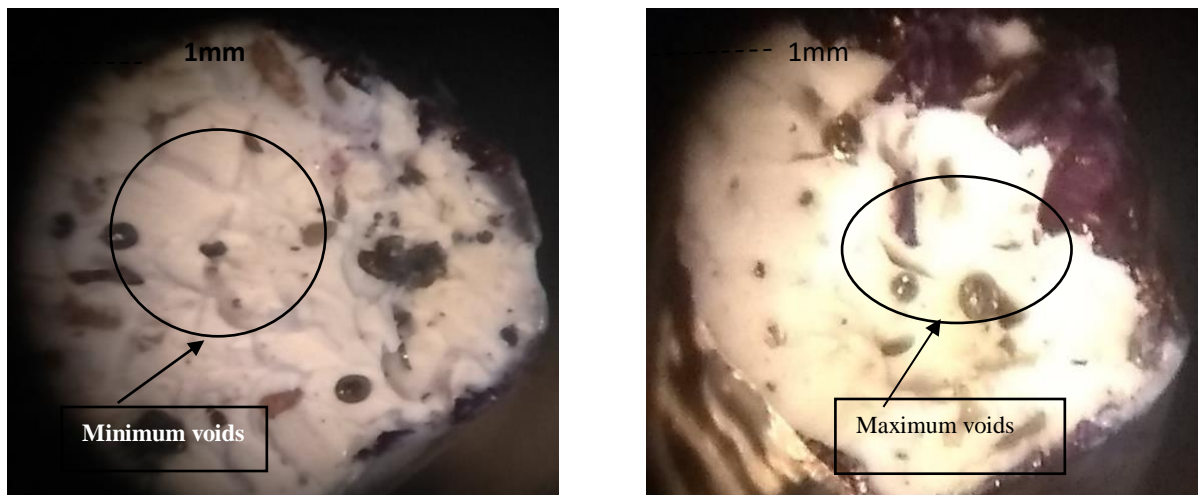


Figure 5.13 Photomicrographs at cross-section for Fe reinforced filament having maximum and minimum peak strength

Further, Signal to noise (S/N) ratio for PS and %BE were calculated based on the ‘larger is better’ approach using Eq. (1) and represented in Table 5.5

Table 5.5 S/N ratios for PS and %BE

S No.	Filament reinforced with BP		Filament reinforced with WD		Filament reinforced with Fe	
	S/N ratio for PS (dB)	S/N ratio for % BE (dB)	S/N ratio for PS (dB)	S/N ratio for % BE (dB)	S/N ratio for PS (dB)	S/N ratio for % BE (dB)
1	29.78	14.52	28.19	15.65	30.15	10.02
2	29.05	12.53	27.77	12.30	29.64	11.70
3	27.55	11.60	26.69	11.71	29.24	11.99
4	29.28	11.55	27.55	11.55	29.76	12.70
5	28.41	9.88	26.09	10.02	29.09	18.32
6	29.48	13.86	27.65	15.19	30.98	10.04
7	28.69	8.69	25.50	10.83	28.45	16.86
8	29.78	14.01	27.11	14.70	29.92	11.64
9	29.01	12.93	26.11	10.55	29.44	11.75

Based on the calculated values of S/N ratios, the mean effect plot for PS and %BE for all filaments were obtained and shown in Figures 5.14-5.16 respectively. The peak strength of BP reinforced filament increases slightly with an increase in load from 10 kg to 15 kg. However, the same decreases sharply as the load changes from 10 kg to 15 kg for WD reinforced filament. While peak strength of ABS reinforced with Fe increases from 10kg to 12.5 Kg load and then decreases by increasing load up to 15kg load. The effect of load on PS for WD and Fe reinforced filament was much higher as compared to BP reinforced filament. As the temperature increases, the PS for all reinforced filament decreases slightly. Speed comes out to be the predominant factor affecting the PS of all fused filaments. With the increase in speed, the PS drops dramatically may be due to poor intermolecular bonding between the ABS and reinforced material. The parametric conditions that yielded maximum PS for BP reinforced filament were 15 kg load, 225°C temperature and 70 rpm speed whereas 10 kg load, 225°C temperature and 70 rpm speed provides maximum strength to WD

reinforced filament, whereas 12.5kg load, 245°C temperature and 70 rpm speed provides maximum strength to Fe reinforced filament

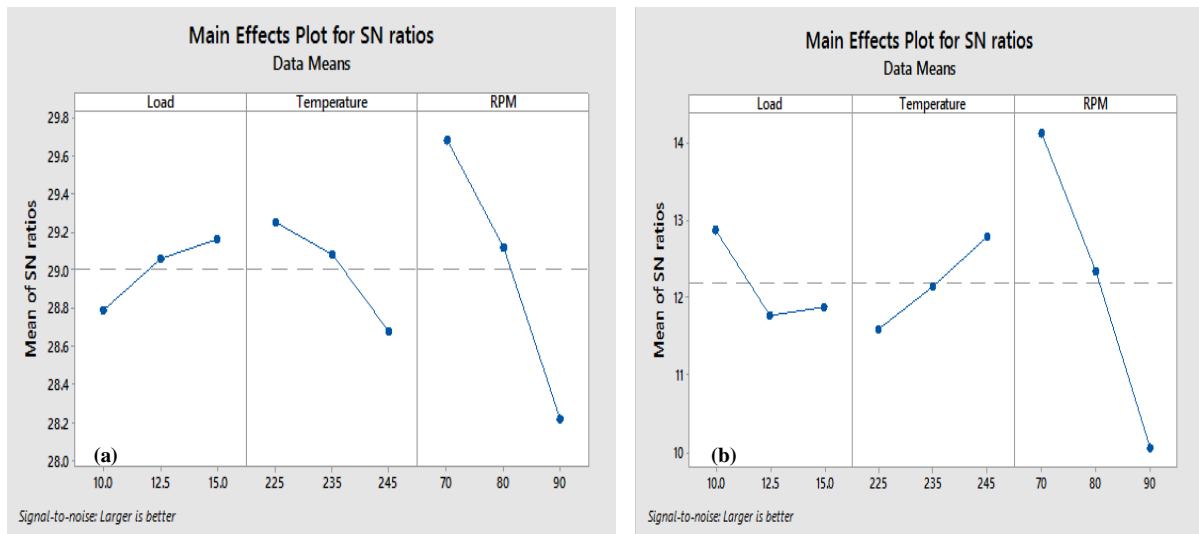


Figure 5.14 Mean S/N ratio plots for PS and % BE of ABS reinforced with BP

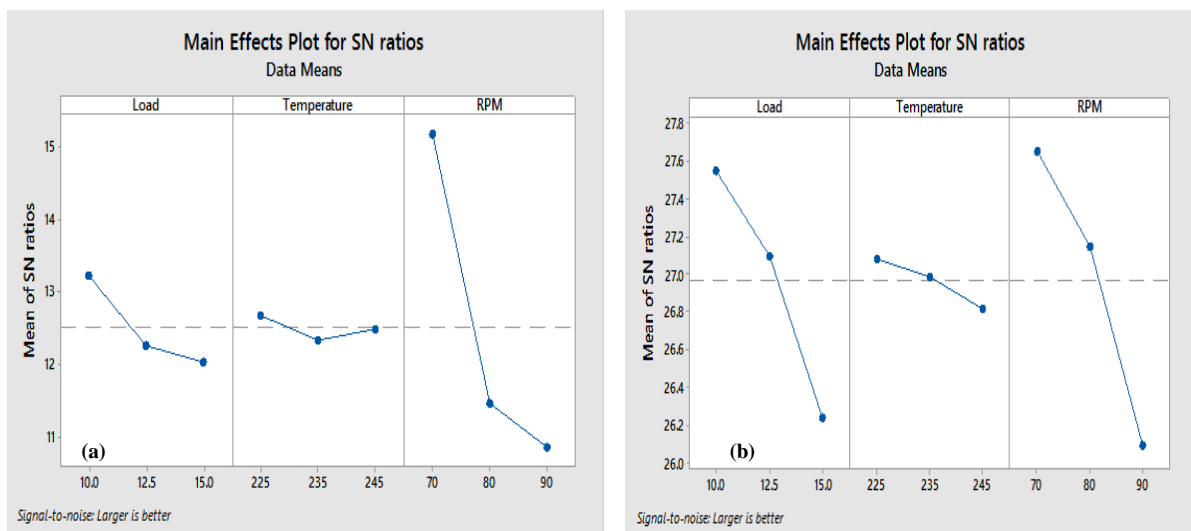


Figure 5.15 Mean S/N ratio plots for PS and % BE of ABS reinforced with WD

The %BE of WD and BP reinforced filament decreases with an increase in load from 10 kg to 15 kg, whereas for Fe reinforced filament it increases with an increase in load up to 12.5kg but after an increase in load up to 15kg it decreases. However, the effect of load on BE for WD reinforced filament was much higher as compared to BP reinforced filament. As the temperature increases, the BE for BP reinforced filament increases whereas it remains almost the same for WD reinforced filament.

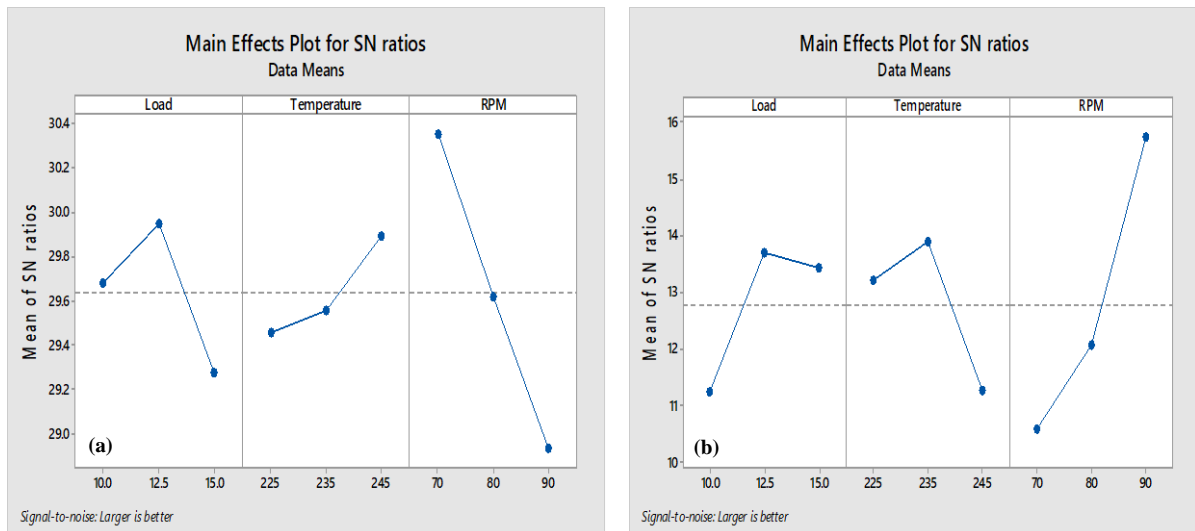


Figure 5.16 Mean S/N ratio plots for PS and % BE of ABS reinforced with Fe

But in the case of Fe reinforced filament, it increases with an increase in the temperature but after 235°C it starts decreasing. With the increase in speed, the BE drops significantly may be due to improper mixing of ABS and reinforced material results in comparatively brittle filaments. The parametric conditions that yields maximum BE for BP reinforced filament were 10 kg load, 245°C temperature and 70 rpm speed whereas 10 kg load, 225°C temperature and 70 rpm speed provide the favorable results in the case of WD reinforced filament, whereas 12.5 kg load, 235°C temperature and 70 rpm speed provide the favorable results in case of Fe reinforced filament.

Table 5.6 Results of ANOVA for PS of BP reinforced filament

Source	DOF	Adj SS	Adj MS	F-value	P-value
Load	2	0.2150	0.1075	2.59	0.278
Temperature	2	0.5063	0.2532	6.10	0.141
Speed	2	3.2643	1.6321	39.33	0.025
Error	2	0.0829	0.0415		
Total	8	4.0688			

Since PS and %BE of the filaments were the most important mechanical characteristic among the various observed characteristics, therefore, analysis of variance (ANOVA) has been applied on the S/N ratio of PS and %BE to determine the significant factors for BP, Fe and WD reinforced filaments (Table 5.6-5.11).

Table 5.7 Results of ANOVA for %BE of BP reinforced filament

Source	DOF	Adj SS	Adj MS	F-value	P-value
Load	2	2.396	2.3963	5.93	0.059
Temperature	2	24.883	24.8826	61.58	0.001
Speed	2	1.571	1.5713	3.89	0.106
Error	2	2.020	0.4041		
Total	8	30.871			

Table 5.8 Results of ANOVA for PS of WD reinforced filament

Source	DOF	Adj SS	Adj MS	F-value	P-value
Load	2	2.6484	1.3242	17.21	0.055
Temperature	2	0.1048	0.0524	0.68	0.595
Speed	2	3.7761	1.8880	24.53	0.039
Error	2	0.1539	0.0769		
Total	8	6.6832			

Table 5.9 Results of ANOVA for %BE of WD reinforced filament

Source	DOF	Adj SS	Adj MS	F-value	P-value
Load	2	0.0373	0.0373	0.03	0.870
Temperature	2	29.3750	29.3750	23.41	0.005
Speed	2	2.3646	2.3646	1.88	0.228
Error	2	6.2740	1.2548		
Total	8	38.0509			

The factors having P-value less than 0.05 were considered significant. Based on the results, speed emerges as the only significant factor that affects the PS of the Fe and BP filaments. However, in the case of WD reinforced filaments, the contribution of load on affecting the PS cannot be ignored as P-value for this factor was very close to 0.05.

Table 5.10 Results of ANOVA for PS of Fe reinforced filament

Source	DOF	Adj SS	Adj MS	F-value	P-value
Load	2	0.697	0.348	27.97	0.035
Temperature	2	0.312	0.156	12.55	0.074
Speed	2	3.039	1.519	121.9	0.008
Error	2	0.0249	0.1024		
Total	8	4.074			

Table 5.11 Results of ANOVA for %BE of Fe reinforced filament

Source	DOF	Adj SS	Adj MS	F-value	P-value
Load	2	10.835	5.147	4.54	0.180
Temperature	2	11.112	5.556	4.66	0.177
Speed	2	42.328	21.164	17.74	0.053
Error	2	2.386	1.193		
Total	8	66.661			

The Porosity analysis has been performed using Tool Maker Microscope equipped with software (X 100) for all the composite filaments. The software first captured the image of the cross-section and then automatically gives the value of the porosity percentage as per the ASTM B276 standard in the form of an image. In general, the results of porosity analysis indicated that filaments reinforced with BP and Fe possess less porosity as compared to WD-reinforced filaments. It was mainly because spherical shaped Fe and BP particles (Refer Figure 5.1 and 5.2) occupied more volume in the ABS matrix as compared to 2-D structured WD particles, thus the porosity of the BP and Fe reinforced filament are less. The composite filaments having minimum and maximum porosity reinforced with BP (sample 1 and sample 3), WD (sample 1 and sample 7) and Fe (sample 6 and sample 7) have been shown in Figure 5.17-5.19 respectively which shows that samples with less porosity resulted in better PS and vice versa.

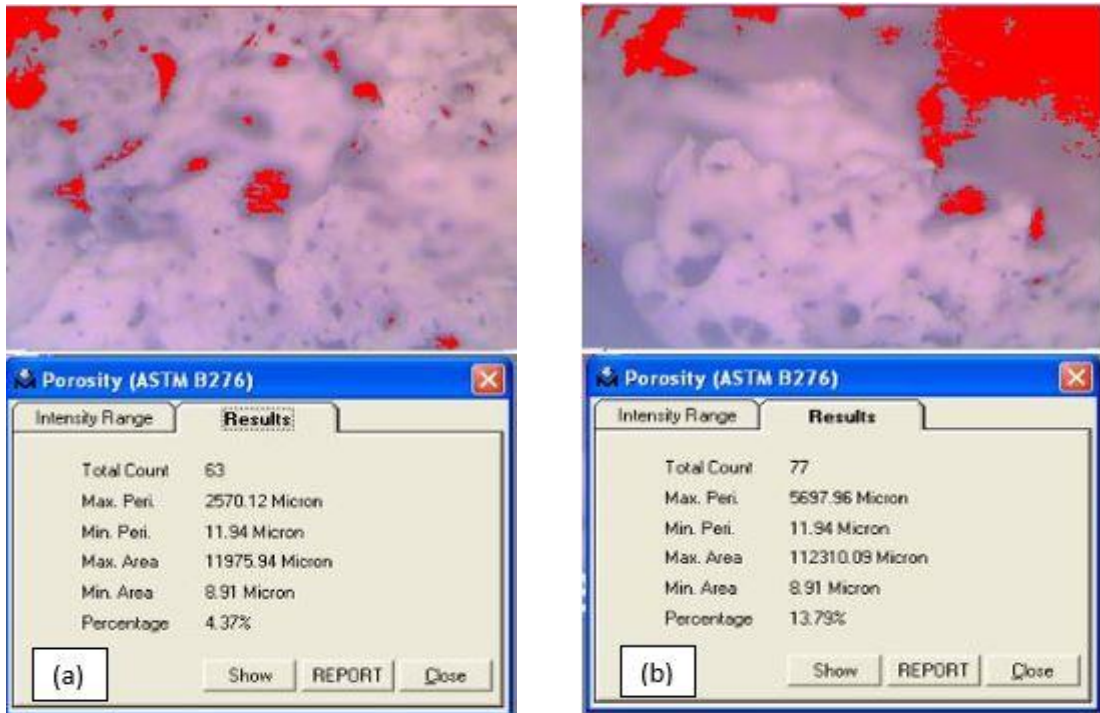


Figure 5.17 Porosity analysis of BP reinforced composite filaments having (a) minimum and (b) maximum porosity percentage

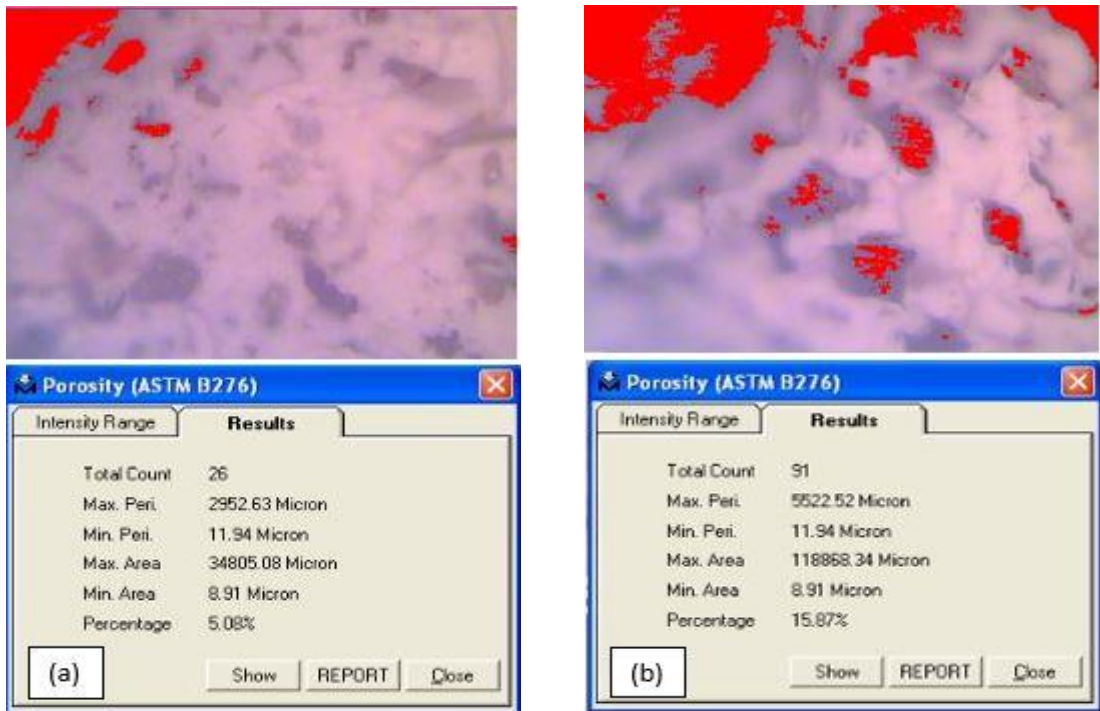


Figure 5.18 Porosity analysis of WD reinforced composite filaments having (a) minimum and (b) maximum porosity percentage

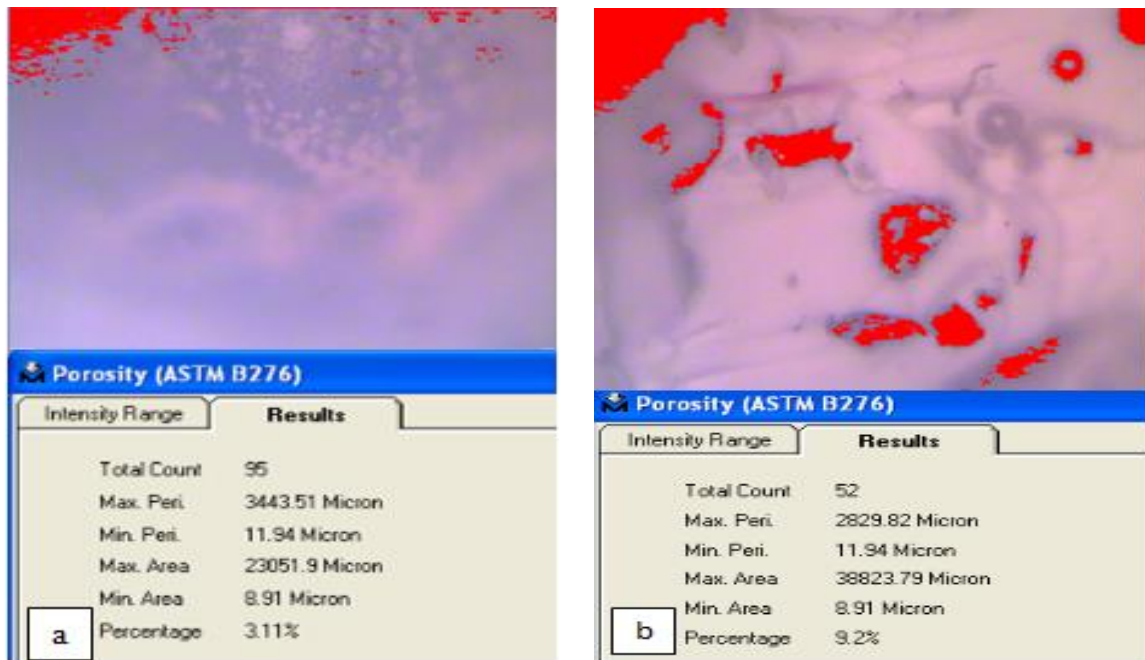
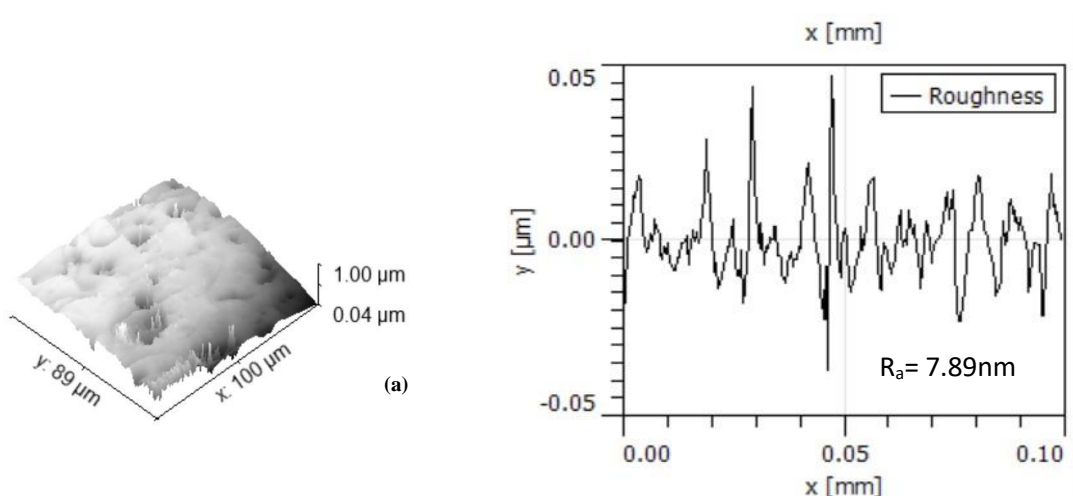
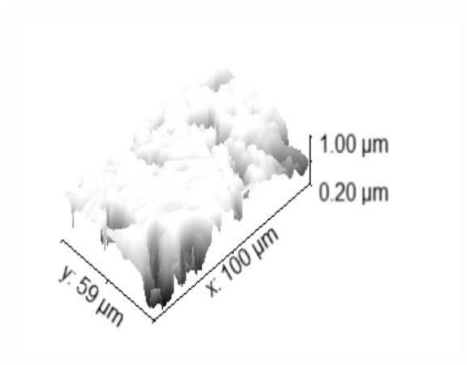


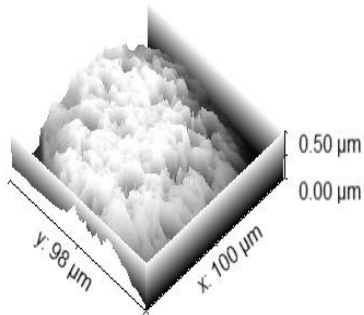
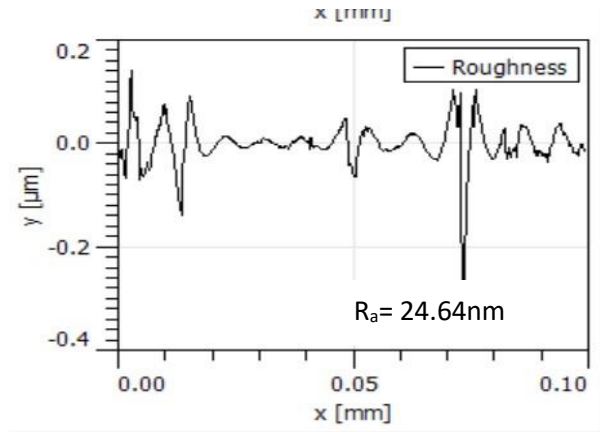
Figure 5.19 Porosity analysis of Fe reinforced composite filaments having (a) minimum and (b) maximum porosity percentage

The photo-micrographic images at $\times 30$ (Figure 5.11-5.12) for the samples having minimum and maximum porosity (sample no. 6 and 5 for Fe reinforced ABS, sample No. 1 and 3 for BP reinforced ABS and sample No. 1 and 7 for WD reinforced ABS as per Table 1.1) were further processed on image processing software to get surface roughness (R_a) value and 3D rendered images (Figure 5.20). It has been observed that Fe reinforced filament possesses a better surface finish ($R_a = 7.89\text{nm}$ and $R_a = 24.64\text{nm}$) as compared to BP reinforced filaments and WD reinforced filament which may also be the reason for their better mechanical properties.

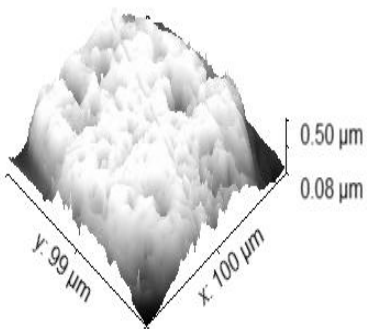
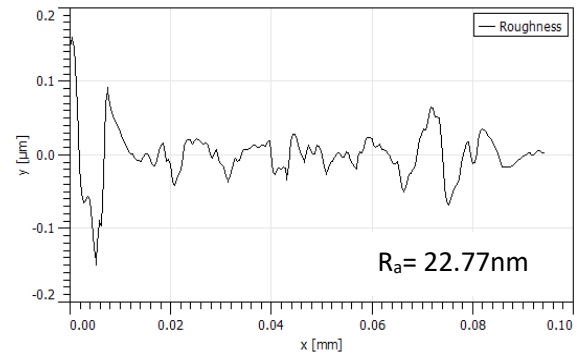




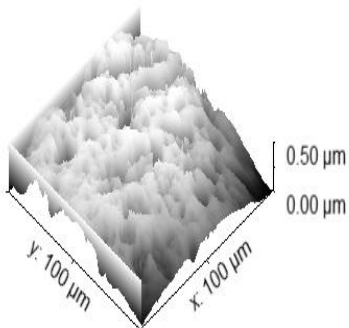
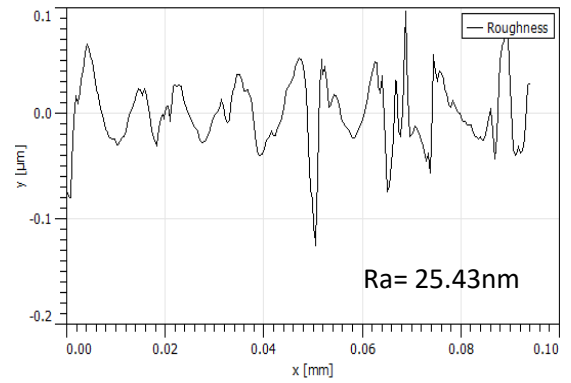
(b)



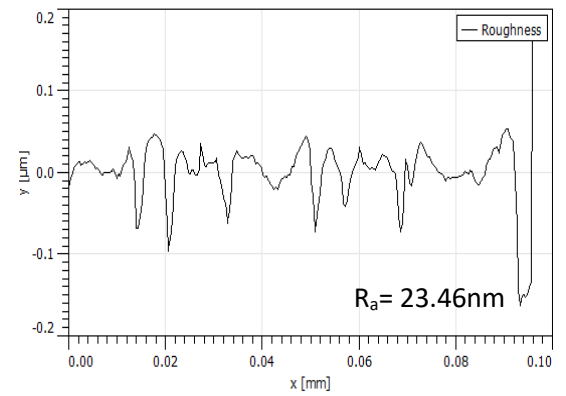
(c)



(d)



(e)



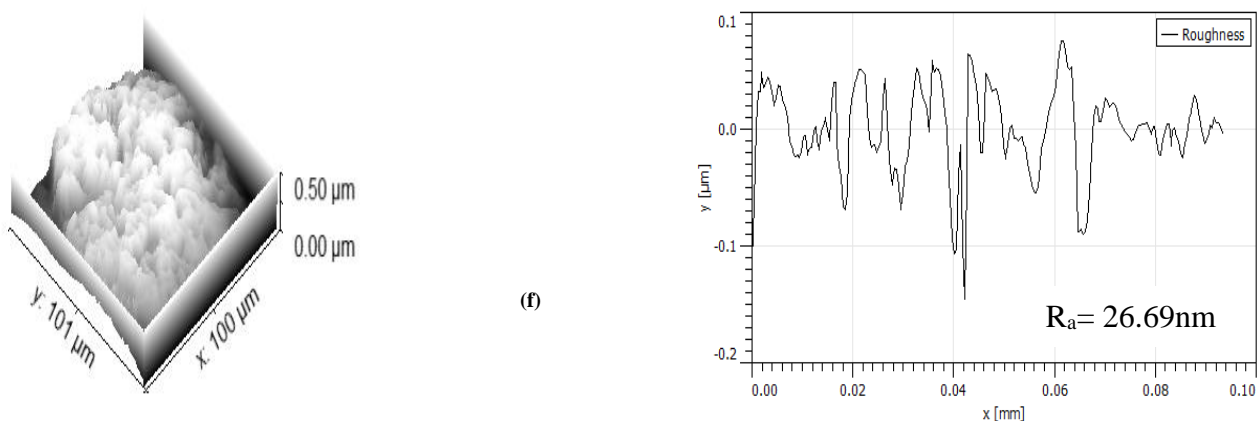


Figure 5.20 3D rendered images of filaments having minimum and maximum porosity

For better understanding the role of reinforcements in non-structural applications, thermal stability analysis using differential scanning calorimeter (DSC) has been performed on BP reinforced samples No. 1, 3 (as per Table 1.1) and WD reinforced sample No. 1, 7 (as per Table 1.1) filaments having minimum and maximum percentage of porosity respectively using three cycles of cooling and heating (Figure 5.21 and 5.22). Thermal stability analysis was executed to determine the exothermic and endothermic reaction at an airflow of 50 ml/min at $10^{\circ}\text{C}/\text{min}$ for exothermic and $-10^{\circ}\text{C}/\text{min}$ for an endothermic reaction. Results of the thermal analysis indicate that glass transition (peak) temperature of filaments having minimum porosity for BP reinforced filament (Sample No. 1) and WD reinforced filament (Sample No. 1) decreases from 102.63°C to 101.13°C and 102.32°C to 100.81°C respectively. Similarly, while analyzing the thermal behavior of filaments having maximum porosity for BP reinforced ABS filament (Sample No. 3), it has been observed that glass transition temperature has increased from 97.0°C to 111.0°C whereas it decreases from 101.41°C to 91.88°C for similar WD reinforced ABS filament (Sample No. 7). Also, during observation of heat capacity of filaments having minimum porosity, it has been observed that the heat carrying ability of BP reinforced ABS filament (2.17 J/g) was much higher as compared to WD reinforced filament (1.46 J/g). It indicates that BP reinforced ABS filament was more thermally stable as compared to WD reinforced filament. So, it can be concluded that ABS reinforced with BP can be used for high temperature and nonstructural applications as compared to ABS reinforced with WD. Further for analyzing the thermal effect thermal analysis of ABS reinforced with Fe powder has been done with the help of Differential Scanning calorimetric (DSC) on filaments having maximum (i.e Sample No.3) and minimum

porosity (i.e Sample No.1). The heat carrying capacity of Sample 6 was decreased from 0.30j/g to 0.48j/g where as sample 7 decreases from 0.24j/g to 0.37j/g. While comparing the heat carrying capacity of all prepared filaments it has been found that the heat carrying capacity of ABS reinforced with BP powder is more as compared to other filaments prepared by reinforcing ABS with Fe and WD.

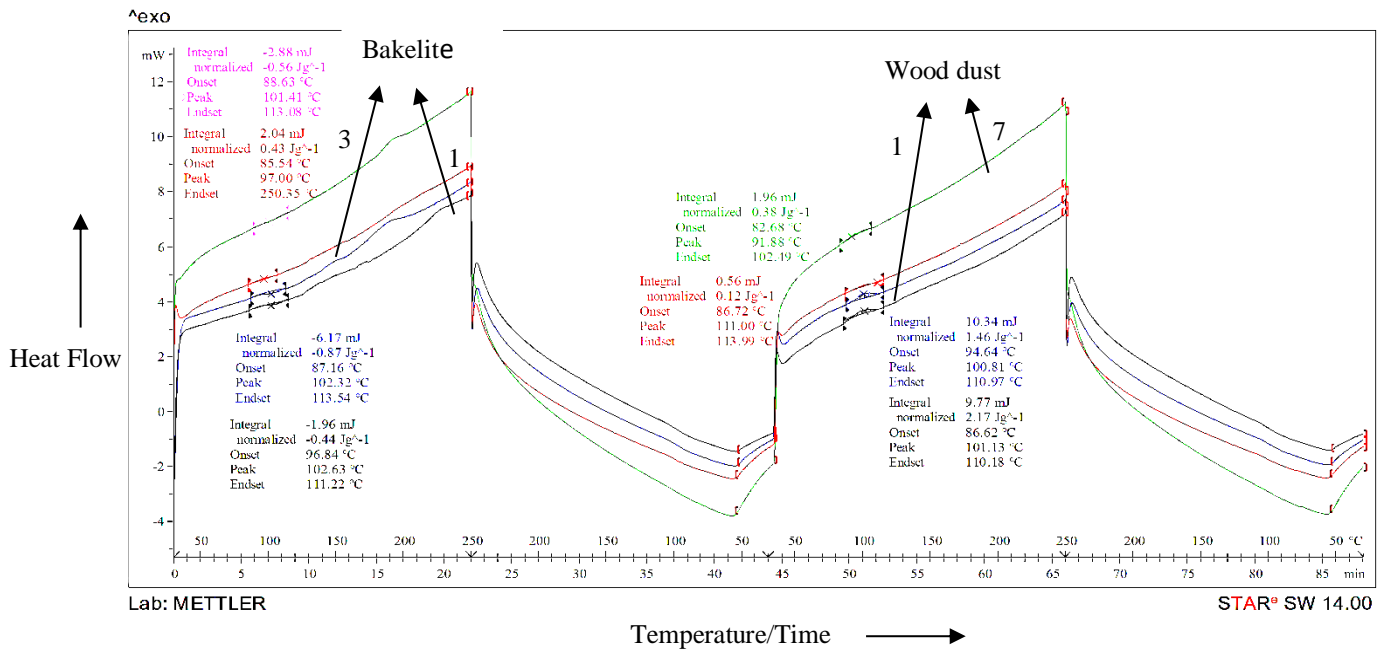


Figure 5.21 Thermal analysis of BP and WD reinforced filaments containing minimum and maximum porosity

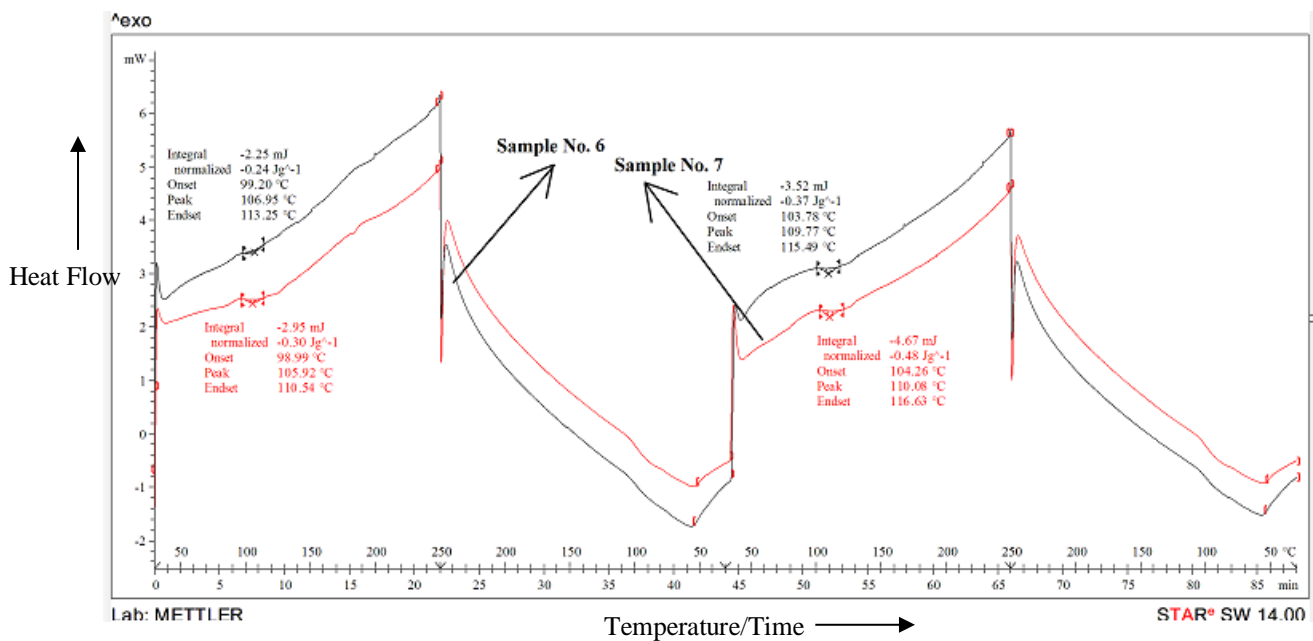


Figure 5.22 Thermal analysis of Fe reinforced filaments containing minimum and maximum porosity

Multi-Response Optimization

Based on the mean effect plots (Figure 5.14-5.16) and various property analyses (Table 5.-5.4), it has been noticed that BP reinforced filament possesses better mechanical, morphological and thermal properties as compared to WD reinforced filament. But the optimum levels of parameters for PS and %BE were different for BP as well as WD reinforced composite filament. So, combined optimized parametric levels have been obtained using Minitab 17 software when both the responses were considered simultaneously [211]. Equal weight and importance have been assigned to each input and output parameter. The suggested parametric levels have been shown in Table 5.12 respectively. The actual value of responses has been calculated based on the S/N ratio by utilizing Eq. (3) and shown in Table 5.12.

Table 5.12 Suggested parametric levels

Parameter	Filament reinforced with BP		Filament reinforced with WD		Filament reinforced with Fe	
	Suggested Value	Actual Value	Suggested Value	Actual Value	Suggested Value	Actual Value
Load	10 Kg	10 Kg	10 Kg	10 Kg	10 Kg	12.5 Kg
Temperature	225°C	225°C	225°C	225°C	225°C	235°C
Speed	70 rpm	70 rpm	70 rpm	70 rpm	70 rpm	80 rpm
S/N ratio (PS)	29.71	30.58 MPa	28.18	25.65 MPa	29.85	31.08
S/N ratio (% BE)	14.24	5.15 %	15.64	6.05 %	14.07	5.05
Desirability	0.962		1.000		0.519	

5.1.2 Chemical Assisted Blending

MFR: After calculating the MFR of 2° recycled ABS with or without reinforcement with mechanical blending, the next step was to investigate the MFR of 2° recycled ABS chemically blended with BP, WD and Fe by varying percentage of reinforcement from 2.5%wt to 10%wt. The MFR of both (ABS+WD, ABS+BP and ABS+Fe) the composites at 2.5%wt proportion of reinforcement was investigated to be higher than MFR of 2° recycled ABS. The results indicated that as the weight proportion of reinforcement raises beyond a critical level, the MFR of all the composites starts decreasing. However, the MFR of WD-

based composite filament decreases once the reinforcement level raises beyond 5% as shown in Table 5.13.

Table 5.13 MFR of 2° recycled ABS with and without reinforcements

S. No.	Sample	MFR (g/10 min)					Average MFR (g/10 min)	Standard Deviation
1	2°recycled ABS +2.5% BP	21.7 6	22.4	22.8	22.5	21.9	22.27	0.43
2	2°recycled ABS +5% BP	19.7	20.4	19.9	20.2	19.8	20.00	0.29
3	2°recycled ABS +7.5% BP	16.8 2	17.2	16.5	16.9	17.5	16.98	0.38
4	2°recycled ABS +10% BP	15.8	14.7	15.4	15.3	14.9	15.22	0.43
5	2°recycled ABS +2.5% WD	22.6	22.8	23.2	22.8	23.1	22.9	0.24
6	2°recycled ABS +5% WD	27.5	28.5	29.3	28.4	28.2	28.38	0.64
7	2°recycled ABS +7.5% WD	18.4 0	18.9	19.4	18.9	19.3	18.98	0.39
8	2°recycled ABS +10% WD	13.5	14.2	14.8	14.2	14.2	14.18	0.46
9	2°recycled ABS + 2.5% Fe powder	22.8	23.2	22.9	22.7	23.1	22.94	0.20
10	2°recycled ABS +5% Fe powder	24.8	25.2	25	25	25	25	0.14
11	2°recycled ABS + 7.5% Fe powder	23.2	22.4	23.2	22.3	22.8	22.78	0.42
12	2°recycled ABS + 10.0% Fe powder	22.2	19.9	21.2	21.1	22.1	21.3	0.93

The reduction in MFR may be due to the generation of good intermolecular bonding between reinforced and base material (ABS) which ultimately absorb most of the heat to break the bonds and thus restricts the flow of composite material from the nozzle. With a further increase in reinforcement level beyond 10%wt, nozzle clogging was detected in the case of ABS reinforced with WD while brittle filament was formed when ABS was reinforced with BP. From MFR results, it has been concluded that at 10%wt. of reinforcements, the MFR of all composites was near to MFR of 2° recycled ABS. Also, this wt.% of reinforcement gives maximum utilization of waste material and hence the composite filaments were fabricated (using TSE) by reinforcing 10% of BP, WD, Fe respectively in this work.

Tensile Testing: The composite filaments have been fabricated by adding 10% reinforcement (BP, WD and Fe) with 90% chemically blended 2° recycled ABS respectively through TSE. Total 27 filaments were prepared by varying each parameter at three levels following conditions represented in Table 1.1. The effect of selected parameters on both mechanical and morphological properties of the filaments have been compared and discussed separately. Tensile tests using UTM were performed on composite filaments on load rate of 25mm/min. for investigating different properties (mechanical) such as peak elongation (PE), peak strength (PS), break strength (BS), break elongation (BE), modulus of elasticity (E) and modulus of toughness (T). The outcomes obtained after performing tensile tests have been represented in Table 5.14- 5.16 respectively.

Table 5.14 Responses for 2° recycled ABS reinforced with 10% BP

S. No.	BS (MPa)	PS (MPa)	% BE	% PE	T (MPa)	E (GPa)
1	30.30±1.6	34.87±1.8	4.19±0.45	3.80±0.4	0.719±0.15	0.786±0.15
2	31.38±1.5	32.07±1.6	4.65±0.6	4.43±0.5	0.590±0.1	0.675±0.12
3	24.88±0.9	27.98± 1.2	5.07±0.55	4.75±0.45	0.645±0.12	0.736±0.18
4	31.22±1.2	31.68± 1.3	3.86±0.4	3.49±0.35	0.425±0.08	0.909±0.2
5	23.91±1.1	26.10± 1.2	4.22±0.4	4.07±0.4	0.790±0.18	0.515±0.1
6	25.18±1.1	27.65± 1.1	5.19±0.5	5.07±0.5	0.560±0.12	0.582±0.12
7	22.14±1.0	24.89±1.1	3.79±0.3	3.48±0.35	0.446±0.1	0.714±0.15
8	23.49±1.2	26.56± 1.2	4.56±0.45	4.12±0.4	0.518±0.12	0.645±0.12
9	22.40±1.2	24.60± 1.1	5.01±0.3	2.98±0.3	0.383±0.1	0.734±0.15

Table 5.15 Responses for 2° recycled ABS reinforced with 10% WD

S.No	BS (MPa)	PS (MPa)	% BE	% PE	T (MPa)	E (GPa)
1	32.81±1.5	36.46±1.7	6.02±0.6	5.38±0.6	0.987±0.18	0.677±0.15
2	18.80±1.2	20.88±1.0	4.43±0.55	4.12±0.5	0.416±0.1	0.507±0.12
3	9.92±1.4	11.02±1.5	2.85±0.4	2.85±0.35	0.141±0.05	0.386±0.08
4	28.89±1.3	32.10±1.5	7.92±0.7	6.87±0.75	1.143±0.22	0.405±0.12
5	16.11±1.4	17.91±1.2	3.75±0.5	3.63±0.4	0.229±0.08	0.706±0.15
6	7.13±1.2	7.92±1.4	2.83±0.3	2.58±0.35	0.056±0.02	0.500±0.1
7	28.49±1.3	31.65±1.6	5.12±0.6	4.43±0.55	0.779±0.15	0.615±0.15
8	21.86±1.2	24.29±1.2	3.81±0.45	3.48±0.4	0.519±0.12	0.547±0.12
9	8.51±1.1	9.45±1.4	1.58±0.35	1.51±0.3	0.067±0.03	0.623±0.15

Table 5.16 Responses for 2° recycled ABS reinforced with 10% Fe

S.No	BS (MPa)	PS (MPa)	% BE	% PE	T (MPa)	E (GPa)
1	28.47±1.5	20.37±1.7	6.97±0.6	4.43±0.6	0.548±0.18	0.642±0.15
2	29.59±1.2	26.33±1.0	5.51±0.55	6.02±0.5	0.843±0.1	0.491±0.12
3	30.27±1.4	16.70±1.5	4.02±0.4	2.22±0.35	0.185±0.05	1.365±0.08
4	18.55±1.3	27.25±1.5	6.33±0.7	5.70±0.75	0.949±0.22	0.325±0.12
5	17.50±1.4	11.97±1.2	4.53±0.5	4.75±0.4	0.322±0.08	0.368±0.15
6	22.63±1.2	25.63±1.4	3.17±0.3	4.43±0.35	0.568±0.02	0.510±0.1
7	9.51±1.3	10.60±1.6	5.38±0.6	3.17±0.55	0.167±0.15	0.300±0.15
8	13.30±1.2	15.75±1.2	4.43±0.45	4.43±0.4	0.349±0.12	0.30±0.12
9	11.78±1.1	8.56±1.4	2.22±0.35	3.80±0.3	0.176±0.03	0.310±0.15

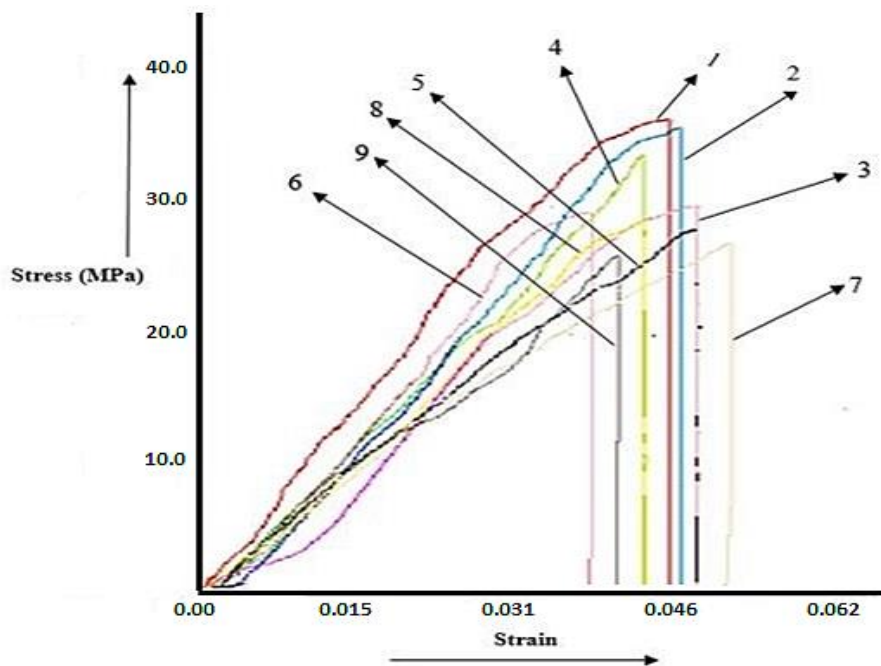


Figure 5.23 Stress versus strain curve of BP reinforced ABS filaments

The composite filaments prepared by reinforcing BP (10% by weight) show more consistent mechanical properties (PS, BS, %PE, %BE) as compared to WD and Fe (10% by weight) reinforced composite filaments as revealed from Table 5.14-5.16. Further, it determined that the BS and PS of all the filaments were affected by extrusion temperature. As the temperature raises (225°C -245°C), the strength (BS and PS) of all the filaments declines abruptly. However, the reduction in PS and BS of WD based filaments was much higher than corresponding BP and Fe based filaments. It was primarily because of the high heat carrying

capacity of WD particles (compared to BP and Fe) that result in a smooth flow of the material even at high temperature and thus gives comparably superior outcomes with regard to mechanical properties. In addition to temperature, the load acted during the extrusion of the composite filaments also affects the PS and BS. With an increase in load from 10 kg to 15 kg, PS and BS reduced slightly for all the filaments.

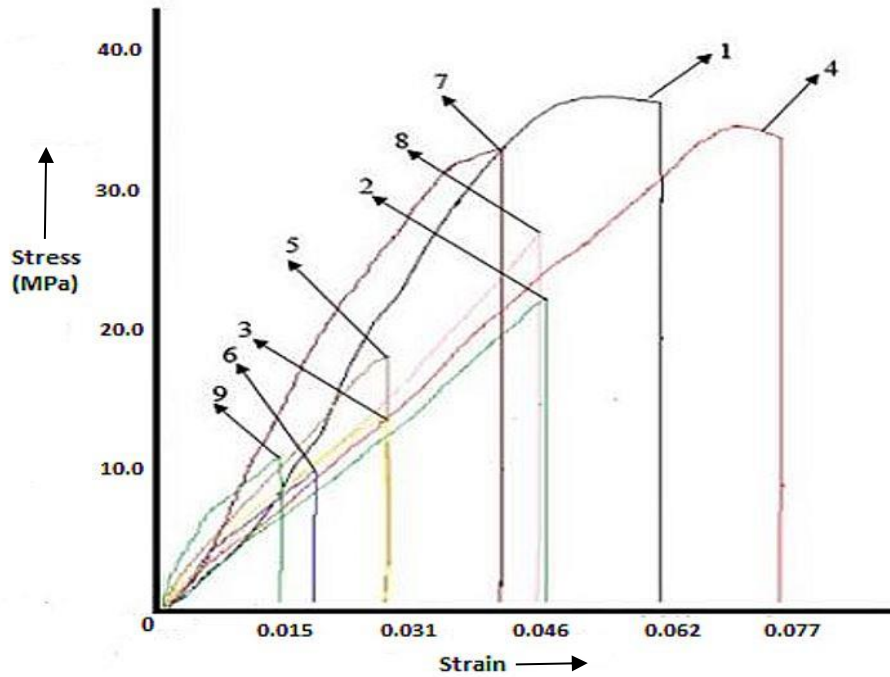


Figure 5.24 Stress versus strain curve of WD reinforced ABS filaments

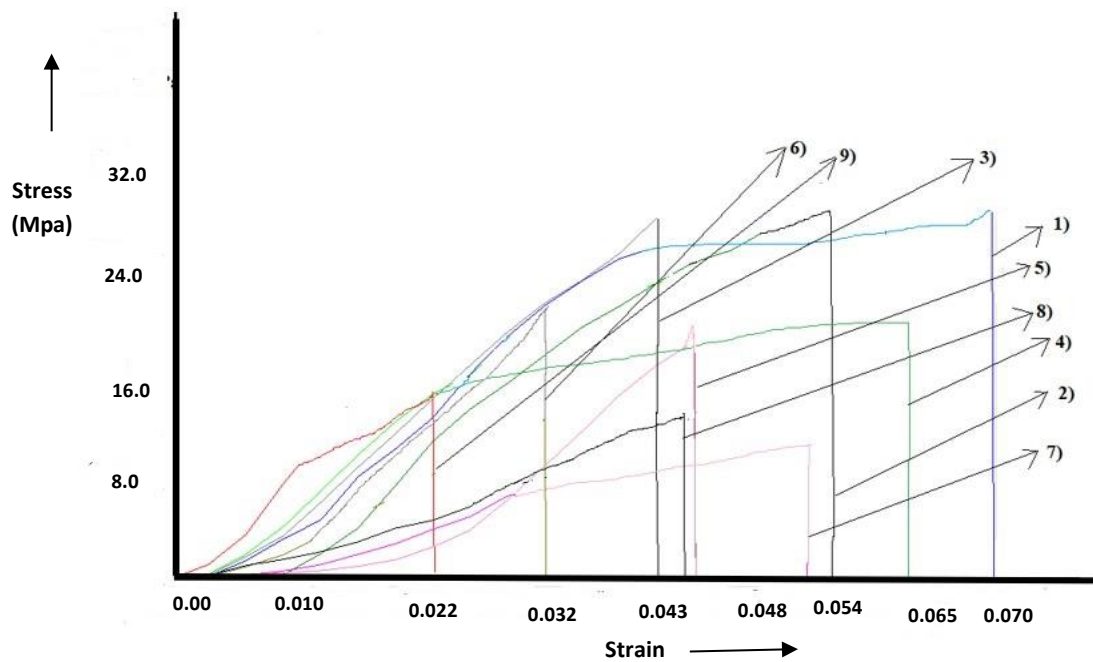


Figure 5.25 Stress versus strain curve of Fe reinforced ABS filaments

Figure 5.23-5.25 represents the stress-strain curves for BP, WD and Fe based filaments respectively. During tensile testing, no negative strain was observed and it was in the direction of load only. The various observations reported in Table 5.14-5.16 were utilized to measure the modulus of toughness (T) and modulus of elasticity (E) of composite filaments. Modulus of toughness (T) is the most important mechanical property of the composite filaments as it gives the estimation of the energy absorbed by the filament per unit volume before its rupture. Modulus of toughness (T) was predicted from the area under the stress-strain curve. It was observed (Refer Table 5.14, 5.15 and 5.16) that there was a drastic change in the value of T for WD and Fe based filaments with a change in process parameters of TSE.

To determine the presence and nature of bonds formed between the base and reinforced materials that ultimately effects the PS of the composite filament, FTIR analysis was performed. The FTIR analysis of filaments having maximum PS fabricated by different blending techniques is shown in Figure 5.26. During FTIR analysis of BP reinforced composite filament (Figure 5.26(a)) the formation of a first medium peak at wave number in the range of 3725 cm^{-1} to 3750 cm^{-1} represents O-H bond stretching confirming the presence of bakelite in the prepared composite. The second sharp peak at wavenumber close to 2925 cm^{-1} indicates C-H bond stretching of ABS thermoplastic (alkane). Both the O-H and C-H bonds require significantly higher bond dissociation energy that ultimately corresponds to better strength of the BP reinforced composite filaments. The small peak formed close to 3700 cm^{-1} during the analysis of WD reinforced composite filament may be due to the existence of the O-H group of water present as an impurity in acetone during the preparation of composite through chemical assisted blending. The second sharp peak in Figure 5.26(c) at wave number in the range of 2925 cm^{-1} to 2980 cm^{-1} indicates C-H bond stretching and the third medium peak at a wavenumber of 1480 cm^{-1} represents C-H bond bending and C-C bond stretching due to aromatic rings present in ABS thermoplastic. The peak formed at a wavenumber of 1706 cm^{-1} (Figure 5.26 (c)) indicates C=O bond stretching. This might be due to the existence of acetone in composite prepared through chemical-assisted blending and could be one of the reasons for the large variation in PS of chemically and mechanically blended WD reinforced composite filaments.

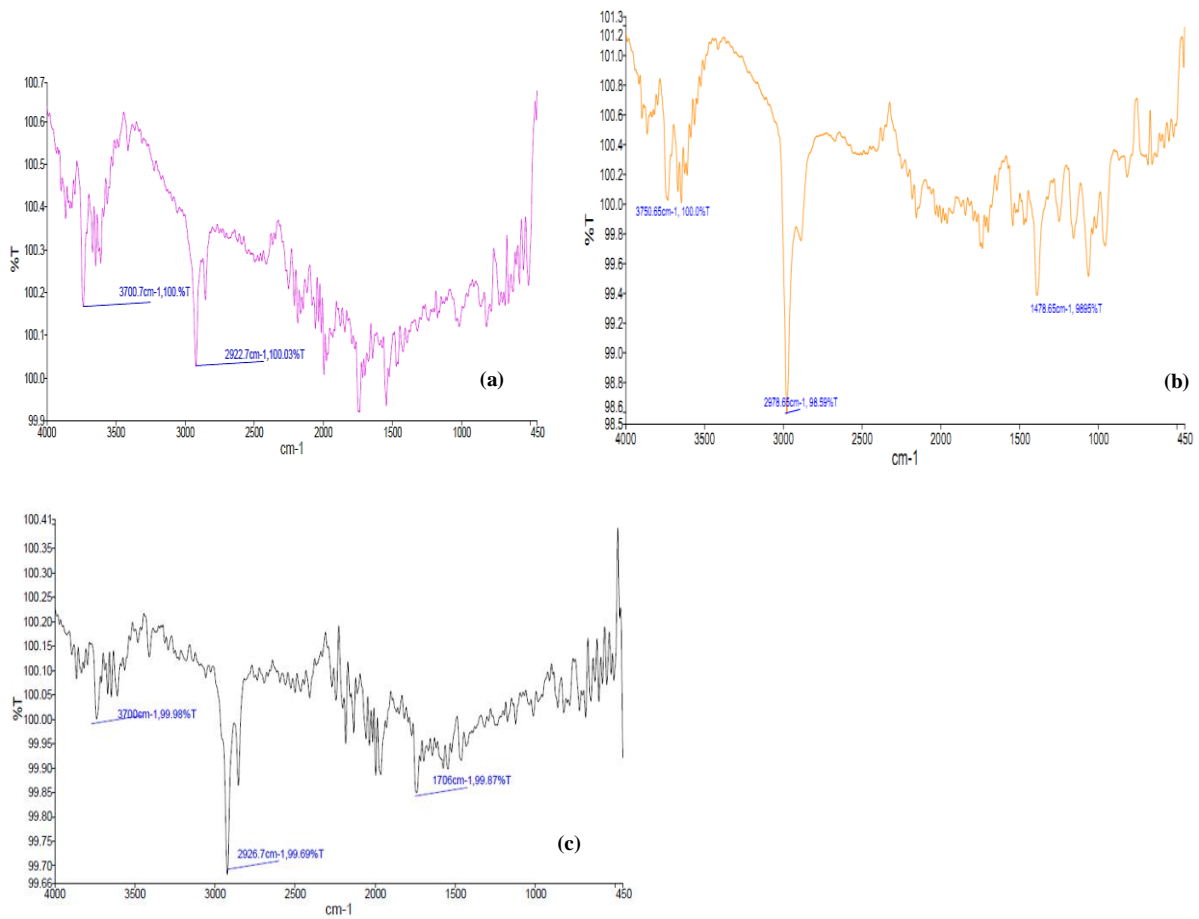


Figure 5.26 FTIR of composite filaments having maximum PS (a) chemically blended ABS+BP, (b) chemically blended ABS+Fe, and (c) chemically blended ABS+WD

The impact of TSE parameters on PS and %BE of composite filaments was analyzed using signal to noise (S/N) ratio analysis. The S/N ratios for all the responses were determined using the ‘larger is better’ approach (Eq. (1)) and reported in Table 5.17.

Table 5.17 S/N ratios for peak strength and percentage break elongation

S No.	Filament reinforced with BP		Filament reinforced with WD		Filament reinforced with Fe	
	S/N ratio for PS (dB)	S/N ratio for %BE (dB)	S/N ratio for PS (dB)	S/N ratio for %BE (dB)	S/N ratio for PS (dB)	S/N ratio for %BE (dB)
1	30.85	12.44	31.24	15.59	29.08	16.86
2	30.12	13.35	26.39	12.93	29.42	14.82
3	28.94	14.10	20.84	9.10	29.60	12.08
4	30.02	11.73	30.13	17.97	25.36	16.02
5	28.33	12.5	25.06	13.53	24.86	13.12
6	28.83	14.30	17.97	9.04	27.09	10.02
7	27.92	11.57	30.01	14.19	19.56	14.61
8	28.48	13.17	27.71	11.62	22.47	12.92
9	27.82	13.99	19.51	3.97	21.42	6.92

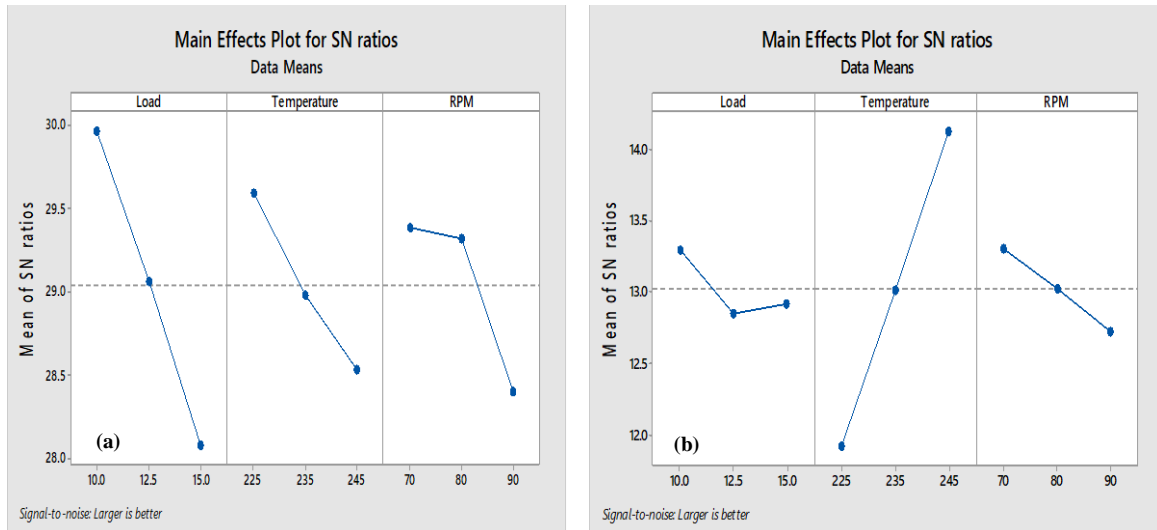


Figure 5.27 S/N analysis for peak strength and %BE of BP reinforced filaments

The PS and %BE of all the filaments were further analyzed by plotting mean S/N ratio graphs (Figure 5.27-5.29 respectively). The selection of load or force applied during the extrusion process seems to be the most critical parameter affecting the flow through the cavity. If the load acting during the extrusion process is low, the semi-molten material might get struck in the cavity and thus causes the seizing. In contrast, if the value of the load is too high, the various properties of the extruded filament might get adversely affected. The increase of load from 10 kg to 15 kg in the case of composite filament reinforced with BP and Fe causes the PS to decline abruptly as observed in Figures 5.27 (a) and 5.29 (a). However, the same (PS) for WD reinforced filament first reduces and then rises slightly as the load increased from 10 kg in steps of 2.5 kg each. The PS for all types of filaments was prominently impacted by the temperature of the extrusion process. The PS for all the filaments falls off rapidly as the temperature rises. However, the reduction in PS of WD reinforced composite filaments was much greater because WD possesses poor heat capacity (specific) which ultimately hinders the steady flow of material at high temperatures and thus results in poor PS.

At a temperature of 225°C, the PS was investigated to be maximum for WD and BP types of filaments but in the case of Fe reinforced filament it was maximum at 245°C. The PS of filaments reinforced with WD was not affected by the variation in speed/rpm of the extruder. But the serious conflicting effect on PS was observed for filaments reinforced with BP and Fe as the speed surges. It was mainly because when the speed of screw rotation is

low, extruded material gets sufficient time to melt and exhibit ductile behavior. Both the filaments i.e (WD and BP) displayed optimum PS at the first level of each selected parameter (10 kg, 225°C, 70 rpm), whereas Fe reinforced filament shows optimum PS at 10 kg, 245°C, 70 rpm. In general, the %BE declines for all the composite filaments as the force or load acting during the extrusion process raises from 10 kg to 15 kg. Similar to PS outcomes, %BE for all types of filaments was also prominently impacted by the temperature of the extrusion process. But the effect of temperature on the %BE of Fe and WD the filaments was opposite to BP reinforced filament.

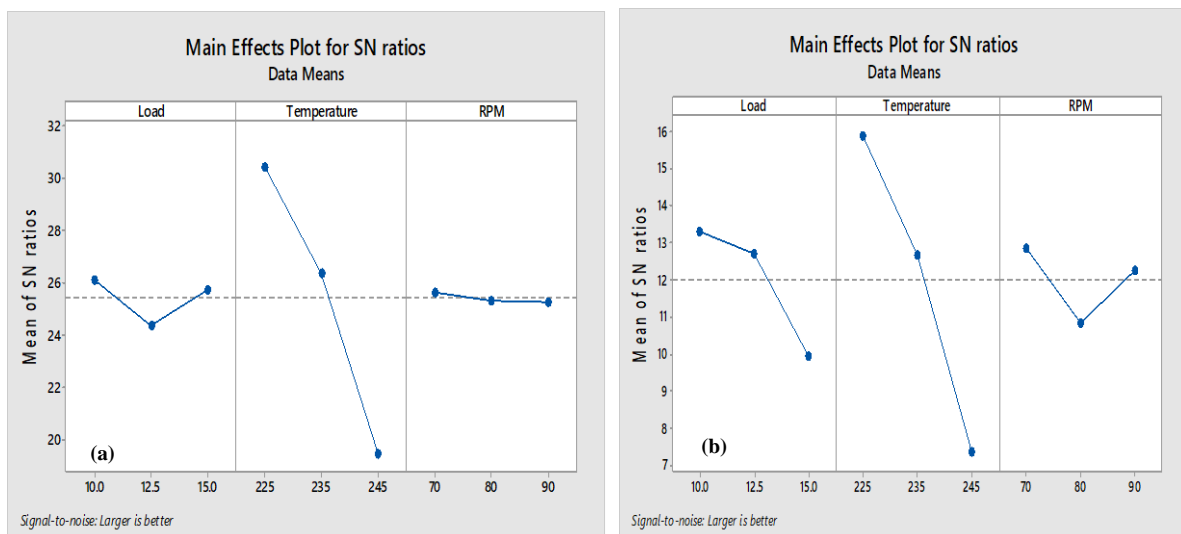


Figure 5.28 S/N analysis for percentage Peak strength and %BE of WD reinforced filaments

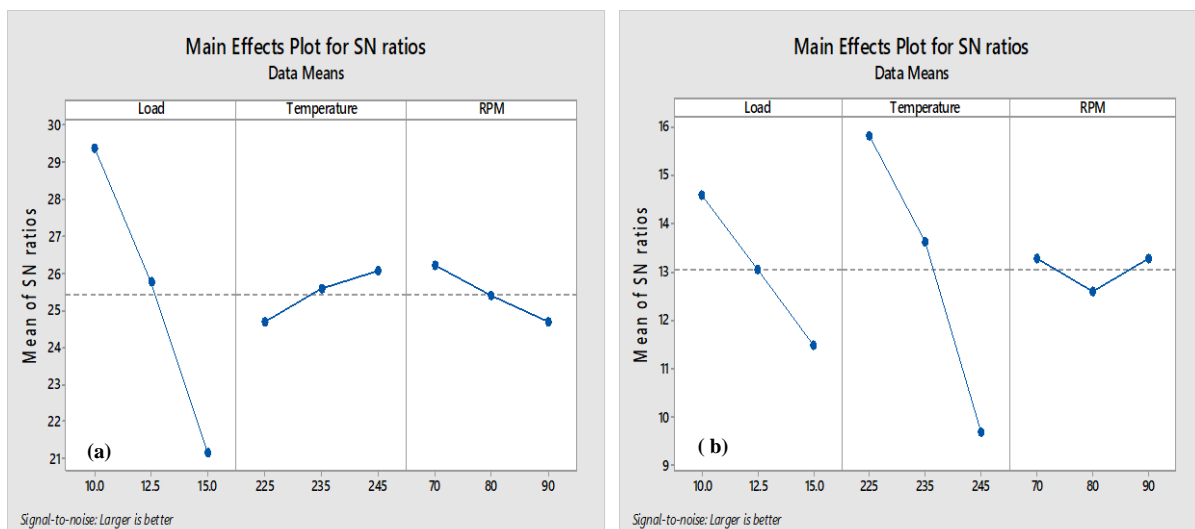


Figure 5.29 S/N analysis for percentage Peak strength and %BE of Fe reinforced filaments

At higher extrusion temperature, BP reinforced filaments displays improved %BE whereas the same decreases abruptly as the temperature rises for WD and Fe reinforced

filaments. It was basically due to the huge difference in the specific heat capacity of two reinforced materials that influence their capacity to hold heat energy and ultimately change their mechanical behavior. Further, the lowest value (70 rpm) of screw speed produces the utmost %BE for both types of filaments. WD reinforced filament displayed optimum %BE at the first level of each selected parameter (10 kg, 225°C, 70 rpm) whereas the levels for optimum %BE for filaments reinforced with BP were 10 kg, 245°C, and 70 rpm, where the optimum levels for %BE of Fe reinforced filament was 10 kg, 225°C, 70 rpm. Among all the concerning mechanical properties measured in this research work, the peak strength (PS) and %BE were the most critical property that affects/influences the performance, applications and utilization of the filaments extensively. So, the analysis of variance (ANOVA) was done for PS and %BE of the composite filaments only. ANOVA results provide the most influential parameters as well as their percentage contribution that affects the mechanical properties of all the composite filaments (Table 5.18-5.23). The analysis was performed at 95% confidence level (parameter significant if P-value < 0.05). The results of the analysis highlighted that all the selected parameters (i.e. load, temperature, speed) influenced the PS and %BE of BP and Fe reinforced filaments critically. On the other hand, extrusion temperature was the only significant parameter in the case of WD reinforced filaments.

Table 5.18 ANOVA analysis for PS of BP reinforced filament

Parameter	DOF	Adj SS	Adj MS	F-value	P-value
Load	2	5.3880	2.6940	93.14	0.011
Temperature	2	1.7157	0.8578	29.66	0.033
Speed	2	1.8400	0.9200	31.81	0.030
Error	2	0.0578	0.0289		
Total	8	9.0016			

Table 5.19 ANOVA analysis for %BE of BP reinforced filament

Parameter	DOF	Adj SS	Adj MS	F-value	P-value
Load	2	0.353	0.176	25.03	0.038
Temperature	2	7.373	3.686	522.12	0.002
Speed	2	0.509	0.254	36.06	0.027
Error	2	0.014	0.007		
Total	8	8.250			

Table 5.20 ANOVA analysis for PS of WD reinforced filament

Parameter	DOF	Adj SS	Adj MS	F-value	P-value
Load	2	5.134	2.5670	1.60	0.384
Temperature	2	186.15	93.078	58.07	0.017
Speed	2	0.201	0.1007	0.06	0.941
Error	2	3.206	1.6029		
Total	8	194.69			

Table 5.21 ANOVA analysis for %BE of WD reinforced filament

Parameter	DOF	Adj SS	Adj MS	F-value	P-value
Load	2	19.79	9.89	154.56	0.006
Temperature	2	111.82	55.913	873.07	0.001
Speed	2	6.624	3.312	51.72	0.019
Error	2	0.128	0.0640		
Total	8	138.377			

Table 5.22 ANOVA analysis for PS of Fe reinforced filament

Parameter	DOF	Adj SS	Adj MS	F-value	P-value
Load	2	101.93	50.965	134.96	0.007
Temperature	2	2.931	1.465	3.88	0.205
Speed	2	3.552	1.776	4.70	0.175
Error	2	0.755	0.3776		
Total	8	109.168			

Table 5.23 ANOVA analysis for %BE of Fe reinforced filament

Parameter	DOF	Adj SS	Adj MS	F-value	P-value
Load	2	14.420	7.210	4.99	0.167
Temperature	2	58.396	29.198	20.20	0.047
Speed	2	0.924	0.462	0.32	0.758
Error	2	2.890	1.445		
Total	8	76.631			

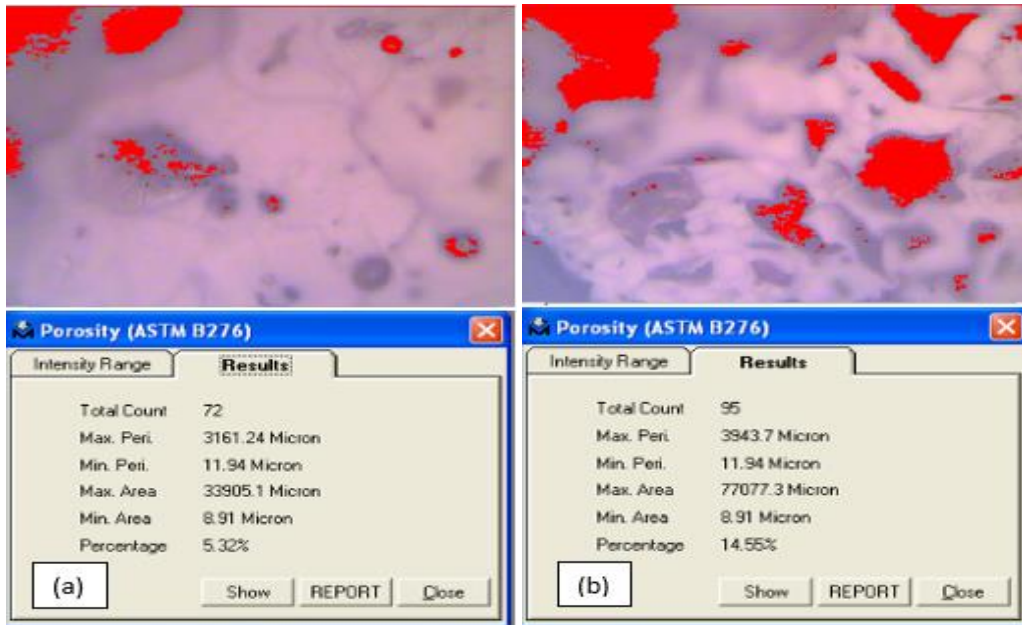


Figure 5.30 (a) Minimum and (b) Maximum porosity at break cross-section of filaments reinforced with BP

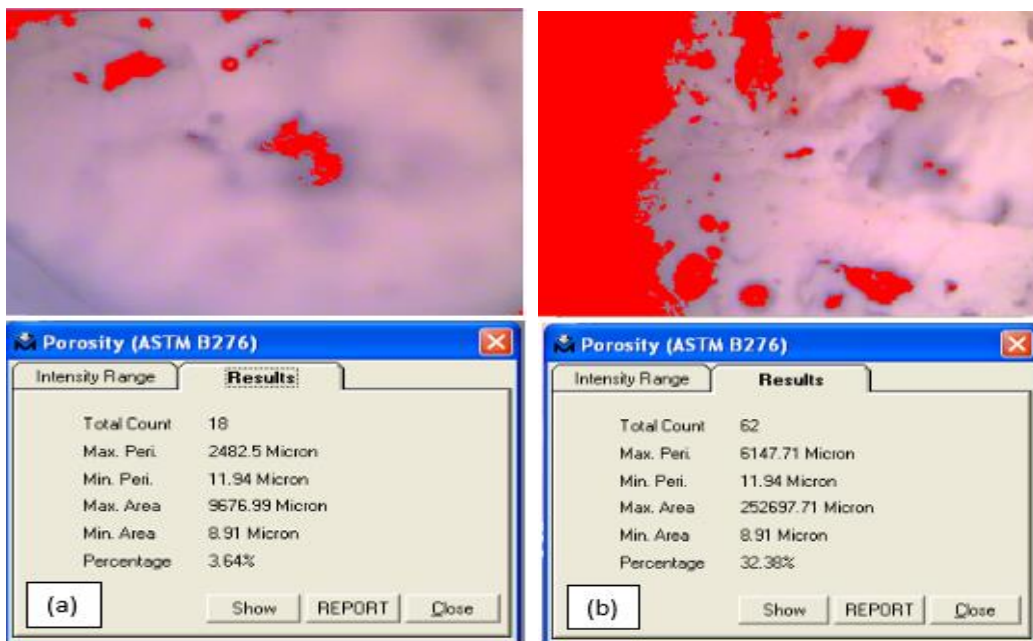


Figure 5.31 Minimum and (b) Maximum porosity at break cross-section of filaments reinforced with WD

Metallurgical image analysis software (at $\times 100$), an integral part of Tool Maker's Microscope was utilized to estimate the percentage porosity in filaments fractured during the tensile tests (according to Table 1.1). The software followed the instructions of the ASTM B276 standard to determine the level of porosity and highlight the results in terms of pictorial view. Sample (1,9) (Figure 5.30) and sample (1,6) (Figure 5.31) and sample (4,9) (Figure 5.32) contain the lowest and highest porosity for BP, WD and Fe reinforced filaments

respectively. The results revealed that percentage porosity directly influenced the strength of fabricated filaments. High strength (both BS and PS) was investigated for all types of composite filaments possessing lesser percentage porosity and vice-versa.

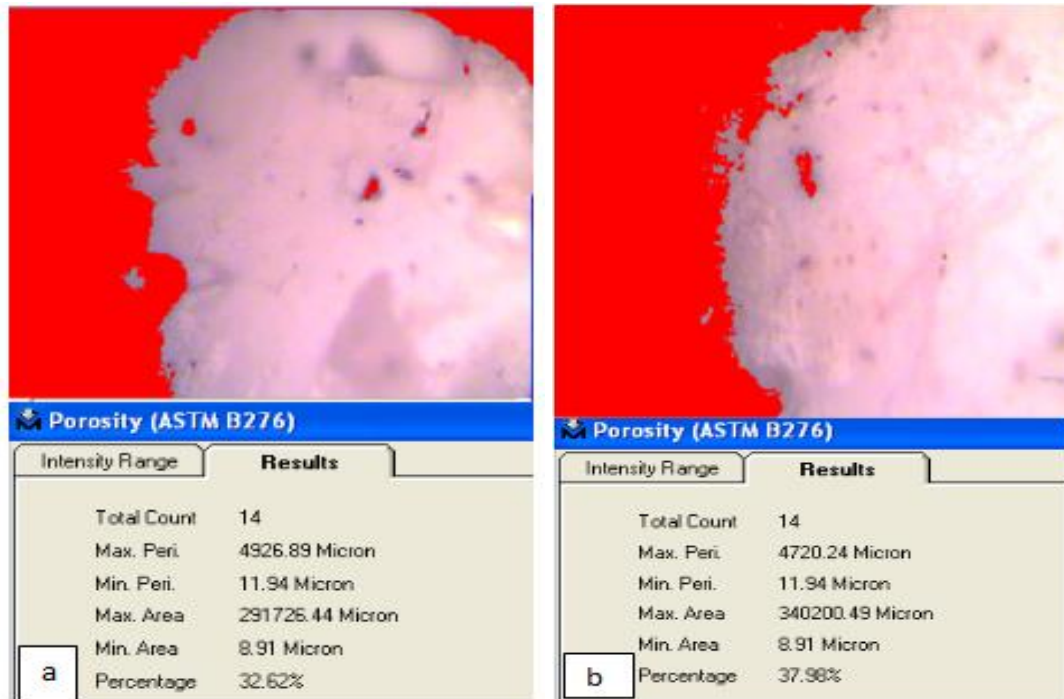


Figure 5.32 Minimum and (b) Maximum porosity at break cross-section of filaments reinforced with Fe

Optical photomicrographs of the cross-section (break) at $\times 30$ were also captured for the composite filaments containing the lowest and highest porosity (Figure 5.33, 5,34, 5,35). Sample (1,9), sample (1,6) and sample (4,9) contain the lowest and highest porosity (Refer Table 5.24) for BP, WD and Fe reinforced filaments respectively. It was predicted from the photomicrographs that each sample contains some voids at the point where the filament breaks into two halves during the tensile test.

However, the quantity of voids present at the cross-section varies in all the composite filaments due to different processing conditions. These voids adversely affect the mechanical behaviour of the filaments during the tensile test. So, it has been predicted that the presence of a higher number of asperities/voids in the fabricated filaments could be responsible for poor mechanical behaviour. Filaments containing lesser number of voids exhibit better mechanical properties and vice versa.

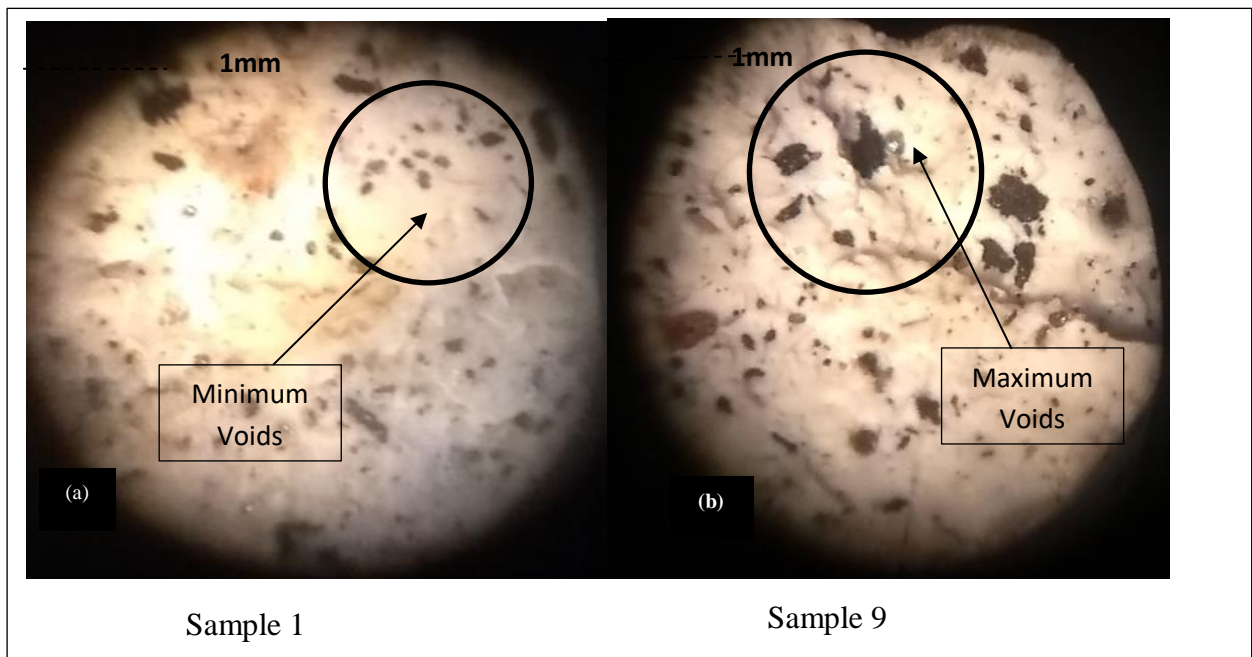


Figure 5.33 Photomicrograph analysis at the cross-section of samples reinforced with BP

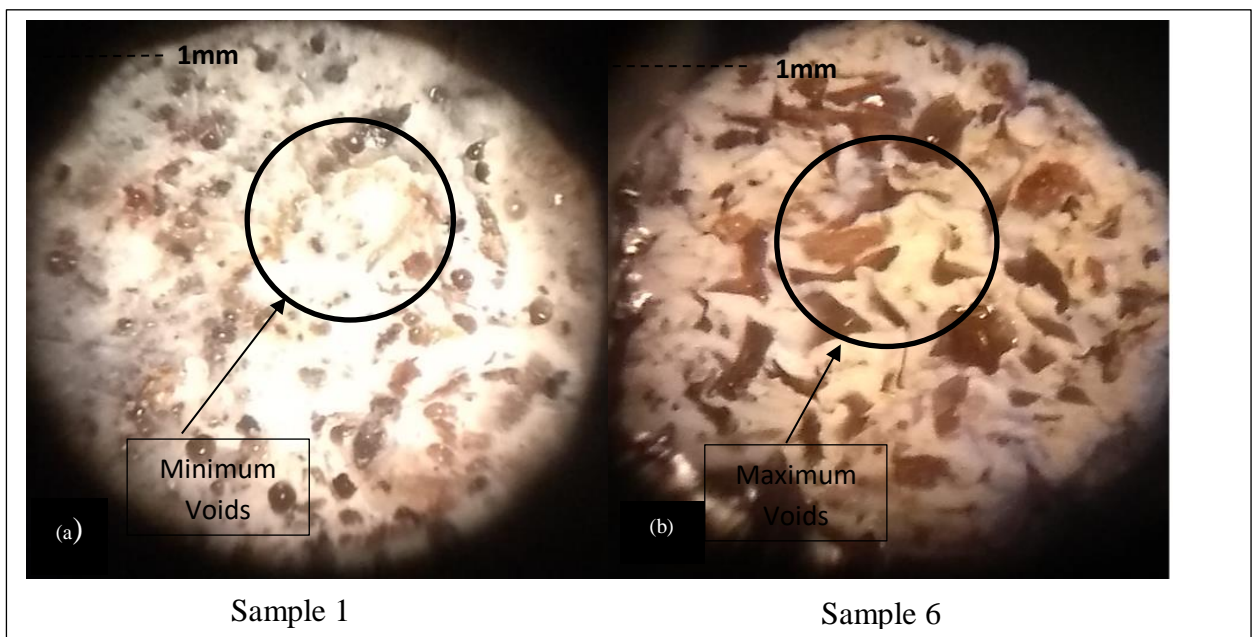


Figure 5.33 Photomicrograph analysis at the cross-section of samples reinforced with WD

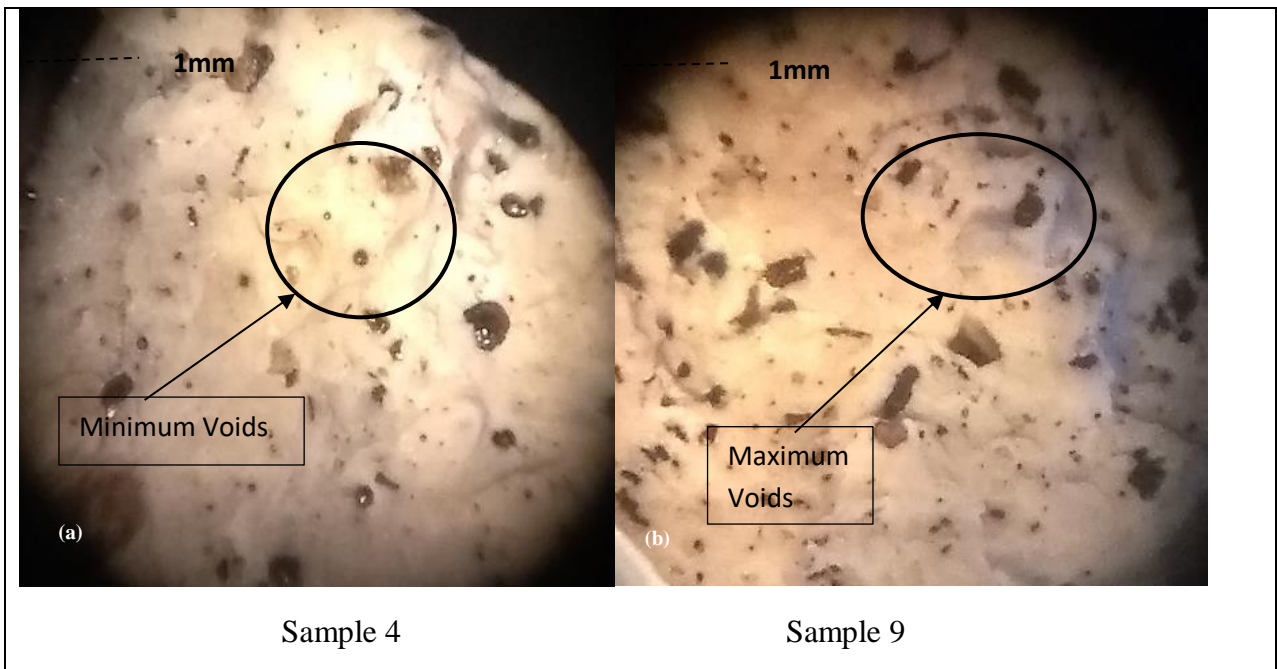
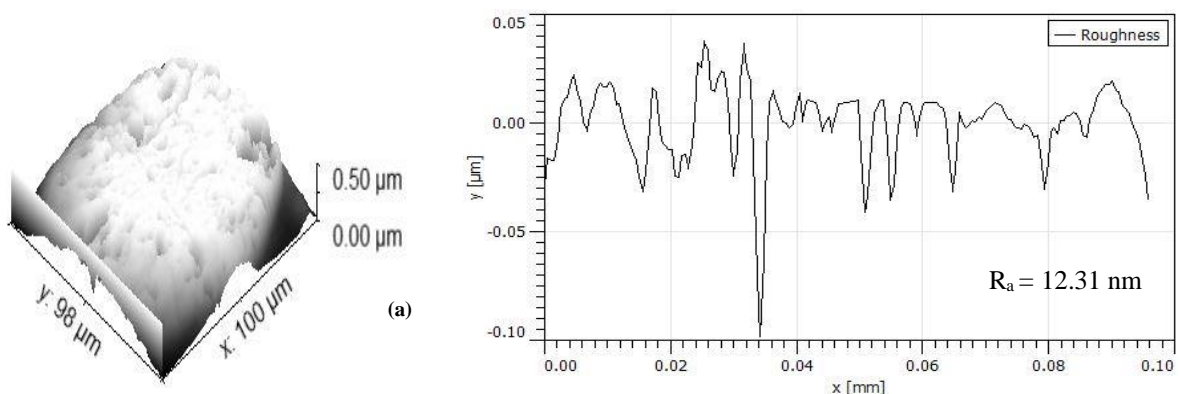
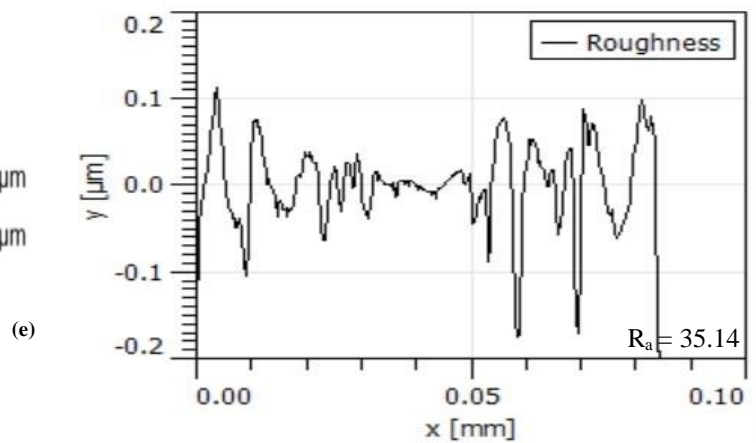
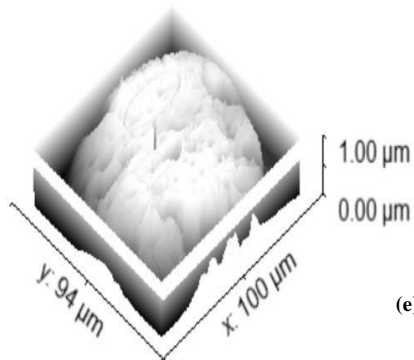
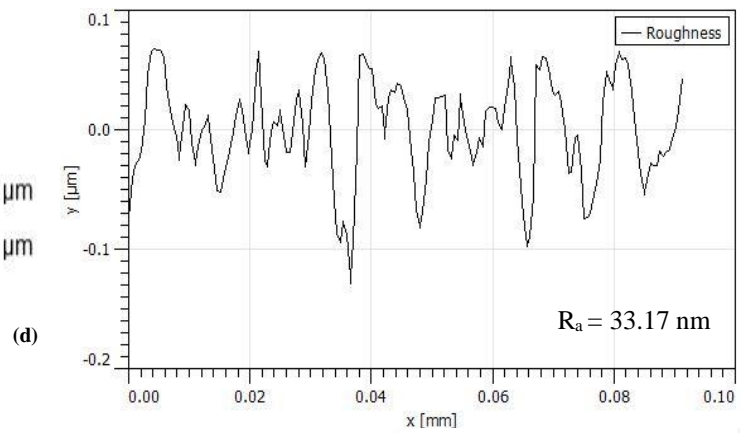
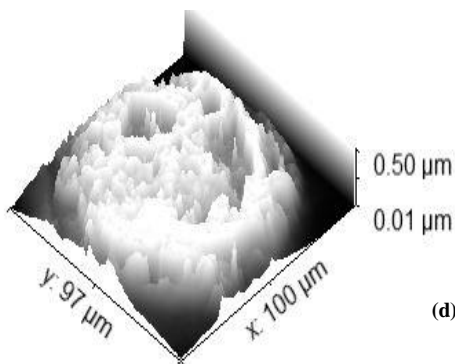
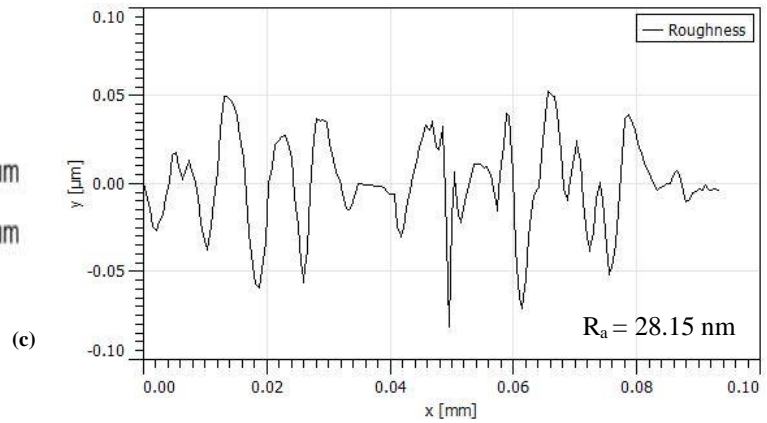
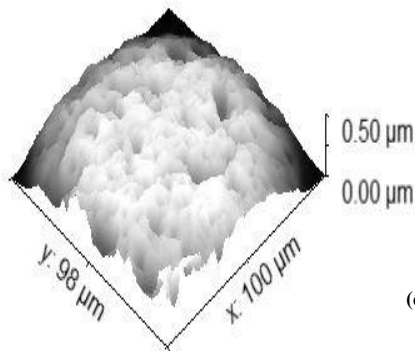
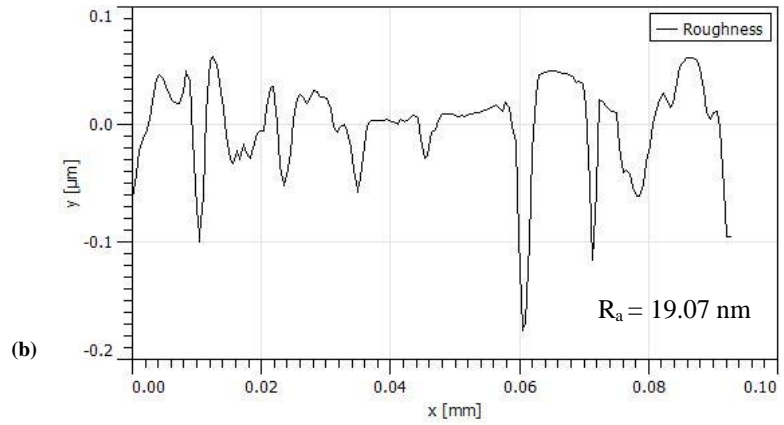
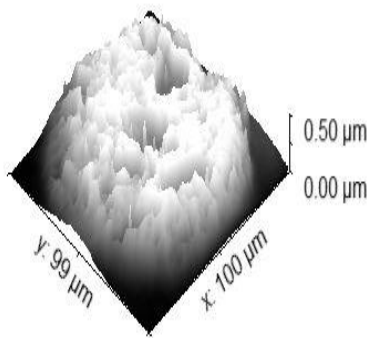


Figure 5.35 Photomicrograph analysis at a cross-section of samples reinforced with Fe

The optical micrographic images (Figure 5.33-5.35) for all the composite filaments were then utilized to obtain the surface morphology and average surface roughness (R_a) value through the processing (image) software (Figure 5.36). The results obtained through the software highlighted that the filaments prepared by reinforcing BP (Figure 5.36(a) and 5.36 (b)) possess better surface texture as indicated by their lesser roughness values ($R_a = 12.31$ nm and $R_a = 19.07$ nm) compared to WD (Figure 5.36 (c) and 5.36 (d)) based composite filaments ($R_a = 28.15$ nm and $R_a = 33.17$ nm) and Fe (Figure 5.36 (e) and 5.36 (f)) based composite filaments ($R_a = 35.14$ nm and $R_a = 88.28$ nm). Such variation in R_a value indeed affects the properties of fabricated filaments. The poor surface finish of composite filaments prepared by Fe was more as compared to other filaments prepared by WD and BP.





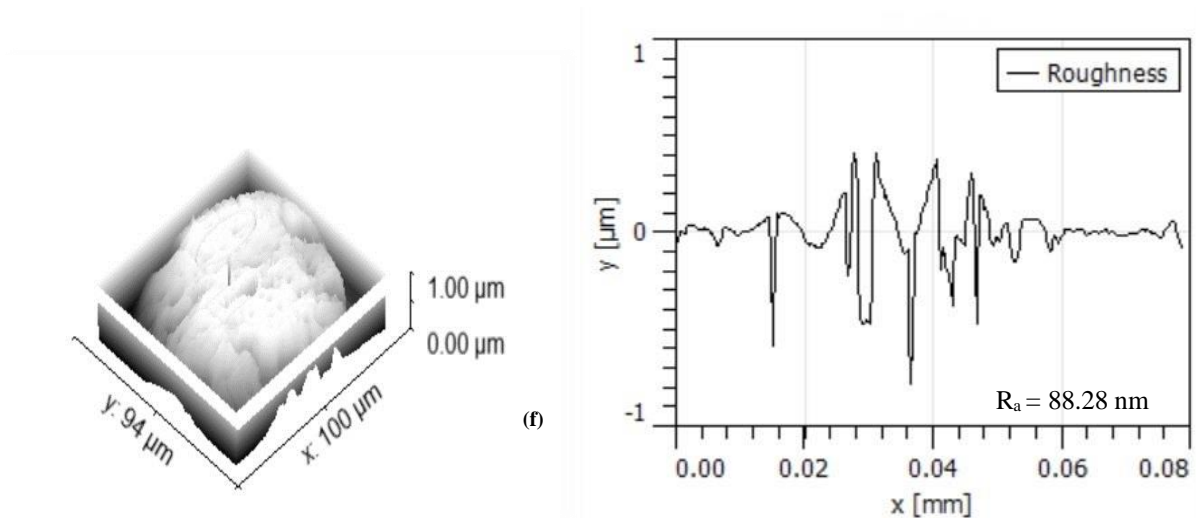


Figure 5.36 Surface morphology of BP (a, b), WD (c, d) and Fe (e,f) reinforced filaments possessing lowest and highest porosity respectively.

The presence and structure (spherical) of BP and Fe in the ABS matrix were confirmed through the scanning electron microscopic (SEM) image (Figure 5.37 and 5.39). But the two-dimensional WD particles being non-conductive were not identifiable in the SEM image (Figure 5.38). To determine the compositional proportion of various materials in the composite filaments, electron dispersive spectroscopy analysis (Point mapping) was performed and the results were shown in the form of an image (Figure 5.40-5.42).

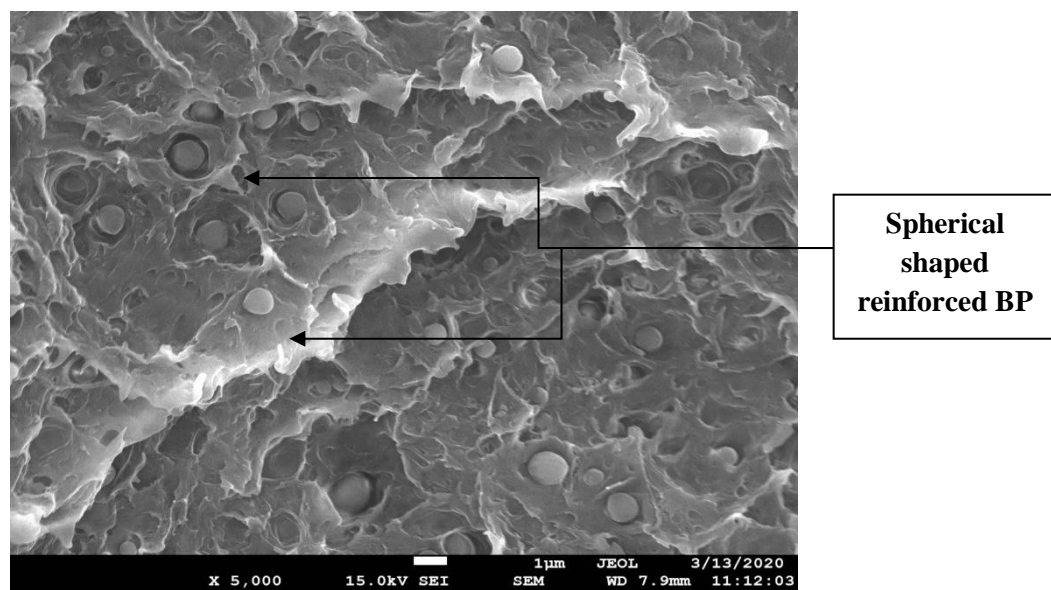


Figure 5.37 SEM analysis of filament at $\times 5000$ (BP reinforced)

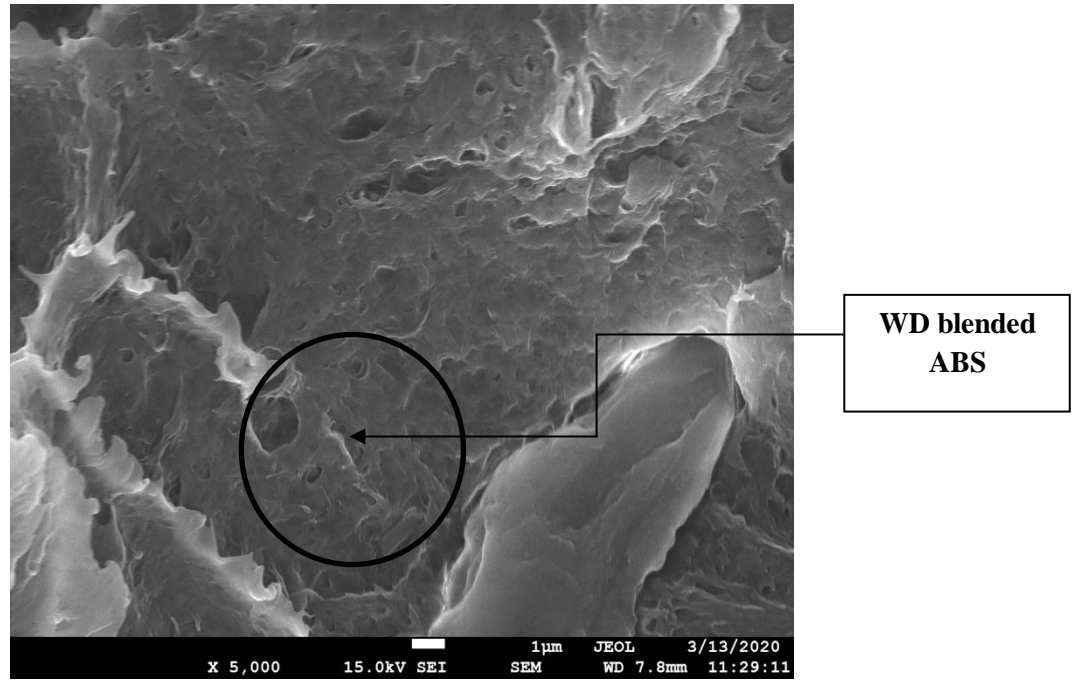


Figure 5.38 SEM analysis of filament at $\times 5000$ (WD reinforced)

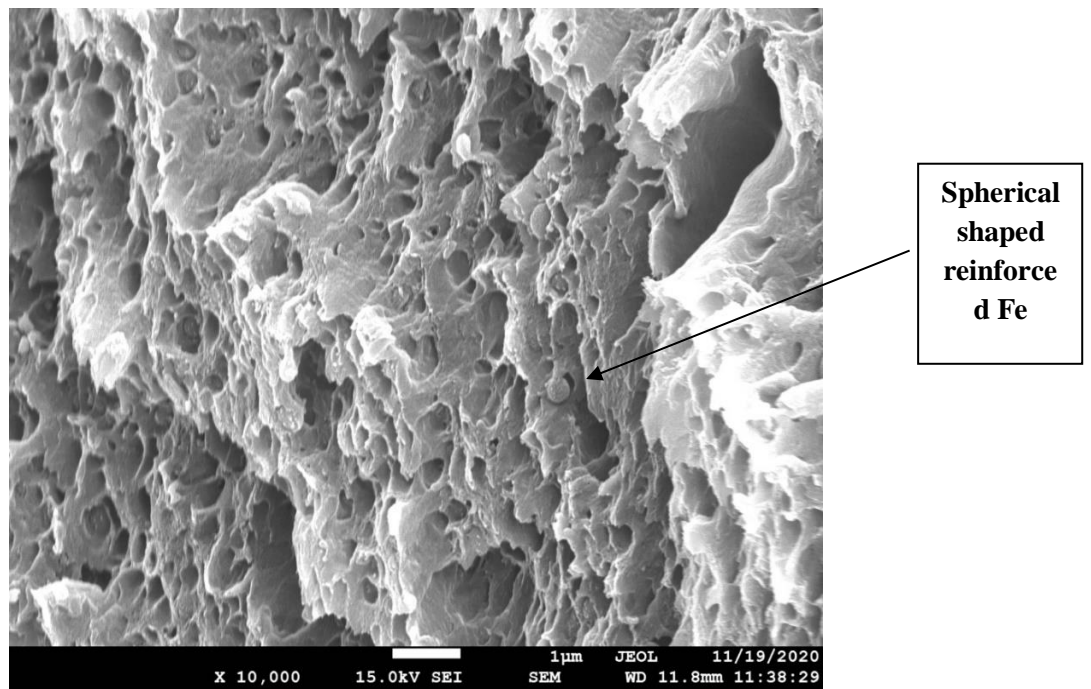


Figure 5.39 SEM analysis of filament at $\times 10,000$ (Fe reinforced)

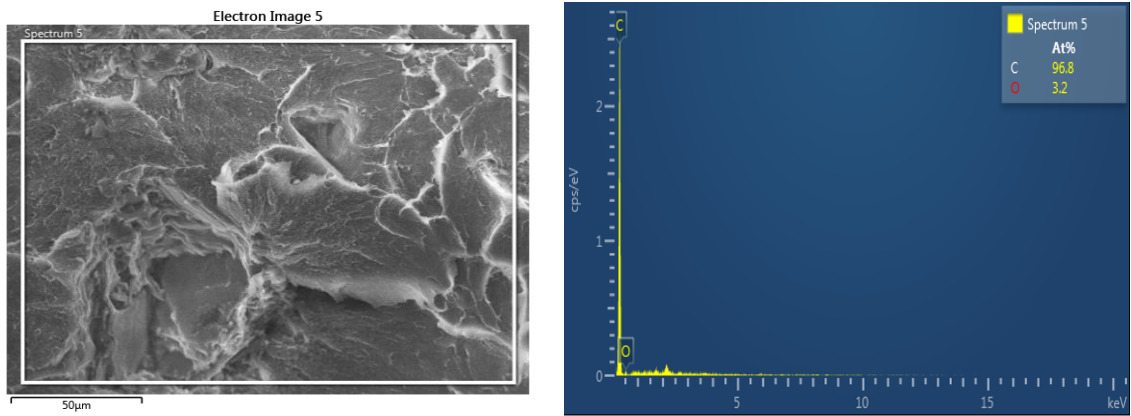


Figure 5.40 EDS analysis of filament possessing maximum PS fabricated by reinforcing BP

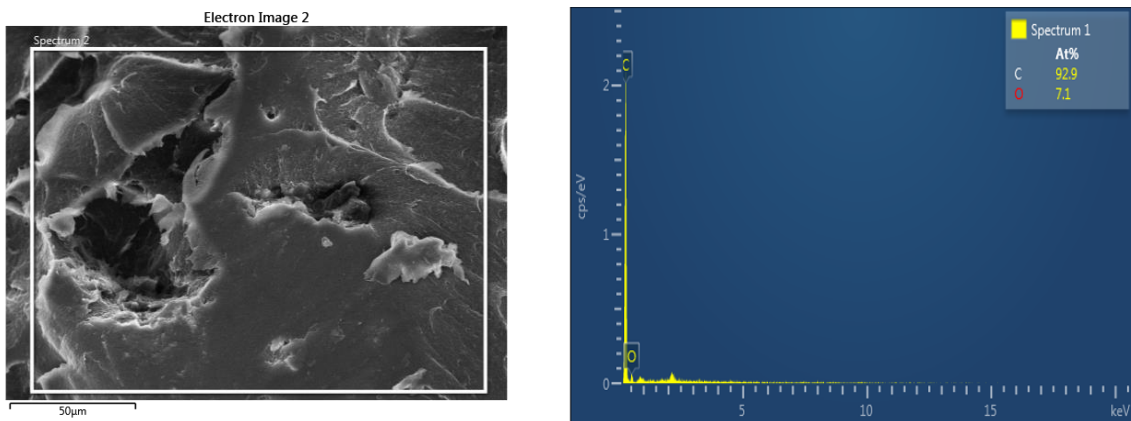


Figure 5.41 EDS analysis of filament possessing maximum PS fabricated by reinforcing WD

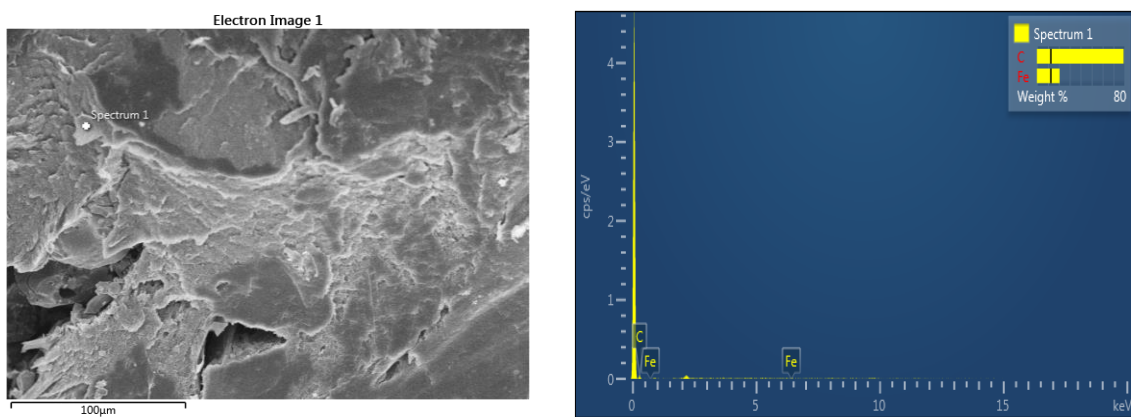


Figure 5.42 EDS analysis of filament possessing maximum PS fabricated by reinforcing Fe

To determine the properties like heat capacity, glass transition temperature, peak temperature, etc of the composite filaments, the thermal stability analysis can be executed using a differential scanning calorimeter (DSC). Since the ABS thermoplastic exhibits amorphous nature, the peak and glass transition temperature cannot be predicted accurately. So, in this work, only the heat carrying capacity of the composite filaments was determined through thermal analysis. The analysis was performed on the sample (1,9), sample (1,6) and sample (4,9) possessing the lowest and highest porosity for BP, WD, and Fe reinforced filaments respectively (Figure 5.43 and 5.44).

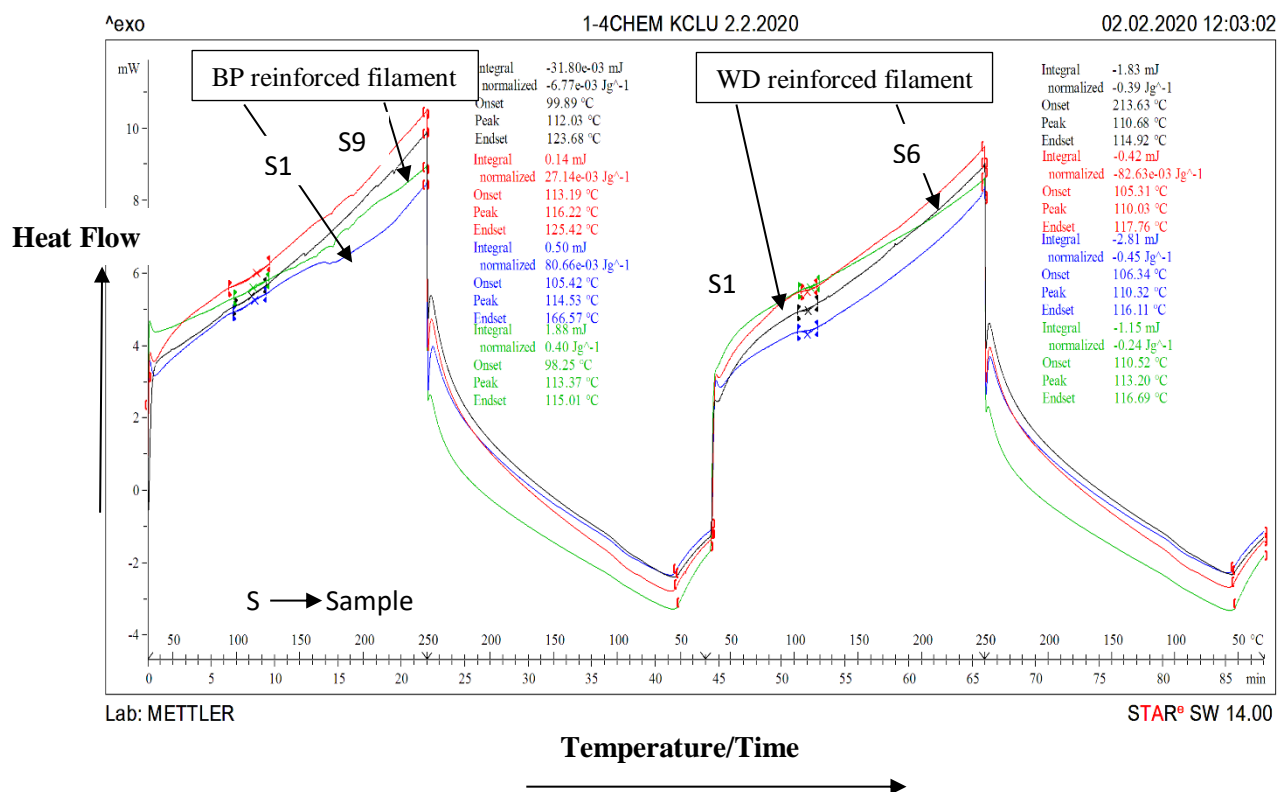


Figure 5.43 Thermal analysis of BP and WD composite filaments

The process consists of repeated heating and cooling of the composite sample by flowing air (50 ml/min) at -10°C/min for endothermic reaction and 10°C/min for an exothermic reaction. The amount of heat absorbed and released during the particular reaction gives the estimation of the heat carrying capacity of the samples. The results revealed that during the alternate heating cycles, BP reinforced filaments show much better heat capacity may be due to the higher thermal conductivity of BP than the corresponding WD reinforced filaments. For instance, the increase in heat capacities was from 80.66×10^{-3} J/g to 0.45 J/g

and 6.77×10^{-3} J/g to 0.39 J/g for samples 1 and 9 (composite filaments reinforced with BP) respectively. Negligible improvement in heat capacity during the alternate heating cycles was indicated by sample 6 whereas a decrease in heat capacity was observed for sample 1 (composite filaments reinforced with WD). Similarly for Fe reinforced filament heat carrying capacity of Sample 4 was 0.57j/g as compared to Sample 9. As per the observations obtained through the thermal investigations, it was predicted that filaments reinforced with WD were not capable of absorbing the heat. On the other hand, improvement in heat carrying capability/behavior during each cycle was demonstrated by the BP reinforced filament and thus indicated the stability of the filament with an increase in temperature.

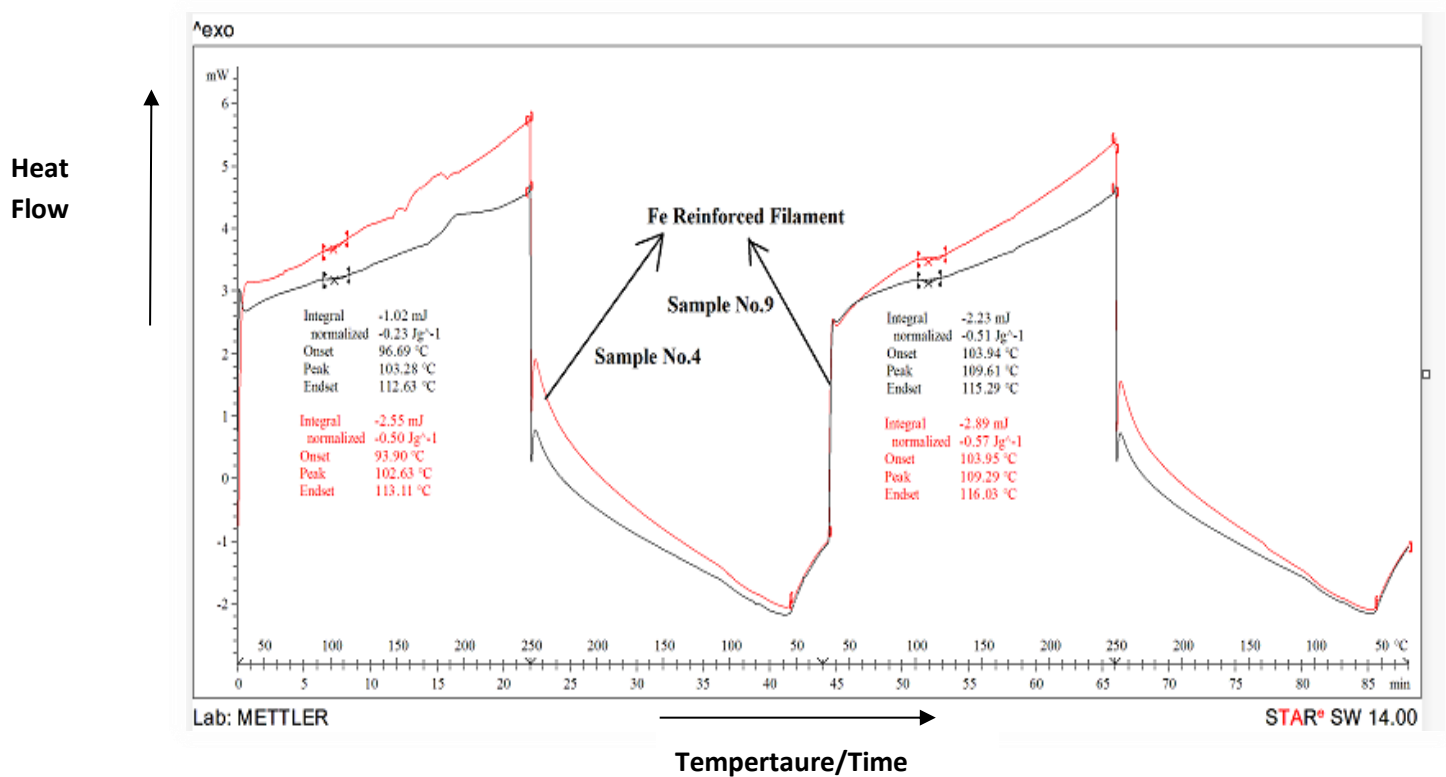


Figure 5.44 Thermal analysis of Fe composite filaments

Optimization of Multiple Responses

BP reinforced composite filaments exhibit better thermal, morphological and mechanical (by and large) properties when contrasted with WD and Fe composite filaments because of the mean effect plots (Figure 5.18-5.23).

Table 5.24 Optimized levels for different responses

Parameters	BP reinforced filament		WD reinforced filament		Fe reinforced filament	
	Optimized Value	Real Value	Optimized Value	Real Value	Optimized Value	Real Value
Load	10 Kg	10 Kg	10 Kg	10 Kg	10 Kg	10 Kg
Temperature	245 °C	245 °C	225 °C	225 °C	245 °C	245 °C
Speed	70 rpm	70 rpm	70 rpm	70 rpm	70 rpm	70 rpm
S/N ratio (PS)	29.81	30.93 MPa	31.06	35.72MPa	29.39	29.18MPa
S/N ratio (% BE)	14.70	5.43 %	16.74	6.87%	15.39	5.88%
Desirability	0.812		0.948		0.988	

But the ideal parametric levels for both composite filaments with their PS and %BE were quite diverse. So, it was obvious to investigate the parametric levels that produce optimum results when both the PS and %BE were given considerable significance and weightage. The current objective was fulfilled by performing the optimization of multiple responses using Minitab 17 software [211]. The requirements optimized levels proposed by the software were reported in Table 5.24.

5.1.3 Mechanical-Hybrid Assisted Blending

In the present objective 2° recycled ABS has been reinforced with 10% reinforcements (BP + WD + Fe). Then the MFR (Melt flow rate) of the prepared composite was determined as per ASTM D1238 standards which indicates the ability of the polymer to flow through a nozzle in 10 minutes under standard conditions. After doing five repeated trials for prepared composite, MFR comes out as 18.35g/10min. On further increase in reinforcement proportion clogging of the nozzle took place. Further, with the help of L9 O.A as per the conditions mentioned in Table 1.1 nine different filaments have been prepared for performing tensile testing with the help of a UTM machine on load rate of 25mm/min. The different mechanical properties obtained for the fabricated filaments were represented in Table 5.25. A stress-strain curve has been plotted with the obtained values as shown in Figure 5.45. From the stress-strain curve, it has been observed that sample 6 possesses maximum toughness of 0.550 MPa while sample 3 gives a minimum 0.10 MPa among all the filaments.

Table 5.25 Different Mechanical properties obtained after tensile testing

S.No	PS (MPa)	BS (MPa)	% PE	% BE	E (GPa)	T (MPa)
1	9.65±1.7	8.6±1.6	4.4±0.6	3.23±0.7	0.380±0.15	0.122±0.3
2	9.55±1.5	8.54±1.4	3.5±0.4	2.53±0.5	0.376±0.25	0.107±0.2
3	9.21±0.9	9.11±0.8	3.8±0.5	1.9±0.4	0.484±0.2	0.10±0.15
4	11.76±1.4	10.1±1.3	3.1±0.3	2.22±0.4	0.530±0.35	0.125±0.2
5	10.21±1.2	9.51±1.2	2.8±0.2	3.82±0.3	0.104±0.4	0.466±0.25
6	13.79±1.4	8.69±1.1	3.1±0.2	1.27±0.6	1.08±0.3	0.550±0.2
7	14.38±1.3	11.13±1.4	2.2±0.3	2.22±0.3	0.648±0.3	0.123±0.25
8	20.47±1.6	16.29±1.5	4.3±0.4	1.2±0.5	3.2±0.2	0.210±0.35
9	17.89±1.3	10.59±1.2	3.4±0.3	1.9±0.4	0.941±0.4	0.117±0.15

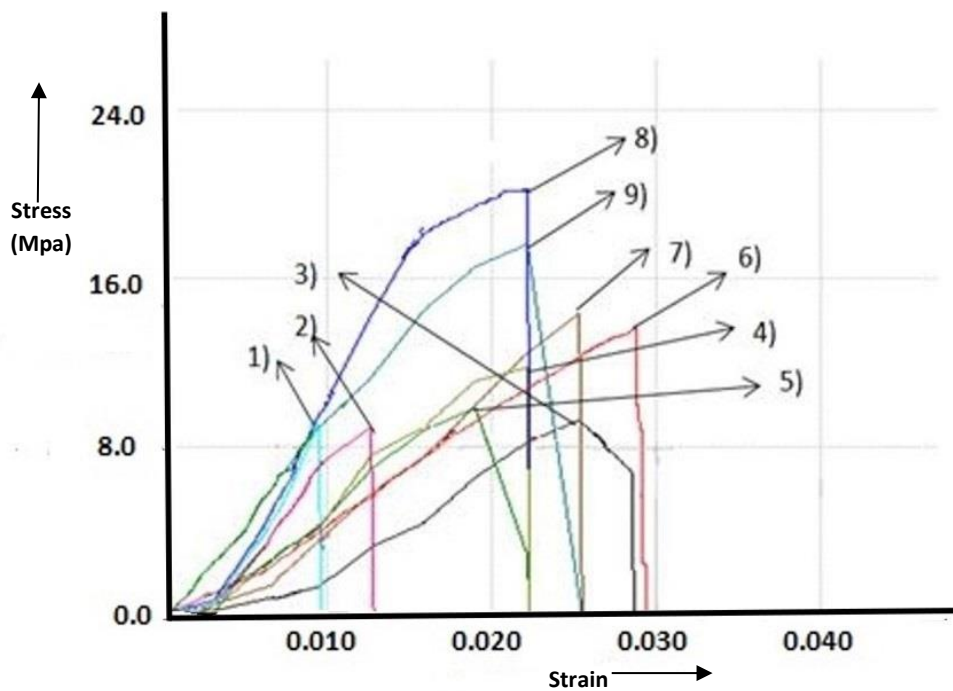


Figure 5.45 Stress-strain curve for prepared filaments

Optical photomicrographs were taken at the break cross-section for samples no. 8 and 3 having maximum and minimum peak strength (PS) as shown in Figure 5.46.

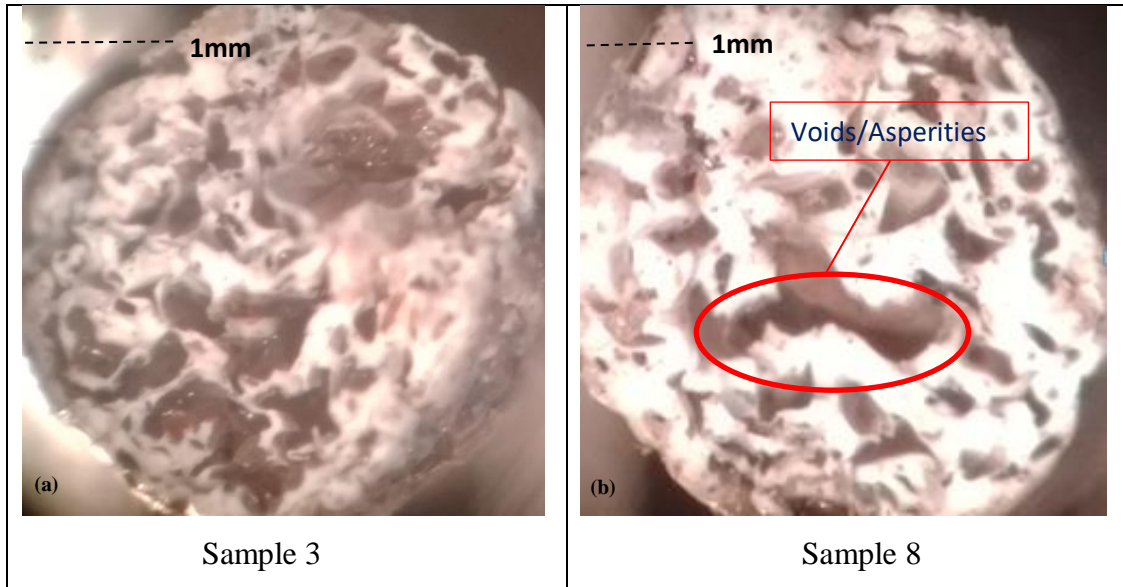


Figure 5.46 Optical Photomicrograph of filaments having least and highest voids

To determine the presence and nature of bonds formed between the base and reinforced materials that ultimately effects the PS of the composite filament, FTIR analysis was performed. The FTIR analysis of filaments having maximum PS fabricated by different blending techniques is shown in Figure 5.47.

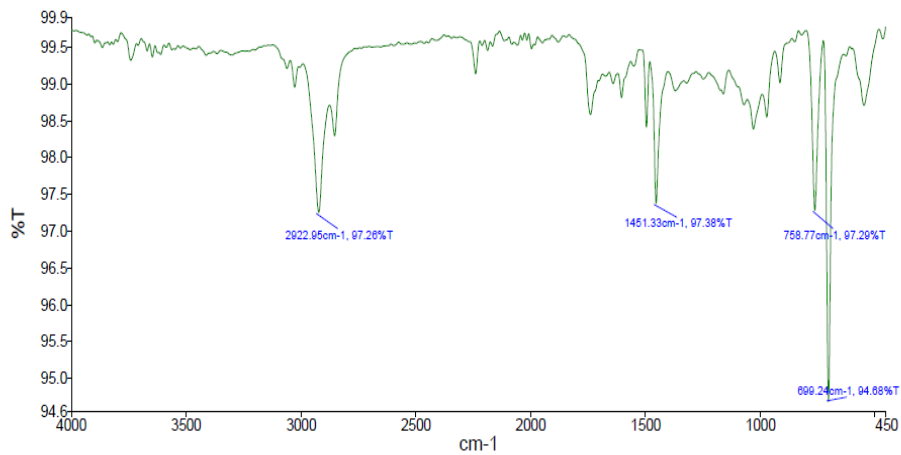


Figure 5.47 FTIR of composite filaments having maximum PS prepared by mechanical-hybrid blended

The first sharp peak was at wave number in the range of 2922 cm^{-1} indicates C-H bond stretching and the second medium peak at a wavenumber of 1450 cm^{-1} represents C-H bond bending and C-C bond stretching due to aromatic rings present in ABS thermoplastic. The sharp significant peak at 699.2 cm^{-1} corresponds to the Fe-O bond present in the mechanical-hybrid composite may be responsible for lower PS.

From photomicrograph analysis, it has been found that the number of voids in all the filaments were not the same and filaments fabricated at low speed contain a relatively higher number of voids as compared to other samples. Further, both selected optical photomicrograph images were processed on image processing software for estimating the average surface roughness (R_a) and surface topology. The results obtained for average surface roughness (R_a) in the form of the graph has been shown in Figure 5.48. From analysis, it has been found that sample 8 has minimum R_a (24.38 nm) whereas sample 3 has maximum R_a (32.43 nm) which could be due to the presence of a higher number of voids. Therefore, it has been found that the presence of a higher number of asperities/voids in the fabricated filaments could be one of the reasons for showing poor mechanical properties.

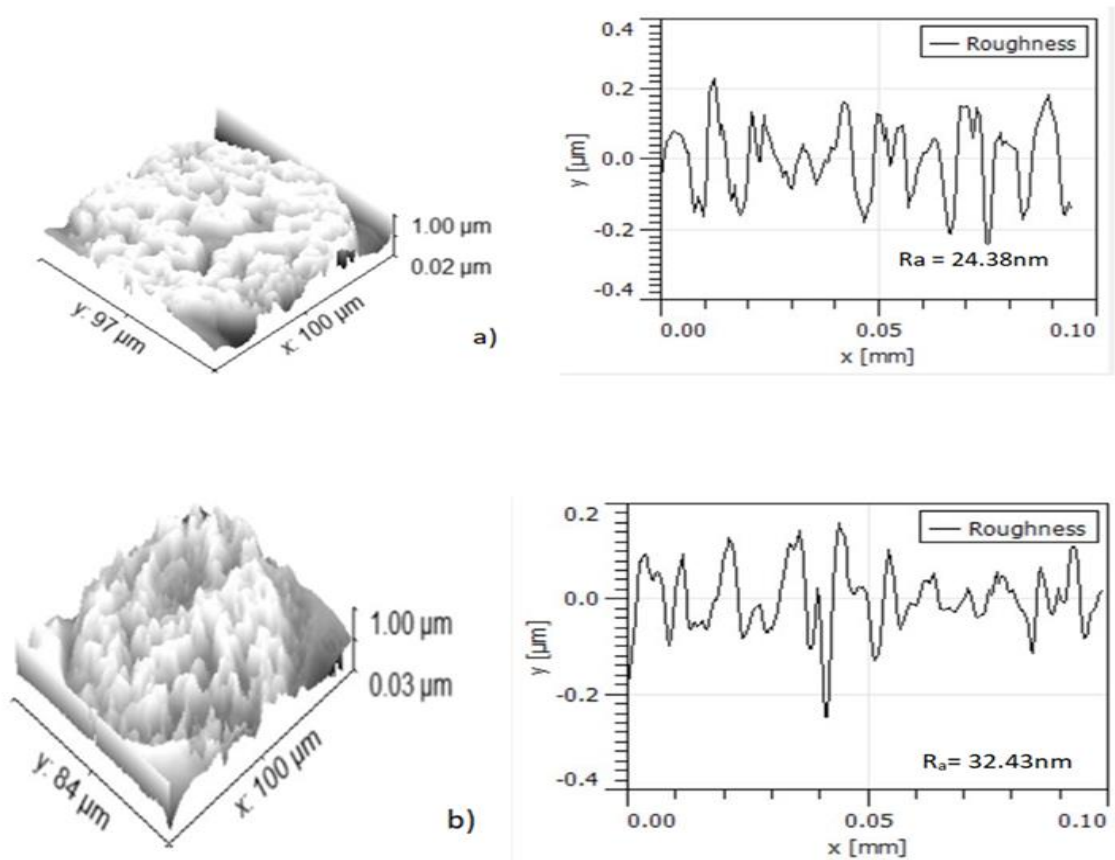


Figure 5.48 Surface topology of filaments having a) minimum and b) maximum voids

Tool Maker Microscope has been used to determine the porosity of filaments at $\times 100$ as per standard ASTM B276. The porosity results obtained in the form of the image has been shown in Figure 5.49.

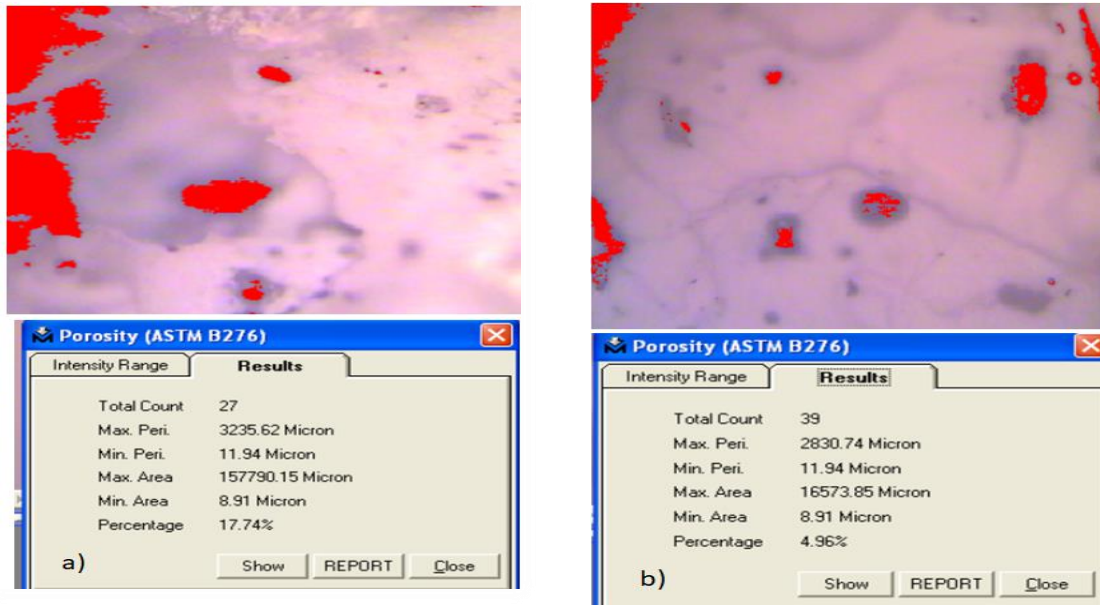


Figure 5.49 Porosity presence along with percentage in composite filaments

From SEM analysis as shown in Figure 5.50 it has been found that filaments having poor mechanical bonding due to improper mixing of reinforced material especially Fe particles with base matrix results in the formation of higher number of voids.

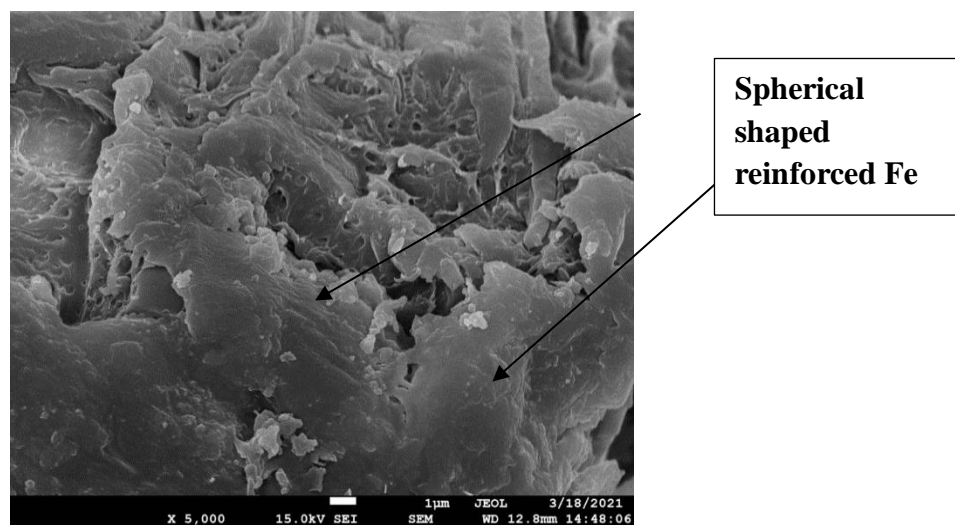


Figure 5.50 SEM analysis of filament prepared by hybrid blending

Further EDS analysis (Area mapping) has been done for determining the composition of elements present in the filament. From EDS analysis it has been found that the red color shows the percentage of Carbon atoms i.e 90.25%, and the green color shows the percentage of Iron atoms i.e 9.75% as shown in Figure 5.51.

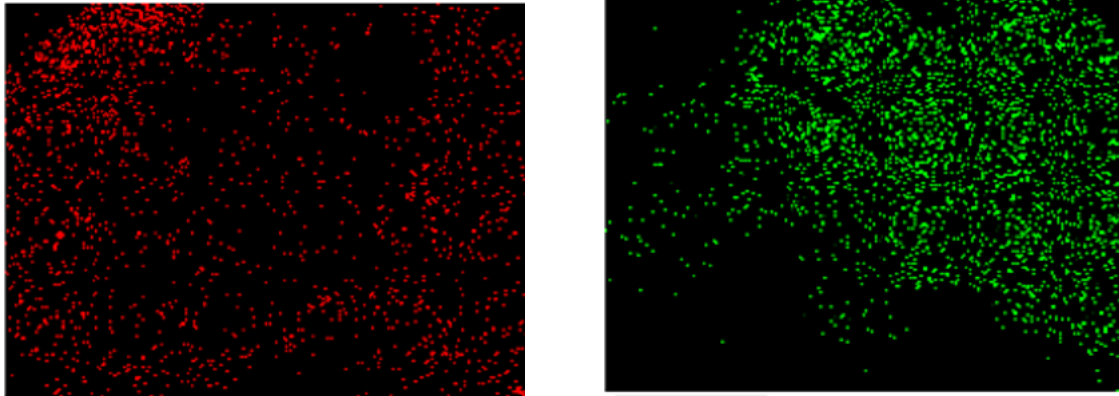


Figure 5.51 EDS analysis of filament prepared by hybrid blending

Further, the signal to noise (S/N) ratio has been calculated for PS and %BE based on a larger is a better approach using equation (1) as represented in Table 5.26.

Table 5.26 Calculated S/N values for PS

Sample No.	1	2	3	4	5	6	7	8	9
S/N value for PS	19.69	19.60	19.28	21.40	20.10	22.79	23.15	26.22	25.05
S/N value for %BE	10.1841	8.0624	5.5751	6.9271	11.6413	2.0761	6.9721	1.5836	5.5751

Based on calculated S/N, the mean effect plot for PS and %BE has been obtained as shown in Figure 5.52. As PS and %BE both are important parameters affecting the strength of filament, therefore ANOVA has been applied on calculated S/N values for determining the predominant factor that affects the PS and %BE of the filaments. The results of ANOVA have been shown in Table 5.27- 5.28. From mean S/N ratio plots as shown in Figure 5.52. It has been observed that with an increase in extrusion load and temperature, PS of the composite filament increases but in the case of %BE it is opposite. The increase in load helps in the easy flow of the material. Also, maximum PS has been obtained at low speed i.e 70

rpm because at low-speed reinforced material forms sufficient strong bonds with a base material which results in maximum PS. But in the case of %BE it is maximum at 90 rpm. Therefore, suitable parametric conditions for obtaining maximum PS are 15 kg load, 245° C temperature and 70 rpm speed but while for %BE were 10 kg load, 225° C temperature and 90 rpm speed.

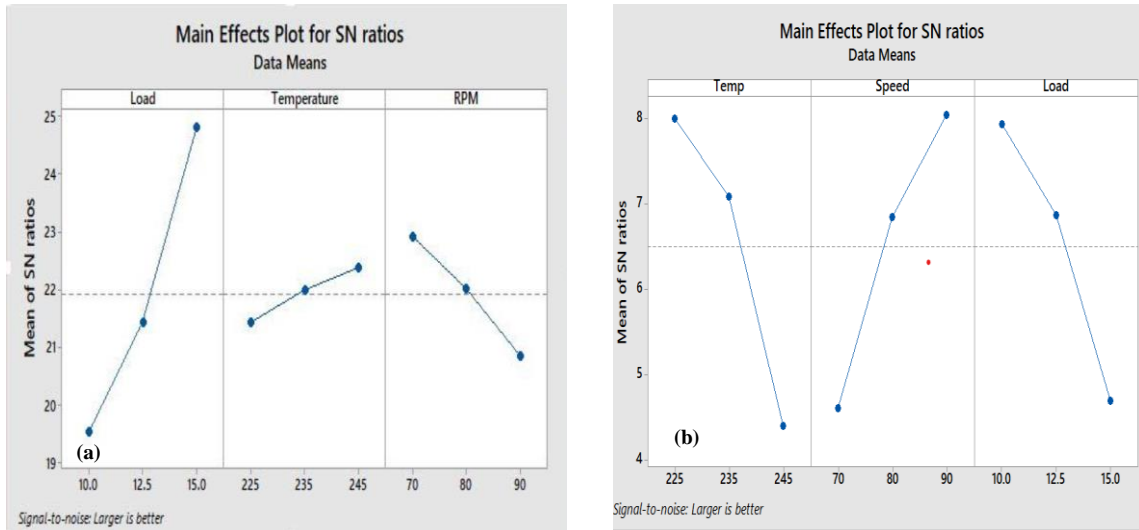


Figure 5.52 Mean S/N ratio for a) PS b) %BE of composite filaments

Table 5.27 ANOVA analysis for PS of composite filaments

Source	DOF	Adj SS	Adj MS	F-value	P-value
Temperature	2	1.399	0.699	2.02	0.331
Speed	2	6.202	3.101	8.96	0.100
Load	2	42.892	21.446	61.94	0.016
Error	2	0.692	0.346		
Total	8	51.1871			

Table 5.28 ANOVA analysis for %BE of composite filaments

Source	DOF	Adj SS	Adj MS	F-value	P-value
Temperature	2	21.05	10.52	0.65	0.607
Speed	2	18.23	9.11	0.56	0.141
Load	2	16.43	8.21	0.50	0.065
Error	2	32.55	16.27		
Total	8	88.26			

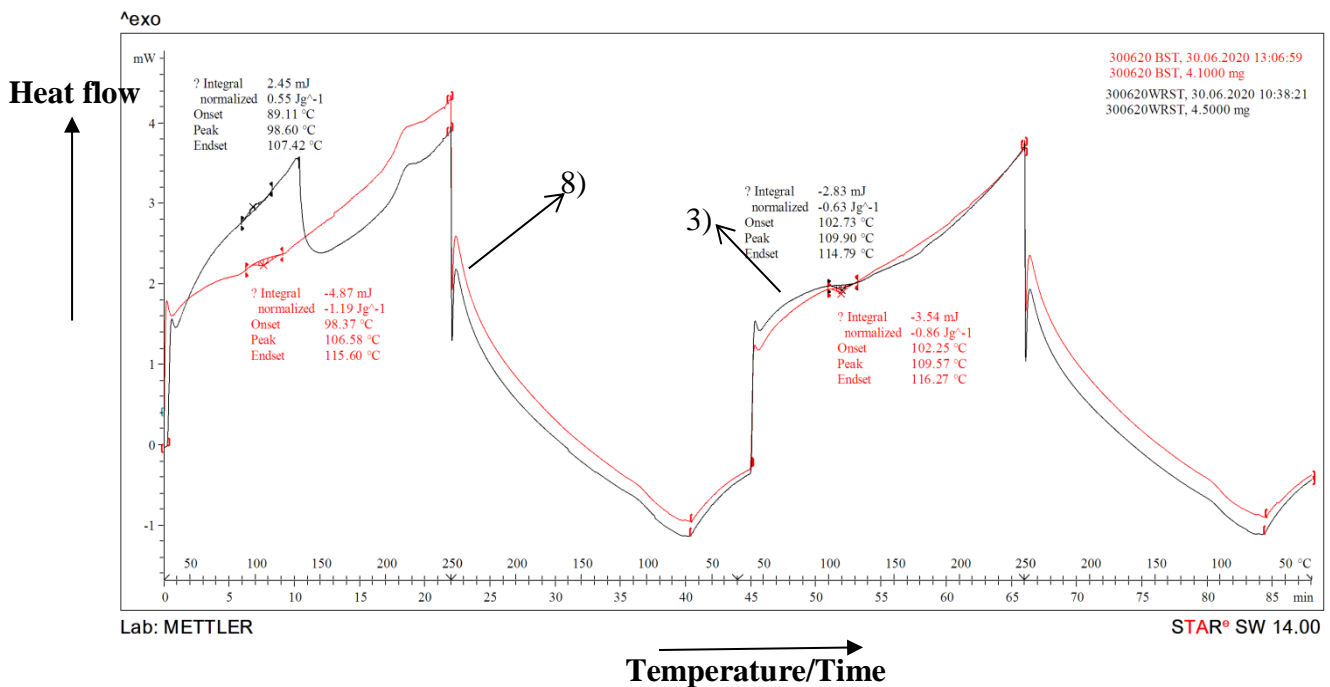


Figure 5.53 Thermal analysis of filaments having maximum and least porosity

At last thermal analysis of filaments (having maximum and minimum porosity) has been performed with the help of DSC for studying the effect of reinforcements. Thermal analysis was done at an airflow of 50 ml min^{-1} using three cycles of heating and cooling for both exothermic and endothermic reaction as shown in Figure 5.53. From the thermal analysis, it has been observed that the heat carrying capacity of sample 8 (0.86 J/g) is more as compared to sample 3 (0.63 J/g). Therefore, filament fabricated as per the processing conditions of sample 8 might be suitable for high-temperature applications.

The selected thermal and mechanical (%BE and PS) properties of the composite filaments (BP, WD and Fe) fabricated through different routes of blending (mechanical, chemical and mechanical- hybrid assisted) were compared to estimate the variation in properties of fused filaments. The observations of comparison (Table 5.29) revealed that chemical (acetone) blending of reinforcements in ABS matrix yields improved mechanical properties (especially WD reinforced filament) as compared to mechanical and hybrid blending. However, maximum heat capacity (one of the most important thermal properties of composite filaments) was achieved through mechanical blending. Further filaments having maximum peak strength have been prepared with the help of a Twin Screw Extruder for multilayer and hybrid layer printing.

Table 5.29 Comparison of properties for composite filaments

	Mechanical Blending			Chemical Blending			Hybrid Blending
Property	BP reinforced filament	WD reinforced filament	Fe reinforced filament	BP reinforced filament	WD reinforced filament	Fe reinforced filament	Hybrid Reinforced Filament
PS	30.58 MPa	25.65 MPa	32.82MPa	30.93 MPa	35.72 MPa	30.27MPa	20.49MPa
%BE	5.15 %	6.05 %	8.25%	5.43 %	6.87 %	6.97%	1.2%
Heat capacity	2.17 J/g	0.38J/g	0.48j/g	0.45 J/g	0.24 J/g	0.57j/g	0.83j/g

5.2 PHASE 2- (3D PRINTING)

5.2.1 Print functional prototypes via mechanical-assisted blending

The next step was a printing of function prototypes with the help of Fused Deposition Modeling, total 18 samples have been prepared (9 samples of tensile and 9 samples of flexural) as per the L9 orthogonal array mentioned in Table 4.4. Prepared specimens were further processed on a UTM machine on load rate of 25mm/min. for calculating their mechanical properties as shown in Tables 5.30 and 5.31.

Table 5.30 Different observations obtained during tensile testing

S.No	PS (MPa)	BS (MPa)	% PE	% BE	E (GPa)	T (MPa)
1	11.85	10.66	3.72	3.92	0.4416	0.1616
2	13.84	12.45	6.23	6.20	0.2428	0.4731
3	15.35	13.10	6.92	7.82	0.242	0.5043
4	11.08	9.98	3.84	4.15	0.4961	0.14471
5	12.45	11.08	3.48	5.95	0.3572	0.2105
6	12.97	11.31	4.43	7.32	0.3723	0.2148
7	8.96	7.35	6.33	3.80	0.2021	0.1745
8	7.68	6.35	5.70	4.75	0.6063	0.0502
9	9.98	8.76	6.23	5.88	0.6173	0.0934

Table 5.31 Different observations obtained during flexural testing

S.No	PS (MPa)	BS (MPa)	% PE	% BE	E (MPa)	T (MPa)
1	23.39	28.90	7.6	13.78	0.4004	1.2354
2	25.38	22.84	7.7	11.88	0.7120	0.90408
3	32.11	22.27	7.13	9.98	0.7406	0.7404
4	17.44	12.49	6.65	15.21	0.4451	0.6526
5	20.11	18.09	6.95	11.44	0.6446	0.6874
6	24.74	15.70	6.65	13.80	0.5593	0.7208
7	13.88	17.48	7.6	14.73	0.5450	0.8579
8	17.89	16.10	9.03	18.53	0.4228	1.2236
9	19.43	21.05	10.93	15.68	0.4566	1.2998

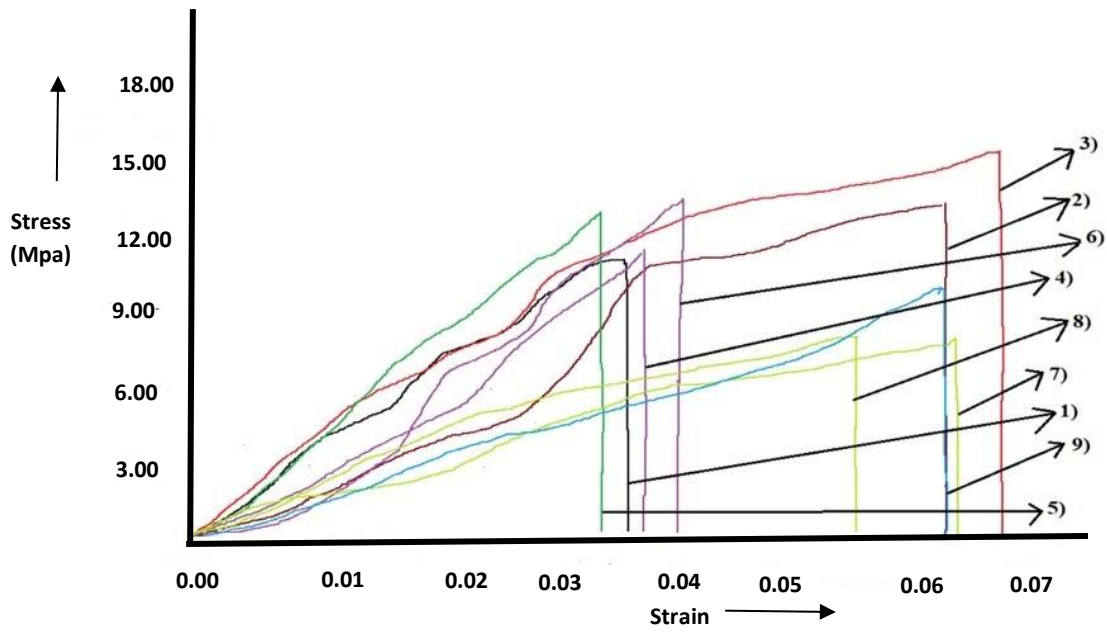


Figure 5.54 Stress-Strain curve of 3D printed specimens after tensile testing

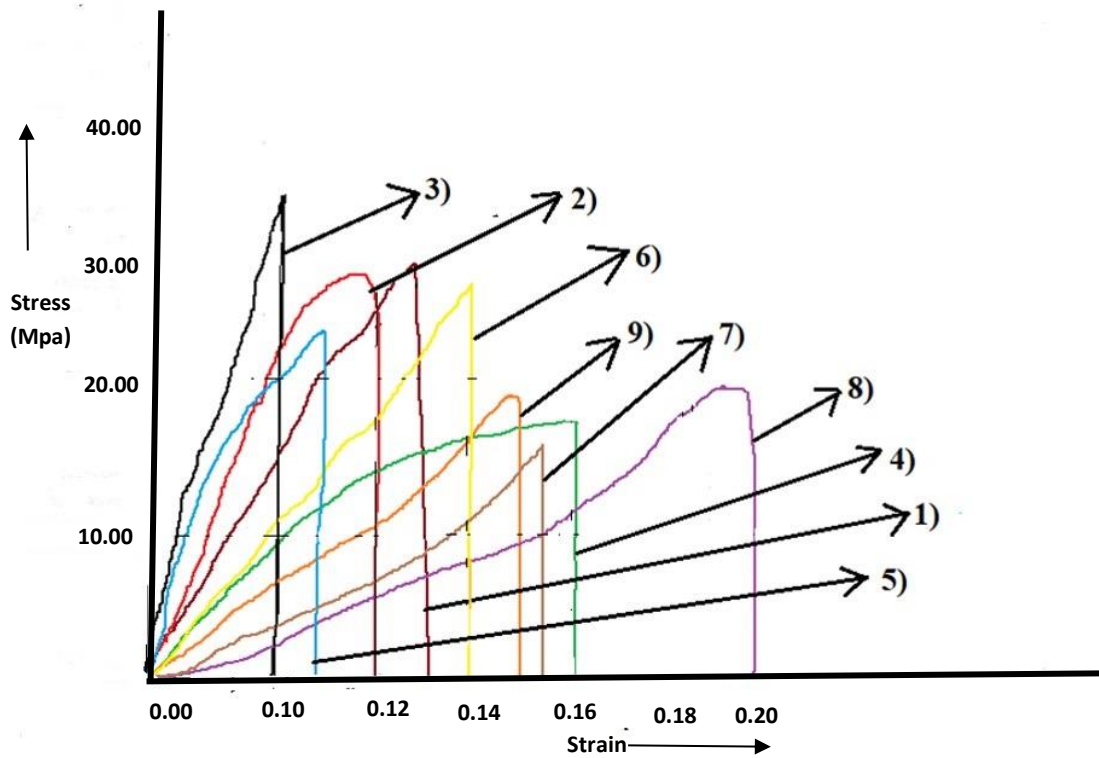


Figure 5.55 Stress-Strain curve of 3D printed specimens after flexural testing

From stress-strain analysis (Figure 5.54 and 5.55) it has been found that maximum peak strength of tensile specimen has been found for Sample No. 3 and least for Sample No. 8, similarly while analysing peak strength of flexural specimen it has been found that Sample No. 3 has maximum flexural strength as compared to Sample No. 7. This shows that samples prepared at 100% infill density have maximum strength as compared to samples prepared at 90% and 80% infill density. It may be because at higher infill density less gap was there between the layers which lead to give better mechanical strength. Further, for better understanding, the effect of input variables ANOVA and S-N ratio analysis has been done.

After tensile testing SEM analysis at 33X Zoom has been done on both tensile and flexural as shown in Figures 5.56 and 5.57. From SEM analysis, it has been found that there was a fractured surface between the adjacent layers that were responsible for showing poor mechanical properties. EDS analysis (Area Mapping) of 3D printed specimen was done to determine the weight percentage of the elements present in the 3D printed specimen. From EDS analysis of the 3D printed tensile specimen, it has been found that the percentage of carbon in the composite was 94.72% by wt. whereas Iron was 5.28% by wt. as shown in Figure 5.58.

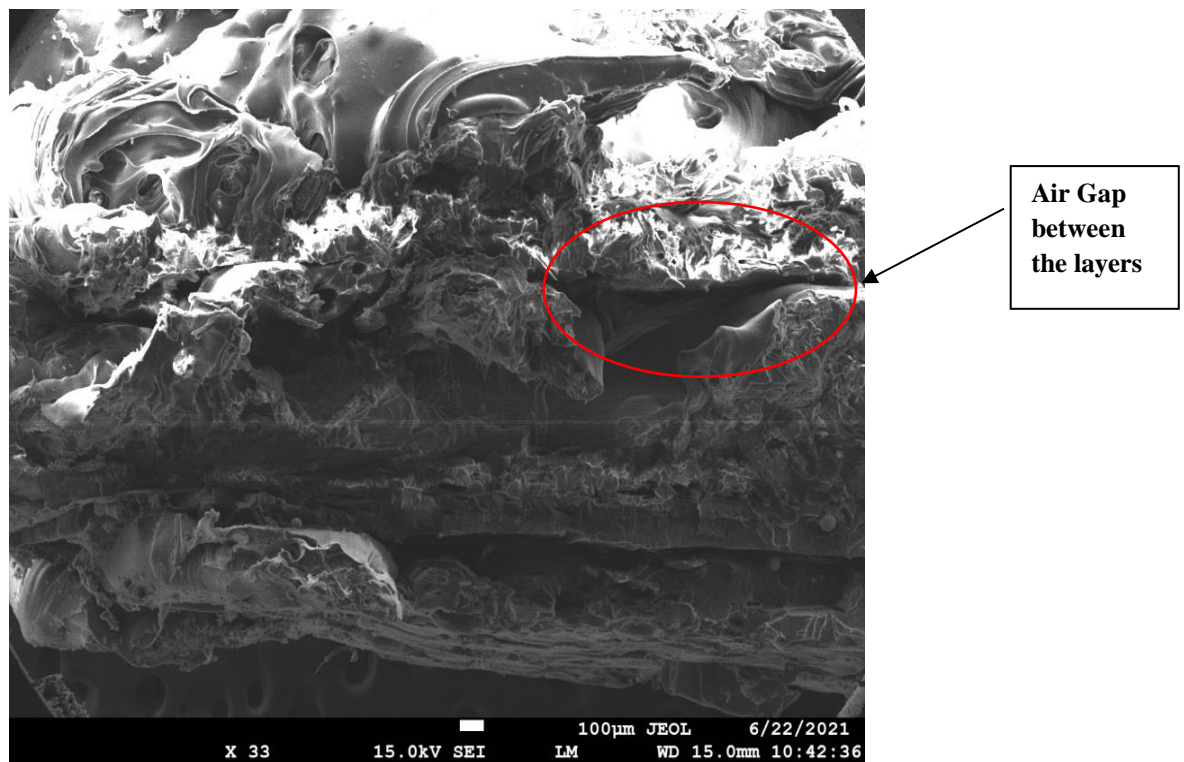


Figure 5.56 SEM analysis of 3D printed tensile specimen

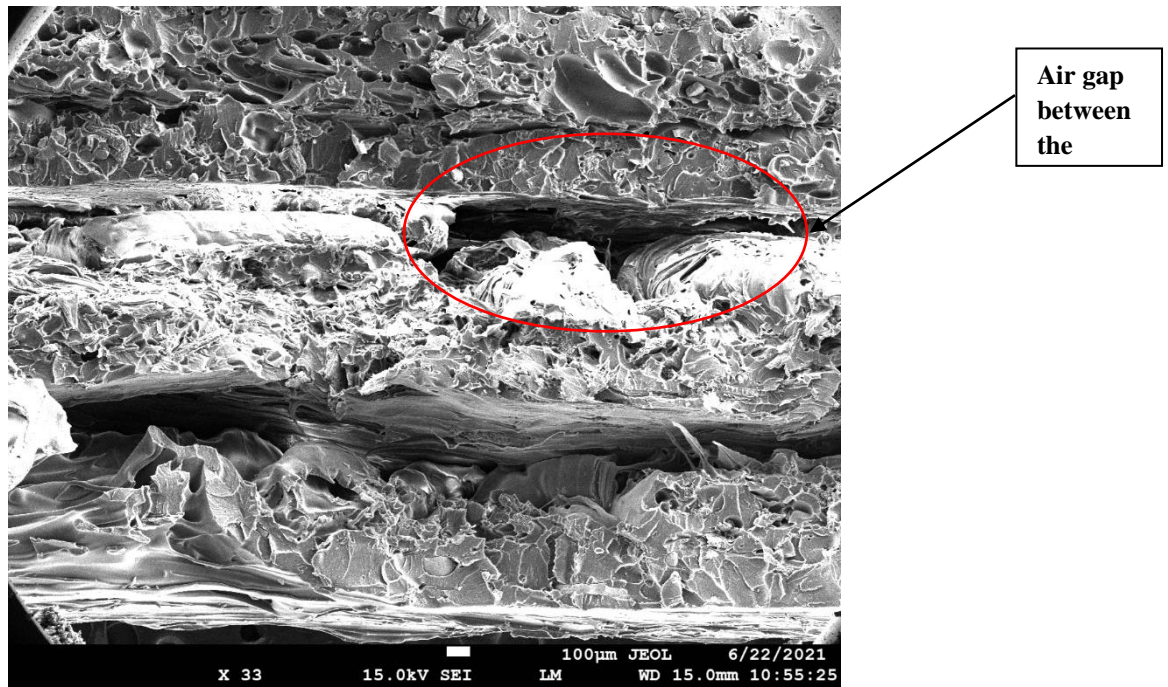


Figure 5.57 SEM analysis of 3D printed Flexural specimen

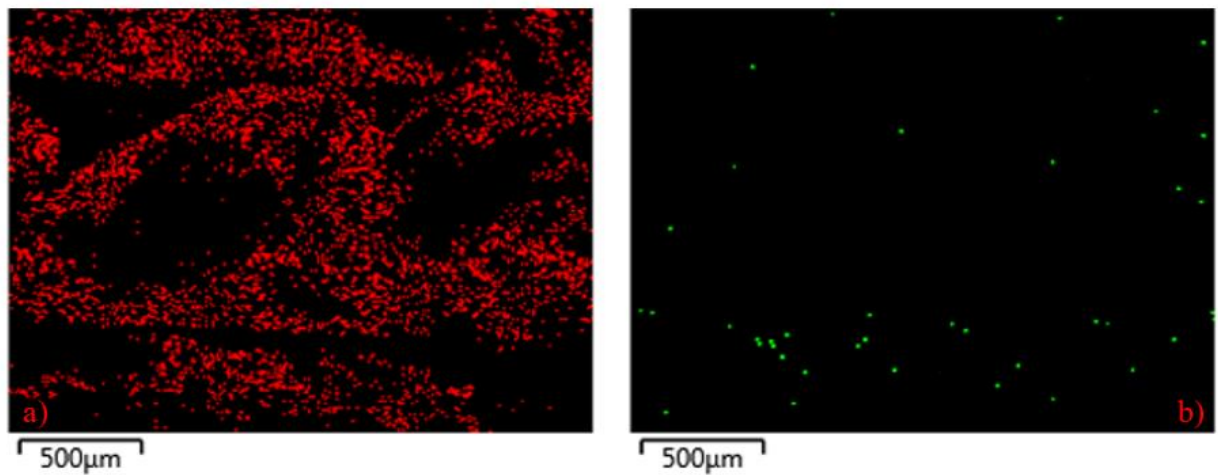


Figure 5.58 EDS analysis of 3D printed tensile specimen a) shows wt.% of carbon particles
b) shows wt.% of Fe particles

Similarly, EDS analysis (Area Mapping) of 3D printed flexural specimen has been done and it was found that carbon percentage is 96.27 % by wt. whereas iron percentage is 3.73% by weight as shown in Figure 5.59.

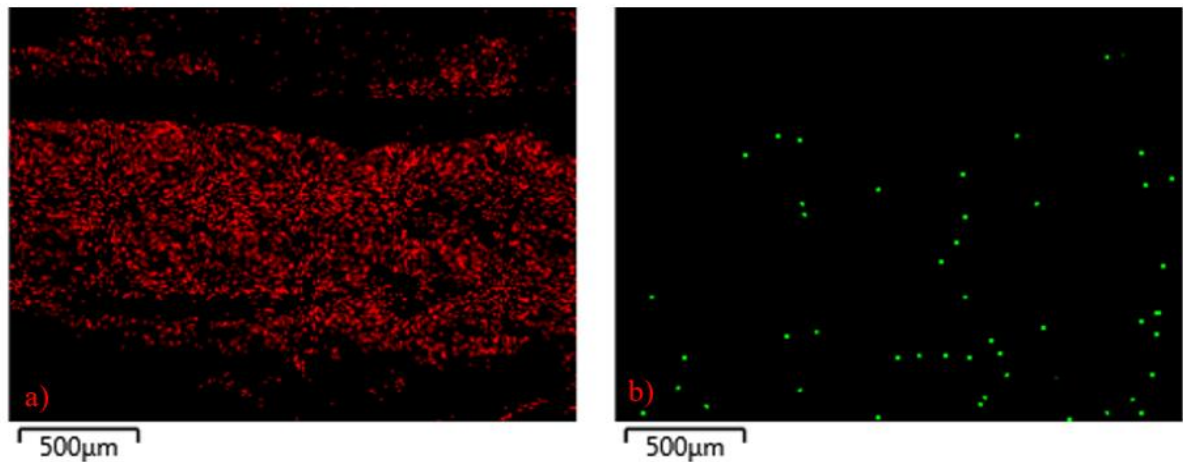


Figure 5.59 EDS analysis of 3D printed flexural specimen a) shows wt.% of carbon particles
 b) shows wt.% of Fe particles

Analysis of variance (ANOVA)

From ANOVA analysis S/N ratio plots have been drawn for PS and %BE for both specimens as shown in Figures 5.60 and 5.61. From Peak strength analysis it has been found that maximum strength was found at 0° raster angle as raster angle increases peak strength has been decreased, the same type of behavior has been found for flexural specimens. But the effect of raster angle on the Peak strength of the flexural specimen was more as compared to 3D printed tensile specimen. While analyzing the effect of infill density it has been found that with a decrease in infill percentage peak strength has been decreased and maximum peak strength was found at 100% infill density for both 3D printed specimens. It could happen because at lower infill density there is a gap between the adjacent layers which ultimately leads to poor bonding and decreased strength of the printed specimen. The next parameter was printing speed it was found that the maximum peak strength of the tensile specimen was found at 40mm/s it could be due to because at lower printing speed there is sufficient cooling time between the subsequent layers due to which poor bonding was formed. The parametric conditions that yield maximum PS for 3d printed tensile specimen were 0° raster angle, 100% infill density and 40 mm/s infill speed whereas 0° raster angle, 100% infill density and 20mm/sec infill speed provides better results in the case of 3D printed flexural specimen.

Table 5.32 S-N ratio analysis of peak strength and % break elongation for both tensile and flexural specimen

Exp. No.	Tensile specimen		Flexural specimen	
	S/N ratio for PS (dB)	S/N ratio for % BE (dB)	S/N ratio for PS (dB)	S/N ratio for % BE (dB)
1	21.47	11.86	27.38	22.78
2	22.82	15.84	28.08	21.49
3	23.72	17.86	30.13	19.98
4	20.89	12.36	24.83	23.64
5	21.90	15.49	26.08	21.16
6	22.25	17.29	27.86	22.81
7	19.70	11.59	22.84	23.36
8	17.70	13.53	25.02	25.35
9	19.98	15.38	25.76	23.90

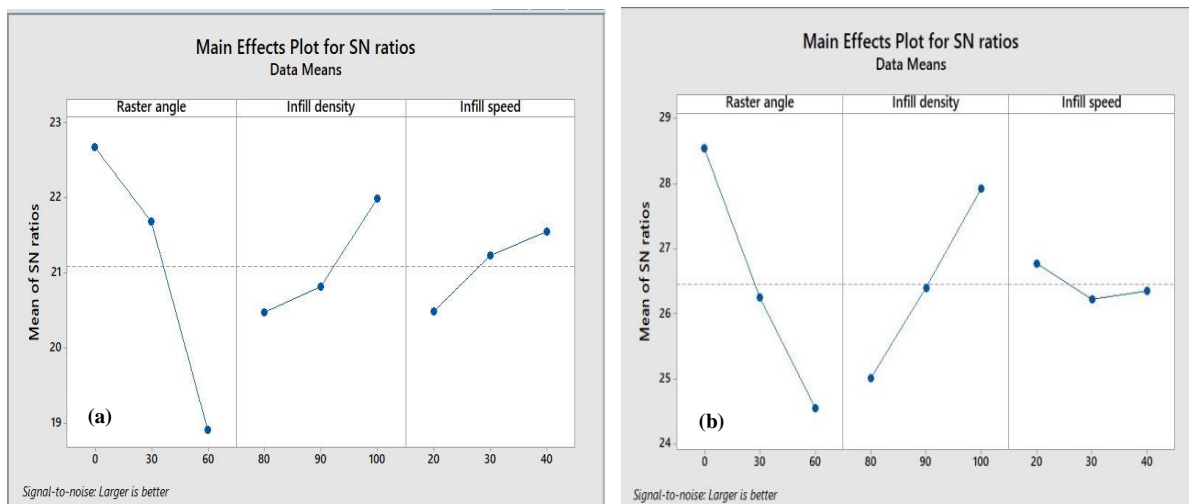


Figure 5.60 Mean S/N ratio plots for PS of tensile and flexural specimen

The %BE of 3D printed tensile specimens increases with an increase in infill density from 80 % to 100 % as shown in Figure 5.61. While in the case of flexural specimen it was maximum for 80% infill density. However, the effect of raster angle on %BE for flexural specimen was much higher as compared to 3D printed tensile specimen. As the infill speed increases, the %BE for 3D printed tensile specimen increases whereas for flexural specimen

maximum flexural strength was obtained at 20mm/sec it may be due to lower speed there was better bonding between the layers as compared to specimen prepared at higher speed. The parametric conditions that yield maximum %BE for 3D printed tensile specimen was 0° raster angle, 100% infill density and 40 mm/s infill speed whereas 60° raster angle, 80% infill density and 20mm/sec infill speed provides better results in the case of 3D printed flexural specimen.

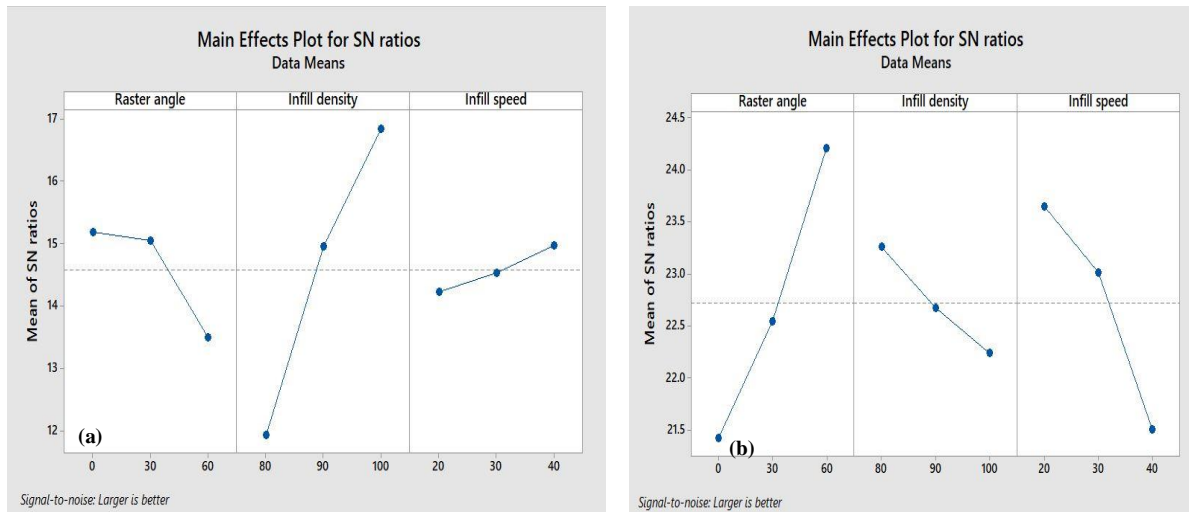


Figure 5.61 Mean S/N ratio plots for %BE of tensile and flexural specimen

Since PS and %BE of the 3D printed specimen was the most important mechanical characteristic among the various observed characteristics, therefore, analysis of variance (ANOVA) has been applied on the S/N ratio of PS and %BE to determine the significant factors for 3D printed tensile and flexural specimen (Table 5.33- 5.36).

Table 5.33 ANOVA analysis for PS of 3D printed Tensile specimen

Source	DF	Adj SS	Adj MS	F- Value	P-Value
Raster angle	2	22.8092	11.4046	41.57	0.023
Infill Density	2	3.8034	1.9017	6.93	0.126
Infill Speed	2	1.813	0.9156	3.34	0.231
Error	2	0.5486	0.3743		
Total	8	28.9925			

Table 5.34 ANOVA analysis for %BE of 3D printed Tensile specimen

Source	DF	Adj SS	Adj MS	F- Value	P-Value
Raster angle	2	5.2428	2.6214	7.94	0.112
Infill Density	2	36.7455	18.3727	55.66	0.018
Infill Speed	2	0.8626	0.4313	1.31	0.434
Error	2	0.6602	0.3301		
Total	8	43.511			

Table 5.35 ANOVA analysis for PS of 3D printed Flexural specimen

Source	DF	Adj SS	Adj MS	F- Value	P-Value
Raster angle	2	23.9038	11.9519	94.71	0.010
Infill Density	2	12.6560	6.3280	50.15	0.020
Infill Speed	2	0.4767	0.2383	1.89	0.346
Error	2	0.2524	0.1262		
Total	8	37.288			

Table 5.36 ANOVA analysis for %BE of 3D printed Flexural specimen

Source	DF	Adj SS	Adj MS	F- Value	P-Value
Raster angle	2	11.809	5.905	35.45	0.027
Infill Density	2	1.5983	0.7991	4.80	0.172
Infill Speed	2	7.3010	3.650	21.91	0.044
Error	2	0.3332	0.1666		
Total	8	21.0423			

The factors having P-value less than 0.05 were considered significant. Based on the results, raster angle and infill density both emerge as the significant factor that affects both PS and %BE of the specimens.

Multi response optimization

Based on the mean effect plots (Figure 5.60 and 5.61) and various property analysis it has been noticed that 3D printed flexural specimens possesses better mechanical, morphological and thermal properties as compared to 3D printed tensile specimens. But the

optimum levels of parameters for PS and %BE were different for both tensile and flexural. So, process optimization for both specimens has been done with the help of Minitab 17 software as shown in Table 5.37. From the analysis, it has been found that specimens prepared at 0° raster angle, 100% infill density and 20mm/sec printing speed give 71.97% desirability as compared to other printing parameters.

Table 5.37 Multi response of 3D printed specimens

Parameter	Suggested Value	Actual Value
Raster angle	0°	0°
Infill Density	100%	100%
Infill speed	20mm/sec	20mm/sec
S/N ratio for PS of Tensile specimen	22.96	14.06MPa
S/N ratio for % BE of Tensile specimen	17.10	7.162
S/N ratio for PS of Flexural specimen	30.32	32.82MPa
S/N ratio for % BE of Flexural specimen	21.86	12.39%
Desirability	71.9%	

5.2.2 Print functional prototypes via chemical assisted blending

In the present step, tensile and flexural specimens have been prepared with the help of fused filaments prepared via chemical blending. A total of 18 samples have been prepared 9 samples of tensile and 9 samples of flexural as per L9 OA mentioned in Table 4.4, they were further processed on a UTM machine on load rate of 25mm/min for calculating different mechanical properties as shown in Table 5.38 and 5.39. Based on different observations stress-strain curves have been drawn for both 3D printed specimens as shown in Figures 5.62 and 5.63. From stress-strain curves, nonlinear behavior has been found it could be due to necking occurring between the layers as specimens have been prepared at different conditions.

Table 5.38 Obtained mechanical properties of 3D Printed tensile specimens

S.No	PS (MPa)	BS (MPa)	% PE	% BE	E (GPa)	T (MPa)
1	11.45	4.34	2.22	3.17	0.516	0.054
2	13.28	7.51	3.17	3.82	0.419	0.118
3	15.55	9.47	3.8	4.75	0.409	0.179
4	10.52	12.34	3.17	3.07	0.332	0.1953
5	12.56	12.04	4.43	3.48	0.283	0.285
6	13.71	13	3.17	4.05	0.432	0.2264
7	8.35	7.98	3.12	2.53	0.410	0.14
8	9.12	11.31	3.80	3.38	0.24	0.21
9	10.38	11.95	3.48	3.81	0.29	0.22

Table 5.39 Obtained mechanical properties of 3D Printed flexural specimens

S.No	PS (MPa)	BS (MPa)	% PE	% BE	E (GPa)	T (MPa)
1	22.09	11.11	3.8	15.20	0.871	0.545
2	24.52	19.88	6.18	14.13	0.5956	0.6610
3	25.15	12.7	6.65	9.98	0.5672	0.744
4	16.54	13.91	7.6	17.08	0.3264	0.682
5	18.75	22.64	9.5	13.70	0.2960	1.03
6	22.09	22.07	8.08	15.73	0.4103	1.39
7	12.35	16.88	7.6	14.83	0.2437	0.775
8	14.11	14.89	5.24	19.48	0.4050	0.966
9	15.46	19.88	5.7	18.48	0.406	1.007

While comparing peak strength of both tensile and flexural specimens it has been found that flexural specimen Sample No. 3 has maximum peak strength i.e 25.15 Mpa while Sample No. 7 has minimum peak strength i.e. 12.35Mpa as compared to a tensile specimen.

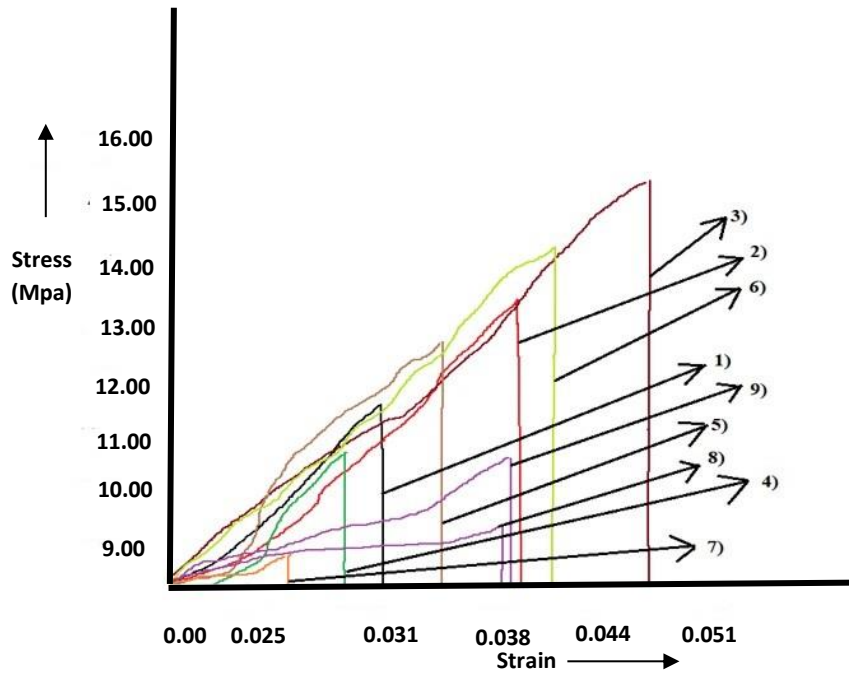


Figure 5.62 Stress-Strain curve of 3D printed specimens after tensile testing

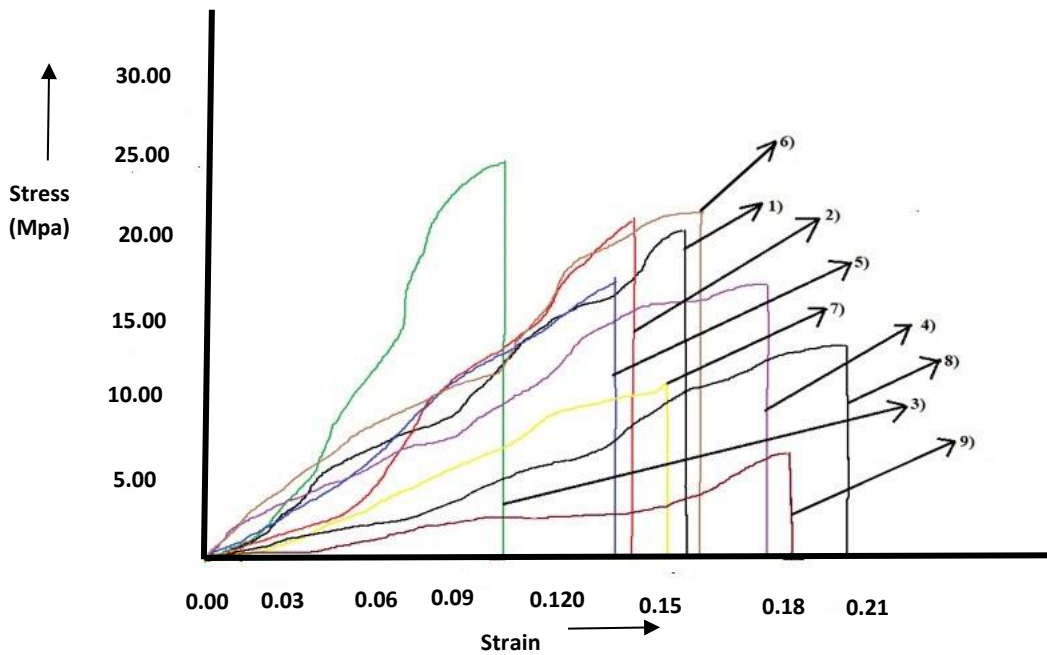


Figure 5.63 Stress-Strain curve of 3D printed specimens after flexural testing

After tensile testing SEM analysis of both specimens has been done on 33X zoom as shown in Figures 5.64 and 5.65. From SEM analysis, it has been found that there is a fractured surface between the adjacent layers that were responsible for showing poor mechanical properties.

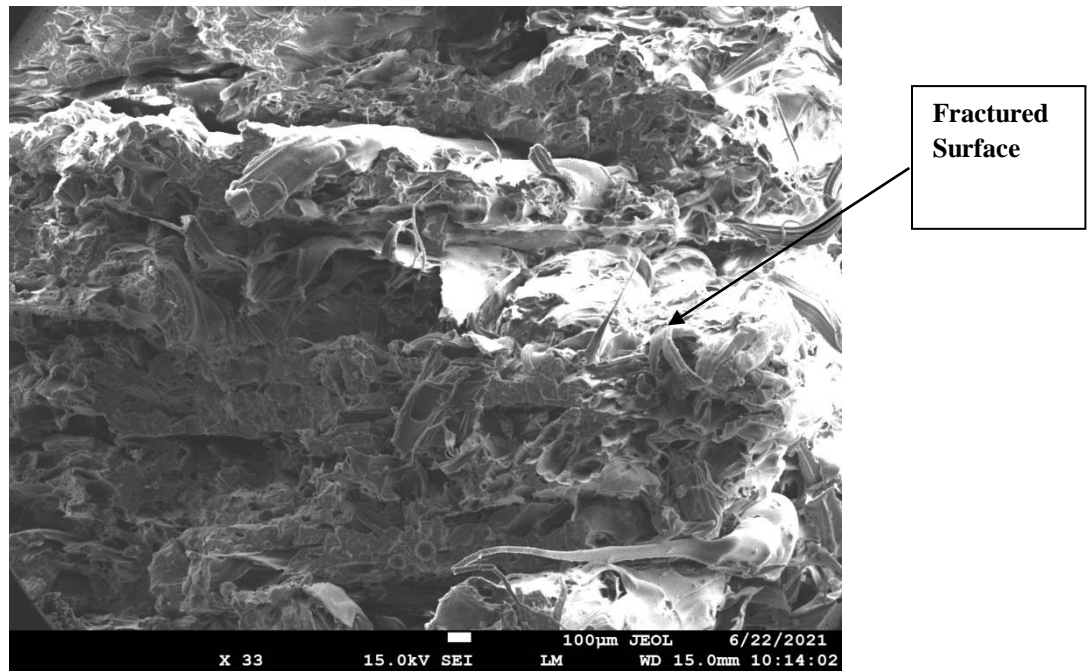


Figure 5.64 SEM analysis of 3D printed tensile specimen

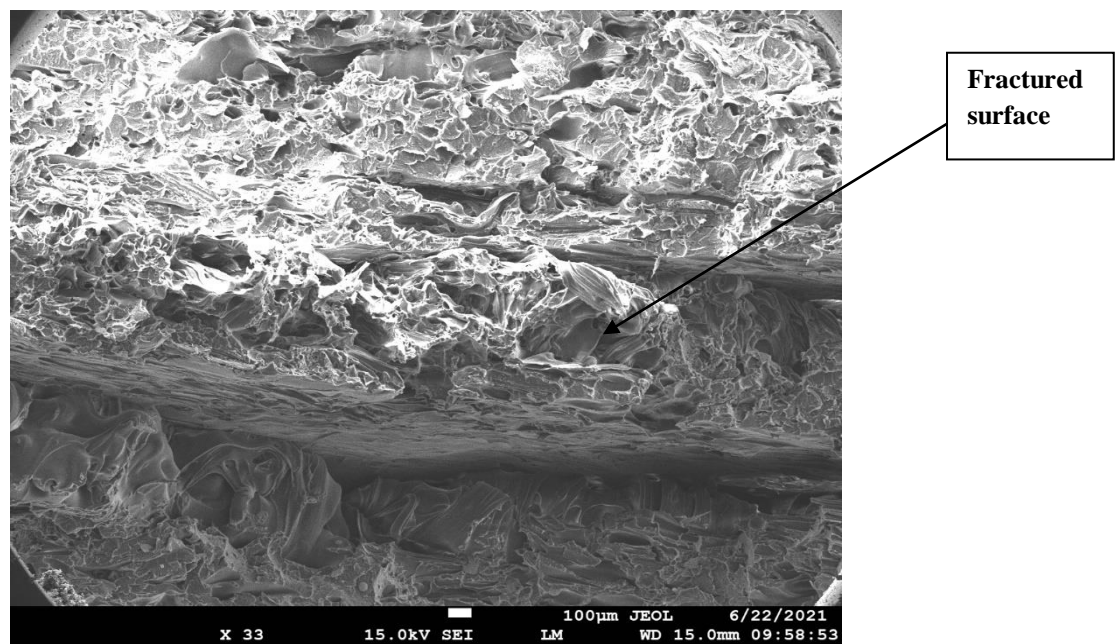


Figure 5.65 SEM analysis of 3D printed flexural specimen

EDS analysis (Area Mapping) of 3D printed specimen was done to determine the weight percentage of the elements present in the 3D printed specimen. From EDS analysis of the 3D printed tensile specimen, it has been found that the percentage of carbon in the composite is 98% by wt. whereas Iron is 2% by wt. as shown in Figure 5.66. Similarly, EDS

analysis of 3D printed flexural specimen has been done and it was found that carbon percentage is 99 % by wt. whereas iron percentage is 1% by weight as shown in Figure 5.67.

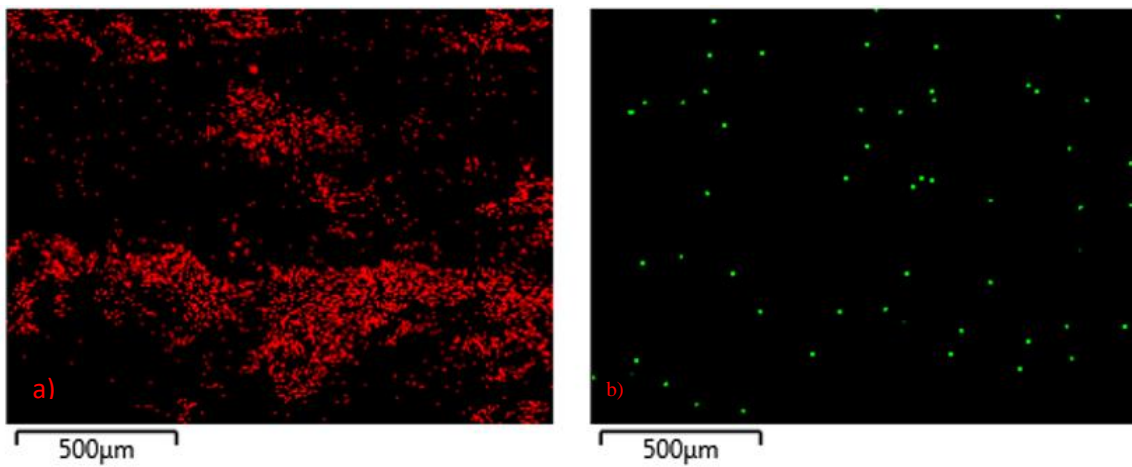


Figure 5.66 EDS analysis of 3D printed tensile specimen a) shows wt.% of carbon b) shows wt.% of Fe particles

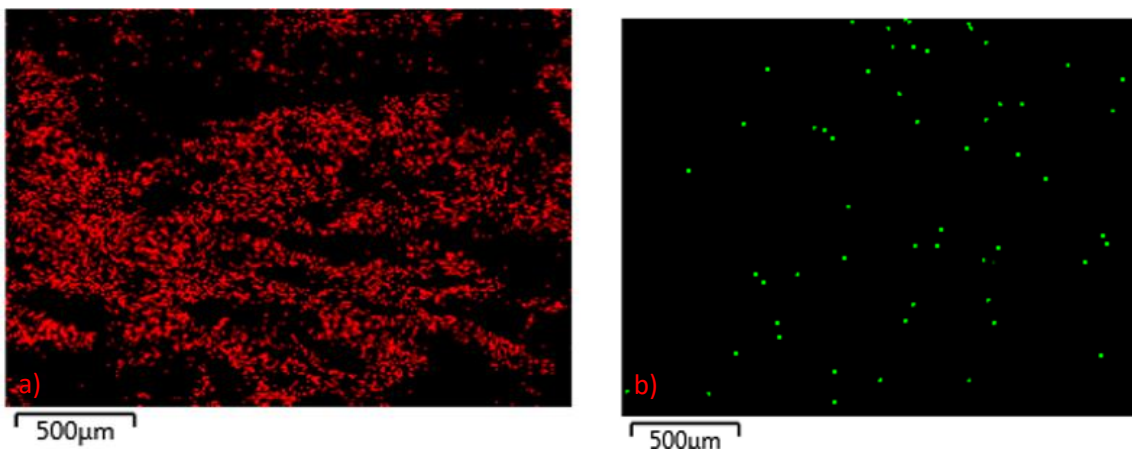


Figure 5.67 EDS analysis of 3D printed flexural specimen a) shows wt.% of carbon b) shows wt.% of Fe particles

Analysis of variance (ANOVA)

From S/N ratio analysis plots have been drawn for both PS and %BE of both specimens as shown in Figures 5.68 and 5.69. From Peak strength analysis it has been found that maximum strength was found at 0° raster angle for both 3D printed tensile and flexural specimens. But the effect of raster angle on the Peak strength of the flexural specimen was more as compared to 3D printed flexural specimen. While analyzing the effect of infill density it has been found that with a decrease in infill percentage peak strength has been decreased and maximum peak strength was found at 100% infill density for both 3D printed

specimens. With the increase in printing speed in the case of the flexural specimen from 20mm/sec to 30mm/sec, peak strength decreases may be due to insufficient time for making proper bonding with the intermediate layer. But in the case of 3D printed tensile specimens this effect was opposite for 3D printed tensile specimens maximum peak strength was obtained for specimens printed at 40mm/sec.

Table 5.40 S-N ratio analysis of peak strength and % break elongation for both tensile and flexural specimen

Exp. No.	S/N ratio for PS (dB) Tensile specimen	S/N ratio for %BE (dB) Tensile specimen	S/N ratio for PS (dB) Flexural specimen	S/N ratio for %BE (dB) Flexural specimen
1	21.76	10.021	26.88	23.636
2	22.43	11.641	27.79	23.002
3	23.83	13.533	28.01	19.982
4	20.44	9.742	24.37	24.649
5	21.97	10.831	25.46	22.734
6	22.74	12.149	26.88	23.934
7	18.43	8.062	21.83	23.422
8	19.19	10.578	22.99	25.791
9	20.32	11.618	23.78	25.334

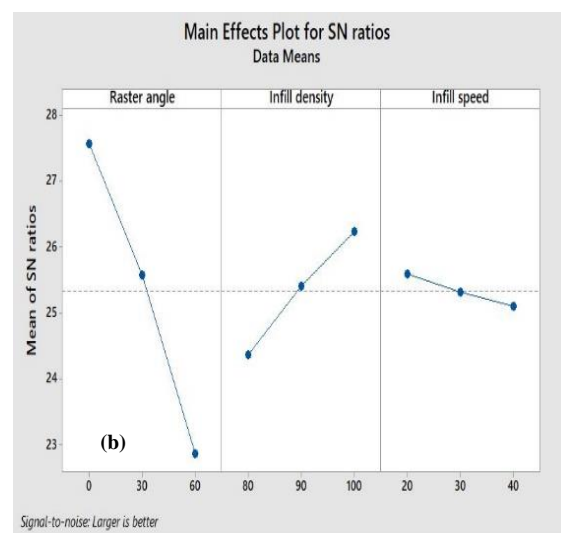
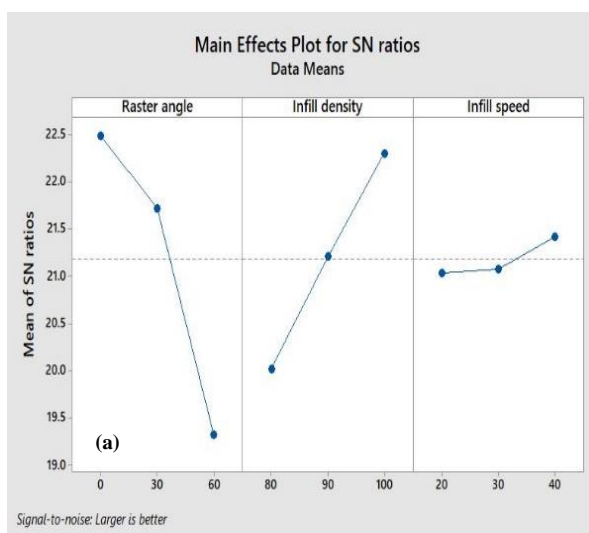


Figure 5.68 S/N ratio peak strength of the tensile and flexural specimen

While analyzing the effect of %BE on 3D printed tensile specimens, it has been found that maximum %BE was obtained at 0° raster angle, 100% infill density because of less gap between adjacent layers which increase the strength of the specimen. The effect of %BE for flexural specimens was more as compared to 3D printed tensile specimens. The parametric conditions that yield maximum PS for 3d printed tensile specimen were 0° raster angle, 100% infill density and 40 mm/s infill speed whereas 0° raster angle, 100% infill density and 20mm/sec infill speed provides better results in the case of 3D printed flexural specimen.

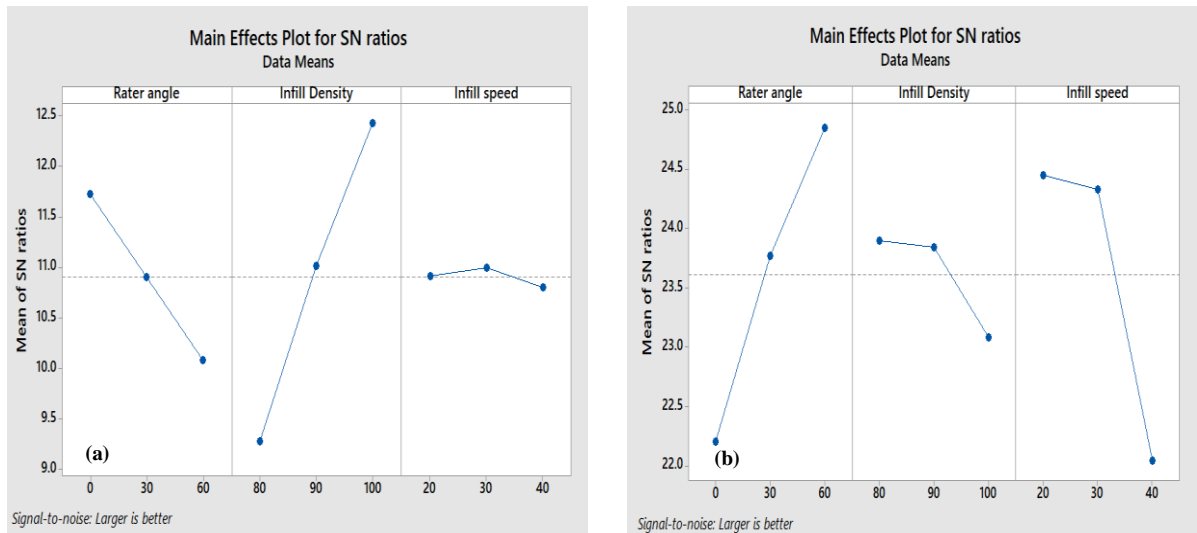


Figure 5.69 S/N ratio %BE of tensile and flexural specimen

Table 5.41 ANOVA analysis of PS for the tensile specimen.

Source	DF	Adj SS	Adj MS	F- Value	P- Value
Raster angle	2	16.424	8.212	2845.47	0.000
Infill Density	2	7.824	3.912	1355.65	0.001
Infill Speed	2	0.259	0.129	44.90	0.022
Error	2	0.005	0.002		
Total	8	24.513			

Table 5.42 ANOVA analysis of %BE for tensile specimen

Source	DF	Adj SS	Adj MS	F- Value	P-Value
Raster angle	2	4.062	2.0312	5.80	0.147
Infill Density	2	15.015	7.507	21.43	0.045
Infill Speed	2	0.055	0.0276	0.08	0.927
Error	2	0.700	0.350		
Total	8	19.834			

Table 5.43 ANOVA analysis of PS for Flexural specimen

Source	DF	Adj SS	Adj MS	F- Value	P-Value
Raster angle	2	33.2806	16.640	149.3	0.007
Infill Density	2	5.238	2.619	23.51	0.041
Infill Speed	2	0.354	0.177	1.59	0.386
Error	2	0.222	0.114		
Total	8	39.0956			

Table 5.44 ANOVA analysis of %BE for flexural specimen

Source	DF	Adj SS	Adj MS	F- Value	P-Value
Raster angle	2	10.590	5.295	27.59	0.035
Infill Density	2	1.251	0.625	3.26	0.235
Infill Speed	2	11.022	5.511	28.71	0.034
Error	2	0.383	0.191		
Total	8	23.247			

Since PS and %BE of the 3D printed specimen were the most important mechanical characteristic among the various observed characteristics, therefore, analysis of variance (ANOVA) has been applied on the S/N ratio of PS and %BE to determine the significant factors for 3D printed tensile and flexural specimen as shown in Table 5.41-5.44. The factors having P-value less than 0.05 were considered significant. Based on the results, it has been found that infill density and speed both emerge as the significant factor that affects both PS and %BE of the specimens.

Multi response optimization

Based on the mean effect plots (Figure 5.68 and 5.69) and various property analysis it has been noticed that 3D printed flexural specimens possesses better mechanical, morphological and thermal properties as compared to 3D printed tensile specimens. But the optimum levels of parameters for PS and %BE were different for both tensile and flexural. So, process optimization for both specimens has been done with the help of Minitab 17 software as shown in Table 5.45. From the analysis, it has been found that specimens prepared at 0° raster angle, 100% infill density and 20mm/sec printing speed give 78.9% desirability as compared to other printing parameters.

Table 5.45 Multi response analysis of 3D printed specimens

Parameter	Suggested Value	Actual Value
Raster angle	0°	0°
Infill Density	100%	100%
Infill speed	20mm/sec	20mm/sec
S/N ratio for PS of Tensile specimen	23.47	14.92MPa
S/N ratio for % BE of Tensile specimen	13.26	4.83%
S/N ratio for PS of Flexural specimen	28.70	27.31MPa
S/N ratio for % BE of Flexural specimen	22.52	13.37%
Desirability	78.95%	

5.2.3 Print functional prototypes via hybrid- mechanical assisted blending

In this step 3D printing of tensile and flexural specimens has been done by varying different printing parameters as per L9 OA shown in Table 4.4. 9 tensile specimens and 9 flexural specimens were processed on UTM on load rate of 25mm/min for determining their mechanical properties as shown in Tables 5.46 and 5.47. Based on obtained mechanical properties stress-strain curves have been drawn as shown in Figures 5.70 and 5.71. From stress-strain curves, nonlinear behavior has been found it may be due to necking occurring

between the layers as specimens have been prepared at different conditions. While comparing peak strength of both tensile and flexural specimens it has been found that flexural specimen Sample No. 4 has maximum peak strength i.e 15.08 Mpa while Sample No. 9 has minimum peak strength i.e. 9.89Mpa as compared to the tensile specimen.

Table 5.46 Obtained mechanical properties of 3D Printed tensile specimens

S.No	PS (MPa)	BS (MPa)	% PE	% BE	E (GPa)	T(MPa)
1	10.66	10.45	3.72	4.92	0.40	0.142
2	12.84	12.45	6.23	5.20	0.22	0.369
3	13.1	12.88	6.92	6.82	0.22	0.449
4	9.98	9.78	3.84	4.15	0.45	0.111
5	11.08	10.58	3.48	4.95	0.328	0.182
6	11.31	11.27	4.43	6.32	0.343	0.158
7	7.35	7.13	6.33	4.80	0.179	0.150
8	6.35	6.15	5.7	5.75	0.685	0.052
9	8.36	8.16	6.23	6.88	0.61	0.093

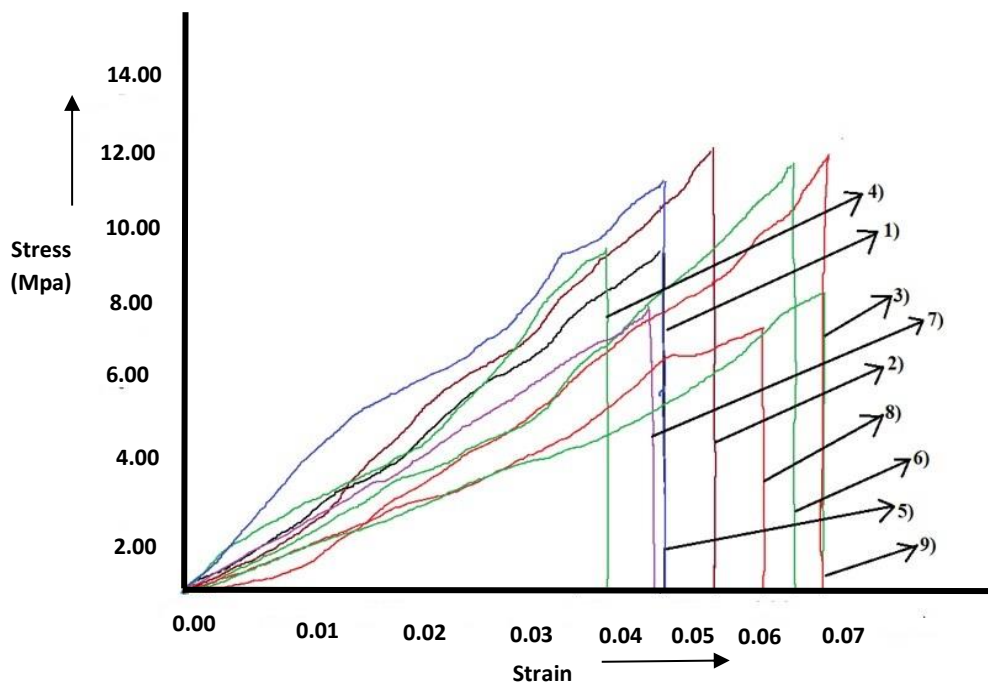


Figure 5.70 Stress- Strain curve of 3D printed specimens after tensile testing

Table 5.47 Obtained mechanical properties of 3D Printed flexural specimens

S.No	PS (MPa)	BS (MPa)	% PE	% BE	E (GPa)	T (MPa)
1	17.48	4.95	10.93	15.25	0.1073	0.195
2	13.31	10.51	8.55	13.28	0.2911	0.382
3	11.88	6.73	8.08	10.48	0.1975	0.277
4	15.08	12.33	10.45	11.56	0.2796	0.527
5	12.35	10.91	9.4	10.32	0.2268	0.483
6	14.21	11.52	9.03	12.51	0.3024	0.401
7	11.69	10.48	6.45	8.32	0.3283	0.448
8	12.83	12.49	3.3	7.35	0.8903	0.158
9	9.98	9.13	8.08	9.38	0.2678	0.477

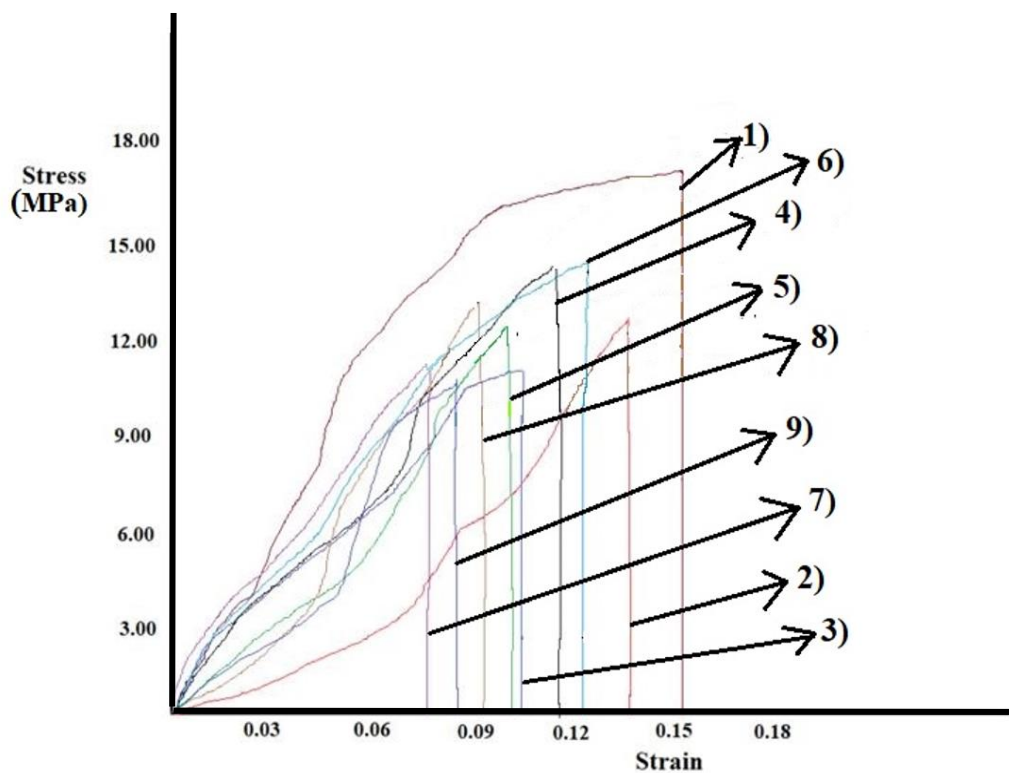


Figure 5.71 Stress-Strain curve of 3D printed specimens after Flexural testing

After performing tensile testing SEM analysis has been done for both specimens having the least peak strength at 50X zoom as shown in Figures 5.72 and 5.73. From SEM analysis, it has been found that there is a fractured surface between the adjacent layers that was responsible for showing poor mechanical properties. EDS analysis (Area Mapping) of

3D printed specimen was done to determine the weight percentage of the elements present in the 3D printed specimen as shown in Figure 5.74. From EDS analysis it has been found that red color shows the percentage of Carbon atoms i.e 90.25%, and green color shows the percentage of Iron atoms i.e 9.75% as shown in Figure 5.74.

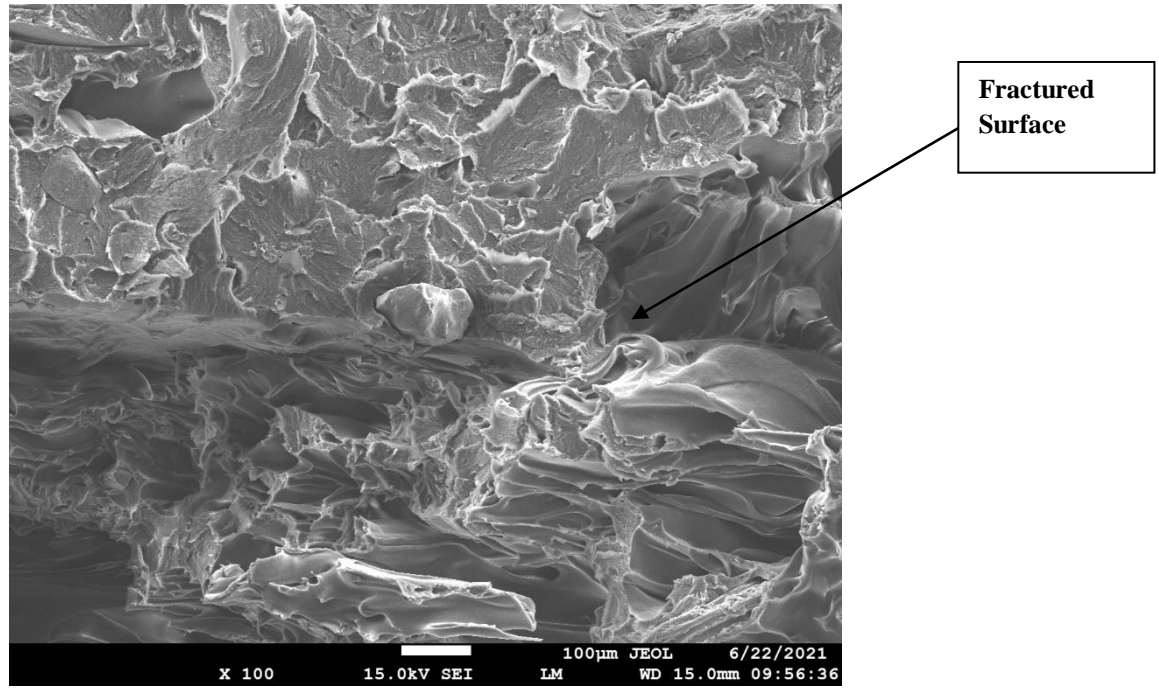


Figure 5.72 SEM analysis of tensile specimen

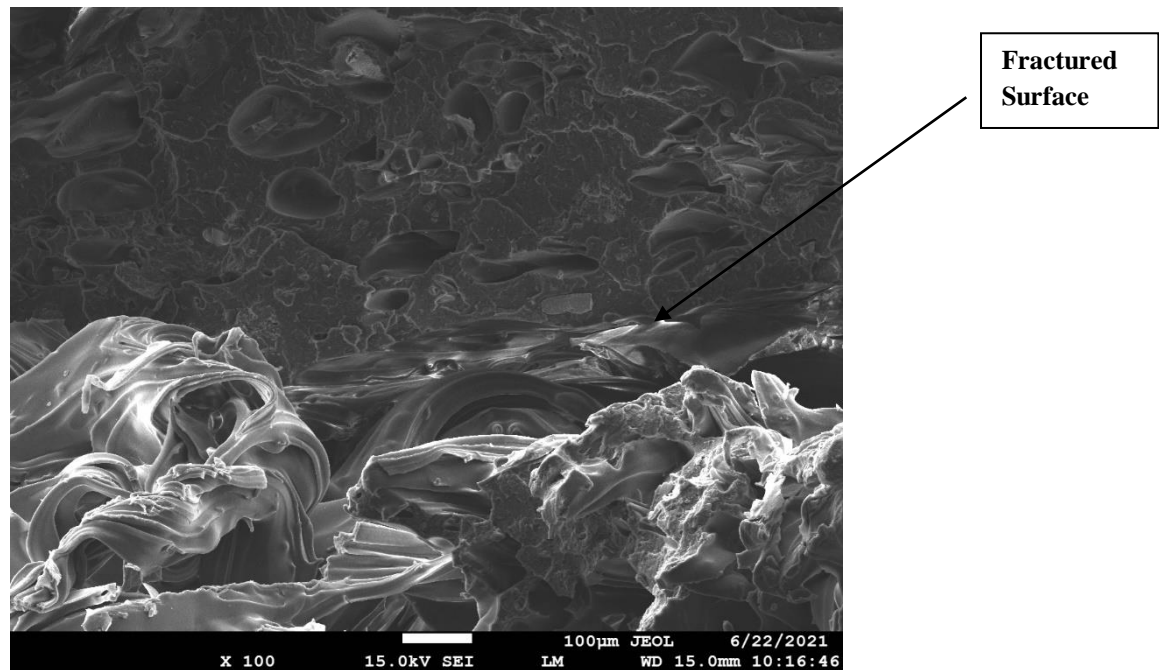


Figure 5.73 SEM analysis of flexural specimen

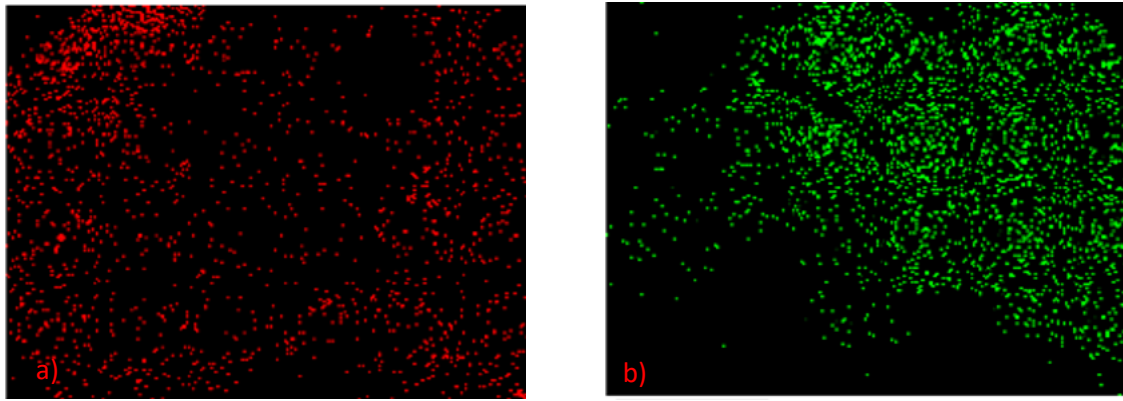


Figure 5.74 EDS analysis of hybrid specimen a) shows wt.% of carbon b) shows wt.% of Fe particles

Analysis of variance (ANOVA)

From S/N ratio analysis plots have been drawn for both PS and %BE as shown in Figures 5.75 and 5.76. From Peak strength analysis it has been found that maximum strength was found at 0° raster angle as raster angle increases peak strength has been decreased. But the effect of raster angle on the Peak strength of the flexural specimen was more as compared to 3D printed flexural specimen.

Table 5.48 S-N ratio analysis of peak strength and % break elongation for both tensile and flexural specimen

Exp. No.	S/N ratio for PS (dB) Tensile specimen	S/N ratio for %BE (dB) Tensile specimen	S/N ratio for PS (dB) Flexural specimen	S/N ratio for %BE (dB) Flexural specimen
1	20.555	13.839	24.850	23.665
2	21.903	14.320	22.483	22.464
3	22.345	16.675	21.496	20.464
4	19.982	12.361	23.568	21.259
5	20.890	13.892	21.833	20.273
6	21.069	16.014	23.051	21.954
7	18.040	13.624	21.356	18.402
8	16.055	15.193	22.164	17.325
9	18.850	16.751	29.982	19.444

While analyzing the effect of infill density it has been found that with a decrease in infill percentage peak strength has been decreased and maximum peak strength was found at 100% infill density for 3D printed flexural specimen but for 3D printed tensile specimens it was maximum at 80% infill density. With the increase in printing speed for a flexural specimen from 20mm/sec to 400mm/sec, peak strength decreases may be due to insufficient time for making proper bonding with the intermediate layer. The parametric conditions that yield maximum PS for 3d printed tensile specimen were 0° raster angle, 80% infill density and 20 mm/s infill speed whereas 0° raster angle, 100% infill density and 40mm/sec infill speed provides better results in the case of 3D printed flexural specimen. But in the case of %BE maximum strength was found at 20mm/s and 0° raster angle.

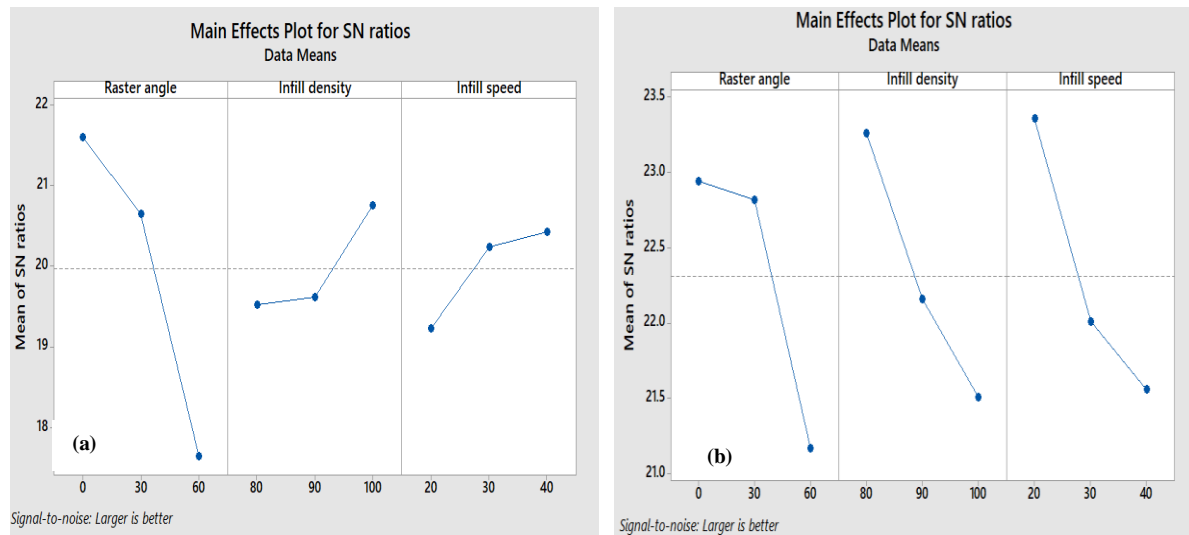


Figure 5.75 Mean effect plot for PS of 3D printed flexural and tensile specimen

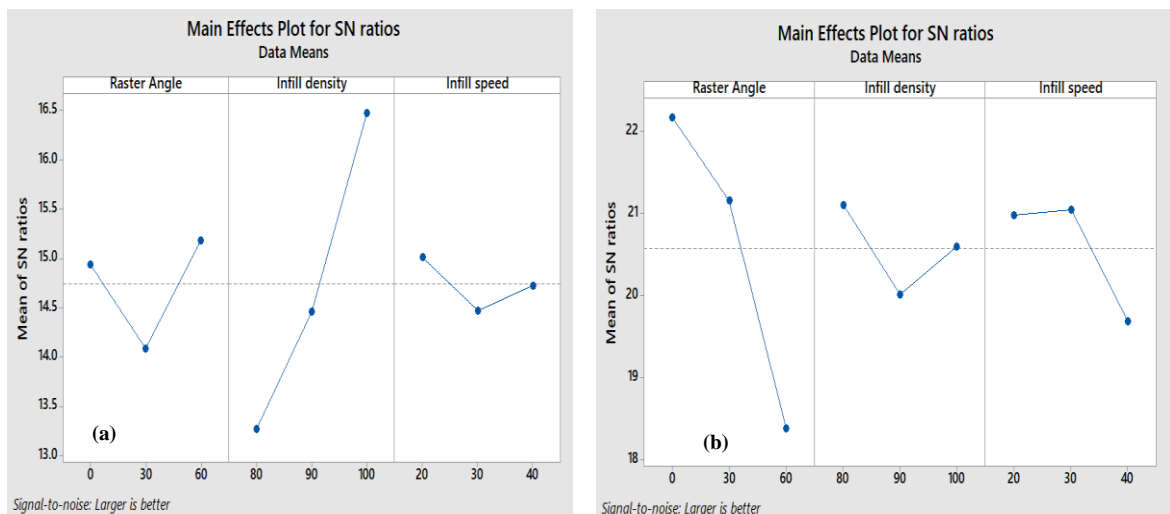


Figure 5.76 Mean effect plot for %BE of 3D printed flexural and tensile specimen

Since PS and %BE of the 3D printed specimen were the most important mechanical characteristic among the various observed characteristics, therefore, analysis of variance (ANOVA) has been applied on the S/N ratio of PS and %BE to determine the significant factors for 3D printed tensile and flexural specimen (Table 5.49- 5.52). The factors having P-value less than 0.05 were considered significant. Based on the results both raster angle and infill density emerge as the significant factor that affects both PS and %BE of the specimens.

Table 5.49 ANOVA analysis for PS of tensile specimen

Source	DF	Adj SS	Adj MS	F- Value	P-Value
Raster angle	2	28.52	14.476	35.58	0.027
Infill Density	2	3.556	1.778	4.37	0.186
Infill Speed	2	1.964	0.982	2.41	0.293
Error	2	0.813	0.4069		
Total	8	35.286			

Table 5.50 ANOVA analysis for %BE of tensile specimen

Source	DF	Adj SS	Adj MS	F- Value	P-Value
Raster angle	2	2.004	1.002	43.79	0.022
Infill Density	2	15.748	7.874	344.08	0.003
Infill Speed	2	0.434	0.217	9.50	0.095
Error	2	0.045	0.0228		
Total	8	18.2335			

Table 5.51 ANOVA analysis for PS of flexural specimen

Source	DF	Adj SS	Adj MS	F- Value	P-Value
Raster angle	2	5.820	2.910	87.11	0.011
Infill Density	2	4.706	2.353	70.43	0.014
Infill Speed	2	5.335	2.66	79.82	0.012
Error	2	0.0668	0.0334		
Total	8	15.9274			

Table 5.52 ANOVA analysis for %BE of flexural specimen

Source	DF	Adj SS	Adj MS	F- Value	P-Value
Raster angle	2	23.054	11.527	6.08	0.141
Infill Density	2	1.778	0.888	0.47	0.681
Infill Speed	2	3.509	1.754	0.92	0.520
Error	2	3.3799	1.899		
Total	8	32.140			

Multi-process optimization

Based on the mean effect plots (Figure 5.75-5.76) and various property analysis, it has been noticed that 3D printed flexural specimens possesses better mechanical, morphological and thermal properties as compared to 3D printed tensile specimens. But the optimum levels of parameters for PS and %BE were different for both tensile and flexural. So, process optimization for both specimens has been done with the help of Minitab 17 software as shown in Table 5.53.

Table 5.53 Multi response analysis of 3D printed specimens

Parameter	Suggested Value	Actual Value
Raster angle	0°	0°
Infill Density	100%	100%
Infill speed	20mm/sec	20mm/sec
S/N ratio for PS of Tensile specimen	21.80	11.48MPa
S/N ratio for % BE of Tensile specimen	16.95	7.05%
S/N ratio for PS of Flexural specimen	23.20	14.45MPa
S/N ratio for % BE of Flexural specimen	22.60	5.33%
Desirability	.8427	

The selected mechanical (%BE and PS) properties of the printed specimens (multilayer and hybrid printing) printed through different routes of blending (mechanical, chemical and mechanical- hybrid assisted) were compared to estimate the variation in properties. The observations of comparison (Table 5.54) revealed that mechanical-assisted 3D printed specimens yield better properties as compared to specimens printed through chemical and hybrid- mechanical-assisted blending. Further printing conditions show superior properties were used to print rectangular specimens via multi-layer mechanical-assisted printing.

Table 5.54 Comparison of properties for composite filaments

	Multi-Layer Printing				Single Layer Printing	
	Mechanical Assisted Blending		Chemical Assisted Blending		Hybrid-Mechanical Assisted Blending	
3D printed specimens	Tensile	Flexural	Tensile	Flexural	Tensile	Flexural
PS(MPa)	22.96	30.32	23.47	28.70	21.80	23.20
%BE	17.10	21.86	13.26	22.52	16.98	22.60

5.3 PHASE 3- (PRE AND POST PROCESSING)

5.3.1 Pre- Processing Techniques

The surface finish plays an important role for parts prepared via FDM. Many researchers have done extensive research on improving the surface finish of 3D printed parts by controlling various parameters of FDM but unfortunately, the surface roughness exists as it's an inherent characteristic of layered manufacturing. Many researchers have controlled various FDM parameters for improving surface finish. Some researchers tried to improve the finish by modifying the slicing technique but still, it was not eliminated completely. Different parameters affecting surface properties of parts prepared by FDM along with their effects are discussed below.

Layer thickness: It is defined as the height of the layer deposited by the extrusion layer on the printing bed. It is one of the most significant parameters that affect the surface finish and other properties of the printed part. However, the effect of layer thickness on surface quality diminishes after vapor smoothing. Because during vapor smoothing reflow of material took place and it fills the gap between the adjacent layers [212]. Therefore, in the present study layer thickness taken is 0.4mm.

Air Gap: It is defined as the distance between the two adjacent layers, it is also known as Road Gap. Normally the air gap is zero it means adjacent layers are touching each other. When there is a gap between the adjacent layers it is known as the positive gap, when layers are overlapping with each layer it means a negative gap which gives dense structure and requires more material and build time [213]. Few researchers suggested that to get a good surface finish and accurate dimensional accuracy air gap should be zero [214].

Raster width: It is the width of molten material which is going to deposit on the bed. It varies from 1.2 to 1.5 times the nozzle diameter [215]. The effect of raster width on the surface finish is the same as the effect of layer thickness on surface finish and dimensional accuracy [216]. It was noticed that superior mechanical properties, surface properties and dimensional accuracy were obtained with lesser raster width [217].

Model Temperature: It is the temperature at which the heater is maintained to get material in the form of molten stage. Extrusion temperature is usually equal or slightly less than the melting temperature of the polymer. Extrusion temperature is also an important parameter for surface properties. Higher extrusion temperature with respect to melting temperature of

polymer results in high flowability, poor adhesion. Therefore, it should be slightly less than the melting temperature of polymer material and thus kept constant during the study.

Raster angle: It is the angle between the X-axis of the printing bed and the nozzle path. Generally, researchers have opted two raster angle techniques first is criss- cross ($-45^{\circ}/+45^{\circ}$) and the second is cross ($0^{\circ}/90^{\circ}$). Some authors found better surface finish and dimensional surface finish at 0° as compared to specimens printed at other raster angles [218-219].

Infill Density: Gap between the adjacent layer can be controlled as per the requirement. Generally, there are three types of infill density pattern used one is medium, high and solid. The parts prepared with solid density have more weight, more density, and take more manufacturing time as compared to other infill density patterns. As different infill density patterns are directly linked with internal raster arrangement, it does not affect the surface roughness of the printed FDM parts if surface roughness and tensile strength is not the main objective, some researchers found that after post-treatment gap between adjacent layers due to different infill pattern will reduce due to flow of material.

Build orientation: The build orientation is defined as the orientation at which part is printed. This is one of the most important parameters that affects the surface finish as studied by many researchers. Some researchers studied the effect of build angle on surface finish and found that parts printed at 0° raster angle yield superior surface properties as compared to specimens printed at 90° orientation [220]. However, the rectangular specimens printed during this work at 0° and 90° build orientation shows almost similar surface roughness, therefore, 0° build orientation was taken while printing rectangular specimens in this work.

Infill pattern: Another parameter that affects the surface properties of the printed specimen is the infill pattern. It is the technique of printing the internal structure of the component to be printed. There are different types of infill pattern are available such as honeycomb, hexagonal, rectilinear, linear, diamond. A more dense infill structure gives superior mechanical properties as less gap between the adjacent layers, more will be the strength. Therefore, among different infill patterns, rectilinear infill pattern has more dense structure.

Printing speed: It is the speed of the build nozzle while depositing material on the printing bed along the XY plane. Printing speed is one of the predominant factors that affect the formation of the build component. During maximum printing speed printing, the nozzle

developed residual stress which results in a faster extrusion process and gives a poor surface finish. Therefore printing speed should be minimum while printing thinner layers.

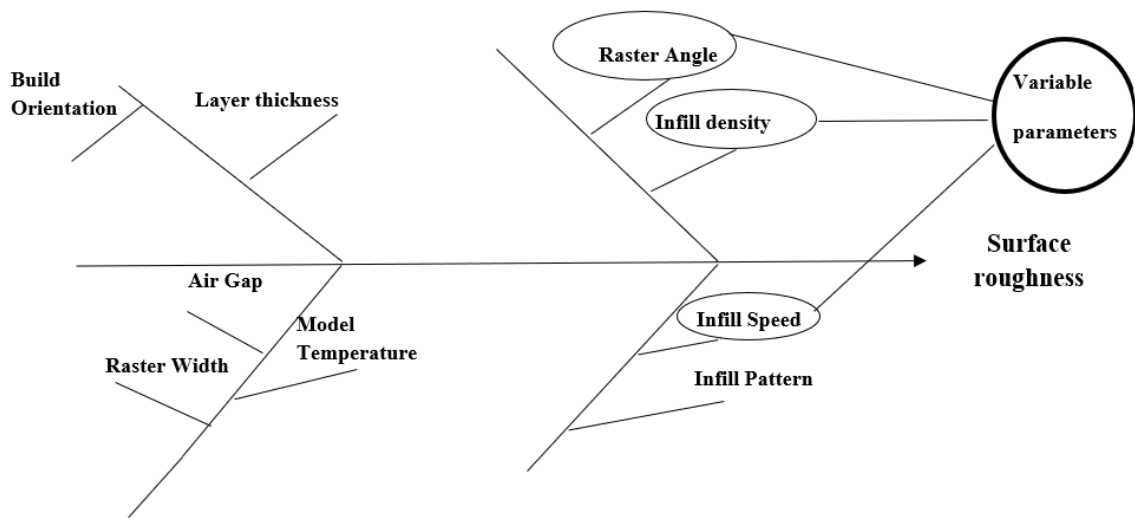


Figure 5.77 Different pre-processing parameters of FDM

From the above discussion, it has been found that by controlling different FDM parameters surface finish can be improved but still it is not possible to make parts with exact precision. Based on the optimization 18 rectangular specimens of dimensions (60x12.7x3.2mm have been prepared by fixing different pre-processing parameters of FDM) as shown in Figure 5.78. Following parameter have been fixed while printing parts via FDM they were layer thickness (0.407mm), raster width (0.254mm), air gap (0mm), Extrusion temperature (270°C), raster angle (0°), infill density (100%) and infill speed (20mm/sec). Therefore, to improve surface finish and shore hardness post-processing technique has been applied.

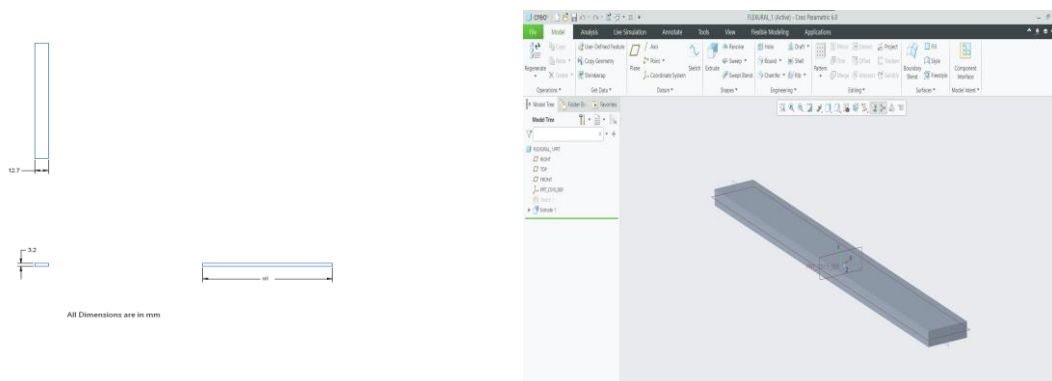


Figure 5.78 2D drawing and 3D CAD model of a rectangular specimen

5.3.2 Post Processing Techniques

The parts prepared by FDM need some post-processing techniques for removing flakes, debris, small cavities and removal of extra material. Although Stratasys has developed an ultrasonic cleaner for cleaning the FDM parts the surface finish improved by this technique is not appropriate as surface finish improved by chemical vapor smoothing. Acetone was used as a smoothing agent and also used for finishing the parts. Few researchers have improved the surface finish of the part by dipping them in acetone solution for 5 min. Anthamatten et al. improved the surface finish of the parts by varying number of cycles and found that with an increase in the number of cycles surface finish has been improved [221]. The second post-processing technique used was heat treatment means heating the prepared specimen above the glass transition temperature. Few researchers reported that on surface annealing of 3D printed ABS specimen nearby or above glass transition temperature of polymer both surface finish and shore hardness have been improved up to some remarkable point. Therefore, three variables of vapor smoothing (i.e soaking time, number of cycles and smoothing time) and two parameters (heating time and heating temperature) for the second parameter have been selected. In the last surface roughness has been calculated with the help of a surface roughness tester (Make: Mutututo).

5.3.3 Study the effect of post-processing on the surface and mechanical properties of 3D printed functional prototypes.

Two post-processing techniques first was chemical vapor smoothing and the second was heat treatment has been used in the present objective for determining the effect of different process parameters on surface roughness and shore Hardness. The different experiment has been performed as per the conditions mentioned in Table 4.5 and 4.6 and change in surface roughness and shore hardness were obtained after CVs and Heat Treatment has been shown in Table 5.55 and 5.56 below. From Table 5.55 it has been found that the maximum percentage change in surface roughness was 91.69% i.e for Sample No.9, similarly, the maximum change in shore hardness was 12.12% for sample No.9 after CVs. Similarly, while analyzing the effect of heat treatment on surface roughness and shore hardness it has been found that sample heat-treated for maximum duration along with maximum heating time shows improvement in surface roughness and shore hardness. From Table 5.56 it has been found that the maximum percentage change in surface roughness was 81.59% i.e for Sample No.8, similarly, the maximum change in shore hardness was 12% for

sample No.9. While comparing both tables it has been found that the CVS process shows better surface roughness improvement as compared to the heat-treatment process.

Table 5.55 Percentage change in Shore Hardness and Surface Roughness after CVS

S.No	Surface Roughness (μm)			Shore Hardness (Hd)		
	Before CVS	After CVS	Percentage change	Before CVS	After CVS	Percentage change
1	14.361	2.745	80.89	26.5	28	5.66
2	15.732	2.638	83.23	34.5	36.55	6.00
3	14.088	2.015	85.70	33	35.95	9.00
4	12.711	1.635	87.14	30	32.40	8.00
5	12.982	1.461	88.75	34	37.40	10.00
6	13.211	1.858	85.94	27	29.95	11.00
7	10.661	1.112	89.56	31	34.45	11.10
8	11.201	1.356	87.89	21.5	24.05	12.00
9	10.31	0.856	91.69	33	40.00	12.10

Table 5.56 Percentage change in Shore Hardness and Surface Roughness after Heat treatment

S.No	Surface Roughness (μm)			Shore Hardness (Hd)		
	Before HT	After HT	Percentage change	Before HT	After HT	Percentage change
1	14.258	4.528	68.24	26.5	27.5	4.00
2	14.625	4.254	70.91	34.5	26.5	5.00
3	14.114	4.025	71.48	33	35.5	7.50
4	12.514	3.528	71.80	30	32.45	8.000
5	13.012	3.178	75.57	34	37.50	10.00
6	13.115	3.369	74.31	27	29.53	10.50
7	10.788	1.985	81.59	31	34.15	10.00
8	11.014	2.256	79.51	21.5	23.95	11.00
9	10.452	1.862	82.19	33	36.95	12.00

After calculating a change in surface roughness and shore Hardness after CVS and Heat treatment process SEM image has been taken before and after the CVs treatment as shown in Figure 5.79. This clearly shows the gap between the adjacent layers i.e., Stair case effect but after CVS treatment these gaps get disappeared due to the deposition of acetone on the surface which ultimately improves the surface finish and shore hardness.

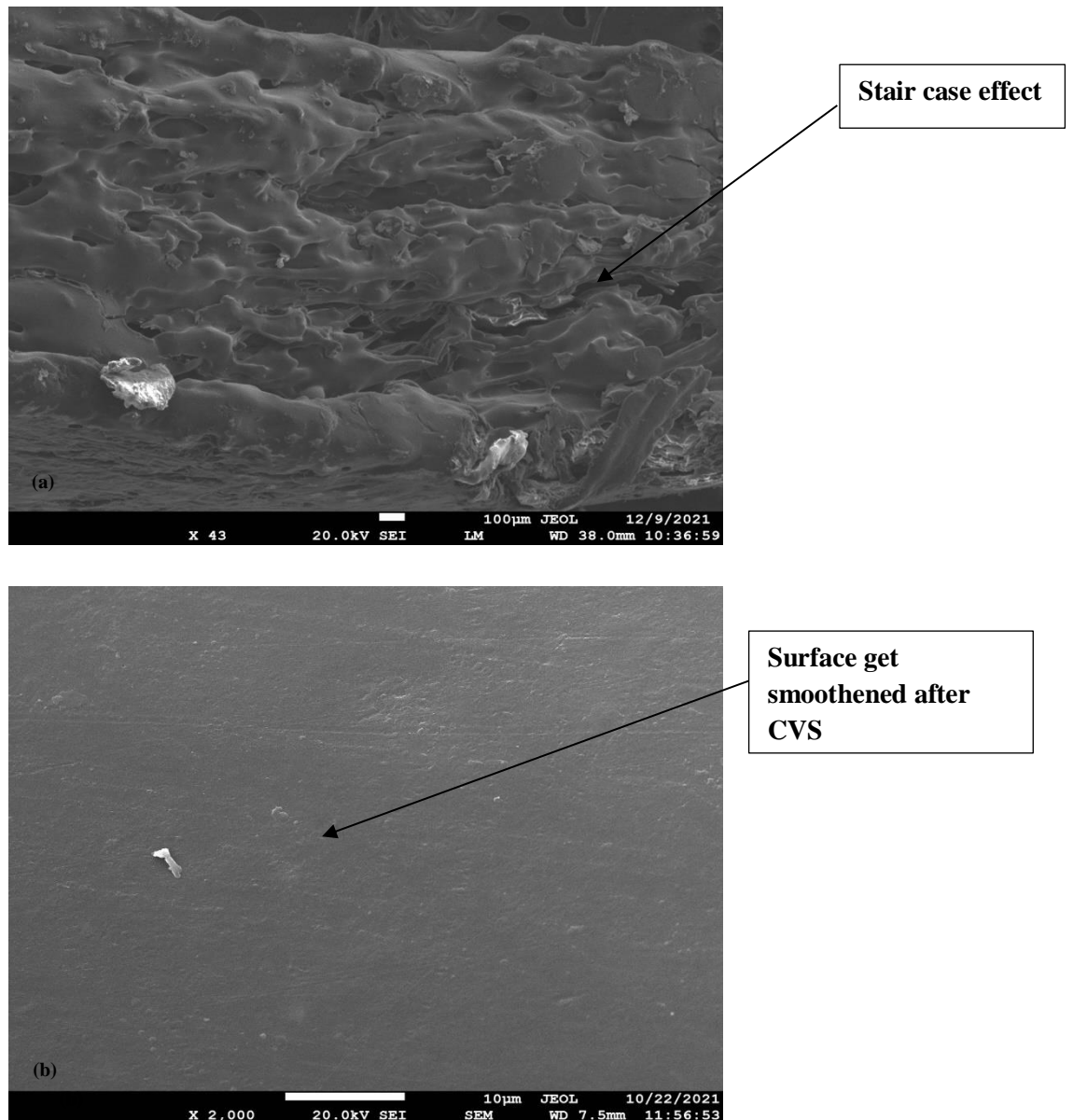


Figure 5.79 SEM image before and after CVS

Further ANOVA analysis has been used to determine the effect of CVs and heat treatment on surface roughness and shore hardness as shown in Table 5.57.

Table 5.57 S/N ratio after CVS and Heat treatment

S/N ratio of percentage change in Shore Hardness		S/N ratio of percentage change in Surface roughness	
After CVS	After HT	After CVS	After HT
15.05	12.04	38.15	36.6811
15.56	13.97	38.40	37.0145
19.08	17.50	38.65	37.0840
18.06	18.06	38.80	37.1234
20.00	20.00	38.96	37.5677
20.82	20.42	38.68	37.4212
20.90	20.00	39.04	38.2338
21.58	20.82	38.87	38.0092
21.65	21.58	39.24	38.2959

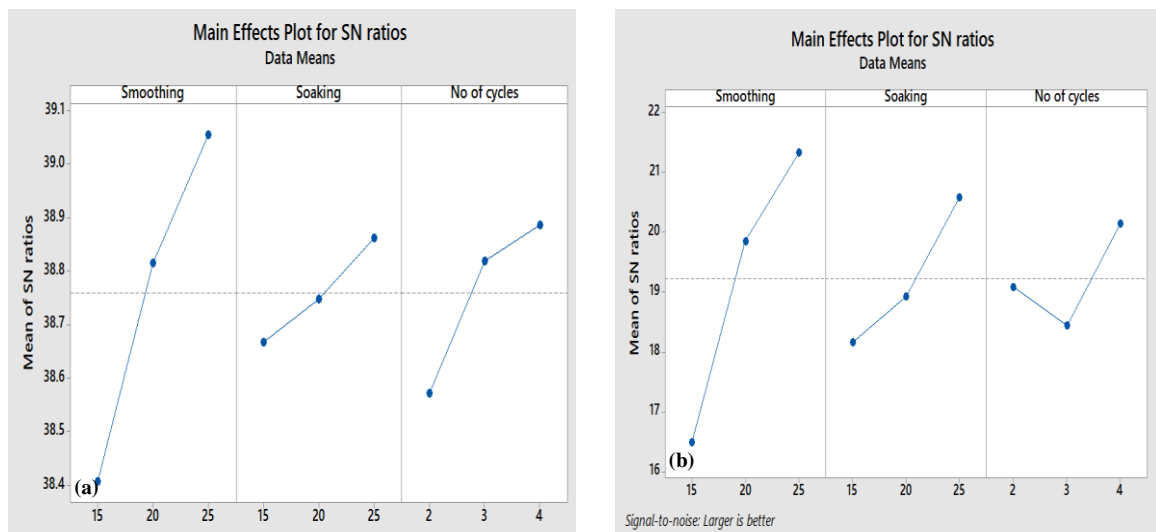


Figure 5.80 Mean SN ratio plot of percentage change in a) surface roughness and b) shore Hardness after CVS

While analyzing the mean S/N curve as shown in Figure 5.79 and 5.80 for percentage change in surface roughness after CVs and Heat treatment it has been found that with an increase in smoothing time and number of cycles there was a significant improvement in surface roughness has been obtained because as several cycles increases and smoothing time increases more vapors get deposited on the surface of the specimen which means there is no space between the adjacent layers

and ultimately improved surface roughness has been obtained. Along with surface roughness, shore Hardness was also improved up to some extend.

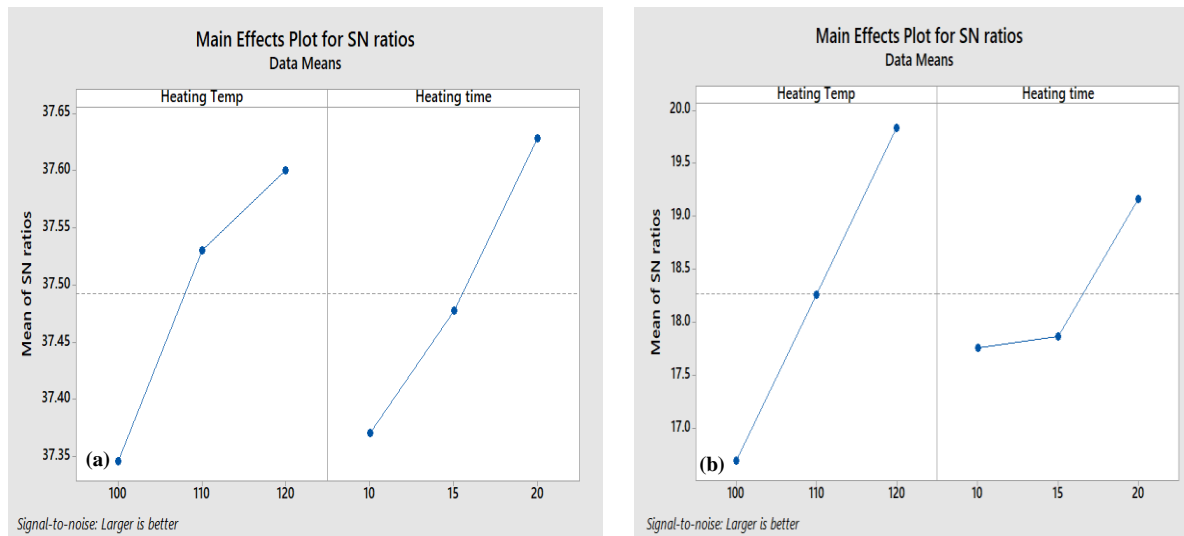


Figure 5.81 Mean SN ratio plot of percentage change in a) surface roughness and b) shore hardness after Heat Treatment

While analyzing the effect of heat treatment on surface roughness and shore hardness it was found that with an increase in heating time more heat will flow between the layers and it will fill the air gap between the layers, also it helps in removing all peaks and valleys on the surface of the prepared specimen. Due to this improved surface finish was obtained. On comparing both surface finish and shore hardness after heat treatment and vapor smoothing results of CVs are superior as compared to heat treatment. Predominant factors that affect both surface roughness and shore Hardness after CVs treatment were 25sec. smoothing time, soaking time 25 min and 4 no. of cycles. Similarly, predominant factors that affect both surface roughness and shore Hardness after Heat treatment were 120°C heating temperature and heating time i.e 25 min.

Table 5.58 ANOVA analysis of percentage change in Shore Hardness after CVS

Source	DF	Adj SS	Adj MS	F- Value	P-Value
Smoothing Time	2	34.760	17.38	40.12	0.001
Soaking Time	2	9.485	4.74	10.099	0.021
No of cycles	2	1.061	0.530	1.23	0.318
Error	2	4.314	0.862		
Total	8	49.620			

Table 5.59 ANOVA analysis of percentage change in surface roughness after CVS

Source	DF	Adj SS	Adj MS	F- Value	P-Value
Smoothing Time	2	0.631	0.315	75.58	0.00
Soaking Time	2	0.0572	0.0286	6.86	0.07
No of cycles	2	0.1486	0.0743	17.80	0.008
Error	2	0.0417	0.0083		
Total	8	0.8788			

Table 5.60 ANOVA analysis of percentage change in shore Hardness after heat Treatment

Source	DF	Adj SS	Adj MS	F- Value	P-Value
Heating Temp.	2	10.543	5.17	1.51	0.026
Heating Time	2	1.411	0.705	0.20	0.66
Error	2	41.801	6.967		
Total	6	53.746			

Table 5.61 ANOVA analysis of percentage change in Surface roughness after heat Treatment

Source	DF	Adj SS	Adj MS	F- Value	P-Value
Heating Temp.	2	57.029	28.51	2.93	0.013
Heating Time	2	3.39	1.69	0.16	0.491
Error	2	116.75	19.459		
Total	6	177.174			

Therefore, analysis of variance (ANOVA) has been applied on the S/N ratio of surface roughness and shore Hardness to determine the significant factors after post-processing. The factors having P-value less than 0.05 were considered significant. Based on the results soaking time, smoothing time, no of cycles, heating time and heating temperatures were emerging as the significant factor that affects both surface roughness and shore Hardness.

Multi-process optimization

Based on the mean effect plots and various property analyses, it has been noticed that surface roughness of 3D printed rectangular specimens post-treated via CVs possesses exhibit better improvement in surface roughness as compared to the surface roughness of 3D printed

specimen post-treated via heat treatment. So, process optimization for both post-processing techniques has been done with the help of Minitab 17 software. From the analysis, it has been found that specimens heated at 110°C for 15min gave desirability of 57% whereas specimens chemically treated for no of cycles 4, vapor smoothing time 25sec gave 100% desirability.

Further surface roughness of the specimens having maximum percentage change in surface roughness and shore Hardness after both post-processing techniques have been calculated with the help of surface roughness tester (Make: Mitutoyo) While measuring the surface roughness among various roughness parameters only R_a was considered because it uses an algorithm that averages the absolute values of the profile height deviation from the mean line on the entire surface within the sampling length and then neutralizes the few outlying points so that the extreme points have no significant impact on the outcome. The surface roughness profile of the sample having good improvement after heat treatment and vapor smoothing has been shown in Figures 5.82 and 5.83 below.

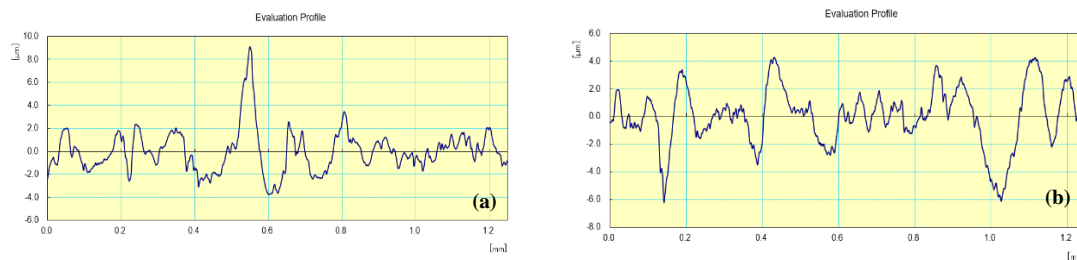


Figure 5.82 Surface roughness profile shows improvement in a) surface roughness and b) shore hardness after CVs treatment

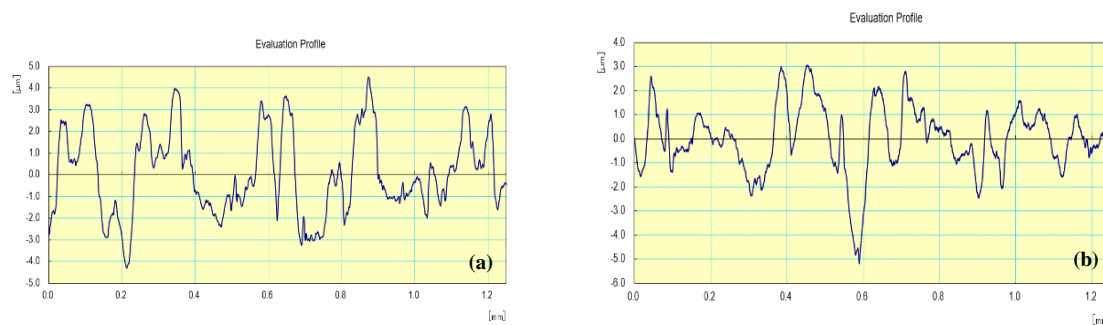


Figure 5.83 Surface roughness profile shows improvement in a) surface roughness and b) shore hardness after heat treatment

From post-processing treatment, it has been found that fixing pre-processing parameters of the FDM surface finish of the specimen can be improved up to some extent. While comparing the CVS and HT it has been found that better surface finish and shore

harness were obtained from the CVS process. Therefore to make tiles have a better surface finish and improved shore hardness can be post-treated with chemical vapor smoothing process at following parameters i.e smoothing time 25sec, soaking time 25 min and no of cycles 4.

Post Processing Technique	CVS	Heat Treatment
Maximum percentage change in Surface Roughness	91.69%	82.19%
Maximum percentage change in Shore Hardness	12.10 %	12.00%

CHAPTER 6

CONCLUSIONS

Based on outcomes received from experimentation performed in the different phases, the following conclusions have been drawn:

Composite filament preparation:

- The BP, WD and Fe powder were successfully reinforced into ABS matrix to achieve desired properties for non-structural applications as well as for the recycling of these wastes.
- From the rheological study, it has been observed that the addition of any of the reinforcements initially increases the MFR irrespective of the type of blending. However, with an increase of reinforcement level beyond a certain limit, the MFR of all the composite filaments starts decreasing.
- In mechanical blended composite filaments, extrusion speed emerges as the highly influencing factor affecting the mechanical properties. As the speed increases, the mechanical properties start reducing. Also, the selected mechanical properties for ABS+Fe powder based composite filaments were quite higher as compared to filament reinforced with WD and BP. On the other hand, the temperature during the extrusion process comes out as the most influential parameter followed by the load that affects the properties of composite filaments prepared through chemical assisted blending. Further, BP reinforced (10% by weight) composite filaments exhibit more uniform mechanical properties (PS, BS, %PE, %BE, etc.) compared to WD (10% by weight) and Fe (10% by weight) reinforced filaments. But at optimized parametric conditions, the WD reinforced filaments possess better mechanical properties as compared to BP and Fe reinforced filaments. The composite filaments fabricated through mechanical-hybrid blending possess relatively poor mechanical properties due to the brittle nature of the fabricated filaments.
- Mechanical properties of the composite filaments were drastically influenced by the percentage of porosity. The filaments possessing less porosity show better mechanical behaviour and consequently superior properties.
- The outcomes of DSC highlighted that the composite filaments fabricated by reinforcing BP possesses better heat capacity due to the high thermal conductivity of

bakelite and thus are suitable for applications subjected to relatively high temperature. The results of FTIR spectroscopy helps in predicting the mechanical behavior of composite filaments based on the presence of various compounds and their bonding with the base matrix.

- The chemical assisted blending of BP, WD and Fe as reinforcement in ABS matrix yields improved mechanical properties as compared to mechanical blending. However, thermal properties in terms of heat-carrying capacity achieved through chemical blending were degraded may be due to the presence of a higher porosity percentage.
- Combined optimized extrusion parameter settings for mechanically blended composite filaments that maximized the peak strength and percentage break elongation simultaneously was investigated as 10 kg load, 225°C temperature and 70 rpm speed for all composite filaments. However, the peak strength at the optimized parametric setting for BP, WD and Fe powder reinforced composite filament were 30.58 MPa, 25.65 MPa and 35.39 MPa respectively. Similarly, for chemically blended composite filaments, the optimized parametric levels that simultaneously maximize the PS and %BE of BP and Fe reinforced composite were: 10 kg load, 245°C temperature 70 rpm speed whereas for WD reinforced filament are 10 kg load, 225°C temperature, 70 rpm speed respectively. The optimized values of PS obtained were 30.93 MPa, 30.20 MPa and 35.72 MPa for the composite (BP, Fe and WD reinforced) filaments respectively.

Printing (FDM) and Post-processing:

- Multi-layer and single hybrid filament based tensile and flexural specimens were successfully printed (through FDM) from 2° recycled ABS based composite filaments to obtain the desired properties.
- Infill density and infill speed during printing come out as the most influential parameter that affects the properties of all prepared specimens. Further, specimens prepared through the mechanical blending route shows better mechanical and morphological properties as compared to specimen prepared through chemical and hybrid-mechanical assisted blending route.

- The tensile and flexural specimens printed from mechanical-hybrid blended composite filaments exhibit minimum strength and elongation among all the printed specimens primarily due to the brittle nature of the fused filaments.
- The SEM characterization indicated that higher density and lower raster angle results in uniform deposition of layers that leads to lesser void formation and consequently good bonding between the adjacent layers.
- The multi-objective optimization technique suggested that specimens prepared at 0° raster angle, 100% infill density and 20 mm/sec infill speed exhibit superior properties for all type of composite filaments (mechanical, chemical and mechanical-hybrid blended) with different desirability value.
- Both the CVS and heat treatment processes improve the surface finish of ABS based rectangular printed specimen significantly. Improvement in surface finish of more than 90% and 80% was achieved through CVS and heat treatment process respectively.
- With each smoothing cycle, the surface finish improves as some amount of material re-flows from peaks to valleys and thus almost eliminates the staircase effect of layered fabrication.
- The reflow of material caused by chemical vapors (acetone) enhances the shore hardness also during the CVS process. An improvement in shore hardness of 12% was observed after CVS and heat treatment process.
- The parameter that gives optimum surface finish and shore hardness after the CVS were four number of cycles, smoothing time of 25 seconds, and soaking time of 25 min.
- The composite filaments prepared in this research work would be employed to print multi-material smart tiles for low temperature regions. The BP reinforced filaments can be printed as outer surface layers of the tiles because of its thermal stability and high heat carrying capacity, WD reinforced filaments as inner layers due to insulating properties to retain the heat inside the room and Fe powder reinforced filaments as outer layers to impart magnetic properties and self-assembly features.

LIMITATIONS AND SCOPE OF FUTURE RESEARCH WORK

- The present research work focused on the material development for the fabrication of smart tiles. The work related to product development, product behaviour and life cycle can be explored in future studies.
- The present work utilizes BP, WD and Fe powder as reinforcement in 2° recycled ABS for studying the mechanical and thermal properties. Further, studies can be performed by taking other reinforcements and their impact on various properties.
- The limited and constrained set of processing parametric levels was one of the limitation of the present work.
- In this work, the non-structural applications of ABS composite matrix were investigated whereas the structural applications of recycled ABS composite matrix can be explored in future work.

REFERENCES

1. Brown SB. (2003), "Reactive compatibilization of polymer blends", In: Polymer blends handbook, pp. 339-415.
2. Paul D. and Barlow J. (1980), "Polymer blends", Journal Macromolecule Science Review, Vol. 18, No. 1, pp. 109-68.
3. Thomas S., Grohens Y. and Jyotish Kumar P. (2014), "Characterization of polymer blends: miscibility, morphology and interfaces", John Wiley & Sons.
4. Utracki LA. and Wilkie CA. (2002), "Polymer blends handbook", Springer.
5. Lithner D., Larsson A. and Dave G. (2011), "Environmental and health hazard ranking and assessment of plastic polymers based on chemical composition", Science Total Environment Vol. 409, No.18, pp. 3309–3324.
6. Mwanza, B. G. and Mbohwa, C. (2017), Drivers to sustainable plastic solid waste recycling: a review. Procedia Manufacturing, Vol. 8, pp. 649-656.
7. Ackerman F. (2000), "Waste management and climate change", Local Environment, Vol.5, pp. 223-229.
8. Kozderka, M., Rose, B., Kočí, V., Caillaud, E. and Bahlouli, N. (2016), "High impact polypropylene (HIPP) recycling–Mechanical resistance and Lifecycle Assessment (LCA) case study with improved efficiency by preliminary sensitivity analysis", Journal of cleaner production, Vol.137, pp. 1004-1017.
9. Jambeck, J., Hardesty, B. D., Brooks, A. L., Friend, T., Teleki, K., Fabres, J. and Wilcox, C. (2018), "Challenges and emerging solutions to the land-based plastic waste issue in Africa", Marine Policy, Vol.96, pp. 256-263.
10. Silvarrey, L. D. and Phan, A. N. (2016), "Kinetic study of municipal plastic waste", International journal of hydrogen energy, Vol.41, pp. 16352-16364.
11. Geyer, R., Jambeck, J. R. and Law, K. L. (2017), "Production, use, and fate of all plastics ever made", Science advances, Vol. 3, No.7. pp.1-5.
12. Cole, M., Lindeque, P., Halsband, C. and Galloway, T. S. (2011), "Microplastics as contaminants in the marine environment: a review", Marine pollution bulletin, Vol. 62, pp. 2588-2597.
13. Singh, N., Hui, D., Singh, R., Ahuja, I. P. S., Feo, L. and Fraternali, F. (2017), "Recycling of plastic solid waste: A state of art review and future applications", Composites Part B: Engineering, Vol. 115, pp. 409-422.

14. Milios, L., Christensen, L. H., McKinnon, D., Christensen, C., Rasch, M. K. and Eriksen, M. H. (2018), "Plastic recycling in the Nordics: A value chain market analysis", *Waste Management*, Vol. 76, pp. 180-189.
15. Gondal, M. A. and Siddiqui, M. N. (2007), "Identification of different kinds of plastics using laser-induced breakdown spectroscopy for waste management", *Journal of Environmental Science and Health Part A*, Vol. 42, No. 13, pp.1989-1997.
16. Strategic Management Group, (2014), "T. Potential of plastic industry in northern India with special focus on plasticulture and food processing".
17. da Silva, D. J. and Wiebeck, H. (2020), "Current options for characterizing, sorting, and recycling polymeric waste. Progress in Rubber", *Plastics and Recycling Technology*, Vol. 36, pp. 284-303.
18. Eriksen, M. K., Pivnenko, K., Olsson, M. E. and Astrup, T. F. (2018), "Contamination in plastic recycling: Influence of metals on the quality of reprocessed plastic", *Waste management*, Vol. 79, pp. 595-606.
19. Yu J., Sun L., Ma C., Qiao Y. and Yao H. (2016), "Thermal degradation of PVC: A review", *Waste Management*, Vol.48, pp. 300-314.
20. Dodiuk, H. (Ed.), *Handbook of thermoset plastics*. William Andrew, (2013).
21. Al-Salem, S. M., Antelava, A., Constantinou, A., Manos, G. and Dutta, A. (2017), "A review on thermal and catalytic pyrolysis of plastic solid waste (PSW)", *Journal of Environmental Management*, Vol. 197, pp.177-198.
22. Spinacé, M. A. D. S. and De Paoli, M. A. (2005), "A tecnologia da reciclagem de polímeros", *Química nova*, Vol.28, pp.65-72.
23. Hamad, K., Kaseem, M. and Deri, F. (2013), "Recycling of waste from polymer materials: An overview of the recent works", *Polymer degradation and stability*, Vol. 98, pp.2801-2812.
24. Cruz, S. A., Oliveira, É. C., Oliveira, F., Garcia, P. S. and Kaneko, M. L. (2011), "Polímeros reciclados para contato com alimentos", *Polímeros*, Vol.21, pp.340-345.
25. Al-Salem, S. M., Lettieri, P. and Baeyens, J. (2019), "Recycling and recovery routes of plastic solid waste (PSW): A review," *Waste management*, Vol.29, pp.2625-2643.
26. Garcia, J. M. and Robertson, M. L. (2017), "The future of plastics recycling", *Science*, Vol. 358, pp. 870-872.
27. da Silva, D. J. (2016), "Novel preparation technique for polycarbonate/titanium dioxide nanocomposites", *SPE Plast Res Online*, pp. 1-4.

28. da Silva, D. J., Escote, M. T., Cruz, S. A., Simião, D. F., Zenatti, A. and Curvello, M. S.(2018),“Polycarbonate/TiO₂ nanofibers nanocomposite: preparation and properties”, *Polymer Composites*, Vol. 39, pp.780-790.
29. Rahimi, A. and García, J. M. (2017), “Chemical recycling of waste plastics for new materials production”, *Nature Reviews Chemistry*, Vol.1, pp.1-11.
30. Chawla, K., Singh, R., and Singh, J. (2020), “Segregation and Recycling of Plastic Solid Waste: A Review”, *Advances in Materials Science and Engineering*, pp. 205-221.
31. Kumar, S., Panda, A. K. and Singh, R. K. (2011), “A review on tertiary recycling of high-density polyethylene to fuel”, *Resources, Conservation and Recycling*, Vol.55, pp.893-910.
32. Ignatyev, I. A., Thielemans, W. and Vander Beke, B. (2014), “Recycling of polymers: a review”, *Chem Sus Chem*, Vol.7, pp.1579-1593.
33. Rezaei, F., Rownaghi, A. A., Monjezi, S., Lively, R. P. and Jones, C. W. (2015), “SO_x/NO_x removal from flue gas streams by solid adsorbents: a review of current challenges and future directions”, *Energy and fuels*, Vol.29, pp.5467-5486.
34. Sun, Y., Zwolińska, E. and Chmielewski, A. G. (2016), “Abatement technologies for high concentrations of NO_x and SO₂ removal from exhaust gases: A review”, *Critical Reviews in Environmental Science and Technology*, Vol.46, pp.119-142.
35. Chawla, K., Singh, J. and Singh, R. (2020), “On recyclability of thermosetting polymer and wood dust as reinforcement in secondary recycled ABS for nonstructural engineering applications”, *Journal of Thermoplastic Composite Materials*, doi: 0892705720925135.
36. Singh J., Singh R., Singh H. and Verma, A.K. (2018a), “Investigations for mechanical properties and biocompatibility of SS-316L implant prepared as rapid investment casting for batch production”, *Sadhana - Academy Proceedings in Engineering Sciences*, Vol. 43, No. 5, pp. 1-10.
37. Chua C.K, Matham M.V, and Kim Y. (2017), “Lasers in 3D printing and manufacturing”, *World Scientific Publishing Company, Singapore*, Vol. 12.
38. CustomPartNet (2008), Online available at: <http://www.custompartnet.com> [accessed on February 3, 2017].
39. Redwood, B., Schöffner, F. and Garret, B. (2017), “The 3D printing handbook: technologies, design and applications”, *3D Hubs B.V.*

40. Gebhardt, A. (2012), "Understanding additive manufacturing: rapid prototyping-rapid tooling-rapid manufacturing", Carl Hanser Verlag GmbH Co., Munich, Germany, doi.org/10.3139/9783446431621.
41. Vaezi, M., Chianrabutra, S., Mellor, B. and Yang, S. (2013), "Multiple material additive manufacturing–Part 1: a review", *Virtual and Physical Prototyping*, Vol. 8, No. 1, pp.19-50.
42. Gibson, I. (2006), "Advanced manufacturing technology for medical applications: reverse engineering, software conversion and rapid prototyping", John Wiley and Sons, New York, USA, [doi:10.1002/0470033983](https://doi.org/10.1002/0470033983).
43. Shah, J., Snider, B., Clarke, T., Kozutsky, S., Lacki, M. and Hosseini, A. (2019), "Large-scale 3D printers for additive manufacturing: design considerations and challenges", *The International Journal of Advanced Manufacturing Technology*, Vol. 104, pp. 3679-3693.
44. Mikula, K., Skrzypczak, D., Izydorzyc, G., Warchoń, J., Moustakas, K., Chojnacka, K. and Witek-Krowiak, A. (2021), "3D printing filament as a second life of waste plastics—A review", *Environmental Science and Pollution Research*, Vol. 28, No. 10, pp. 12321-12333.
45. Baechler, C., DeVuono, M. and Pearce, J. M. (2013), "Distributed recycling of waste polymer into RepRap feedstock", *Rapid Prototyping Journal*, Vol. 19, No.2, pp. 118-125.
46. Singh, R., Singh, S. and Fraternali, F. (2016a), "Development of in-house composite wire based feedstock filaments of fused deposition modeling for wear-resistant materials and structures", *Composites Part B: Engineering*, Vol. 98, pp. 244-249.
47. Singh, R., Kumar, R., Feo, L. and Fraternali, F. (2016b), "Friction welding of dissimilar plastic/polymer materials with metal powder reinforcement for engineering applications", *Composites Part B: Engineering*, Vol. 101, pp.77-86.
48. Farina, I., Fabbrocino, F., Carpentieri, G., Modano, M., Amendola, A., Goodall, R. and Fraternali, F. (2016), "On the reinforcement of cement mortars through 3D printed polymeric and metallic fibers", *Composites Part B: Engineering*, Vol.90, pp.76-85.
49. Lanzotti, A., Martorelli, M., Maietta, S., Gerbino, S., Penta, F. and Gloria, A. (2019), "A comparison between mechanical properties of specimens 3D printed with virgin and recycled PLA", *Procedia Cirp*, Vol.79, pp.143-146.

50. Duval, C. (2014), "Plastic waste and the environment. Environmental Impact of Polymers", doi: 10.1002/9781118827116.ch2.
51. Brüster, B., Addiego, F., Hassouna, F., Ruch, D., Raquez, J. M. and Dubois, P. (2016), "Thermo-mechanical degradation of plasticized poly (lactide) after multiple reprocessing to simulate recycling: Multi-scale analysis and underlying mechanisms", *Polymer Degradation and Stability*, Vol.131, pp.132-144.
52. Anderson, I. (2017), "Mechanical Properties of Specimens 3D Printed with Virgin and Recycled Polylactic Acid", *3d printing and additive manufacturing*, Vol. 4, No.2, pp. 110-115.
53. Zhao P., Rao C., Gu F., Sharmin N. and Fu J. (2018a), "Close-looped recycling of polylactic acid used in 3D printing: An experimental investigation and life cycle assessment", *Journal of Cleaner Production*, Vol.197, pp.1046–1055.
54. Zhao XG., Hwang KJ., Lee D., Kim T. and Kim N. (2018b), "Enhanced mechanical properties of self-polymerized polydopamine-coated recycled PLA filament used in 3D printing", *Applied Surface Science*, Vol.441, pp.381–387.
55. Adhikary, K. B., Pang, S. and Staiger, M. P. (2008), "Dimensional stability and mechanical behaviour of wood–plastic composites based on recycled and virgin high-density polyethylene (HDPE)", *Composites Part B: Engineering*, Vol.39, pp. 807-815.
56. Jen, Y. M. and Huang, C. Y. (2014), "Effect of temperature on fatigue strength of carbon nanotube/epoxy composites", *Journal of Composite Materials*, Vol.48, pp.3469-3483.
57. Lu, N. and Oza, S. (2013), "A comparative study of the mechanical properties of hemp fiber with virgin and recycled high density polyethylene matrix", *Composites Part B: Engineering*, Vol.45, pp. 1651-1656.
58. Oliveux, G., Dandy, L. O. and Leeke, G. A. (2015), "Current status of recycling of fibre reinforced polymers: Review of technologies, reuse and resulting properties", *Progress in Materials Science*, Vol. 72, pp. 61-99.
59. Onwudili, J. A., Miskolczi, N., Nagy, T. and Lipóczy, G. (2016), "Recovery of glass fibre and carbon fibres from reinforced thermosets by batch pyrolysis and investigation of fibre re-using as reinforcement in LDPE matrix", *Composites Part B: Engineering*, Vol. 91, pp.154-161.
60. Yildirim, E., Miskolczi, N., Onwudili, J. A., Németh, K. E., Williams, P. T. and Sója, J. (2015), "Evaluating the mechanical properties of reinforced LDPE composites

- made with carbon fibres recovered via solvothermal processing”, *Composites Part B: Engineering*, Vol. 78, pp.393-400.
61. Pan, G. T., Chong, S., Tsai, H. J., Lu, W. H. and Yang, T. C. K. (2018), “The effects of iron, silicon, chromium, and aluminum additions on the physical and mechanical properties of recycled 3D printing filaments”, *Advances in Polymer Technology*, Vol. 37, pp.1176-1184.
 62. Singh, S. and Singh, R. (2015), “Wear modelling of Al-Al₂O₃ functionally graded material prepared by FDM assisted investment castings using dimensionless analysis”, *Journal of Manufacturing Processes*, Vol.20, pp.507-514.
 63. Hamad, K., Kaseem, M. and Deri, F. (2013), “Recycling of waste from polymer materials: An overview of the recent works”, *Polymer degradation and stability*, Vol. 98, pp. 2801-2812.
 64. Simón, D., Borreguero, A. M., De Lucas, A. and Rodríguez, J. F. (2018), “Recycling of polyurethanes from laboratory to industry, a journey towards the sustainability”, *Waste Management*, Vol.76, pp.147-171.
 65. Unnisa, S. A. and Hassanpour, M. (2017), “Development circumstances of four recycling industries (used motor oil, acidic sludge, plastic wastes and blown bitumen) in the world”, *Renewable and sustainable energy reviews*, Vol. 72, pp. 605-624.
 66. Silveira, A. V. M., Cella, M., Tanabe, E. H. and Bertuol, D. A. (2018), “Application of tribo-electrostatic separation in the recycling of plastic wastes”, *Process Safety and Environmental Protection*, Vol.114, pp. 219-228.
 67. Butler, E., Devlin, G. and McDonnell, K. (2011), “Waste polyolefins to liquid fuels via pyrolysis: review of commercial state-of-the-art and recent laboratory research”, *Waste and biomass valorization*, Vol.2, pp.227-255.
 68. Wu, W., Geng, P., Li, G., Zhao, D., Zhang, H. and Zhao, J. (2015) “Influence of layer thickness and raster angle on the mechanical properties of 3D-printed PEEK and a comparative mechanical study between PEEK and ABS”, *Materials*, Vol. 8, No.9, pp. 5834-5846.
 69. Singh, R. Kumar, R. and Kumar S. (2017b) “Polymer Waste as Fused Deposition Modeling Feed Stock Filament for Industrial Applications”, *Materials Science and Materials Engineering*, doi: 10.1016/B978-0-12-803581-8.04153-9.
 70. Ryder Matthew A., Lados Diana A., Iannacchione Germano S. and Peterson Amy M. (2017), “Fabrication and properties of novel polymer-metal composites using fused deposition modeling”, *Composites science and technology*, Vol. 158, pp. 43-50.

71. Sezer, H. K. and Eren, O. (2019), "FDM 3D printing of MWCNT re-inforced ABS nano-composite parts with enhanced mechanical and electrical properties", *Journal of Manufacturing Processes*, Vol. 37, pp- 339-347.
72. Mojarrad, A., Ramazani SA, A., Ghasemi, I. and Vaziri, A. (2014), "Rheological and morphological behaviors of polyamide 6/acrylonitrile-butadiene-styrene/nanoclay nanocomposites", *Journal of Thermoplastic Composite Materials*, Vol. 27, No.10, pp. 1399-1416.
73. Billah, K. M. M., Lorenzana, F. A., Martinez, N. L., Wicker, R. B. and Espalin, D. (2020), "Thermomechanical characterization of short carbon fiber and short glass fiber-reinforced ABS used in large format additive manufacturing", *Additive Manufacturing*, Vol.35, pp.1-9.
74. De León, A. S., Domínguez-Calvo, A. and Molina, S. I. (2019), "Materials with enhanced adhesive properties based on acrylonitrile-butadiene-styrene (ABS)/thermoplastic polyurethane (TPU) blends for fused filament fabrication (FFF)", *Materials & Design*, Vol. 182, pp. 1-11.
75. Kumar, V., Singh, R. and Ahuja, I. P. S. (2020), "Effect of extrusion parameters on primary recycled ABS: mechanical, rheological, morphological and thermal properties", *Materials Research Express*, Vol.7, No.1, pp.1-16.
76. Kumar, V., Singh, R. and Ahuja, I. P. S. (2021), "On 4D capabilities of chemical assisted mechanical blended ABS-nano graphene composite matrix", *Materials Today: Proceedings*, Vol.48, pp.952-957.
77. Tambrallimath, V., Keshavamurthy, R., Saravanabavan, D., Koppad, P. G. and Kumar, G. P. (2019), "Thermal behavior of PC-ABS based graphene filled polymer nanocomposite synthesized by FDM process", *Composites Communications*, Vol.15, pp. 129-134.
78. Weng, Z., Wang, J., Senthil, T. and Wu, L. (2016), "Mechanical and thermal properties of ABS/montmorillonite nanocomposites for fused deposition modeling 3D printing", *Materials & Design*, Vol.102, pp. 276-283.
79. Torrado, A. R., Shemelya, C. M., English, J. D., Lin, Y., Wicker, R. B. and Roberson, D. A. (2015), "Characterizing the effect of additives to ABS on the mechanical property anisotropy of specimens fabricated by material extrusion 3D printing", *Additive Manufacturing*, Vol.6, pp. 16-29.
80. Schmitz, D. P., Dul, S., Ramoa, S. D. A. S., Soares, B. G., Barra, G. M. O. and Pegoretti, A. (2021), "Effect of printing parameters on the electromagnetic shielding

- efficiency of ABS/carbonaceous-filler composites manufactured via filament fused fabrication”, *Journal of Manufacturing Processes*, Vol.65, pp.12-19.
81. Kariz, M., Sernek, M., Obućina, M. and Kuzman, M. K. (2018), “Effect of wood content in FDM filament on properties of 3D printed parts”, *Materials Today Communications*, Vol.14, pp.135-140.
 82. Kumar, S., Singh, R., Singh, T. P. and Batish, A. (2019), “Investigations of polylactic acid reinforced composite feedstock filaments for multimaterial three-dimensional printing applications”, *Proceedings of the Institution of Mechanical Engineers, Part C: Journal of Mechanical Engineering Science*, Vol. 233, No.17, pp. 5953-5965.
 83. Yang, L., Li, S., Zhou, X., Liu, J., Li, Y., Yang, M. and Zhang, W. (2019). “Effects of carbon nanotube on the thermal, mechanical, and electrical properties of PLA/CNT printed parts in the FDM process”, *Synthetic Metals*, Vol. 253, pp- 122-130.
 84. Singh, R., Kumar, R., Pawanpreet, Singh, M. and Singh, J. (2019), “On mechanical, thermal and morphological investigations of almond skin powder-reinforced polylactic acid feedstock filament”, *Journal of Thermoplastic Composite Materials*, doi:10.1177/ 0892705719886010.
 85. Stoof, D., Pickering, K. and Zhang, Y. (2017), “Fused deposition modelling of natural fibre/polylactic acid composites”, *Journal of Composites Science*, Vol.1, No. 1, doi.org/10.3390/jcs1010008.
 86. Montava-Jordà, S., Quiles-Carrillo, L., Richart, N., Torres-Giner, S. and Montanes, N. (2019), “Enhanced interfacial adhesion of polylactide/poly (ϵ -caprolactone)/walnut shell flour composites by reactive extrusion with maleinized linseed oil”, *Polymers*, Vol.11, No.5, pp.758.
 87. Singh, R., Kumar, R. and Kumar, S. (2017), “Polymer waste as fused deposition modeling feedstock filament for industrial applications”. *Materials Science and Materials Engineering*, DOI:10.1016/B978-0-12-803581-8.04153-9, pp. 1-12.
 88. Kumar, S., Singh, R., Singh, T. P. and Batish, A. (2019), “On investigation of rheological, mechanical and morphological characteristics of waste polymer-based feedstock filament for 3D printing applications”, *Journal of Thermoplastic Composite Materials*, doi: 0892705719856063.
 89. Liu, Z., Lei, Q. and Xing, S. (2019), “Mechanical characteristics of wood, ceramic, metal and carbon fiber-based PLA composites fabricated by FDM. *Journal of Materials Research and Technology*”, Vol. 8, No.5, pp.3741-3751.

90. Masood, S. H. and Song, W. Q. (2005). Thermal characteristics of a new metal/polymer material for FDM rapid prototyping process. *Assembly Automation*, Vol.25, No.4, pp. 309-315.
91. Singh, R., Kumar, R., Mascolo, I. and Modano, M. (2018), “On the applicability of composite PA6-TiO₂ filaments for the rapid prototyping of innovative materials and structures”, *Composites Part B: Engineering*, Vol. 143, pp. 132-140.
92. Mergen, Ö. B., Arda, E. and Evingür, G. A. (2020), “Electrical, mechanical, and optical changes in MWCNT-doped PMMA composite films”, *Journal of Composite Materials*, Vol. 54, No.18, pp. 2449-2459.
93. Chen, J., Lu, H. Y., Yang, J. H., Wang, Y., Zheng, X. T., Zhang, C. L. and Yuan, G. P. (2014), “Effect of organoclay on morphology and electrical conductivity of PC/PVDF/CNT blend composites”, *Composites Science and Technology*, Vol. 94, pp.30-38.
94. Novais, R. M., Carvalheiras, J., Seabra, M. P., Pullar, R. C. and Labrincha, J. A. (2017), “Effective mechanical reinforcement of inorganic polymers using glass fibre waste”, *Journal of Cleaner Production*, Vol. 166, pp. 343-349.
95. Sodeifian, G., Ghaseminejad, S. and Yousefi, A. A. (2019), “Preparation of polypropylene/short glass fiber composite as Fused Deposition Modeling (FDM) filament”, *Results in Physics*, Vol.12, pp.205-222.
96. Colorado H A., Gutireere E. and Heei C. (2020), “Cantilever creep method for testing ceramic composites and a case study for chemically bonded phosphate ceramic composites reinforced with glass, carbon and basalt fibers, including both experiments and simulations”, *Journal of composite materials*, doi.org/10.1177/00211998320902510.
97. Sharma, R., Singh, R. and Batish, A. (2021). “Study on barium titanate and graphene reinforced PVDF matrix for 4D applications”, *Journal of Thermoplastic Composite Materials*, Vol. 34, No. 9, pp. 1234-1253.
98. Karaman, E. and Çolak, O. (2020), “The effects of process parameters on mechanical properties and microstructures of parts in fused deposition modeling”, *Duzce University Journal of Science & Technology*, Vol. 8, pp.617–630.
99. Patan, Z. Y. (2019). Karbon fiber takviyeli ABS kompozitlerin FDM 3B yazıcı ile üretimi ve “ansys ile modellenmesi”, (Doctoral dissertation, Onsekizmart Üniversitesi).

100. Ning, F., Cong, W., Qiu, J., Wei, J. and Wang, S. (2015), "Additive manufacturing of carbon fiber reinforced thermoplastic composites using fused deposition modeling", *Composites Part B: Engineering*, Vol. 80, pp.369-378.
101. Zhong, W., Li, F., Zhang, Z., Song, L. and Li, Z. (2001), "Short fiber reinforced composites for fused deposition modeling", *Materials Science and Engineering: A*, Vol.301, pp.125-130.
102. Hill, C., Rowe, K., Bedsole, R., Earle, J. and Kunc, V. (2016), "Materials and process development for direct digital manufacturing of vehicles", In SAMPE Long Beach (2016), Conference and Exhibition.
103. Kunc, V. (2015), "Advances and challenges in large scale polymer additive manufacturing", In Proceedings of the 15th SPE Automotive Composites Conference, Novi, MI, USA, Vol. 9.
104. Mori, K. I., Maeno, T., and Nakagawa, Y. (2014)," Dieless forming of carbon fibre reinforced plastic parts using 3D printer", *Procedia engineering*, Vol. 81, pp.1595-1600.
105. Hwang, S., Reyes, E. I., Moon, K. S., Rumpf, R. C. and Kim, N. S. (2015), "Thermo-mechanical characterization of metal/polymer composite filaments and printing parameter study for fused deposition modeling in the 3D printing process", *Journal of Electronic Materials*, Vol. 44, pp.771-777.
106. Duty, C. E., Drye, T. and Franc, A. (2015), "Material development for tooling applications using big area additive manufacturing (BAAM) (No. ORNL/TM-2015/78)", Oak Ridge National Lab. (ORNL), Oak Ridge, TN (United States), Manufacturing Demonstration Facility (MDF), doi.org/10.2172/1209207.
107. Perez, A. R. T., Roberson, D. A. and Wicker, R. B. (2014), "Fracture surface analysis of 3D-printed tensile specimens of novel ABS-based materials", *Journal of Failure Analysis and Prevention*, Vol. 14, No.3, pp. 343-353.
108. Gao, X., Zhang, D., Qi, S., Wen, X. and Su, Y. (2019), "Mechanical properties of 3D parts fabricated by fused deposition modeling: Effect of various fillers in polylactide", *Journal of Applied Polymer Science*, doi.org/10.1002/app.47824.
109. Ferreira, R. T. L., Amatte, I. C., Dutra, T. A. and Bürger, D. (2017), "Experimental characterization and micrography of 3D printed PLA and PLA reinforced with short carbon fibers", *Composites Part B: Engineering*, Vol. 124, pp. 88-100.
110. Hodzic, D. and Pandzic, A. (2019), "Influence of carbon fibers on mechanical properties of materials in FDM technology", In Proceedings of the 30th DAAAM

- International Symposium on Intelligent Manufacturing and Automation, Zadar, pp.1726-9679.
111. Liu, Z., Lei, Q. and Xing, S. (2019), “Mechanical characteristics of wood, ceramic, metal and carbon fiber-based PLA composites fabricated by FDM”, *Journal of Materials Research and Technology*, Vol. 8, pp. 3741-3751.
 112. Tian, X., Liu, T., Wang, Q., Dilmurat, A., Li, D. and Ziegmann, G. (2016), “Recycling and remanufacturing of 3D printed continuous carbon fiber reinforced PLA composites”, *Journal of Cleaner Production*, Vol. 30, pp.1-10.
 113. Van Der Klift, F., Koga, Y., Todoroki, A., Ueda, M., Hirano, Y. and Matsuzaki, R. (2016), “3D printing of continuous carbon fibre reinforced thermoplastic (CFRTP) tensile test specimens”, *Open Journal of Composite Materials*, Vol. 6, No.1, pp. 18-27.
 114. Nagendra, J. and Prasad, M. G. (2020), “FDM process parameter optimization by Taguchi technique for augmenting the mechanical properties of nylon–aramid composite used as filament material”, *Journal of The Institution of Engineers (India): Series C*, Vol. 101, pp. 313-322.
 115. Melenka, G. W., Cheung, B. K., Schofield, J. S., Dawson, M. R. and Carey, J. P. (2016), Evaluation and prediction of the tensile properties of continuous fiber-reinforced 3D printed structures”, *Composite Structures*, Vol. 153, pp. 866-875.
 116. Dickson, A. N., Barry, J. N., McDonnell, K. A. and Dowling, D. P. (2017), “Fabrication of continuous carbon, glass and Kevlar fibre reinforced polymer composites using additive manufacturing”, *Additive Manufacturing*, Vol. 16, pp. 146-152.
 117. Gardner, J. M., Sauti, G., Kim, J. W., Cano, R. J., Wincheski, R. A., Stelter, C. J. and Park, S. S. (2016), “Additive manufacturing of multifunctional components using high density carbon nanotube yarn filaments”, *Nasa Technical Reports Server*.
 118. Nabipour, M., Akhoundi, B. and Bagheri Saed, A. (2020), “Manufacturing of polymer/metal composites by fused deposition modeling process with polyethylene”, *Journal of Applied Polymer Science*, Vol. 137, doi.org/10.1002/app.48717.
 119. Gebhardt, A. (2003), “Rapid Prototyping”, *Hanser Gardner Publications, Inc., Cincinnati, USA*, ISBN: 978-3-446-21259-6.
 120. Azadi, M., Dadashi, A., Dezianian, S., Kianifar, M., Torkaman, S. and Chiyani, M. (2021), “High-cycle bending fatigue properties of additive-manufactured ABS and

- PLA polymers fabricated by fused deposition modeling 3D-printing”, *Forces in Mechanics*, doi.org/10.1016/j.finmec.2021.100016.
121. Singh, R. (2013), “Some investigations for small-sized product fabrication with FDM for plastic components”, *Rapid Prototyping Journal*, doi:10.1108/13552541311292745.
 122. Liu, Z., Lei, Q. and Xing, S. (2019), “Mechanical characteristics of wood, ceramic, metal and carbon fiber-based PLA composites fabricated by FDM”, *Journal of Materials Research and Technology*, Vol. 8, No.5, pp.3741-3751.
 123. Maurya, N.K., Rastogi, V. and Singh, P. (2020), “Experimental and computational analysis of mechanical properties of RGD840 material manufactured through PolyJet process”, *Rapid Prototyping Journal*, Vol. 27, No. 1, pp. 207-214.
 124. Kumar, R., Singh, R. and Farina, I. (2018), “On the 3D printing of recycled ABS, PLA and HIPS thermoplastics for structural applications”, *PSU Research Review*, doi: 10.1108/PRR-07-2018-0018.
 125. Schirmeister, C. G., Hees, T., Licht, E. H. and Muelhaupt, R. (2019), “3D printing of high density polyethylene by fused filament fabrication”, *Additive Manufacturing*, Vol.28, pp.152-159.
 126. Lohar, G. S. and Jogi, B. F. (2018), “Influence of carbon black (CB) on mechanical behaviour and microscopic analysis of poly-propylene (PP)/acrylonitrile-butadiene-styrene (ABS) nanocomposites”, *Procedia Manufacturing*, Vol. 20, pp. 85-90.
 127. Mu, M., Ou, C. Y., Wang, J. and Liu, Y. (2020), “Surface modification of prototypes in fused filament fabrication using chemical vapour smoothing”, *Additive Manufacturing*, doi.org/10.1016/j.addma.2019.100972.
 128. Singh, J. (2017), “Some investigations for biomedical implant prepared by combining fused deposition modeling chemical vapour smoothing silicon moulding and investment casting”, *Doctorate Thesis*.
 129. Bharath, V., Prakash, N. D., Anshuman, R. and Henderson, M., (2000), “Sensitivity of RP surface finish to process parameter variation”, In: *Solid free form fabrication proceedings*. The University of Texas, Austin, pp. 252-258.
 130. Chakraborty, D., Reddy, A., Roy, B. and Choudhury, A. (2008), “Extruder Path Generation for Curved Layer Fused Deposition Modeling”, *Computer-Aided Design*, Vol. 40, pp. 235–243.
 131. Lay, M., Thajudin, N. L. N., Hamid, Z. A. A., Rusli, A., Abdullah, M. K. and Shuib, R. K. (2019), “Comparison of physical and mechanical properties of PLA,

- ABS and nylon 6 fabricated using fused deposition modeling and injection molding”, *Composites Part B: Engineering*, Vol.176, doi.org/10.1016/j.compositesb.2019.107341.
132. Roy, R. and Mukhopadhyay, A. (2021), “Tribological studies of 3D printed ABS and PLA plastic parts”, *Materials Today: Proceedings*, Vol. 41, pp. 856-862.
133. Yap, Y. L., Toh, W., Koneru, R., Lin, K., Yeoh, K. M., Lim, C. M. and Zheng, G. (2019), “A non-destructive experimental-cum-numerical methodology for the characterization of 3D-printed materials—polycarbonate-acrylonitrile butadiene styrene (PC-ABS)”, *Mechanics of Materials*, Vol.132, pp. 121-133.
134. Al Rashid, A., Khan, S. A., Al-Ghamdi, S. G. and Koç, M. (2021), “Additive manufacturing of polymer nanocomposites: needs and challenges in materials, processes, and applications”, *Journal of Materials Research and Technology*, Vol. 14, pp. 910-941.
135. Petroni, J. M., Neves, M. M., de Moraes, N. C., da Silva, R. A. B., Ferreira, V. S. and Lucca, B. G. (2021), “Development of highly sensitive electrochemical sensor using new graphite/acrylonitrile butadiene styrene conductive composite and 3D printing-based alternative fabrication protocol”, *Analytica Chimica Acta*, Vol. 1167, doi: 10.1016/j.aca.2021.338566.
136. Kaur, G., Singari, R. M. and Kumar, H. (2021), “A review of fused filament fabrication (FFF): Process parameters and their impact on the tribological behavior of polymers (ABS)”, *Materials Today: Proceedings*, doi: 10.1016/j.matpr.2021.06.274.
137. Boparai, K. S. (2020). “Thermal and Dynamic Mechanical Analysis of 3D Printed Bakelite Reinforced ABS”, *Reference Module in Material Science and Material Engineering*, doi:10.1016/B978-0-12-820352-1.00037-7.
138. Jayanth, N. and Senthil, P. (2019), “Application of 3D printed ABS based conductive carbon black composite sensor in void fraction measurement”, *Composites Part B: Engineering*, Vol.159, pp.224-230.
139. Dul, S., Fambri, L. and Pegoretti, A. (2016), “Fused deposition modelling with ABS–graphene nanocomposites”, *Composites Part A: Applied Science and Manufacturing*, Vol. 85, pp. 181-191.
140. Sahay, R., Nayak, R., Naik, N. and Tambrallimath, V. (2021), “Influence of silicon carbide reinforcement on mechanical behavior of 3D printed polymer composites”, *Materials Today: Proceedings*, doi:10.1016/j.matpr.2020.12.787.

141. Abdullah, Z., Ting, H. Y., Ali, M. A. M., Fauadi, M. H. F. M., Kasim, M. S., Hambali, A. and Handoko, F. (2018), "The Effect of Layer Thickness And Raster Angles On Tensile Strength And Flexural Strength For Fused Deposition Modeling (FDM) Parts", *Journal of Advanced Manufacturing Technology (JAMT)*, Vol.12, pp.147-158.
142. Singh, B., Kumar, R. and Chohan, J. S. (2021), "Multi-objective optimization of 3D Printing process using genetic algorithm for fabrication of copper reinforced ABS parts", *Materials Today: Proceedings*, Vol.48, pp.981-988.
143. Kumar, R., Singh, R., Ahuja, I. P. S., Amendola, A. and Penna, R. (2018), "Friction welding for the manufacturing of PA6 and ABS structures reinforced with Fe particles", *Composites Part B: Engineering*, Vol.132, pp.244-257.
144. Travieso-Rodriguez, J. A., Zandi, M. D., Jerez-Mesa, R. and Lluma-Fuentes, J. (2020), "Fatigue behavior of PLA-wood composite manufactured by fused filament fabrication", *Journal of Materials Research and Technology*, Vol. 9, No.4, pp.8507-8516.
145. Yubo, T. A. O., Peng, L. I. and Ling, P. A. N. (2020), "Improving tensile properties of polylactic acid parts by adjusting printing parameters of open source 3D printers", *Materials Science*, Vol. 26, No.1, pp.83-87.
146. Kumar, S., Singh, R., Singh, T. P. and Batish, A. (2020), "On flexural and pull out properties of 3D printed PLA based hybrid composite matrix", *Materials Research Express*, Vol.7, No.1, pp.1-14.
147. Gavali, V. C., Kubade, P. R. and Kulkarni, H. B. (2020), "Mechanical and thermo-mechanical properties of carbon fiber reinforced thermoplastic composite fabricated using fused deposition modeling method", *Materials Today: Proceedings*, Vol.22, pp. 1786-1795.
148. Kwok, S. W., Goh, K. H. H., Tan, Z. D., Tan, S. T. M., Tjiu, W. W., Soh, J. Y. and Goh, K. E. J. (2017), "Electrically conductive filament for 3D-printed circuits and sensors", *Applied Materials Today*, Vol.9, pp.167-175.
149. Torrado, A. R., Shemelya, C. M., English, J. D., Lin, Y., Wicker, R. B. and Roberson, D. A. (2015), "Characterizing the effect of additives to ABS on the mechanical property anisotropy of specimens fabricated by material extrusion 3D printing", *Additive Manufacturing*, Vol.6, pp.16-29.
150. Angelopoulos, P. M., Kenanakis, G., Viskadourakis, Z., Tsakiridis, P., Vasilopoulos, K. C., Karakassides, M. A. and Taxiarchou, M. (2021),

- “Manufacturing of ABS/expanded perlite filament for 3D printing of lightweight components through fused deposition modeling”, *Materials Today: Proceedings*, Vol. 54, pp.14-21.
151. Jiang, D. and Ning, F. (2020), “Fused filament fabrication of biodegradable PLA/316L composite scaffolds: effects of metal particle content”, *Procedia Manufacturing*, Vol. 48, pp. 755-762.
152. Sang, L., Han, S., Peng, X., Jian, X. and Wang, J. (2019), “Development of 3D-printed basalt fiber reinforced thermoplastic honeycombs with enhanced compressive mechanical properties”, *Composites Part A: Applied Science and Manufacturing*, Vol. 125, pp.105518.
153. Leist, S. K., Gao, D., Chiou, R. and Zhou, J. (2017), “Investigating the shape memory properties of 4D printed polylactic acid (PLA) and the concept of 4D printing onto nylon fabrics for the creation of smart textiles”, *Virtual and Physical Prototyping*, Vol.12, No.4, pp. 290-300.
154. Bilkar, D., Keshavamurthy, R. and Tambrallimath, V. (2021), “Influence of carbon nanofiber reinforcement on mechanical properties of polymer composites developed by FDM”, *Materials Today: Proceedings*, Vol. 46, pp. 4559-4562.
155. Peng, X., Zhang, M., Guo, Z., Sang, L. and Hou, W. (2020), “Investigation of processing parameters on tensile performance for FDM-printed carbon fiber reinforced polyamide 6 composites”, *Composites Communications*, Vol. 22, doi.org/10.1016/j.coco.2020.100478.
156. Ramesh, M. and Panneerselvam, K. (2021), “Mechanical investigation and optimization of parameter selection for Nylon material processed by FDM”, *Materials Today: Proceedings*, Vol. 46, pp. 9303-9307.
157. Yao, T., Ye, J., Deng, Z., Zhang, K., Ma, Y. and Ouyang, H. (2020), “Tensile failure strength and separation angle of FDM 3D printing PLA material: Experimental and theoretical analyses”, *Composites Part B: Engineering*, Vol. 188, doi.org/10.1016/j.compositesb.2020.107894.
158. Singh, S., Singh, M., Prakash, C., Gupta, M. K., Mia, M. and Singh, R. (2019), “Optimization and reliability analysis to improve the surface quality and mechanical characteristics of heat-treated fused filament fabricated parts”, *The International Journal of Advanced Manufacturing Technology*, Vol. 102, No.5, pp. 1521-1536.

159. Wittbrodt, B. and Pearce, J. M. (2015), "The effects of PLA color on material properties of 3-D printed components", *Additive Manufacturing*, Vol. 8, pp. 110-116.
160. Tao, Y., Wang, H., Li, Z., Li, P. and Shi, S. Q. (2017), "Development and application of wood flour-filled polylactic acid composite filament for 3D printing", *Materials*, Vol. 10, No.4, doi: 10.3390/ma10040339.
161. Wu, W., Geng, P., Li, G., Zhao, D., Zhang, H. and Zhao, J. (2015), "Influence of layer thickness and raster angle on the mechanical properties of 3D-printed PEEK and a comparative mechanical study between PEEK and ABS", *Materials*, Vol. 8, No.9, pp. 5834-5846.
162. Shenavar, A. and Abbasi, F. (2007), "Morphology, thermal, and mechanical properties of acrylonitrile-butadiene-styrene/carbon black composites", *Journal of applied polymer science*, Vol. 105, No.4, pp. 2236-2244.
163. Roberson, D., Shemelya, C. M., MacDonald, E. and Wicker, R. (2015), "Expanding the applicability of FDM-type technologies through materials development", *Rapid Prototyping Journal*, Vol. 21, No.2, pp.147-143.
164. Gkartzou, E., Koumoulos, E. P. and Charitidis, C. A. (2017), "Production and 3D printing processing of bio-based thermoplastic filament", *Manufacturing Review*, Vol. 4, pp. 1-14.
165. Idrees, M., Jeelani, S. and Rangari, V. (2018), "Three-dimensional-printed sustainable biochar-recycled PET composites", *ACS Sustainable Chemistry & Engineering*, Vol. 6, pp. 13940-13948.
166. Singh R, Singh H, and Farina I, (2019), "On the additive manufacturing of an energy storage device from recycled material", *Composite Part B Engineering*, Vol.156, pp. 259–265.
167. Alexander, P., Allen, S. and Dutta, D. (1998), "Part orientation and build cost determination in layered manufacturing", *Computer Aided Design*, Vol. 30, pp. 343-356.
168. Tong, K., Joshi, S. and Lehtihet, E.A. (2008), "Error compensation for fused deposition modelling (FDM) machine by correcting slice files", *Rapid Prototyping Journal*, Vol. 14, No. 1, pp. 4–14.
169. Noriega, A., Blanco, D., Alvarez, B.J. and Garcia, A. (2013), "Dimensional accuracy improvement of FDM square cross-section parts using artificial neural

- networks and an optimization algorithm”, *International Journal of Advanced Manufacturing Technology*, Vol. 69, pp. 2301–2313.
170. Hur, J. and Lee, K. (1998), “The development of a CAD environment to determine the preferred build-up direction for layered manufacturing”, *International Journal of Advanced Manufacturing Technology*, Vol. 14, pp. 247-254.
171. Zhang, B., Seong, B., Nguyen, V. and Byun, D. (2016), “3D printing of high-resolution PLA-based structures by hybrid electrohydrodynamic and fused deposition modeling techniques”, *Journal of Micromechanics and Microengineering*, Vol. 26, pp. 1-8.
172. Ramos, A.M. and Jose, S. (2009), “CAD-CAM-RTV–Lost-Wax Casting Technology for Medical Implants”, *Rapid Prototyping Journal*, Vol. 15, pp. 211-215.
173. Peres, F. and Martin, C. (1999), “Design methods applied to the selection of a rapid prototyping resource”, *Emerging Technologies and Factory Automation, Proceedings, 7th IEEE International Conference, 18-21 October, Barcelona, Spain, Vol. 1, pp. 417-422.*
174. Chua, C.K., Feng, C., Lee, C.W. and Ang, G.Q. (2005), “Rapid investment casting: direct and indirect approaches via model maker II”, *International Journal of Advanced Manufacturing Technology*, Vol. 25, pp. 26-32.
175. Kumar, P., Singh, R. and Ahuja, I.P.S. (2016), “Experimental investigations on hardness of the biomedical implants prepared by hybrid investment casting”, *Journal of Manufacturing Processes*, Vol. 21, pp. 160–171.
176. Sopcak J.E. (1986), “*Handbook of Lost Wax or Investment Casting*”, Gem Guides Book Company, Baldwin Park, USA.
177. Byun, H.S. and Lee, K.H. (2003), “Design of a New Test Part for Benchmarking the Accuracy and Surface Finish of Rapid Prototyping Processes”, *Proceedings of Computational Science and Its Applications- ICCSA, May 18-21, Montreal, Canada, pp. 731-740.*
178. Lppolito, R., Luliano, L. and Gatto, A. (1995), “Benchmarking of Rapid Prototyping Techniques in Terms of Dimensional Accuracy and Surface Finish”, *CIRP Annals - Manufacturing Technology*, Vol. 44, pp. 157-160.
179. Grenda, E. (2006), “Castle islands worldwide guide to rapid prototyping”, available at <http://home.att.net/~castleisland/home.htm> (accessed on 08/09/2013).

180. Bakar, N.S.A., Alkahari, M.R. and Boejang, H. (2010), "Analysis on fused deposition modeling performance", *Journal of Zhejiang University Science A*, Vol. 11, pp. 972-977.
181. Percoco, G., Galantucci, L.M. and Lavecchia, F. (2011), "Validation study of an analytical model of FDM accuracy", in *DAAAM International Scientific Book*, B. Katalinic (ed.), DAAAM International, Vienna, Austria, pp. 585-592.
182. Boschetto, A., Giordano, V. and Veniali, F. (2013), "Surface roughness prediction in fused deposition modelling by neural networks", *The International Journal of Advanced Manufacturing Technology*, Vol. 67, pp. 2727–2742.
183. Ayrilmis, N. (2018), "Effect of layer thickness on surface properties of 3D printed materials produced from wood flour/PLA filament", *Polymer testing*, Vol. 71, pp. 163-166.
184. Chohan, J. S., Singh, R. and Boparai, K. S. (2020), "Vapor smoothing process for surface finishing of FDM replicas", *Materials Today: Proceedings*, Vol. 26, pp. 173-179.
185. Garg, A., Bhattacharya, A. and Batish, A. (2016), "On surface finish and dimensional accuracy of FDM parts after cold vapor treatment", *Materials and Manufacturing Processes*, Vol. 31, No.4, pp. 522-529.
186. Boschetto, A. and Bottini, L. (2015), "Roughness prediction in coupled operations of fused deposition modeling and barrel finishing", *Journal of Materials Processing Technology*, Vol. 219, pp. 181-192.
187. Turner B.N. and Gold, S. A. (2015), "A review of melt extrusion additive manufacturing processes: II. Materials, dimensional accuracy, and surface roughness", *Rapid Prototyping Journal*, Vol. 21, pp. 250–261.
188. Jin, Y-a., Li, H., He, Y. and Fu, J-z. (2015), "Quantitative analysis of surface profile in fused deposition modelling", *Additive Manufacturing*, Vol. 8, pp. 142-148.
189. Rattanawong, W., Masood, S.H. and Iovenitti, P. (2001), "A volumetric approach to part-build orientations in rapid prototyping", *Journal of Materials Processing Technology*, Vol. 119, pp. 348-353.
190. Pennington, R. C., Hoekstra, N. L. and Newcomer, J. L. (2005), "Significant Factors in the Dimensional Accuracy of Fused Deposition Modelling," *Proceedings of the Institution of Mechanical Engineers, Part E: Journal of Process Mechanical Engineering*, Vol. 219, pp. 89–92.

191. Gregorian, A., Elliott, B., Navarro, R., Ochoa, F., Singh, H., Monge, E., Foyos, J., Noorani, R., Fritz, B. and Jayanthi, S. (2001), "Accuracy improvement in rapid prototyping machine (FDM-1650)", Solid Freeform Fabrication Proceedings, 12th Solid freeform fabrication symposium, University of Texas, Austin, pp. 77-84.
192. Idris, M.H., Sharif, S. and Harun, W.S.W. (2008), "Evaluation of ABS patterns produced from FDM for investment casting process", Proceedings of the 9th Asia Pacific Industrial Engineering & Management Systems Conference, 3–5 December, Nusa Dua, Bali, Indonesia. pp. 1299–1304.
193. Volpato, N., Foggianto, J.A. and Schwarz, D.C. (2014), "The influence of support base on FDM accuracy in Z", Rapid Prototyping Journal, Vol. 20, pp. 182–191.
194. Nuñez, P.J., Rivas, A., García-Plaza, E., Beamudb, E. and Sanz-Lobera, A. (2015), "Dimensional and surface texture characterization in Fused Deposition Modelling (FDM) with ABS plus", Procedia Engineering, Vol. 132, pp. 856 –863.
195. Thrimurthulu, K., Pandey, P.M. and Reddy, N.V. (2004), "Optimum Part Deposition Orientation in Fused Deposition Modeling", International Journal of Machine Tools and Manufacture, Vol. 44, pp. 585–594.
196. Mahapatra, S.S. and Sood, A.K. (2012), "Bayesian Regularization-Based Levenberg–Marquardt Neural Model Combined With BFOA for Improving Surface Finish of FDM Processed Part", International Journal of Advanced Manufacturing Technology, Vol. 60, pp. 1223-1235.
197. Garcia, C. R., Correa, J., Espalin, D., Barton, J. H., Rumpf, R. C., Wicker, R. and Gonzalez, V. (2012), "3D printing of anisotropic metamaterials", Progress In Electromagnetics Research Letters, Vol.34, pp.75-82.
198. Babae, S., Shim, J., Weaver, J. C., Chen, E. R., Patel, N. and Bertoldi, K. (2013), "3D soft metamaterials with negative Poisson's ratio", Advanced Materials, Vol. 25, No.36, pp. 5044-5049.
199. Compton, B. G. and Lewis, J. A. (2014), "3D-printing of lightweight cellular composites", Advanced materials, Vol. 26, No.34, pp.5930-5935.
200. Singh, R., Singh, I., Kumar, R. and Brar, G. S. (2021), "Waste thermosetting polymer and ceramic as reinforcement in thermoplastic matrix for sustainability: thermomechanical investigations", Journal of Thermoplastic Composite Materials, Vol.34, No.4, pp. 523-535.
201. Teresa, R.H.M., Angulo-Sanchez, J.L. and Pérez-Chantaco, A. (2007), "Determination of the molecular characteristics of commercial polyethylenes with

- different architectures and the relation with the melt flow index”, *Journal of Applied Polymer Science*, Vol. 104, No.3, pp. 1572-1578.
202. Bremner, T., Rudin, A. and Cook, D.G. (1990), “Melt flow index values and molecular weight distributions of commercial thermoplastics”, *Journal of Applied Polymer Science*, Vol. 41, pp. 1617-1627.
203. Covas J.A. and Gaspar-Cunha A. (2001), “A computational investigation on the effect of polymer rheology on the performance of a single screw extruder”, *Erheopt*, Vol.1, pp. 41-62.
204. Ross, P.J. (1996), “Taguchi Techniques for Quality Engineering: loss function, orthogonal experiments, parameter and tolerance design”, McGraw Hill Professional, New York.
205. Patel, J.P., Patel, C.P. and Patel, U.J. (2012) “A Review on Various Approach for Process Parameter Optimization of Fused Deposition Modeling (FDM) Process and Taguchi Approach for Optimization”, *International Journal of Engineering Research and Applications*, Vol.2, No.2, pp. 361-365.
206. Rao, A.S., Dharap, M.A., Venkatesh, J.V.L. and Ojha, D. (2012), “Investigation of post processing techniques to reduce the surface roughness of fused deposition modeled parts”, *International Journal of Mechanical Engineering and Technology*, Vol. 3, No.3, pp. 531-544.
207. Davim, J.P. (2003), “Design of optimization of cutting parameters for turning metal matrix composites based on the orthogonal arrays”, *Journal of Material Processing Technology*, Vol. 132, No. 3, pp. 340-344.
208. Besterfield, H.D., Micna, C.B., Besterfield, G.H. and Sacre, M.B. (2010), *Total Quality Management*, 3rd edition, Prentice Hall.
209. Phadke, M.S. (1986), “Design Optimization Case Study”, *AT & T Technical Journal*, Vol. 65, No. 2, pp. 51-68.
210. Logothetis, N. (1997), *Management for total quality*, Prentice Hall.
211. Singh J, Singh R. and Singh H. (2017), "Investigations for improving the surface finish of FDM based ABS replicas by chemical vapor smoothing process: a case study", *Assembly Automation*, Vol. 37, No. 1, pp.13-21.
212. Galantucci, L. M., Lavecchia, F. and Percoco, G. (2010), “Quantitative analysis of a chemical treatment to reduce roughness of parts fabricated using fused deposition modelling”, *CIRP annals*, Vol. 59, No. 1, pp.247-250.

213. Arumaikkannu, G., Maheshwaraa, N.U. and Gowri, S. (2005), "A Genetic Algorithm with Design of Experiments Approach to Predict the Optimal Process Parameters for FDM", Proceedings of 16th Solid Freeform Fabrication Symposium, August 1-3, Austin, USA, pp. 150-161.
214. Kumar, P., Ahuja, I.P.S. and Singh R. (2012), "Application of Fusion Deposition Modelling for Rapid Investment Casting – A Review" International Journal of Materials Engineering Innovation, Vol. 3, No. 3, pp. 204-227.
215. Agarwala, M.K., Jamalabad, V.R., Langrana, N.A., Safari A., Whalen, P.J. and Danforth, S.C. (1996), "Structural Quality of Parts Processed by Fused Deposition", Rapid Prototyping Journal, Vol. 2, No. 4, pp. 4-19.
216. Sood, A.K. (2011), "Study on Parametric Optimization of Fused Deposition Modelling (FDM) Process", Ph.D. Thesis, National Institute of Technology, Rourkela, India.
217. Gajdoš, I. and Slota, J. (2013), "Influence of Printing Conditions on Structure in FDM Prototypes", Technical Gazette, Vol. 20, No. 2, pp. 231-236.
218. Chaturvedi, V. (2009), "Parametric Optimization of Fused Deposition Modeling Using Response Surface Methodology", M.Tech. Thesis, National Institute of Technology, Rourkela, India.
219. Chouksey, A. (2012), "Study of parametric Optimization of Fused Deposition Modeling Process Using Response Surface Methodology", B. Tech. Thesis, National Institute of Technology, Rourkela, India.
220. Ziemian, C.W. and Crown, P.M (2001), "Computer Aided Decision Support for Fused Deposition Modeling", Rapid Prototyping Journal, Vol. 7, No. 3, pp. 138-147.
221. Anthamatten, A., Letts, S.A. and Cook, R.C. (2004), "Controlling Surface Roughness in Vapor-Deposited Poly(amic acid) Films by Solvent-Vapor Exposure", Langmuir, Vol. 20, pp. 6288-6296.